Atlantic Water advection and glacier responses at the margins of Svalbard since the deglaciation

Dissertation

zur Erlangung des Doktorgrades der Naturwissenschaften
am Fachbereich Geowissenschaften
der Universität Bremen/

submitted for the doctoral degree in natural sciences
at the faculty of Geosciences
of Bremen University

vorgelegt von/

by

Martin Bartels

Bremen, Juli 2017

ArcTrain marum Universität Bremen UQÀM

Gutachter der Dissertation:
Prof. Dr. Dierk Hebbeln (MARUM – Zentrum für Marine Umweltwissenschaften, Universität Bremen)
Prof. Dr. Gerhard Schmiedl (Universität Hamburg)

Datum der Abgabe: 18. Juli 2017
Datum des Kolloquiums: 08. November 2017

To Franca & Ava

Abstract

The Arctic reacts very sensitively to climatic and oceanographic changes as positive feedback mechanisms strengthen climate trends in high latitudes, in particular during the current climate warming. This phenomenon is called "Arctic Amplification". Warm atmospheric temperatures cause melting of sea ice, glaciers and ice sheets thereby reducing the Earth´s albedo, which leads to a further warming (ice–albedo feedback). Furthermore, a retreating sea ice cover insulates the cold Arctic atmosphere lesser from relatively warm ocean waters advected to the high northern latitudes by the North Atlantic Current. The reduced insulation increases the vertical heat transfer to the atmosphere (ice–insulation feedback). Due to this sensitivity, the Arctic may be regarded as an “early warning system” in the context of the progressing climate change.

In order to investigate the long-term consequences of these effects on climatic conditions, marine sediments from the Arctic can act as climate archives, which record climate variations of the past. Palaeoclimate reconstructions, based on these sediment sequences, can help to understand the complex global climate system, especially regarding the "Arctic Amplification" as they add important information to existing historical weather observations. The accessibility to such climate archives in the Arctic is limited or at least complicated by the partial perennial sea ice coverage. In contrast, the shelves of the Svalbard archipelago are bathed in warmer waters than any other Arctic regions at similar latitudes providing seasonally ice-free conditions. Additionally, the archipelago is located at the only deep sea gateway connecting the Arctic Ocean with the North Atlantic, offering ideal conditions to study past environmental conditions in the Arctic. The region is expected to react to even small-scale variations in the interplay of relatively warm Atlantic and cold Arctic waters. Further back in time, during the last Ice Age, the archipelago was even covered by the northwestern part of the Svalbard–Barents Sea Ice Sheet that stretched across the entire Barents Sea between northern Norway and the Arctic Ocean.

In the framework of this thesis, sediment cores from two fjords at the northern margin of Spitsbergen (western Svalbard) and in Nordaustlandet (eastern Svalbard), respectively, as well as from a trough off northwestern Spitsbergen were chosen because fjord (and trough) sediments offer highly resolved climate archives due to high sedimentation rates. A set of various methods was applied to reconstruct the palaeoceanography and ocean–ice interactions during the past ~15,500 years. The benthic foraminiferal fauna was analysed to assess the palaeoenvironmental conditions including the hydrography of the region, whereas sediment properties (grain size distribution and the amount of ice-rafted material) were used to evaluate the past glacier activity. Stable carbon and oxygen isotopes in foraminifera shells were studied to reconstruct palaeoproductivity and temperature/salinity and organic molecules in the sediment were analysed to achieve information on past surface water conditions including sea surface temperature, primary production and sea ice coverage.

This cumulative dissertation comprises three manuscripts summarized as follows: In the first manuscript, a sediment core from the mouth of the Woodfjord (northern Spitsbergen) was investigated spanning the last 15,500 years, although with a 6,000-year gap. Hydrographic conditions and glacier dynamics during the deglaciation were compared with those of the last two millennia. The data indicate that between ~15,500 and ~12,900 years ago, the advection of Atlantic water into the bottom water of the fjord has contributed significantly to the disintegration of the Svalbard–Barents Sea Ice Sheet and its outlet glaciers. During the Younger Dryas (~12,900–11,700 years ago), Atlantic Water rose in the water column and influenced the

intermediate water, while no glacier advances are evident in our record. The subsequent early Holocene, when most glaciers in the investigated fjord system had retreated to inner-fjord positions, was characterized by warmer temperatures than today. Simultaneously with other sites around Svalbard, these ameliorated conditions were briefly interrupted around 11,000 years ago, during the so-called *Preboreal Oscillation*. The period between ~7,800–1,800 years ago could not be interpreted due to disturbances in the sediment sequence. Unlike during the deglaciation, glaciers rather advanced than waned in the course of the last almost two millennia, although a persisting influx of Atlantic Water is evident.

The second manuscript is based on sediment samples from the Wahlenbergfjord, a remote fjord in Nordaustlandet, surrounded by tidal glaciers. The sediment core covers the past ~11,300 years. During the early Holocene, when summer insolation reached its maximum, intense meltwater discharges delivered large amounts of sediments, while at the same time a strong influence of Atlantic-derived water is suggested. At the transition to the mid-Holocene (around 7,700 years ago), a regional hydrographic shift is indicated in the record from this fjord: Arctic Water gained influence, while Atlantic-derived waters became less important. Similar indications were observed at numerous sites in the Svalbard area, which suggest that even remote glacier-proximal fjord sediments reflect regional palaeoceanographic variations. As assumed in the first manuscript, glacier advances are likely during the late Holocene, especially since ~3,000 years ago, when again a strong influence of Atlantic Water is assumed, also in the Wahlenbergfjord. This contradiction may be caused by extending sea ice insulating the cold atmosphere from the relatively warm ocean waters.

In the third manuscript, a sediment core from the Kongsfjord-Trough (northwestern Spitsbergen) covering the period ~15,300–1,300 years ago, was compared with previously published data from a nearby study site (encompassing only the Holocene). These data reveal an early Atlantic Water inflow (starting ~14,800 years before today), which significantly affected the break-up of the Svalbard–Barents Sea Ice Sheet. At the onset of the Younger Dryas, Atlantic Water was forced to sink in the water column by the massive meltwater outburst that triggered this cold spell. Subsequently, the inflow of relatively warm Atlantic Water again contributed to further glacier retreats, while environmental conditions during the Younger Dryas were very variable in the Svalbard area. The deglaciation of the Svalbard–Barents Sea Ice Sheet persisted until ~10,300 years ago, when the deposition of meltwater-derived fine sediments rapidly declined. Glacier melting and meltwater discharge seemingly were the dominant processes during deglaciation compared to glacier calving. The comparison to a nearby core site closer to the coast illustrates that the proximity to the shore had a major impact on productivity, which at times was limited by fine grained sediment-laden meltwater plumes (around 10,500 years ago) or enhanced by a coastward shift of the Arctic Coastal Front enabling Atlantic Water to affect the shelf waters (~10,300–7,700 years ago).

Zusammenfassung

Die Arktis reagiert sehr empfindlich auf klimatische und ozeanographische Veränderungen, da positive Rückkopplungsmechanismen Klimatrends in hohen Breiten verstärken, ein Phänomen, das die „arktische Verstärkung“ (“*Arctic Amplification*“) genannt wird und insbesondere auch die aktuelle Klimaerwärmung betrifft. Bei warmen atmosphärischen Temperaturen schmelzen Meereis, Gletscher und Eisschilder, sodass die Albedo reduziert wird, was zu einer weiteren Erwärmung führt (Eis–Albedo–Feedback). Darüber hinaus kann eine reduzierte Meereisbedeckung die kalte arktische Atmosphäre schlechter gegenüber relativ warmen Meerwasser, das vor allem durch den Nordatlantikstrom in die hohen nördlichen Breiten transportiert wird, isolieren, wodurch sich der vertikale Wärmetransport in die Atmosphäre erhöht (Eis–Isolation–Feedback). Aufgrund dieser Empfindlichkeit kann die Arktis als „Frühwarnsystem“ im Kontext des fortschreitenden Klimawandels angesehen werden.

Um die langfristigen Auswirkungen dieser Effekte auf Klimatrends zu untersuchen bieten sich marine Sedimente aus der Arktis als ein Klima-Archiv an, welches Klima-Variationen der Vergangenheit aufzeichnet. Paläoklima-Rekonstruktionen, die auf diesen Sedimentabfolgen basieren, können dazu beitragen, das komplexe globale Klimasystem vor allem auch im Hinblick auf die „arktische Verstärkung“ zu verstehen, da sie wichtige Informationen zu bestehenden historischen Wetterbeobachtungen hinzufügen. Die Zugänglichkeit zu solchen Klima-Archiven in der Arktis ist durch die teilweise ganzjährige Meereisbedeckung begrenzt oder zumindest kompliziert. Im Gegensatz dazu sind die Schelfe des Svalbardarchipels von wärmeren Gewässern bedeckt als alle anderen arktischen Gebiete in ähnlichen Breiten. Dementsprechend sind dort saisonal eisfreie Bedingungen anzutreffen. Darüber hinaus befindet sich das Archipel an der einzigen Tiefsee-Verbindung, die den Arktischen Ozean mit dem Nordatlantik verbindet. Svalbard bietet somit ideale Voraussetzungen, um vergangene Umweltbedingungen in der Arktis zu studieren. Es wird erwartet, dass die Region schon auf kleinere Variationen im Zusammenspiel von relativ warmem atlantischen und kaltem arktischen Wasser reagiert. Weiter zurück in der Vergangenheit, am Ende der letzten Eiszeit war das Archipel sogar von dem nordwestlichsten Teil des Svalbard–Barentssee Eisschildes bedeckt, der sich über die gesamte Barentssee zwischen Nordnorwegen und dem Arktischen Ozean erstreckte.

Im Rahmen dieser Arbeit wurden Sedimentkerne von zwei Fjorden am nördlichen Rand von Spitzbergen (Westsvalbard) und in Nordaustlandet (Ostsvalbard) sowie aus einem Trog vor Nordspitzbergen ausgewählt, weil Fjord- (und Trog-) Sedimente aufgrund hoher Sedimentationsraten hochaufgelöste Klimaarchive bieten. Eine Reihe von verschiedenen Methoden wurde angewendet, um die Paläozeanographie und Ozean–Eis–Interaktionen während der letzten ~15.500 Jahre zu rekonstruieren. Die Fauna der benthischen Foraminiferen wurde analysiert, um die Paläo-Umweltbedingungen einschließlich der Hydrographie der Region abzuschätzen, während Sediment-Eigenschaften (Korngrößenverteilung und die Menge an eistransportiertem Material) verwendet wurden, um die Gletscheraktivität der Vergangenheit zu bewerten. Stabile Kohlenstoff- und Sauerstoffisotope in Foraminiferenschalen wurden untersucht, um die Paläo-Produktivität bzw. die Temperatur/Salinität zu rekonstruieren, wohingegen organische Moleküle im Sediment Informationen über vergangene Oberflächenwasserbedingungen einschließlich Meeresoberflächentemperatur, Primärproduktion und Meereisbedeckung geliefert haben.

Diese kumulative Dissertation besteht aus drei Manuskripten, die im Folgenden zusammengefasst werden: Im ersten Manuskript wurde ein Sedimentkern von der Mündung des Woodfjords (Nordspitzbergen) untersucht, der die letzten 15.500 Jahre abdeckt, allerdings mit einer 6.000-jährigen Lücke. Hydrographische Bedingungen und Gletscher-Dynamiken während der Deglaziation wurden mit denen der letzten zwei Jahrtausende verglichen. Die Daten deuten darauf hin, dass zwischen ~15.500 und ~12.900 Jahren vor heute die Advektion atlantischen Wassers in das Bodenwasser des Fjords wesentlich zum Zerfall des Svalbard–Barentssee Eisschildes und seiner Auslassgletscher beigetragen hat. Während der Jüngeren Dryas (~12.900–11.700 Jahre vor heute) stieg das atlantische Wasser in der Wassersäule auf und beeinflusste das Zwischenwasser. Zur selben Zeit sind keine Gletschervorstöße überliefert. Das anschließende frühe Holozän, als sich die meisten Gletscher im untersuchten Fjord-System in das Innere der Fjorde zurückzogen hatten, war von wärmeren Temperaturen als heute geprägt. Vor rund 11.000 Jahren, während der sogenannten präborealen Oszillation („*Preboreal Oscillation*“) wurden diese verbesserten Bedingungen kurzzeitig unterbrochen, was gleichzeitig an verschiedenen Orten rund um Svalbard festzustellen ist. Der Zeitraum zwischen ~7.800–1.800 Jahren vor heute konnte aufgrund von Störungen in der Sedimentabfolge nicht interpretiert werden. Im Gegensatz zur Zeit der Deglaziation sind die Gletscher im Laufe der letzten zwei Jahrtausende vorgerückt, obwohl ein anhaltender Zustrom von atlantischem Wasser angenommen wird.

Das zweite Manuskript basiert auf Sedimentproben aus dem Wahlenbergfjord, einem abgelegenen Fjord in Nordaustlandet, der von Gezeitengletschern umgeben ist. Der Sedimentkern umfasst die vergangenen ~11.300 Jahre. Während des frühen Holozäns, als die Sommerinsolation ihr Maximum erreichte, lieferten intensive Schmelzwasserabflüsse große Mengen an Sedimenten, während gleichzeitig ein starker Einfluss von Wassermassen atlantischen Ursprungs vermutet wird. Beim Übergang zum mittleren Holozän (vor etwa 7.700 Jahren) wird in den Daten aus diesem Fjord ein regionaler Wechsel der hydrographischen Bedingungen angezeigt: Das arktische Wasser gewinnt an Einfluss, während der Einstrom von Wasser atlantisch Ursprungs abgeschwächt wird. Ähnliche Hinweise wurden an Lokationen um Svalbard beobachtet, die darauf hindeuten, dass auch abgelegene, gletscher-proximale Fjordsedimente regionale paläozeanographische Variationen widerspiegeln. Wie bereits im ersten Manuskript angenommen, sind Gletschervorstöße während des späten Holozäns wahrscheinlich, besonders seit ~3.000 Jahren, wenn auch für den Wahlenbergfjord wieder ein stärkerer Einfluss atlantischen Wassers angenommen wird. Dieser Widerspruch mag in einer vermehrten Ausbreitung von Meereis begründet sein, die die kalte Atmosphäre von dem relativ warmen Meerwasser isolierte.

Im dritten Manuskript wurde ein Sedimentkern aus dem Kongsfjord-Trog (Nordwestspitzbergen), der die Zeitspanne ~15.300–1.300 Jahre vor heute abdeckt, mit bereits veröffentlichten Daten von einem nahegelegenen Sedimentkern (der nur das Holozän umfasst) verglichen. Diese Daten zeigen einen frühen Einfluss atlantischen Wassers (ab ~14.800 Jahren vor heute), der eine deutliche Einwirkung auf den Zerfall des Svalbard–Barentssee Eisschildes hatte. Zu Beginn der Jüngeren Dryas wurde das atlantische Wasser durch den massiven Schmelzwasserausbruch, der diese Kälteperiode auslöste, gezwungen, in der Wassersäule zu sinken. In der Folge führte der Zufluss relativ warmer atlantischer Wassermassen zu weiteren Gletscherrückzügen, während die Umweltbedingungen während der Jüngeren Dryas in der Region Svalbards sehr variabel waren. Die Deglaziation des Svalbard–Barentssee Eisschildes dauerte bis vor ~10.300 Jahren an, als der Eintrag von Schmelzwasser-transportierten feinen Sedimenten rasch abnahm. Gegenüber dem

Kalben scheint das Schmelzen der Gletscher und der Eintrag von Schmelzwasser der dominierende Prozess während der Deglaziation gewesen zu sein. Der Vergleich zu einer nahegelegenen Kern-Lokation dichter an der Küste zeigt, dass diese Nähe zur Küste einen großen Einfluss auf die Produktivität hatte, die dort zeitweise durch feinkörnige, trübe Sedimentfahnen limitiert wurde (vor etwa 10.500 Jahren), oder durch eine Verschiebung der Arktischen Küstenfront („*Arctic Coastal Front*“) in Richtung Küste, sodass atlantisches Wasser Einfluss auf die Schelfgewässer hatte (~10.300–7.700 Jahre), verstärkt wurde.

Acknowledgements

First of all, I would like to thank Dierk Hebbeln for offering me the PhD position, for supervising and supporting me during the process of my project and lastly for hiring me a second time for a subsequent postdoc position. Thank you, Dierk!

I am also grateful to Gerhard Schmiedl for agreeing to be the second reviewer of this thesis, but also for sparking my enthusiasm for foraminiferal research already during my studies.

I further thank the graduate college *ArcTrain* ("Processes and impacts of climate change in the North Atlantic Ocean and the Canadian Arctic"), funded by the Deutsche Forschungsgemeinschaft (DFG; IRTG 1904 ArcTrain), not only for financial support, e.g., for conference trips, research stays abroad, summer schools and annual meetings in Canada, but above all for offering the unique opportunity to study the Arctic, even travel to the Arctic and to participate in a cruise with the icebreaker RV *Polarstern*, some of my long-standing dreams.

The graduate school *GLOMAR* and its lecturers are acknowledged for offering interesting courses and lots of support. Especially, Karin Boos is thanked for very helpful explanations about the software *R* and statistics.

Moreover, I am grateful to my thesis committee (Dierk Hebbeln, Rüdiger Stein, Mayhar Mohtadi, Claude Hillaire-Marcel and Markus Kienast) for support and fruitful discussions.

The *MARUM – Center for Marine Environmental Sciences* in Bremen is thanked for providing sample material and lab facilities.

My co-authors Claude Hillaire-Marcel, Rüdiger Stein, Kirsten Fahl, Marit-Solveig Seidenkrantz and Jürgen Titschack are acknowledged for performing measurements, data processing, improving my first manuscript, general support and beneficial discussions. I especially thank Jürgen for all the support, answering my endless questions, coming up with the idea of CT scanning my sediment cores, discussing sedimentological issues and creating really nice maps. Marit-Solveig is further thanked for the revision of the foraminiferal species during my first identification attempts.

I am obliged to all the people who performed further measurements for me and offered support in the lab: Volker Diekamp, Christina Gnade, Henning Kuhnert, Birgit Meyer, Birgit Lübben, Vera Lukies, Vera Bender, Janet Rethemeyer and Lukas Wacker. Lukas is further thanked for many explanations and discussions regarding radiocarbon measurements.

I am also grateful to my intern Hyunyung Boo as well as to my student assistants Christian Haars, Nele Lamping, Anna-Lena Rugen, Christian Rintisch, Jan Unverfärth and Marco Wolsza. Without your help this thesis would not exist.

The following people are acknowledged for administrative help and support: Gabriella Wehr, Carmen Murken, Nico Dittert and Birgit Volkmann. Furthermore, I am grateful to Jutta Bülten for IT support.

I am very thankful to Anne de Vernal and Claude Hillaire-Marcel for hosting and supervising me at their institute *le Geotop* during my research stay at the *Université du Québec à Montréal*. Moreover, I am grateful to Cynthia Le Duc for sharing her office in Montréal. I also thank all the colleagues at *UQÀM* who supported me with administrative issues, in the lab, at the scanning electron microscope and while learning a new method for age–depth modelling during my stay: Nicole Turcot, Bianca Fréchette and Maryse Henry as well as Raynald Lapointe and André Poirier.

I also want to thank all my *ArcTrain* peers, on the German and on the Canadian side, for very great times on retreats, summer schools, annual meetings and cruises. Special thanks go to the fellows from Montréal for a warm welcome during my stay.

The participants of the RV *Polarstern* cruise PS93.1 are acknowledge for an amazing time on board during this impressing adventure. Especially Matze Forwick is thanked for inspiring discussions about fjords, but also for funny "after hours". Likewise, I thank the participants of the RV *Maria S. Merian* cruise MSM36 for an interesting cruise going beyond my research scope and a relaxed atmosphere even during night shifts.

A great "thank you!" goes to the *Hebbeln Sedimentology Working Group* for amusing coffee and lunch breaks but also inspiring discussions. My office mates Martina Hollstein and Yusuf Awaluddin are especially acknowledged for a comfortable working atmosphere. I really had a great time with you, guys!

I am grateful to Timm Sauer for the revision of the "frame-text" of my thesis.

Last but not least, I am thankful to my family: My parents are acknowledged for any kind of support. My parents-in-law are especially thanked for offering me a calm place in their flat during busy weekend hours finalising my dissertation. And, above all, I am grateful to my wife Franca and our daughter Ava for just being there, motivating me and providing a "safe haven" every time. Without you, Franca, it would not have been possible to "conquer this mountain". Thank you!

Table of Contents

1 Introduction

As documented during the past decades (recently summarised in IPCC, 2014), we are facing a global warming, which will likely have significant consequences for our society's future life quality, e.g., due to catastrophic events like floodings, droughts, extreme weather events, crop failures etc. Averaged global temperatures exceeding values experienced during the time span of instrumental weather observations are expected in the near future (IPCC, 2014). To minimise a further warming and to develop adaptation strategies, it is very important to understand the global climate system and its internal responses and interactions. During geological time spans (even within the last 11,000 years), the Earth experienced warmer temperatures than today. Accordingly, palaeoclimate reconstructions offer a valuable contribution to deeper insights, e.g., into atmospheric, hydrographic and cryospheric interconnections during those temperature maxima (Masson-Delmotte et al., 2014). Polar regions are of particular importance as those regions react extremely sensitive to climate changes (as outlined in the following chapter). Especially, the interplay of relatively warm ocean currents with glaciers and sea ice is of great interest (Cook et al., 2016; Luckman et al., 2015; Motyka et al., 2003; Straneo et al., 2010; Wouters et al., 2015). Hence, the past ocean–ice interactions in Arctic fjords were reconstructed in the framework of this thesis.

1.1 The role of the Arctic in the climate system

Since the beginning of satellite-based sea ice observations (1978/79), the extension of summer sea ice in the Arctic is shrinking (Stroeve et al., 2012), very likely caused by the anthropogenic emission of greenhouse gases inducing a global warming (Notz and Marotzke, 2012; Notz and Stroeve, 2016). In modelled scenarios of the future, this global warming is accelerating the melting of Arctic ice sheets (especially, the Greenland Ice Sheet), which is assumed to contribute largely to global sea level rise (Alley et al., 2005; Gregory et al., 2004; Gregory and Huybrechts, 2006). These examples illustrate that the Arctic plays an important role in the global climate system. Due to its exceptionally sensitive responses to climate variability it can be regarded as an "early warning system", especially in the context of the ongoing anthropogenic climate change. Temperatures in the Arctic are rising twice as rapidly as the global mean owing to positive feedback mechanisms – this effect is known as "Arctic amplification" (Serreze and Barry, 2011; Fig. 1a): Warmer temperatures cause the melting of sea ice, consequently, the albedo (the percentage of sunlight reflection) decreases due to the darker sea surface (compared to sea ice) further warming the planet. Additionally, relatively warm ocean currents are no longer insulated by sea ice leading to warmer atmospheric temperatures (Fig. 1b, c). Recent studies examined a linkage between those rapid changes in the Arctic (especially the loss of sea ice and snow melting) and extreme weather events in mid-latitudes (Cohen et al., 2014a; Mori et al., 2014). However, mid-latitude responses to the Arctic amplification are chaotic and linkages between the Arctic warming and, e.g., severe Eurasian winters are very complex (Overland et al., 2016).

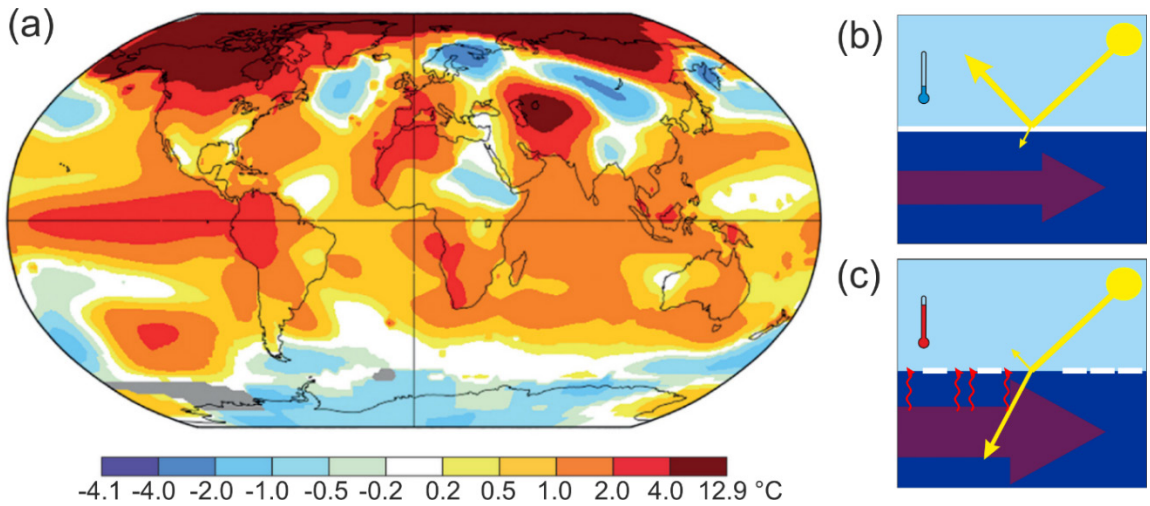

Fig. 1: Arctic Amplification and feedback mechanisms: (a) Atmospheric temperature anomalies [°C] for January 2016 compared to the temperature record since 1880 showing a significantly warmer Arctic (modified after Overland et al., 2016). (b) A closed sea ice cover insulates the cool atmosphere from warm ocean currents while radiation from the sun is mostly reflected (high albedo). (c) Less sea ice coverage leads to a lower albedo (less sunlight is reflected) while the ocean is warmed up and heat loss from the ocean to the atmosphere results in further warming consequentially melting more sea ice (positive feedback).

On monthly and annual timescales, Arctic climate is strongly influenced by sea level pressure anomalies north of 20°N, the so-called Arctic Oscillation (AO; Thompson and Wallace, 1998). During a positive AO (Fig. 2a), strong winds at ~55°N prevent cold air masses from moving southwards, whereas during a negative AO (Fig. 2b), Arctic air can reach lower latitudes (e.g., Darby et al., 2012). The AO is directly linked to the North Atlantic Oscillation (NAO; e.g., Delworth and Dixon, 2000; Deser, 2000; Mysak, 2001). During a positive NAO index (high pressure gradient between the Icelandic low and the Azores high; Fig. 2c), intensified westerlies lead to mild and wet winters in Northern Europe (Hurrell, 1995). In the Arctic, a high NAO index strengthens northerly winds resulting in cold and dry conditions in Greenland and north-eastern Canada and vice versa (Fig. 2c, d). Additionally, a north-eastward shift of Atlantic storms can be associated with a positive NAO index (Hurrell, 1995; Hurrell et al., 2003). Strong southerly winds over the Norwegian Sea cause an enhanced inflow of warm Atlantic Water (AW) far into the Arctic Ocean when the NAO index is high (Mysak, 2001). The distribution of sea ice is also linked to the NAO. During a positive phase, sea ice in the Labrador Sea extends southwards while sea ice around Greenland retreats farther north (Hurrell et al., 2003). Furthermore, the recently increasing NAO index also has a decelerating effect on the general trend of a weakened Atlantic Meridional Overturning Circulation (AMOC): Global warming results in warmer and fresher and, thus, less dense surface waters reducing the AMOC, while a positive NAO index causes stronger westerlies, which cool the surface layer delaying the reduction of the overturning circulation (Delworth and Dixon, 2000).

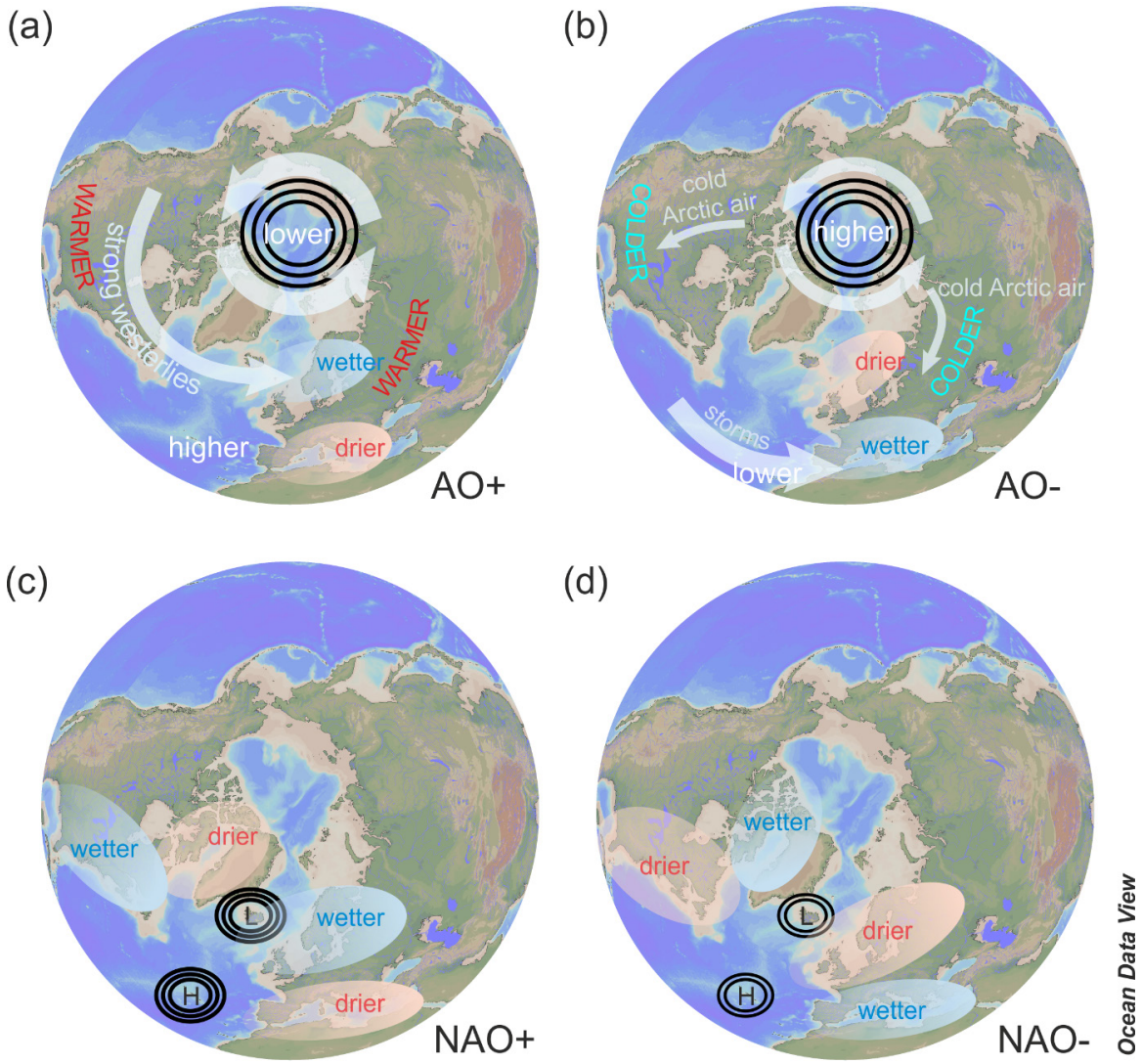

Fig. 2: Arctic Oscillation (AO) and North Atlantic Oscillation (NAO). (a) positive AO: lower than average sea level pressure over the Arctic Ocean and higher than average sea level pressure at lower latitudes leads to strong westerlies "trapping" cold Arctic air in polar regions. Hence, Eurasia and North America experience warmer temperatures while northern Europe gets wetter and the Mediterranean area drier. (b) negative AO: opposite climate conditions as cold Arctic air is able to reach lower latitudes while storms over the central Atlantic transport moisture to the Mediterranean region. (c) positive NAO index (high pressure gradient between Iceland low and Azores high): drier western Arctic (Greenland and Canada) and wetter eastern North America as well as wetter northern Europe and drier Mediterranean area. (d) negative NAO index (low pressure gradient between Iceland low and Azores high): opposite climate conditions. Basemap created with Ocean Data View (Schlitzer, 2015).

The latter example as well as the example of the connection between the Arctic amplification and mid-latitude weather phenomena illustrate the complexity of climate interconnections and the interweaving of anthropogenic and natural forcings and variabilities. Therefore, several studies emphasised the importance of palaeoclimate reconstructions in the Arctic to understand its role in the climate system (e.g., Axford et al., 2013; Sejrup et al., 2011; Spielhagen, 2012). Miller et al. (2010) showed that especially the Arctic amplification can be traced during the past three million years in proxy-based palaeo-records as well as in modelling studies. Palaeoclimate reconstructions offer an insight into climatic conditions almost undisturbed by human activities (animal farming, land use, deforestation, burning of fossil fuels etc.). For this purpose, continuous, ideally highly resolved sedimentary records are needed.

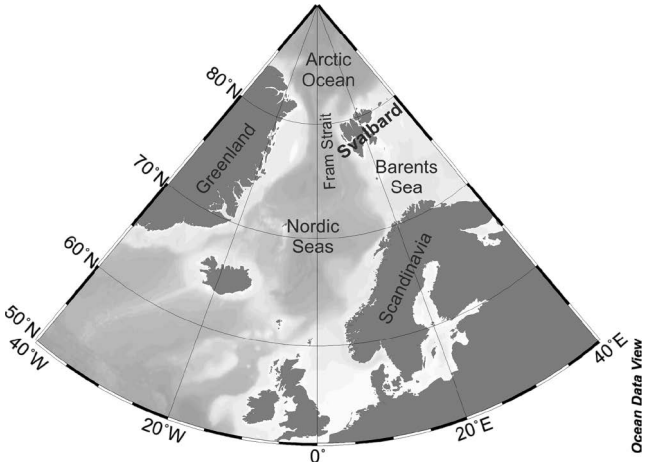

Fig. 3: Northern North Atlantic with location of the Svalbard Archipelago at the north-western Barents shelf. Basemap created with Ocean Data View (Schlitzer, 2015).

1.2 Svalbard´s unique position within the Arctic system

The Svalbard Archipelago is situated at the only deep sea gateway (namely the Fram Strait) connecting the Atlantic and the Arctic Ocean (Fig. 3). Due to a strong influence of the northernmost extension of the "Gulf Stream", Svalbard is bathed in warmer waters than any other Arctic location. Accordingly, Svalbard´s climate is comparably mild concerning its position at high latitudes. Directly located at the interconnection of Arctic and Atlantic waters (see chapter 2.2), very sensitive responses to climatic variabilities are expected at Svalbard´s margins. Due to comparably high sedimentation rates, sedimentary records from Svalbard´s shelves and fjords are very well suitable, highly resolved Arctic climate archives, ideal to reconstruct past hydrographic, cryospheric and climatic developments, at least since the last deglaciation (since ~20,000 years).

In the Arctic Ocean, the recovery of sediment cores is only possible under great effort and for the most part merely with the help of an icebreaker as the Arctic Ocean is largely covered by sea ice. Contrastingly, Svalbard´s shelves and fjords are, partly perennial, comparably easy accessible due to relatively warm ocean currents preventing heavy sea ice conditions.

1.3 The palaeoenvironmental development of the Svalbard region since the deglaciation

Based on the available information from previous reconstructions of the palaeoenvironment, the development of the Svalbard region since the Last Glacial Maximum (LGM) can be described as follows: During the LGM (~21,700–18,200 years ago), Svalbard and the Barents Sea were covered by a massive ice sheet extending to the shelf edge of Svalbard (Landvik et al., 1998). Analyses of cosmogenic radionuclides revealed that this ice sheet started to retreat at its westernmost extend already around ~20,500 years ago and the southwestern part around ~19,000–18,000 years ago while the deglaciation of the northern shelf started not before 15,900 years ago (Hormes et al., 2013). Sedimentary records from the northern Barents Sea consistently illustrate a retreat of the ice sheet from the troughs of the northern shelf between ~16,500 and ~15,000 years ago (Hogan et al., 2017). The ice sheet continuously thinned while its inner part deglaciated between ~15,000 and ~14,000 years ago (Hormes et al., 2013). Most fjords in Svalbard were deglaciated in the course of the Bølling interstadial (starting at ~15,100 years ago) and became ice-free during the early Holocene (between ~11,300 and ~9,800 years ago; e.g., Baeten et al., 2010; Flink et al., 2017; Fransner et al., 2017; Hormes et al., 2013). Hormes et al. (2013) assumed that the collapse of the ice sheet was induced by increasing summer insolation, a reduced moisture supply and the advection of relatively warm AW.

The variability of AW inflow and glacier activity at the western Barents and Svalbard shelves during the past ~20,000 years were examined applying various methods, including faunal assemblages of planktic and benthic foraminifera, stable oxygen and carbon isotopes as well as sediment properties, especially the amount

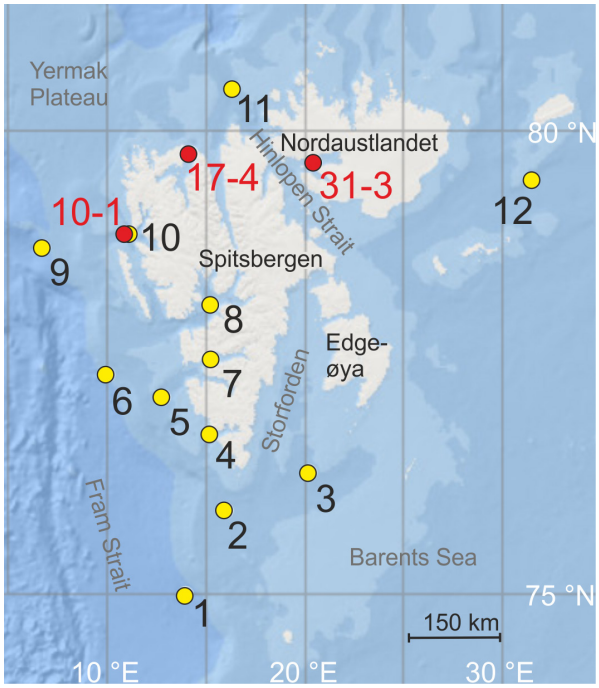

Fig. 4: Palaeoceaongraphic studies in the Svalbard area. Red dots mark core sites used in the studies of this thesis: GeoB108*17-4* at the mouth of the Woodfjord (manuscript I; chapter 5; Bartels et al., 2017), GeoB108*31-3* in the Wahlenbergfjord (manuscript II; chapter 6), GeoB108*10-1* in the Kongsfjord Trough (manscript III; chapter 7). Yellow dots mark core locations of further palaeo-studies: 1. 23258 (Sarnthein et al., 2003); 2. JM02-460 (Rasmussen et al., 2007; Rasmussen and Thomsen, 2014); 3. JM09-020 (Łącka et al., 2015); 4. HR3 (Majewski et al., 2009); 5. JM02-440 (Rasmussen et al., 2007; Ślubowska-Woldengen et al., 2007); 6. MD99-2304 (Hald et al., 2004); 7. MD99-2305 (Hald et al., 2004); 8. JM98-845 (Rasmussen et al., 2012); 9. MSM5/5-712-1 (Müller et al., 2012; Müller and Stein, 2014; Spielhagen et al., 2011; Werner et al., 2011, 2013, 2014); 10. NP05-11-21 (Jernas et al., 2013; Rasmussen et al., 2014b; Skirbekk et al., 2010); 11. NP94-51 (Jernas et al., 2013; Koç et al., 2002; Ślubowska-Woldengen et al., 2007; Ślubowska et al., 2005); 12. NP05-71 (Klitgaard Kristensen et al., 2013). Basemap created with ArcGIS online (http://www.arcgis.com).

of ice-rafted material (e.g., Hald et al., 2004; Łącka et al., 2015; Rasmussen et al., 2007, 2012; Sarnthein et al., 2003; Skirbekk et al., 2010; Ślubowska-Woldengen et al., 2007; see Fig. 4 for locations). At the southwestern Svalbard margin, AW was present since ~20,000 years, although submerged under polar surface waters during the deglaciation (until the onset of the Holocene ~11,700 years ago; Rasmussen et al., 2007). An increasing AW influence, starting between ~15,000 and ~14,500 years ago and peaking during the early Holocene, was reported from the western and northern Svalbard margins (Ślubowska-Woldengen et al., 2007; Ślubowska et al., 2005). Correspondingly, sea ice retreated parallel to this strengthened AW inflow in the eastern Fram Strait (Müller et al., 2009; Müller and Stein, 2014).

Several authors (e.g., Rasmussen et al., 2007; Ślubowska et al., 2005) presumed a continuous AW influence in the Svalbard area during the Younger Dryas (YD; ~12,900–11,700 years ago). The YD has been a matter of debate at least since the early 1990s (e.g., Berger, 1990; see also Fiedel, 2011, and references therein). This cold reversal is clearly evident in Greenland ice cores, e.g., NGRIP (North Greenland Ice Core Project; Rasmussen et al., 2014a). The ending of the YD is clearly defined based on various ice core data (e.g., deuterium excess, stable oxygen isotopes, dust; Walker et al., 2009), whereas the onset is still discussed (Fiedel, 2011). The trigger for the YD was most likely a gigantic meltwater intrusion into the Arctic Ocean that reduced the thermohaline circulation (Broecker, 2006; Broecker et al., 1989; Murton et al., 2010; Tarasov and Peltier, 2005). Whereas this meltwater flood evidently derived from the Laurentide Ice Sheet covering North America, its route is less clear (Broecker, 2006; Levac et al., 2015; Murton et al., 2010; de Vernal et al., 1996). It has been doubted that this freshwater outburst was triggered by an extra-terrestrial impact (van Hoesel et al., 2014; Pinter et al., 2011) as proposed by Firestone et al. (2007). Bradley and England (2008) presumed that the meltwater discharge entailed an extremely thick sea ice coverage on the Arctic Ocean that contributed to the reduced deep water formation decelerating the thermohaline circulation. An increased sea ice export from the central Arctic Ocean during the YD has been suggested by several authors (Bauch et al., 2001; Fahl and Stein, 2012; Not and Hillaire-Marcel, 2012). Despite rapidly dropping temperatures in this time interval (Alley, 2000), no glacier advances have been

reported from most Arctic locations, including Svalbard (e.g., Badding et al., 2013; Mangerud and Landvik, 2007; Reusche et al., 2014; Salvigsen and Österholm, 1982; Slabon et al., 2016; Young et al., 2012). However, several glaciers in western and northernmost Greenland expanded during the YD (Larsen et al., 2016; Ó Cofaigh et al., 2013) while also some Svalbard glaciers may have waned (e.g., Boulton, 1979; Forwick, 2005; Svendsen et al., 1996).

The succeeding early Holocene and especially the so-called Holocene Thermal Maximum were characterized by increasing sea surface temperatures: In the Nordic Seas (e.g., Hald et al., 2007; Telesiński et al., 2015) as well as at the southern (Łącka et al., 2015; Rasmussen et al., 2007; Sarnthein et al., 2003), western (Hald et al., 2004; Rasmussen et al., 2012; Skirbekk et al., 2010; Ślubowska-Woldengen et al., 2007; Werner et al., 2016) and northern Svalbard margins (Koç et al., 2002; Ślubowska et al., 2005) warmer temperatures were detected with a similar timing (starting between ~11,000 and ~10,000 years ago). In contrast, maximum temperatures were reached almost 3,000 years later in the area of Franz Josef Land further to the east (e.g., Duplessy et al., 2001, 2005). Subsequently, a general cooling trend, starting in the course of the mid-Holocene, is evident in the above-mentioned records and likely connected to the neoglaciation (Porter and Denton, 1967), while smaller-scale climatic oscillations appeared with a slightly diverging timing. Rapid hydrographic shifts in the Svalbard area around 7,500 years ago were implied in some studies, when a stronger influence of Arctic Water is assumed while the AW inflow weakened (Rasmussen et al., 2012; Skirbekk et al., 2010; Ślubowska et al., 2005). Indications for glacier re-advances during the late Holocene were found at different locations in Svalbard (e.g., Baeten et al., 2010; Furrer et al., 1991; Røthe et al., 2015; Svendsen and Mangerud, 1997). Simultaneously, AW advection increased in the Nordic Seas, in the western Barents Sea and west of Svalbard (e.g., Dylmer et al., 2013; Jernas et al., 2013; Wilson et al., 2011). During the last two millennia, short-term climate shifts were detected in the Svalbard area (e.g., Bonnet et al., 2010; D'Andrea et al., 2012; Jernas et al., 2013; Majewski et al., 2009; Spielhagen et al., 2011; Werner et al., 2011). Various authors found the largest Holocene glacier extents during the Little Ice Age (cold period between the 14th and 19th century; e.g., Lønne, 2014; Mangerud and Landvik, 2007; Salvigsen and Høgvard, 2006).

1.4 Open questions in palaeo-research regarding the Svalbard area

As depicted above, the evolution of AW advection is well studied at the western Svalbard margin – including its southern and northern extensions (Fig. 4). Study sites directly affected by the West Spitsbergen Current (WSC; the northernmost extension of the North Atlantic Current; see chapter 2.2) appear to act as valuable archives to record past variations of AW inflow, however, often recording only large scale shifts. So far, little is known about the eastward continuation of the WSC, i.e., the Svalbard Branch flowing along northern Spitsbergen and Nordaustlandet, during the past ~15,000 years. Nonetheless, this region is of considerable interest, as the remote extensions of the WSC can be expected to react more sensitive to changes in the strength of AW advection and, thus, to provide a more detailed picture on the variability of AW advection to the high north. This might be even more pronounced, when sensitive climate archives such as inner and outer fjord settings are considered.

As for the northern Svalbard margin, palaeoceanographic records only exist for one site in the Hinlopen Trough, for which the AW advection and the retreat of the ice sheet in the Hinlopen Trough (northern Svalbard; Fig. 4) since ~15,000 years have been reconstructed (Koç et al., 2002; Ślubowska-Woldengen et

al., 2007; Ślubowska et al., 2005) followed by a further high-resolution study on this site covering the last two millennia (Jernas et al., 2013). Apart from this study location, further information only has been provided by the means of benthic foraminiferal assemblage studies from the Murchisonfjord in northwestern Nordaustlandet (Kubischta et al., 2010, 2011). The influence of AW was tracked further to the east of Nordaustlandet, to west of Franz Josef Land and even to the Laptev Sea, north of Siberia (e.g., Duplessy et al., 2001, 2005; Klitgaard Kristensen et al., 2013; Lubinski et al., 2001; Taldenkova et al., 2010). Nevertheless, locations expected to be less affected by the extensions of the WSC, including remote fjords of central Svalbard, have not been studied yet.

Therefore, the following research questions arise:

a) Did the inflow of relatively warm AW during the deglaciation contribute to glacier retreat at the northern Svalbard margin? How did the deglaciation differ from the late Holocene in this area?
b) Are regional hydrographic variations reflected in a remote glacier-proximal fjord? Did AW also penetrate the fjords of Nordaustlandet?
c) How did the deglaciation evolve at the northwestern Svalbard margin before the onset of the Holocene? Did environmental conditions diverge depending on the proximity to the coast at this location?

To answer those questions, the following methods (a "multi-proxy" approach), as described in chapter 3, have been applied. The sample site at the mouth of the Woodfjord (sediment core *GeoB10817-4*; Fig. 4; discussed in chapter 5), a fjord at the northern Spitsbergen margin likely affected by the waters of the Svalbard Branch, is well suited to answer question a). Due to its proximal setting in relation to the ice sheet covering Svalbard during the deglaciation, it can be expected that glacier responses to AW inflow are well reflected.
Sediment samples from the Wahlenbergfjord, situated in western Nordaustlandet (sediment core *GeoB10831-3*; Fig. 4), were investigated for the first time (discussed in chapter 6). The location of this fjord is ideal to answer question b) because it is surrounded by tidewater glaciers, which are expected to have a major influence on sedimentation processes while the fjord has no direct contact to the Svalbard Branch.
Previous studies (Rasmussen et al., 2014b; Skirbekk et al., 2010) have shown that the Kongsfjord Trough (Fig. 4) is well suitable to record hydrographic variations during the Holocene, especially the response to the proximal Arctic Coastal Front. The sediment core *GeoB10810-1* examined in chapter 7, is covering 15,500 years, thus, adding an important time period (the deglaciation) to previous records from that area. Additionally, the core site is presumably located more distal to the coast. Accordingly, question c) can be answered with the help of this sediment core.

2 Regional setting

2.1 The Svalbard Archipelago – modern situation

The Svalbard archipelago is located in the Arctic between ~74–81 °N and ~10–35 °E on the northwestern Barents shelf (Fig. 5). The northern shelf of Svalbard extends as far as ~50–100 km, bordered by a steep continental slope (up to ~10°), whereas the western shelf is ~40–80 km wide (Dallmann, 1999). The archipelago is surrounded by the Arctic Ocean in the north, the Barents Sea in the south and in the east, and the Greenland Sea in the west (Fig. 3). Spitsbergen is the main island of the archipelago; Svalbard also comprises the second largest island Nordaustlandet and several smaller islands: e.g., Edgeøya, Kong Karls Land, Kvitøya, Prins Karls Forland, Hopen and Bjørnøya (øya = island [norw.]; Fig. 5). Spitsbergen and Nordaustlandet are separated by the ~170 km long Hinlopen Strait. Svalbard´s islands are carved by deep fjords, formed by glacier erosion and partly aligned along the north(-west)–south(-east) oriented main fault zones (Harland, 1998). The largest fjord is the Isfjord in central Spitsbergen with a length of ~70 km and water depths up to ~425 m (Fig. 5). Longyearbyen, the largest settlement of Svalbard (~2,000 inhabitants), is located at the Adventfjord, a small tributary fjord of the Isfjord. Large areas of Spitsbergen have an alpine character with peaks up to ~1,700 m in the eastern part (Newtontoppen in Ny Friesland is the highest mountain in Spitsbergen). Gjermundsen et al. (2015) observed that Spitsbergen´s topography withstood glacial erosion during the last glacial periods. The bedrock of Svalbard includes igneous and metamorphic rocks of Precambrian to Silurian age, especially shaped by the Caledonian orogeny (Dallmann, 1999). In Nordaustlandet, e.g., at the northern coast of the Wahlenbergfjord (Fig. 5), Pre-Devonian basement rocks (*Hecla Hoek*) crop out, while younger formations, as Permo-Carboniferous limestones, dolomites (e.g., *Gipshuken* formation) and sandstones (*Hårbardbreen* formation), are encountered at the southern coast of that fjord (Dallmann, 1999; Harland, 1998). Large outcrops of Devonian *Old Red* rocks (e.g., *Wood Bay* formation) are found in Svalbard, e.g., at the northwestern coast of the Woodfjord, northern Spitsbergen (Fig. 5). Additionally, sedimentary deposits from Late Paleozoic to Quaternary age occur in Svalbard, shaped by several orogenetic phases (Dallmann, 1999). In northwestern Spitsbergen and Ny Friesland (Fig. 5), Mid- to Late Miocene and Pleistocene volcanites appear (Harland, 1998). Nowadays, ~60% of Svalbard are covered by glaciers and ice caps, in total ~33,840 km^2 (Radić et al., 2014), while only small areas of the archipelago have a soil or vegetation cover. The ground is perennially frozen down to ~100–400 m (in Spitsbergen ~300 m on average). Only the upper ~1–1.5 m of the permafrost soil, the so-

Fig. 5: The Svalbard Archipelago with main island Spitsbergen and smaller islands. Location names mentioned in the text are given. Isf: Isfjord; Kgf: Kongsfjord; Lyb: Longyearbyen; Wbf: Wahlenbergfjord; Wdf: Woodfjord. Basemap created with ArcGIS online (http://www.arcgis.com).

called active layer, thaws during summer (Harland, 1998). At present, Svalbard´s climate is largely influenced by warm AW, which provides comparably mild temperatures in the area (see chapter 2.2). The annual highly variable climate is characterized by the influence of a low pressure area over Iceland and a high pressure area over Greenland and the Arctic Ocean (Isaksson et al., 2003). (South)westerly winds transport mild air masses from lower latitudes towards Svalbard while northern Svalbard is mainly affected by (north-)easterly winds (e.g., Isaksson et al., 2003; Lind and Ingvaldsen, 2012).

2.2 Oceanography in the Fram Strait – the interplay of Atlantic and Arctic waters

The Fram Strait (framed by the eastern Greenland shelf in the east as well as the Barents shelf and the Svalbard Archipelago in the west) is the only deep sea gateway connecting the Arctic Ocean with lower latitude waters. The main heat import into and freshwater export out of the Arctic Ocean take place through this strait. Heat is transported northward by the inflow of AW in the eastern Fram Strait, while freshwater (liquid and solid as sea ice) is transported southward by the East Greenland Current in the western Fram Strait (e.g., Saloranta and Haugan, 2001; Fig. 6). AW comprises the major source of water masses in the Arctic Ocean (Rudels, 2009). Those relatively warm water masses have a fundamental effect on climatic and hydrographic processes in the Arctic: AW transports heat to high northern latitudes warming Arctic waters as well as the atmosphere and contributes to the distribution of sea ice (Yashayaev et al., 2015). Due to its impact on sea ice melting, AW crucially affects the freshwater budget of high northern latitude seas and the southward outflow of freshwater. The amount of cold and brackish water in surface waters controls its density and, thus, deep water formation. Consequentially, it has an important impact on the variability of the AMOC, which, in turn, influences even global climate (Yashayaev et al., 2015).

AW is transported northwards along the Norwegian shelf via the Norwegian Atlantic Current (Fig. 6). South of Bjørnøya (the southernmost island of Svalbard; Fig. 5) at ~73 °N, the Norwegian Atlantic Current divides (Skagseth, 2008); the North Cape Current flows eastward into the southern Barents Sea while the main branch continues northwards as WSC following the western Barents shelf (Aagaard et al., 1987; Fig. 6). A part of the AW recirculates in the Bjørnøya Trough (Skagseth, 2008). The remainder continues eastward as surface layer staying in contact with the atmosphere and therefore cooling down while salinity decreases due to mixing with meltwater (Rudels, 2009).

At ~78 °N, the WSC is forced to sink to greater water depths by less dense, meltwater-influenced surface waters. Subsequently, the current is further divided into the westward recirculating Return Atlantic Current, the northward flowing Yermak Branch following the western margin of the Yermak Plateau and the eastward flowing Svalbard Branch (Manley, 1995; Fig. 6). The Yermak Branch merges with the Svalbard Branch east of the Yermak Plateau (Pérez-Hernández et al., 2017). The Svalbard Branch is regarded as the most important current for heat transport into the Arctic. Because the Svalbard Branch is insulated by a fresh and cold surface layer the current loses less heat to the atmosphere as it is the case in the Barents Sea (Manley, 1995; Saloranta and Haugan, 2001). Therefore, the current is warming the deep basins in the Arctic Ocean circulating along the shelf edge (Koenig et al., 2017; Pérez-Hernández et al., 2017).

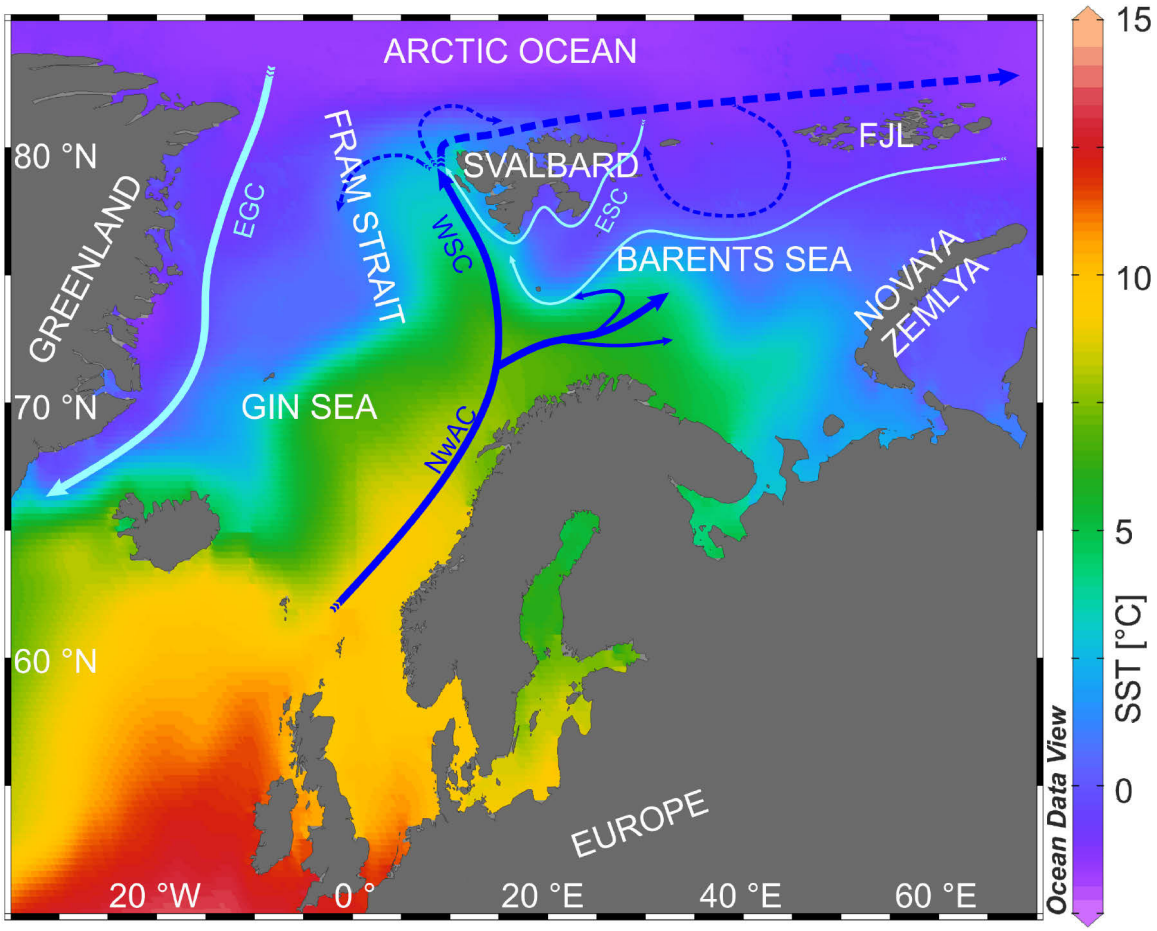

Fig. 6: Main ocean currents and sea surface temperatures in the North Atlantic (annual mean; 1955–2012; World Ocean Atlas; Locarnini et al., 2013). Dark blue arrows symbolise relatively warm currents (dashed: sub-surface currents), light blue arrows symbolise cold currents. NwAC: Norwegian Atlantic Current; WSC: West Spitsbergen Current; ESC: East Spitsbergen Current; EGC: East Greenland Current; FJL: Franz Josef Land; GIN Sea: Greenland–Iceland–Norwegian Sea. Map created with Ocean Data View (Schlitzer, 2015).

Heat advection to high latitudes by AW is more relevant during winter (due to greater temperature gradients than in summer) when it contributes considerably to sea ice melting and to the warming of air temperatures. During summer, the retreat of sea ice is stronger influenced by, e.g., solar radiation and wind while the ocean–atmosphere heat exchange is less important for sea ice melting (Schauer et al., 2004; Walczowski and Piechura, 2011). Additionally, the volume transport of the WSC is significantly larger during winter (~20 Sv = 20 * 10^6 m^3 s^{-1}) than during summer (~5 Sv; Fahrbach et al., 2001), probably induced by stronger winds during winter (Schauer et al., 2004 and references therein).

At the western shelf break of Svalbard, the Arctic Coastal Front separates the WSC from the Arctic Water-derived Coastal Current (Saloranta and Svendsen, 2001). This current is originated in the northern Barents Sea where the East Spitsbergen Current circulates around Edgeøya after entering the Barents Sea east of Nordaustlandet (Skogseth et al., 2005; Fig. 6). The East Spitsbergen Current circuits around the southern tip of Spitsbergen continuing as Coastal Current on the western Spitsbergen shelf (Loeng, 1991). The interplay between those Arctic waters and AW influences the hydrography of Spitsbergen´s fjords. AW intrusion onto the shelf and into the fjords of western Spitsbergen is controlled by various processes. The main mechanism seems to be barotropic instability that allows AW to cross the temperature–salinity front which separates AW from shelf waters (Cottier et al., 2005; Saloranta and Svendsen, 2001; Teigen et al., 2010). Furthermore,

wind-induced upwelling contributes considerably to cross-front transport of AW, especially during winter (Cottier et al., 2005, 2007). Just recently, Nilsen et al. (2016) discovered a slower branch of AW circulating topographically-steered into the troughs of western Spitsbergen (the Spitsbergen Trough Current). During winter this current contributes largely to heat advection to the shelf and fjords of western Spitsbergen. On its northward way the Spitsbergen Trough Current loses heat to the surrounding waters and the atmosphere and is, thus, considered as one of the densest waters when reaching the northern Svalbard shelf (Nilsen et al., 2016). Hydrographic processes inside the fjords are described in the following chapter.

2.3 Fjords – "mini-oceans" and climate archives

The origin of the word *fjord* can be tracked back to the Old Norse term *fjörðr* and appears slightly modified in different regions (e.g., *fjärd* [swe.], *fjordur* [icel.], *firth* [scot.], *Förde* [germ.]; see Howe et al., 2010). Fjords occur in both hemispheres above latitudes of ~42° commonly described as fjord belt (Syvitski et al., 1987). Those are deep troughs, once filled and eroded by glaciers or outlet tongues of ice sheets. Fjords have an estuarine character and as they open into the sea, the steep-sided basins were inundated by sea water after the retreat of the ice (Howe et al., 2010; Syvitski et al., 1987). The direction of fjords is often tied to fault zones (e.g., Harland, 1998; Syvitski et al., 1987). As a result of the glacial processes that formed the fjord, a main feature of most fjords (not all) is a sill (e.g., a moraine) at the mouth, or sometimes additonal sills separating multiple basins (Inall and Gillibrand, 2010; Syvitski et al., 1987). However, sills can also be predefined by the underlying bedrock. Because fjords are semi-closed marine basins, they were often seen as mini-oceans where complex mechanisms can comparably easy be observed and modelled (Forwick et al., 2010; Syvitski et al., 1987). Dependent on the hosting climate zone and the existence of a resident glacier, fjords are classified as polar, subpolar and temperate or glaciated and non-glaciated, respectively (Howe et al., 2010). In this chapter, the focus is on subpolar, glaciated fjords in the northern hemisphere.

Fjord hydrodynamics can – simplified – be described as estuarine, meltwater-influenced, brackish outflow at the surface overlying inflowing saline intermediate waters. Oceanographic processes in fjords are affected by wind forcing and heat exchange at the surface, tidal dynamics, inner basin convection and deep water exchange. The topography significantly influences the circulation in the fjord. Due to a shallow and mostly also narrow entrance to silled fjords, current speeds may be enhanced (Inall and Gillibrand, 2010). Furthermore, a sill restricts the exchange of the seasonally stratified water masses, which can lead to a drastic decrease of the oxygen concentration in bottom waters in fjords and, at the extreme, to anoxia. However, owing to the acceleration at the sill the barotropic flow usually pulls denser water masses across the sill enabling deep water renewal (Inall and Gillibrand, 2010).

Due to great temperature and salinity gradients in the water column of fjords, a stratification develops in a seasonal cycle as illustrated in Fig. 7: Arctic fjords are stratified during summer; advected *Intermediate Water* (e.g., AW) is framed by warmed, meltwater-influenced brackish *Surface Water* and cold, saline *Old winter water*. During autumn, when atmospheric temperatures decrease, heat from the fjord´s surface is released to the atmosphere triggering thermal convection when cooled water masses sink and form the *Local Water*. Additionally, stronger winds cause a mixing of the water column. As *Old winter water* is much more saline than the *Surface Water*, the former is not affected by the mixing during autumn. With the onset of winter, surface temperatures are at freezing point and sea ice forms. During the formation of sea ice, brine is released

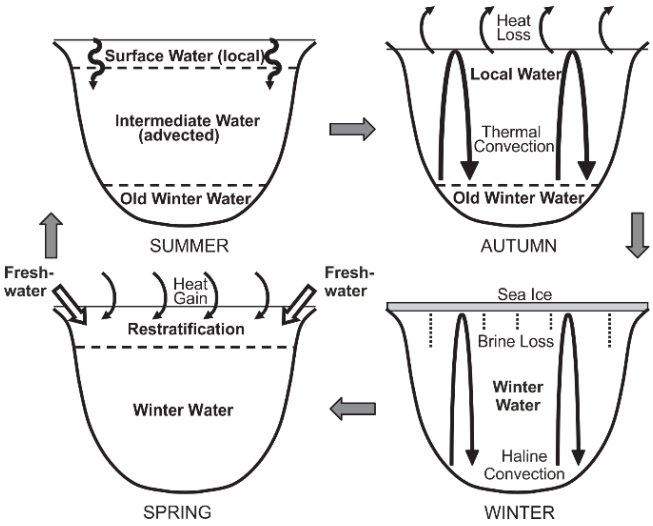

Fig. 7: Seasonal cycle of fjord stratification in a typical Svalbard fjord (modified after Cottier et al., 2010).

increasing the salinity and, thus, the density at the surface. Accordingly, haline convection is induced producing cold and highly saline *winter water*. During spring, melting of sea ice and tributary (land- and sea-terminating) glaciers discharge high amounts of freshwater. Caused by this freshening and successive warming of the surface, the fjord begins to re-stratify while the cold and saline *winter water* remains at the bottom. During summer, the strong stratification of the water column redevelops.

Apart from those seasonal mixing processes, various other mechanisms affect the circulation in fjords. Coriolis forces due to Earth´s rotation have a considerable impact on circulation of stratified Arctic fjords. The importance of these forces on flow dynamics is defined by the so-called Rossby radius (ratio of current velocity, influenced by stratification, to the Coriolis parameter; e.g., Cottier et al., 2010). Circulation in Arctic fjords is significantly influenced by Earth rotation as Coriolis forces increase with latitude leading to a smaller Rossby radius than the width of usually comparably broad Arctic fjords (e.g., Cottier et al., 2010; Inall and Gillibrand, 2010; Svendsen et al., 2002). Consequentially, in the Arctic the outflow of meltwater-derived surface waters as well as the inflow of advected intermediate waters are deflected to the right of the out- and inflow direction, respectively (e.g., Cottier et al., 2010). In east–west orientated fjords, surface waters are accordingly deflected to the north, while intermediate waters are deflected to the south. Furthermore, this current deflection has a considerable effect on sedimentation, because the major part of fjord sediments, e.g., in Svalbard´s fjords, is derived from suspended material in meltwater-plumes and iceberg-rafted material (Howe et al., 2003; Pawłowska et al., 2017). Nonetheless, deposits at the northern coasts of respective fjords differ from its southern counterparts as the former are mainly influenced by surface water transported sediments, while the latter are primarily affected by inflowing waters, which is also reflected in diverging (fossil) benthic foraminiferal faunas (Pawłowska et al., 2017).

Wind stress also has an important influence on fjord circulation as it induces Ekman transport (e.g., Cottier et al., 2010). Also triggered by the Coriolis force, strong wind forcing deflects surface waters to the right of the main wind direction. Subsequently, surface waters are down-welled to the right and underlying water masses are upwelled to the left of the wind direction. At the western and northern shelf of Svalbard, this phenomenon pushes intermediate AW onto the shelves because west of Svalbard northerlies dominate (during winter) while north of Svalbard winds blow primarily from the east (Cottier et al., 2007; Lind and Ingvaldsen, 2012). Apart from the prevalent wind directions, Arctic fjords are significantly affected by katabatic winds. Wind forcing of those down-fjord blowing winds may be so intense that respective strong Ekman pumping enables intermediate waters to reach the surface (Cottier et al., 2010). Sea ice also affects fjord circulation – apart from its influence on convection by brine release – as it insulates fjord waters from the atmosphere preventing wind-induced mixing and heat exchange.

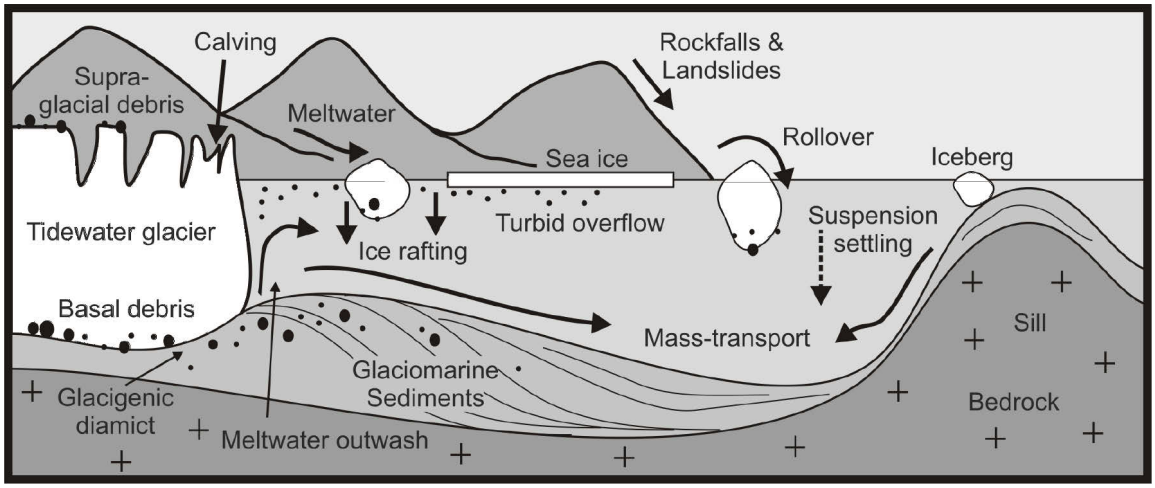

Fig. 8: Physical processes in glaciated fjords (modified after Howe et al., 2010).

While the existence of every fjord is inextricably linked with the occupation of a glacier in the past, Arctic fjords usually host a glacier until today, mostly terminating in the fjord (so-called tidewater glaciers; Fig. 8). Past glacier processes have not only carved the presently inundated valleys, but also have left traces and marks on the sea floor of the fjord during glacier advances and retreats, including terminal and recessional moraines, drumlins, eskers, glacial lineations and iceberg plough marks, as observed in bathymetric data, e.g., from several fjords around Svalbard (Baeten et al., 2010; Flink et al., 2017; Fransner et al., 2017; MacLachlan et al., 2010; Ottesen and Dowdeswell, 2006; Streuff et al., 2015). During advances, grounded tidewater glaciers push sediments forward at the terminating front. After repeated retreats, so-called recessional moraines were left behind. If icebergs or fast flowing ice sheets touch the sea floor, plough marks and glacier lineations were carved, respectively (e.g., Ottesen and Dowdeswell, 2006; Streuff et al., 2015). Drumlins are drop-shaped subglacial elevations consisting of eroded bedrock or accumulated sediments (e.g., Hogan et al., 2010b; MacLachlan et al., 2010). Eskers were formed when meltwater conduits in glaciers were filled with sediments (Ottesen et al., 2008).

Furthermore, sedimentation is presently mainly controlled by glacier processes in Arctic fjords. Where summer temperatures are warm enough, melting results in the transport of large amounts of fine-grained sediment into the (subpolar) fjord (Dowdeswell et al., 1998). The moving glacier incorporates sediments, eroded at the base during its flow (basal debris), aerially transported and deposited on its surface as well as dropped from its steep lateral slopes (e.g., by rockfalls; supra-glacial debris; Fig. 8). While fine-grained material is mainly flushed into the fjord basin by meltwater plumes, coarser material is rafted by icebergs after calving and deposited when the iceberg melts or rolls over dumping sediments deposited on its surface (Fig. 8). Sea ice contributes, to a smaller part, to sedimentation as it also assimilates sediment particles when freezing at beaches or in shallow waters but also sediments fallen on its surface by similar processes as described for glaciers (Dowdeswell et al., 1998). This material will be released when the sea ice melts (Fig. 8). Thus, sedimentation in Arctic fjords occurs predominantly during spring/summer when sea ice and glaciers melt and sea ice no longer prevents icebergs from drifting (Fig. 9).

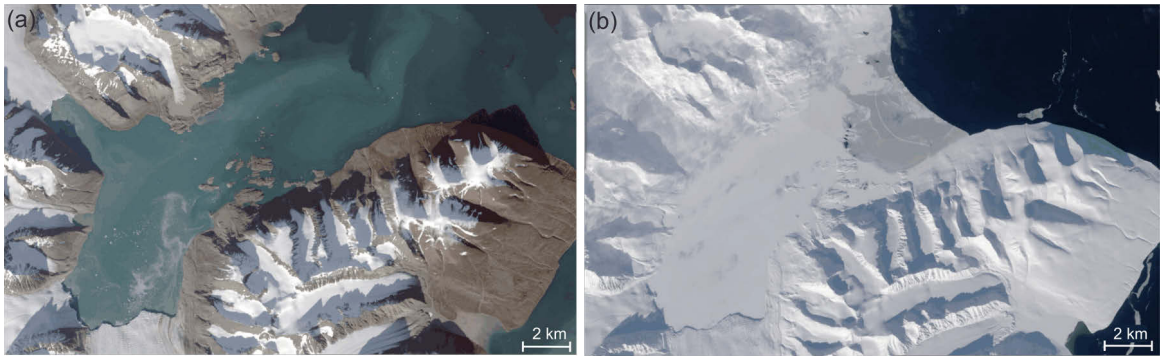

Fig. 9: Satellite images of the Liefdefjord (northern Spitsbergen) during (a) summer and (b) winter. Note sediment plumes and icebergs in (a) showing sediment-laden meltwater discharge and iceberg production during summer while neither suspended sediments nor icebergs are visible during winter (b) when the fjord is partly covered by sea ice. USGS Landsat images: © Norwegian Polar Institute (http://toposvalbard.npolar.no/).

Apart from widespread glaciomarine muds with variable percentages of ice-rafted material, various sedimentary facies were distinguished in the literature, which can be encountered in Arctic fjords. At the base of glaciers, a massive layer with high amounts of coarse debris is deposited (so-called basal till; Forwick and Vorren, 2009). In several Arctic fjords, laminated fine-grained layers were found partly interrupted by coarse-grained diamictions (Cowan et al., 1997; Cowan and Powell, 1990; Dowdeswell et al., 2000; Flink et al., 2017; Ó Cofaigh and Dowdeswell, 2001). Those laminated sediments were interpreted as reflecting annual cycles of high meltwater discharges close to the glacier front (e.g., Cowan et al., 1997; Dowdeswell et al., 2000; Mackiewicz et al., 1984; Ó Cofaigh and Dowdeswell, 2001).

Sediment accumulation rates in fjords can be extremely high, especially at the glacier terminus (up to one metre per year, in Alaska even 13 metres per year; Howe et al., 2010, and references therein). Accordingly, sedimentary records from fjords offer a high temporal resolution when reconstructing the development of the local-to-regional palaeoenvironment and palaeoceanography with the help of sediment cores (see following chapter) making fjord sediments very valuable climate archives especially for the higher latitudes.

3 Methodology and Material

3.1 Sediment cores and the use of proxies

Sediment cores are regarded as climate archives mostly covering greater time spans than the instrumental climate record. Usually, marine sediments are deposited continuously (exceptions will be addressed later; see chapter 3.4). Accordingly, it is assumed that increasing depth in a sediment core corresponds to increasing age of the sediment. Sediment cores are retrieved by ship-based equipment, e.g., boxcorer, multicorer, gravity corer, piston corer or kastenlot. After recovering, sediment cores (e.g., gravity cores, piston cores) are commonly split lengthwise into two halves: Material may be removed (e.g., with syringes; see chapter 3.2) for various measurements and analyses from the *working half*, whereas only non-destructive methods (e.g., computer tomography; see chapter 3.6.2) were performed at the *archive half*.

As no observations are available exceeding the historical climate record (reaching back no longer than the 19th century), environmental, hydrographical and climatic conditions in geological times have to be estimated by approximations and assumptions. It is assumed that physical processes and mechanisms (e.g., sediment dynamics, ocean currents and atmospheric oscillations), chemical processes (e.g., isotope fractionation) as well as responses from biology (e.g., ecological preferences of certain taxa) in the past were analogue to the present. Accordingly, a wide range of so-called "proxies" can be applied, including sediment properties (e.g., grain sizes; see chapter 3.6 and 3.7), geochemical tracers (e.g., stable isotopes in carbonate shells; biogeochemical molecules in the sediments = "biomarkers"; see chapters 3.8 and 3.9) or faunal assemblages (e.g. of benthic foraminifera; see chapter 3.5) on sedimentary records to draw conclusions about past developments.

3.2 Sample Material

The case studies presented in this thesis are based on three gravity cores, recovered during research cruise MSM02/03 with RV *Maria S. Merian* in August 2006 (Lherminier et al., 2009): *GeoB10817-4* (manuscript I; chapter 5; Bartels et al., 2017) from the mouth of the Woodfjord (northern Spitsbergen; 79.80° N, 14.20° E; water depth: 171 m; location shown in Fig. 4), *GeoB10831-3* (manuscript II; chapter 6) from the Wahlenbergfjord (central Nordaustlandet; 79.71 °N, 20.43 °E; water depth: 217 m; Fig. 4) and *GeoB10810-1* (manuscript III; chapter 7) from the Kongsfjord Trough (northwestern Spitsbergen; 79.05 °N, 10.90 °E; water depth: 348 m; Fig. 4).

Sediment core *GeoB10817-4* has a recovery of 275 cm spanning the past ~15,500 years, although a gap of 6000 years (~7,800–1,800 years ago) is evident (see chapter 3.4 for details). The sediment of this core was sampled with syringes every 5 cm for microfossil, grain size and geochemical analyses and the core was scanned with a computer tomograph (CT). Biomarker analyses were carried out in selected depths dependent on significant shifts in, e.g., faunal data.

Sediment core *GeoB10831-3* has a recovery of 575 cm spanning the past ~11,300 years. The sediment of this core was sampled with syringes every 20 cm for microfossil analyses, and every 5 cm for geochemical analyses. Biomarker analyses were carried out in selected depths also according to significant shifts in other data. The core has also been scanned with a CT.

Sediment core *GeoB10810-1* has a recovery of 752 cm and covers the time span ~15,300–1,300 years ago. The sediment of this core was sampled with syringes every 20 cm for microfossil analyses, and every 5 cm

for geochemical analyses (if enough material was available). Biomarker analyses were carried out in selected depths according to significant shifts in the record.

All three sediment cores consist of a fine-grained matrix (ranging from sandy, clayey silt to silty clay) with the occasional occurrence of coarser clasts (ranging from sand to pebbles). Traces of bioturbation are detectable, especially in the upper parts of the cores.

3.3 Sample processing of bulk sediment samples

All bulk sediment samples (volume of syringes: ~10 cm^3) used for microfossil analyses, radiocarbon dating and analyses of ice-rafted debris (IRD), were freeze-dried and washed through 63 µm meshes, dried at 40–60 °C, weighted and dry-sieved through sieves with mesh sizes of 100, 150 and 500 µm (*GeoB10817-4*), 150 and 500 µm (*GeoB10831-3*) as well as 150 and 250 µm (*GeoB10810-1*), respectively. Each size class was weighted. Subsequently, all foraminifera were selected for faunal analyses (complete benthic and occasionally appearing planktic fauna) from the size fraction >100 µm (>150 µm) in sediment core *GeoB10817-4* (*GeoB10831-3* and *GeoB10810-1*). For radiocarbon dating (mixed or monospecific calcareous benthic foraminifera, bivalves) and for stable isotope measurements (benthic foraminifera *Cibicides lobatulus* and *Nonionellina labradorica*; planktic foraminifera *Neogloboquadrina pachyderma* sinistral) the size fraction 150–500 µm was used. Counting of IRD was carried out at the size classes >250 µm (*GeoB10810-1*) and >500 µm (*GeoB10817-4* and *GeoB10831-3*). Samples containing to much specimens (foraminifera or IRD) were split with a microsplitter to receive appropriate numbers (~300 specimens; see chapter 3.5.2).

3.4 Stratigraphy

3.4.1 Radiocarbon-based chronology and its limitations

For the interpretation of sedimentary records, it is necessary to assess the age of the sediment, hence, to create a so-called age–depth model. This model is based on age determinations from several depths. If sediment is not older than ~40,000 years, radiocarbon measurements of organic matter or carbonate (e.g., calcareous shells of foraminifera or bivalves) can be carried out. Besides the two naturally occurring stable carbon isotopes ^{12}C (~98.9 %) and ^{13}C (~1.1 %), a third radioisotope ^{14}C is produced in the upper atmosphere with a half-life of ~5,570 years (e.g., Mangerud, 1972). Living organisms take up traces of ^{14}C from the atmosphere during their lifetimes. After death, the radiocarbon isotopes begin to decay and according to the $^{14}C/^{12}C$ ratio, or in some cases the $^{14}C/^{13}C$ ratio (e.g., determined by accelerated mass spectrometry; AMS), the time of death and, consequently, the age of the sediment can be estimated. Those "radiocarbon ages" can be transformed into calendar ages by calibration. Calibrated calendar ages are given as years before 1950 CE (years before present = a BP) because atomic testing during the 1950s disturbed the natural ^{14}C signal. As the amount of naturally produced atmospheric radiocarbon isotopes changed over time, terrestrial (tree rings, plant macrofossils from lake sediments and speleothems) and marine (corals and foraminifera) ^{14}C data were combined to create calibration curves (e.g., *IntCal13* and *Marine13*; Reimer et al., 2013). Additionally, a so-called "reservoir effect" has to be taken into account in marine environments. Due to the thermohaline circulation in the oceans, water masses loose contact to the atmosphere. As subsurface and benthic calcareous organisms precipitate calcite shells in equilibrium with the surrounding water, the ^{14}C in their shells reflects these "older" water masses. Usually, a constant reservoir age of ~400 years is assumed correcting this offset

(e.g., Reimer et al., 2013), but depending on the area, regional corrections (ΔR) have to be added (Stuiver and Braziunas, 1993).

At high latitudes the reservoir age is believed to be larger than in (sub-)tropical areas (e.g., Eiríksson et al., 2004; Hanslik et al., 2010; Reimer et al., 2013; Sarnthein et al., 2007). Various studies addressed the problem of an additional reservoir age change over time (Austin et al., 1995, 2011; Bard et al., 1994; Björck et al., 2003; Bondevik et al., 2006; Eiríksson et al., 2004; Hanslik et al., 2010; Olsen et al., 2014; Sarnthein et al., 2007; Waelbroeck et al., 2001). During the YD, different reservoir ages were assumed for the North Atlantic ranging from ~700 years (Austin et al., 1995; Bard et al., 1994) to more than 1000 years (Austin et al., 2011; Björck et al., 2003; Waelbroeck et al., 2001). Reservoir corrections of ~1200–1900 years (Waelbroeck et al., 2001) or even more than 2000 years were suggested during Heinrich event 1 (~17,900–14,700 years ago; Sarnthein et al., 2007). Those offsets are likely induced by a reduced AMOC due to the enhanced freshwater input during the deglaciation and the shifted position of deep water formation as well as by an expanded sea ice coverage insulating the North Atlantic from the atmosphere (Austin et al., 1995, 2011; Sarnthein et al., 2007; Waelbroeck et al., 2001). Owing to these uncertainties, in some studies further so-called "tie points" were applied in their age–depth models. Volcanic ashes are a helpful candidate to localise certain time periods, if the eruption date is confidently known, because the mineralogy of those ashes is unique (e.g., van der Bilt et al., 2017; Pearce et al., 2017; Thornalley et al., 2011). Especially the timing of the YD can be defined by findings of the *Vedde Ash* (Austin et al., 1995; Mangerud et al., 1984), tephra particles from a volcanic eruption on Iceland at 12,171 ±57 years BP (in Greenland ice core NGRIP; Svensson et al., 2008), which were found in lake (e.g., Bakke et al., 2009; Lane et al., 2013) as well as marine sediments (e.g., Bauch et al., 2001; Telesiński et al., 2014). But apart from one finding in only one sediment core retrieved in the Fram Strait at 78 °N (Zamelczyk et al., 2012) the distribution of those glass shards is usually limited to lower latitudes and, thus, cannot be applied in the Arctic Ocean or the Svalbard area, respectively.

Further factors may complicate the creation of an age–depth model: In coastal-proximal environments but also at continental slopes, a continuous sedimentation may be interrupted or disturbed. Therefore, the sediment core should be carefully optically examined, e.g., by radiometry or computer tomography, to exclude the existence of a hiatus or a disturbed interval before constructing the age–depth model. A rapid drop of the sedimentation rate can also provide a hint to disconformities/sediment disturbances, which may, e.g., be the result of erosion, slope failures, turbidites, debris flows, heavy bioturbation or iceberg ploughing (e.g., Baeten et al., 2010; Bornhold et al., 2005; Forwick et al., 2010; Howe et al., 2010; Mulder and Alexander, 2001; Ray et al., 2006; Stein, 2008).

3.4.2 Methodological remarks for age–depth modelling

AMS radiocarbon measurements were carried out using carbonate samples (bivalves, mixed or monospecific benthic foraminifera) at twelve, seven and eight depth levels from cores *GeoB10817-4*, *GeoB10831-3* and *GeoB10810-1*, respectively. The uppermost and the lowermost samples in sediment cores *GeoB10817-4* and *GeoB10831-3*, respectively, were measured at *CologneAMS*, University of Cologne (http://www.cologneams.uni-koeln.de), by Janet Rethemeyer. Apart from those samples, all AMS measurements were carried out at the *ETH Laboratory of Ion Beam Physics Zürich* (http://www.ams.ethz.ch/), by Lukas Wacker. This laboratory is able to measure very tiny carbonate samples

(<100 µg according to website; >500 µg with acceptable error, L. Wacker, pers. comm.). Although only small amounts of carbonate were available in our samples, double (or even triple) measurements were possible in most cases.

A constant regional reservoir age correction of 98 ±37 years (averaged ΔR values from six locations in the Svalbard area derived from the Marine Reservoir Correction Database: calib.qub.ac.uk/marine/; Mangerud, 1972; Mangerud and Gulliksen, 1975; Olsson, 1980) was used in all manuscripts. This constant reservoir age correction was applied because no sufficient data for older periods, especially for the YD and the Heinrich Stadial 1, are available until now for the Svalbard area, as already pointed out by Ślubowska-Woldengen et al. (2007), especially for shelves and fjords.

To design an age–depth model, sedimentation rates have to be calculated and interpolated between depths with measured radiocarbon ages. In recent studies, various methods were applied ranging from the "classical" linear interpolation between median calibrated ages to very sophisticated models based on Bayesian statistical approaches (e.g., Balascio et al., 2016; Jackson et al., 2017; Mulitza et al., 2017). Further details about these methods are given below.

In manuscript I (chapter 5; Bartels et al., 2017), sedimentation rates were interpolated linearly between radiocarbon-measured depth levels (using averaged values in case of double measurements). Radiocarbon ages were calibrated into calendar years applying the calibration software CALIB 7.1 (calib.qub.ac.uk/calib/). The interval between 31 and 54 cm was excluded from the age–depth model because sediment disturbances are visible on the CT images in this interval. One radiocarbon sample (from 256.5–257.5 cm depth), which yielded a younger age as the dated sample above (236.5–237.5 cm), was discarded because it is regarded as outlier (age reversal). As the amount of carbonate that was measured from the former depth was four times smaller than the sample at the latter depth, the error range is expected to be much higher for the smaller sample. It is also possible that the sample from 256.5–257.5 cm was affected by bioturbation.

The age–depth models of the sediment cores *GeoB10831-3* and *GeoB10810-1* (manuscript II and III; chapter 6 and 7, respectively) were designed with the Bayesian software *BACON* (Blaauw and Christen, 2011) based on *R* (R Development Core Team, 2011). This software allows a higher variability of sediment accumulation rates because the core is divided into subsections (default = 5 cm) for which individual accumulation rates (in years per centimetres) are calculated applying millions of *Markov Chain Monte Carlo* iterations. Several prior settings (e.g., determining to what degree accumulation rates diverge from each other, depths of a possible hiatus or settings for error estimations) can be adapted to the particular sediment core that shall be examined. Several test runs should be performed to verify which settings are the most appropriate for the specific sediment core. For the sediment cores *GeoB10831-3* and *GeoB10810-1*, default settings were used apart from the settings for error estimation. *BACON* applies a *student's-t* distribution for error estimation, which is set to t.a = 3 and t.b = 4 (allowing long tails). Those were set to t.a = 9 and t.b = 10 to allow more rapid changes of accumulation rates and, thus, a less smoothed age–depth model including all calibrated radiocarbon ages.

Probably due to the 23 centimetres of disturbed sediment, no reasonable results were achieved when creating an age–depth model with *BACON* for sediment core *GeoB10817-4*.

3.5 Microfossil analyses

3.5.1 Benthic foraminifera – an introduction

Foraminifera are single-celled, mostly shelled organisms belonging to the Kingdom of Protista. With approximately 10,000 species, foraminifera have the largest diversity amongst all marine shell-bearing microorganisms (Sen Gupta, 2003). While ~40–50 planktic species can be separated, benthic foraminifera are enormously more diverse. The latter are the oldest group of deep-sea organisms existing since the Pre-Cambrian (since more than ~635 million years; Holbourn et al., 2013), nowadays dwelling in all marine habitats – from deep oceans and continental slopes to fjords, shallow shelves and even in intertidal salt marshes; from the equator to polar regions (Fontanier et al., 2008; Hunt and Corliss, 1993; Jennings et al., 2004; Korsun and Hald, 2000; Milker and Schmiedl, 2012; Müller-Navarra et al., 2016; Wollenburg and Mackensen, 1998). Most benthic species form shells (tests) apart from the small, scarcely studied organic-walled group of allogromiids (e.g., Korsun and Hald, 1998, 2000; Loeblich and Tappan, 1988). Depending on the test material, (non-allogromiid) benthic foraminifera are divided in agglutinants (assembling sediment particles to build their shells) and calcareous species (precipitating carbonate shells), which are further subdivided into hyaline (forming calcite or aragonite walls with ordered carbonate crystals) and porcelaneous species (forming high magnesium calcite walls with non-ordered calcite crystals; Hansen, 2003). Benthic foraminifera live on (epibenthic) or in the sediment (endobenthic). Epibenthic species can live at the sediment–bottom water interface or attached to pebbles, bivalves or other elevated (organic) material on the sea floor. While most endobenthic species live in the upper 1–2 cm below the sediment surface, some can be encountered up to 10 cm deep in the sediment (Hunt and Corliss, 1993; Łącka and Zajączkowski, 2016; Linke and Lutze, 1993). Endosymbionts in epibenthic foraminifera are reported from shallow water inhabiting recent as well as fossil species (e.g., Lee, 2006; Schmidt et al., 2015). But even (temporary) endobenthic species, e.g., *Nonionellina labradorica* or *Elphidium* spp., are able to host symbiotic or, at least, sequestered chloroplasts although some live in the aphotic zone (Bernhard and Bowser, 1999; Cedhagen, 1991). Depending on environmental conditions, endobenthic foraminifera migrate up and down in the sediment (Jorissen et al., 1995; Linke and Lutze, 1993). Jorissen et al. (1995) demonstrated that the so-called average living depth depends, on the one hand, on the food supply and, on the other hand, on the oxygen availability. Numerous studies from Arctic and sub-Arctic locations illustrate that the occurrence of several species is further controlled by sediment properties (e.g., grain sizes), water mass properties (temperature and salinity) or current velocities (Hald and Korsun, 1997; Hunt and Corliss, 1993; Jennings et al., 2004; Korsun and Hald, 1998, 2000; Polyak et al., 2002; Rytter et al., 2002; Steinsund, 1994).

3.5.2 The use of benthic foraminifera as palaeo-ecological proxies and its limitations

The knowledge about the species-dependent ecological preferences of modern benthic foraminifera allows us to reconstruct past hydrographic, climatic and environmental conditions. Thus, the determination and interpretation of faunal assemblages in fossil records is a powerful tool ("proxy") for palaeoceanographic reconstructions. Although foraminifera have already been classified and described in detail in the early nineteenth century, e.g., by d´Orbigny, researchers used them as proxies for palaeo-ecology not before the beginning of the twentieth century (e.g., Cushman; see historical overviews in Boersma, 1998; Jorissen et al., 2007; Murray, 2006). Since then, foraminiferal assemblages were widely used in palaeoceanography for

different time scales in all marine environments, including the Arctic. During recent decades, the past development of climate and hydrographical variability as well as glacier activity and sea ice distribution in the Arctic was estimated by numerous authors based on foraminiferal assemblages (Chauhan et al., 2014; Duplessy et al., 2001; Ezat et al., 2014; Hald et al., 2004; Jernas et al., 2013; Klitgaard Kristensen et al., 2013; Koç et al., 1993, 2002; Lubinski et al., 2001; Majewski et al., 2009; Rasmussen et al., 2012; Rasmussen and Thomsen, 2004; Ślubowska-Woldengen et al., 2007; Ślubowska et al., 2005; Wollenburg et al., 2001)

Nevertheless, this method is restricted by a number of limitations. Jorissen et al. (2007) pointed out that the appearance of benthic foraminifera is predominantly controlled by the organic matter flux and its quality as well as by bottom water ventilation, while current velocities have only a minor influence and physical properties of bottom water are negligible in most study areas. Also in the Arctic Ocean, benthic foraminiferal assemblages rather compete for available food resources than responding to hydrodynamic energy, water mass or sediment properties (Wollenburg and Mackensen, 1998). However, the focus of both studies lays on deep-sea settings.

When interpreting faunal distributions in high resolution, the average living depths of endobenthic foraminifera have to be kept in mind (Alve and Bernhard, 1995; Jorissen et al., 1995; Linke and Lutze, 1993). But, if relatively coarse sampling intervals of 5 cm or more are applied (5 and 20 cm in the studies of this thesis, respectively), the living depths of endobenthic species may be less significant (Zajączkowski et al., 2010a). Just recently, Loubere and Rayray (2016) addressed the problem that the uppermost sediment is homogenised by mixing. Additionally, the first centimetres below the sediment–water interface may be affected by dissolution and mechanical shell destruction. Consequently, fossil assemblages would be dominated by endobenthic species and taxa with more resistant shell material, respectively. Especially in fjord environments, high amounts of organic carbon may lead to anoxia at shallow depths with higher shell preservation below the anoxic boundary than above (Loubere and Rayray, 2016).

Hence, a possible limitation for the use of benthic foraminifera as a proxy is the dissolution of calcareous species: Calcium carbonate will dissolve at low temperatures, high salinities, high pCO_2 values or high hydrostatic pressure. In the literature various causes for low pH values in Arctic environments were discussed: Hald and Steinsund (1996) assumed that dense, very cold and oxygen-rich waters at oceanic fronts lead to an enhanced decay of organic matter at the sediment surface releasing high amounts of CO_2. Brine formation may also trigger carbonate dissolution as it transports cold and saline water to the bottom containing high amounts of CO_2 as well as oxygen, which again contributes to remineralization (Seidenkrantz et al., 2007). High sea surface productivity likewise enhances the oxidation of organic matter at the sea floor leading to decreasing pH values of the bottom water (de Vernal et al., 1992). Accordingly, some studies report about a dominance of agglutinants in samples of high carbonate dissolution (e.g., Hald and Steinsund, 1996; Jennings and Helgadottir, 1994). Various authors propose to quantify the dissolution of foraminifera by calculating a "dissolution index" (percentage of fragments vs. intact specimens; Berger et al., 1982; Pfuhl and Shackleton, 2004; Zamelczyk et al., 2013). However, apart from dissolution, different mechanisms may be involved in the destruction of foraminiferal test, e.g., during sediment accumulation as well as during sample processing (de Vernal et al., 1992).

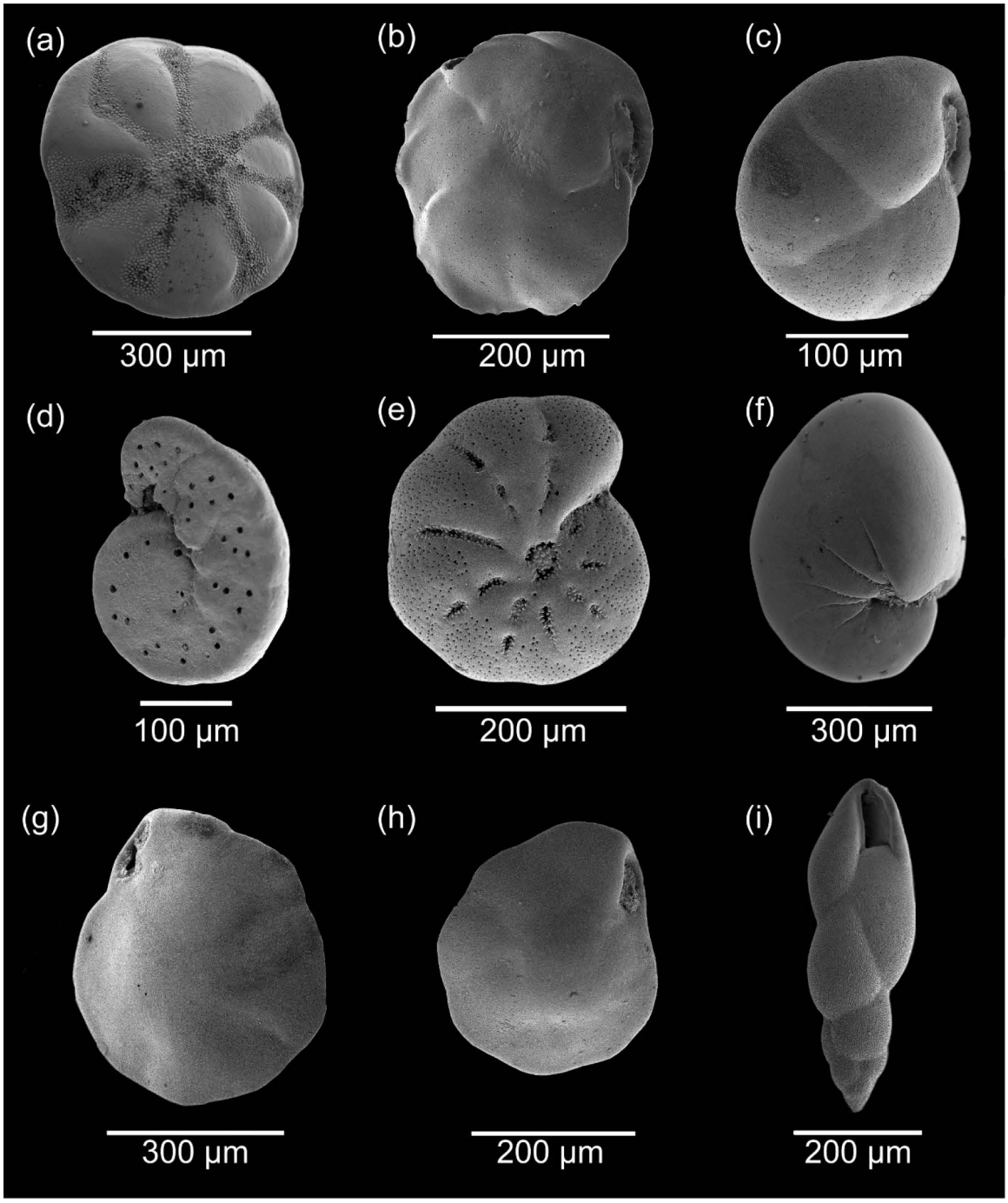

Fig. 10: Abundant benthic foraminifera from the Svalbard area (sediment core *GeoB10817-4*). (a) *Buccella frigida* s.l., (b) *Cassidulina neoteretis*, (c) *Cassidulina reniforme*, (d) *Cibicides lobatulus*, (e) *Elphidium clavatum*, (f) *Nonionellina labradorica*, (g) *Islandiella helenae*, (h) *Islandiella norcrossi*, (i) *Stainforthia loeblichi* s.l.; SEM images produced with a *HITACHI S3400N* Scanning Electron Microscope (accelerating voltage: 3 kV, apart from images (b) and (f): 5 kV) at *le Geotop*, Université du Québec à Montréal (Canada).

3.5.3 Methodological remarks for faunal analyses

The identification of fossil species is carried out following the morphology of the test, i.e., the shape and assembly of chambers as well as the shape and position of the apertures (e.g., Holbourn et al., 2013; Murray, 2006). This is usually done with the help of a stereo-microscope (commonly up to 63-fold magnification). In case of uncertainty when identifying specimens and for documentation, a scanning electron microscope (SEM) can be applied, which allows a much larger magnification (up to 300,000-fold; see images in Fig. 10). In fossil records, only *morphospecies* can be defined; some may match with genetic types while others mismatch as it was reported for planktic (e.g., André et al., 2013) as well as for benthic species (Darling et al., 2016).

In the studies of this thesis, foraminiferal genera were defined following morphological descriptions by Loeblich and Tappan (1988). Abundant species are shown in Fig. 10. The faunal distribution at the studied sites reflects a typical Arctic glaciomarine environment (e.g., Hald and Korsun, 1997; Korsun and Hald, 1998). Ecological preferences of foraminiferal species were estimated following studies of modern (sub-)Arctic shelf faunas, e.g., from Svalbard, Iceland or the Barents and Kara Seas (e.g., Hald and Korsun, 1997; Jennings et al., 2004; Korsun and Hald, 1998, 2000; Polyak et al., 2002; Rytter et al., 2002; Steinsund, 1994).

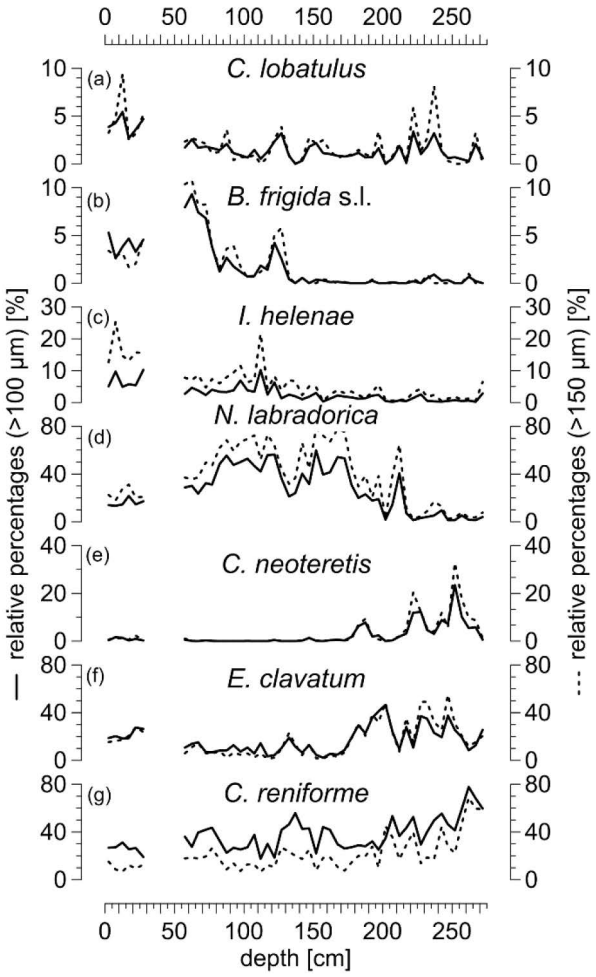

Fig. 11: Comparison of benthic foraminiferal distributions from size classes >100 µm (solid lines) and >150 µm (dashed lines) showing similar patterns (samples obtained from sediment core GeoB10817-4, Woodfjord, northern Spitsbergen; Bartels et al., 2017).

In the Arctic, benthic foraminifera are commonly smaller than in other regions (e.g., Wollenburg, 1992, 1995). Accordingly, most studies analyse specimens appearing in the size fraction >100 µm (e.g., Hald and Korsun, 1997; Hansen and Knudsen, 1995; Seidenkrantz et al., 2007; Skirbekk et al., 2010; Ślubowska-Woldengen et al., 2007). Nevertheless, Wollenburg and Mackensen (1998) reported analogous distribution patterns of benthic foraminiferal faunas from different size classes with the same dominant species. Fig. 11 consistently illustrates parallel faunal patterns of the size fractions >100 µm and >150 µm in a palaeo-record from the mouth of the Woodfjord (northern Spitsbergen; see manuscript I; Bartels et al., 2017).

For the interpretation of species that comprise >10 % of the fauna, at least 300 individuals should be counted in one sample to obtain a 95 % confidence. If less abundant species shall be taken into account even more individuals should be considered (Patterson and Fishbein, 1989). Accordingly, in micropalaeontological studies

>250 individuals are counted in each sample for statistical reasons (Murray, 2006). Count data of selected samples from the sediment core *GeoB10817-4* (examined for an uncertainty analysis; see below) reveal still increasing numbers of species after counting 200 individuals but no considerable change after counting >300 specimens (Fig. 12). Correspondingly, samples containing less than 200 foraminifera should be interpreted very cautiously or even be disregarded.

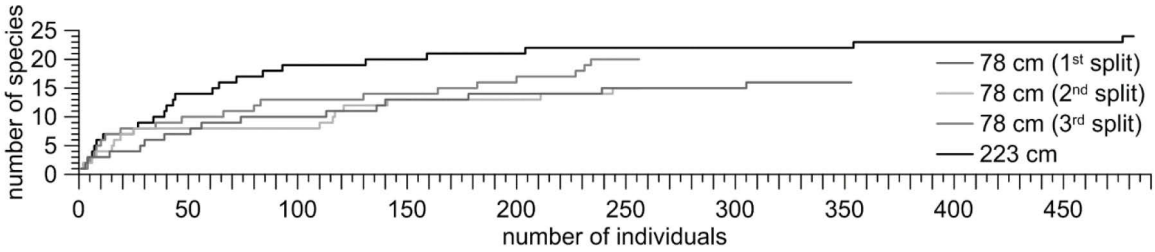

Fig. 12: Census data of benthic foraminifera obtained in two depths of sediment core *GeoB10817-4* (splitted sample from 78 cm counted three times).

For an uncertainty analysis, three replicates of samples from sediment core *GeoB10817-4* (78 cm and 223 cm core depth) were counted. The sample from 78 cm depth was split as it contained a very large number of foraminifera (>8,000 specimens), each split was counted three times. The entire (non-split) sample from 223 cm depth has also been counted three times. The true standard error of the mean was calculated for both depths including the initially counted sample, which was used for the faunal analysis: The standard error of the split sample (78 cm) was 2.95 %, while statistical calculations of the non-split sample (223 cm) yielded a standard error of 3.52 %.

In all three sediment cores, the number of agglutinating species decreases with increasing core depth (Fig. 13). This is very likely connected to the lower preservation potential of agglutinants compared to calcareous species (the so-called taphonomic effect; Hald and Korsun, 1997; Murray, 2006). Similar distribution patterns of arenaceous species have also been found by Ślubowska et al. (2005). Therefore, agglutinants were excluded when calculating relative percentages in the following studies.

To estimate the abundance of foraminifera considering sedimentation rates, accumulation rates of benthic foraminifera were computed as proposed by Ehrmann and Thiede (1985):

$$\mathrm{ARBF} = \mathrm{LSR} * \rho * \mathrm{BFN} \quad (1)$$

with:

ARBF = accumulation rate of benthic foraminifera [specimens cm^{-2} ka^{-1}];

LSR = linear sedimentation rate [cm ka^{-1}];

ρ = density of dry sediment [g cm^{-3}];

BFN = Benthic Foraminifera Number (per gram dry sediment) [specimens g^{-1}]

Accumulation rates of benthic foraminifera were widely used as (surface water) productivity proxies although various limitations exist, e.g., in case of carbonate dissolution (Murray, 2006 and references therein; Wollenburg et al., 2001). Loubere and Fariduddin (2003) pointed out that every benthic foraminiferal species would have to respond similarly on organic matter flux when using their accumulation rate as productivity proxy while taphonomic processes would be ignored (which indeed affects the accumulation rate). Thus, accumulation rates of benthic foraminifera should be interpreted cautiously and ideally in comparison with

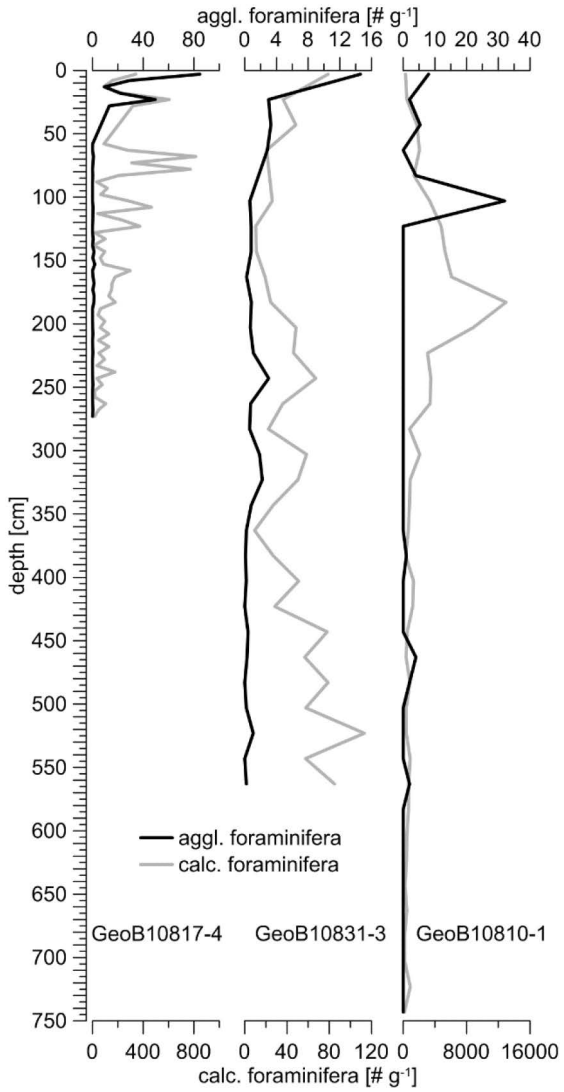

Fig. 13: Number of agglutinating vs. calcareous foraminifera per gram dry sediment. Note different scales at x-axis for agglutinating and calcareous foraminifera.

further productivity proxies (e.g., the offset between epi- and endobenthic stable carbon isotopes, $\Delta\delta^{13}C$, as discussed in chapter 3.8.1).

If faunas are very complex with more than two to three dominant species it might be reasonable to perform a principle components analysis (PCA). This statistic approach reduces a complex data set to two (or more) variables (principle components) explaining a certain percentage of the variance of the fauna (e.g., Davis, 2003). The output of the PCA comprises two data sets: *Scores* describe the proportion of each variable (species) with respect to the principle component (assemblage). Applied at faunal analyses, *scores* highlight the dominant species of the respective assemblages. *Loadings* illustrate the distribution of the principle components over respective sample events; in faunal analyses the distribution of assemblages over time. Faunas in the studied sediment cores in the following manuscripts are to a large degree dominated by three species. Hence, a PCA has only been applied for sediment core *GeoB10831-3* to identify "foraminiferal intervals" (time intervals dominated by certain species/assemblages).

3.6 Ice-Rafted Debris (IRD)

3.6.1 IRD as proxy for glacier activity

Icebergs as well as sea ice can provide a significant contribution to sedimentation processes in Arctic marine environments (e.g., Dowdeswell et al., 1998; Hebbeln, 2000; Stein, 2008). Both incorporate terrigenous grains (e.g., by glacier erosion or freezing in shallow waters, respectively), which are transported ("rafted") by drifting and deposited after melting. While in the deep sea, coarse lithogenic particles can easily be identified as ice(berg)-rafted debris according to their grain size (commonly >500 µm; e.g., Elverhøi et al., 1995; Hebbeln et al., 1998), in fjord environments the identification of IRD is less obvious as various sedimentation processes apart from ice-rafting can entail the accumulation of coarse sediments, including mass wasting events like debris flows. Nevertheless, the interpretation of coarse sediment as IRD is widely used in fjord settings (Baeten et al., 2010; Forwick et al., 2010; Hald et al., 2004; Rasmussen et al., 2012). This is reasonable, if the IRD analysis is combined with further data, e.g., swath bathymetry or acoustic data, which may exclude sedimentation processes apart from ice-rafting.

A wide range of size fractions were assumed to be ice(berg)-rafted (e.g., >63, >150, >250, >500 or >1,000 µm). While IRD analyses based on grains <500 µm might be statistically more robust due to the

higher number of grains that is usually found in this size fraction, processes not related to ice(berg)-rafting can nearly be excluded when interpreting grains >500 µm as IRD while even the mineralogy of these grains can be estimated (Hebbeln et al., 1998). Contrastingly, sea ice mainly transports finer-grained particles (e.g., Dowdeswell et al., 1998; Hebbeln, 2000). Hebbeln (2000) analysed the particle flux in sediment traps deployed in the eastern Fram Strait and found particles >40 µm linked to sea ice-rafting detritus. However, it remains difficult to distinguish between iceberg- and sea ice-rafted debris as both can incorporate fine-grained sediments (e.g., Dowdeswell et al., 1998; Hebbeln et al., 1998). Therefore, it remains hardly possible to reconstruct the sea ice margin with the help of sea ice-rafted debris if other processes or sources cannot be ruled out. In the following chapters, IRD is related to iceberg-rafted detritus if not specified otherwise.

The IRD analysis is further complicated by the fact that different mechanisms can lead to the deposition of ice-rafted material: High amounts of IRD can reflect climatically induced glacier advances or retreats as well as glacier surges because calving glacier fronts are simply the result of instabilities of the tidewater glacier. Furthermore, large amounts of (e.g., meltwater-derived) fine-grained sediments will dilute and, hence, drastically lower the IRD content, while IRD deposition will seem to be enhanced during a reduced input of fine-grained sediments although the IRD accumulation probably stayed constant in both cases (Forwick et al., 2010). Sea surface temperatures will also influence the deposition of ice-rafted material as warmer temperatures will melt icebergs at glacier-proximal positions whereas during cooler temperatures icebergs are able to drift to glacier-distal positions (Forwick et al., 2010). In contrast to lower latitudes, where IRD has been used as proxy for cold pulses (Bond et al., 1997; Heinrich, 1988), enhanced IRD deposition at high latitudes characterizes rather relatively warm conditions with seasonally open water and the presence of tidewater glaciers (Elverhøi et al., 1998). In the Arctic, very cold sea surface temperatures would prevent iceberg melting and a closed, possibly shorefast sea ice cover would hamper iceberg rafting (e.g., Dowdeswell et al., 2000; Elverhøi et al., 1998). Accordingly, IRD records should never be interpreted alone but in the context of further data (e.g., sea floor morphology, radionuclides). For the Svalbard area, e.g., ^{10}Be studies by Hormes et al. (2013), which were combined with radiocarbon-dated beach ridges offer a good overview about glacier retreats during the deglaciation, while the examination of submarine morphologies in various studies elucidate the glacier pathways during a similar time interval (Dowdeswell et al., 2010; Flink et al., 2017; Fransner et al., 2017; Hogan et al., 2010b, 2017; Ottesen et al., 2007). Hence, those data are very well suitable to be combined with local IRD records.

3.6.2 Methodological comparison: Computer tomography vs. IRD accumulation rates

In sediment cores *GeoB10817-4* and *GeoB10831-3*, two methods for the assessment of IRD have been applied and will here be compared. Archive halves of both cores were scanned by a computer tomograph (CT) at the hospital *Klinikum Bremen-Mitte* (*Toshiba Aquilion 64*™, x-ray source: 120 Kv; 600 mA). The resolution of the CT image stacks (produced with Toshiba's patented helical cone beam reconstruction technique) is 0.35 mm in x- and y-direction and 0.5 mm in z-direction (0.3 mm per reconstruction unit). The scanned core sections were merged applying the *Amira* software (ZIB edition; version 2016.25; Stalling et al., 2005) while the core liner and ~2 mm at the core margins were cut. Based on the processed CT data, the number of clasts (>1 mm) per cm^3 and the volume percentages of clasts (>1 mm) in relation to the total volume of the sediment were calculated. Those clasts are considered to be ice-rafted. The size class of >1 mm is selected for technical

reasons as the CT cannot detect clast <1 mm due to its resolution (J. Titschack, pers. comm.). Clasts were defined based on density thresholds (measured in Hounsfield units [HU]) separating clasts (>1,500 HU), matrix sediment (601–1,499 HU) and open voids (filled by air and/or water; 1–600 HU) as well as surrounding air/water (<1 HU). The mean value and its standard deviation of the matrix sediment were determined to assess the x-ray density in each slice. Unusual shifts in the x-ray density as well as the raw orthogonal CT images may provide information about disconformities and disturbances in the sediment (see chapters 3.2 and 3.4).

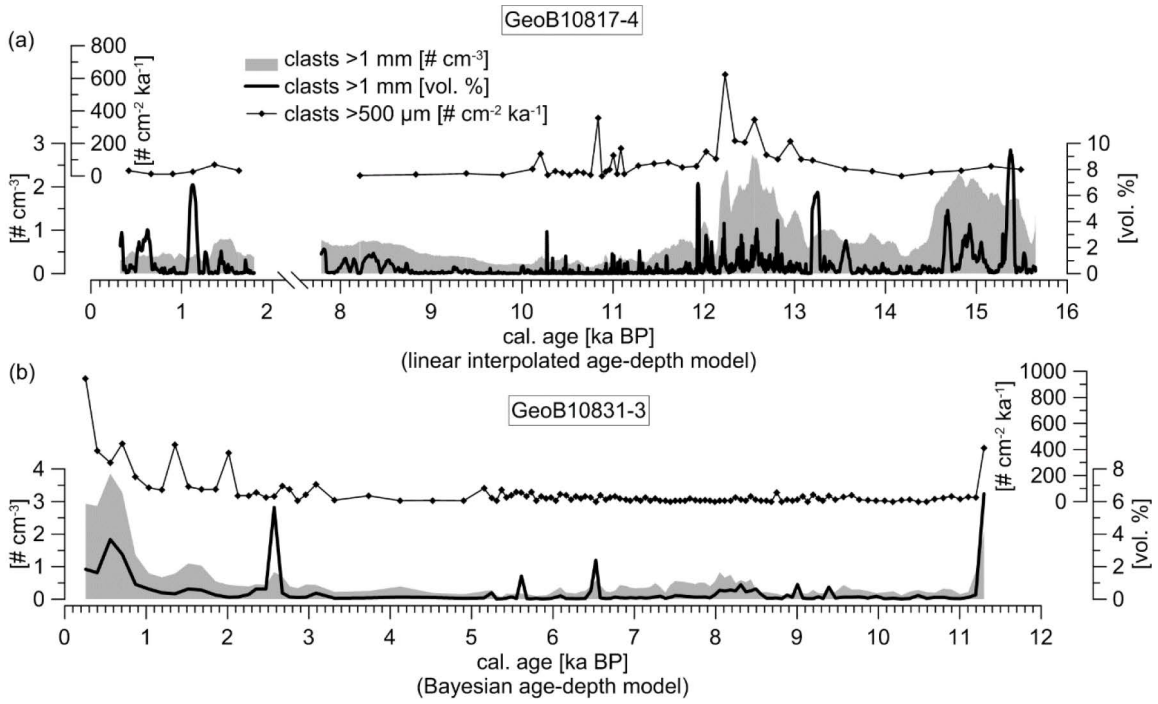

Fig. 14: Comparison of methods to determine the input of ice-rafted debris (IRD): Accumulation rates of clasts >500 µm based on count data as well as volume percentages and number of clasts >1 mm per cm^3 based on CT analyses. CT data in (a) are shown in high resolution (0.3 mm) because the age–depth model of sediment core GeoB10817-4 is based on linear interpolation. Running means (every 5 cm) of CT data are shown in (b) because the age–depth model of sediment core GeoB10831-3 is based on a Bayesian approach performed with *BACON* (Blaauw and Christen, 2011), which is unable to provide high (sub-millimetre) resolution models. Resolution of accumulation rates [# cm^{-2} ka^{-1}] in (a) and (b): 5 cm.

For comparison, lithogenic particles >500 µm were counted in sediment cores *GeoB10817-4* and *GeoB10831-3* before accumulation rates were calculated following Ehrmann and Thiede (1985). Both data sets show comparable patterns illustrated in Fig. 14. The figure further demonstrates that data based on CT scans provide a much higher precision, not only due to the extremely higher resolution (in Fig. 14a), but also due to the combination of volume percentages and numbers per unit. The combination of those data is crucial because volume percentages may overestimate large clasts while the number of clasts per cm^3 may overemphasise high numbers of small debris, which were possibly deposited during a single event (e.g., when an iceberg rolls over releasing rafted debris from its surface). Above all, the CT scan considers the entire core (or at least one half of the core on its full length) compared to only 10 cm^3 (syringes) in certain depth intervals. Especially in Fig. 14a, it is apparent, that the accumulation rates of grains >500 µm do not capture the obviously high IRD input between ~15,500 and ~14,500 years BP illustrated by the CT data.

Sediment core *GeoB10810-1* was not scanned by a CT. Clasts >250 µm were counted because the amount of lithogenic grains in the size class >500 µm was too small. Accumulation rates were also determined using the formula by Ehrmann and Thiede (1985).

3.7 Grain size

3.7.1 Sedimentation processes in fjord environments

In glaciomarine environments, fine-grained sediments play a very crucial role. Most glaciomarine sediments are dominated by silt and/or clay with significantly smaller percentages of sand and larger clasts. Those fine-grained sediments are primarily delivered by glacier meltwater. In the Svalbard area, a region dominated by relatively mild conditions compared to other glaciated regions (e.g., East Greenland), meltwater-derived sediments are the main contributor to sediment accumulation in the fjords (Fig. 15), which reach accumulation rates up to 25 cm per year, e.g., in inner fjord basins of western Spitsbergen (Dowdeswell et al., 1998). Close to the glacier fronts, the sediment accumulation is highest, exponentially decreasing towards the fjord mouth where accumulation rates may be two magnitudes lower than at the terminus of the glacier (Dowdeswell et al., 1998; Svendsen et al., 2002). The rapid sedimentation may be caused by the fact that suspended sediments settle close to tidewater glaciers due to flocculation initiated by the mixing of brackish meltwater-derived waters with saline marine water (Szczuciński and Zajączkowski, 2012). An intensive outflow of meltwater is only expected if summer temperatures (or advecting ocean currents) are warm enough to melt glaciers. Accordingly, high amounts of fine-grained sediments in fjord environments can be linked to retreating glaciers.

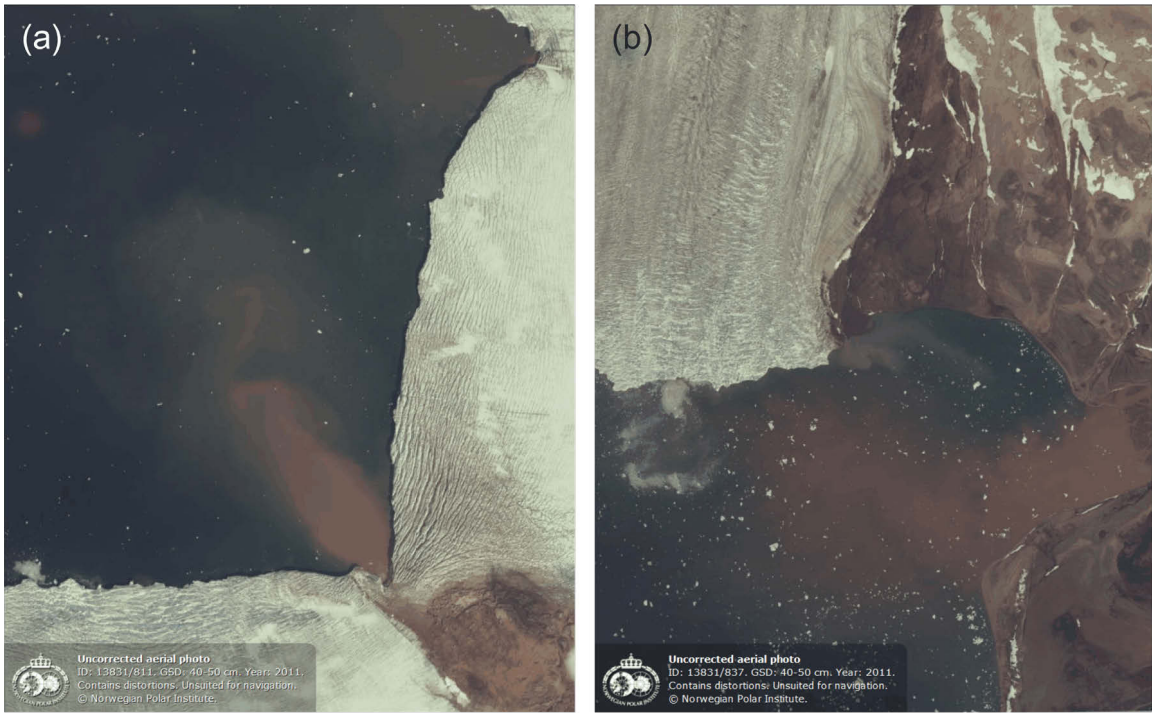

Fig. 15: Uncorrected aerial photos showing meltwater plumes with suspended reddish sediments and icebergs. Photos taken in 2011 at (a) Etonbreen and (b) Bodleybreen at the head of the Wahlenbergfjord (Nordaustlandet). © Norwegian Polar Institute (http://toposvalbard.npolar.no/).

Silt in the size fraction 10–63 µm ("sortable silt") was proposed to trace bottom water current speeds as it is regarded as non-cohesive (McCave et al., 1995a, 1995b). However, the deposition of IRD may disturb the

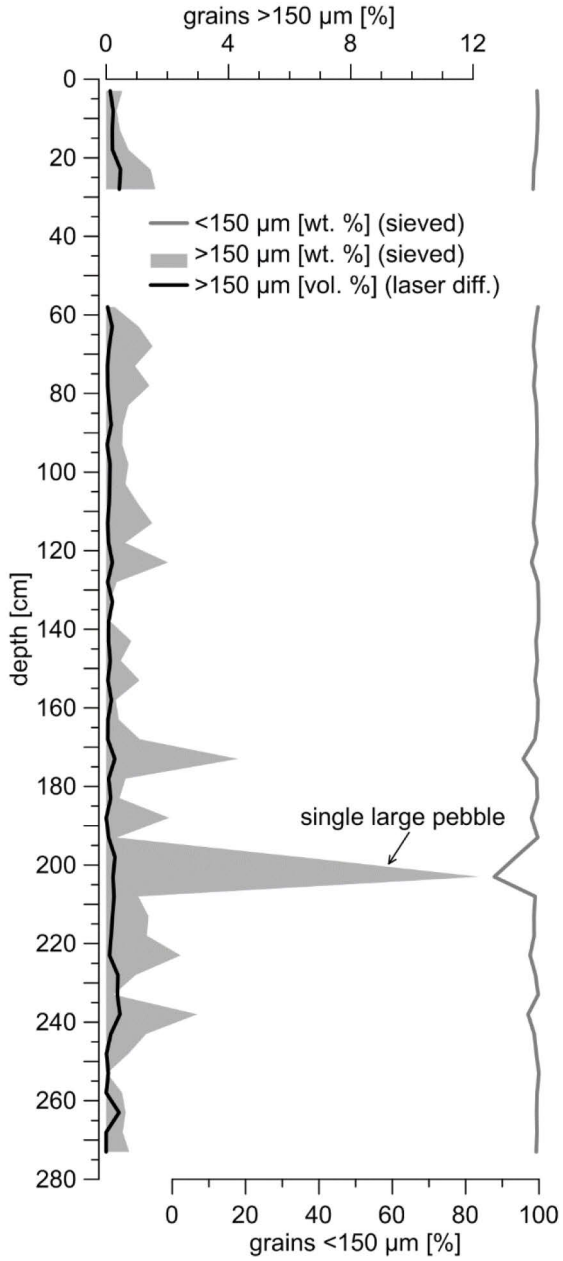

Fig. 16: Comparison of percentages of sediment grains >150 µm determined by the *Laser Diffraction Particle Size Analyser* (volume percentages) and as residuals from sieving (weight percentages) as well as (calculated) weight percentages of sediment grains <150 µm (sediment core *GeoB10817-4*). Note that peak at 203 cm derives from a single large pebble.

sortable silt signal (Jonkers et al., 2012, 2015; McCave and Hall, 2006; Werner et al., 2013). Various attempts to correct the IRD influence were discussed (e.g., Hass, 2002; McCave and Hall, 2006). But, as the latter studies are mainly based on deep sea sediments, the sortable silt approach seems to be not applicable in a fjord setting. Numerous sedimentation processes influence the composition of fjord sediments, including downslope sediment transport, deposition of sea ice- and iceberg-rafted material, settling of meltwater-derived suspended sediments, bottom current activity as well as hemipelagic sedimentation (e.g., Trusel et al., 2010). Nevertheless, hydrodynamic variations of bottom waters may be estimated by interpreting the full grain size spectrum (Jonkers et al., 2015).

3.7.2 Application of grain size measurements

During the usual sample processing for microfossil analyses (see chapter 3.3), the fine sediment fraction (<63µm) is not retained. Thus, only percentages or accumulation rates of the entire size class <63 µm can be calculated but no quantitative analyses of the fine sediment fraction can be carried out. Accordingly, grain size measurements were performed at sediment core *GeoB10817-4* applying the *Beckman Coulter Laser Diffraction Particle Size Analyser LS 13320*™ in the Particle-Size Laboratory at MARUM, University of Bremen. For this purpose, the sediment of this core was sampled with syringes (~10 cm^3) in 5 cm intervals before ~1–2 mm slices from the syringes (~0.5 ml) containing wet bulk sediment were pre-treated as follows:

Only the terrigenous fraction of the sediment should be analysed, hence, organic carbon, calcium carbonate and biogenic opal were removed. Therefore, the samples were boiled in ~200 ml water with 10 ml of 35 % H_2O_2 (until the reaction stopped), 10 ml of 10 % HCl (1 min) and 6 g NaOH pellets (10 min), respectively, diluting the sample after each pre-treatment (dilution factor: >25). For disaggregation, the samples were boiled with ~0.3 g $Na_4P_2O_7$ * $10H_2O$ (3 min; see McGregor et al., 2009). Deionised, degassed and filtered water (filter mesh size: 0.2 µm) was used during sample pre-treatment and analyses to reduce the potential influence of gas bubbles or particles within the water.

The *Particle Size Analyser* is able to detect particle sizes between 0.04 µm and 2 mm, which were divided into 116 size classes. The analyses of particles from 0.4 µm to 2 mm is based on the Fraunhofer diffraction theory, while particles from 0.04 to 0.4 µm were detected due to *Polarization Intensity Differential Scattering*. Replicate analyses of three internal glass-bead standards are carried out regularly. Resulting reproducibility (1σ) is better than ±0.7 µm for the mean and ±0.6 µm for the median grain size, while the average standard deviation is better than ±4 vol. % (including all size classes; standard deviation of the individual size classes varies). All provided statistic values are based on geometric statistics.

The *Particle Size Analyser* principally considers particles as spheres. Thus, clay content may be underestimated because it forms flat sheets (McCave et al., 1995b). In sediment core *GeoB10817-4*, the *Particle Size Analyser* did not identify particles >310 µm whereas the sieved samples used for the microfossil and IRD analyses contained even particles >500 µm. This discrepancy may be caused by the small amount of sediment analysed by the *Particle Size Analyser*. Thus, large pebbles are not captured by measurements with the *Particle Size Analyser* (see Fig. 16). Additionally, low percentages of particles >310 µm may be below the detection limit of the *Particle Size Analyser* (Fig. 16 illustrates that in most samples >98 wt. % of the dried bulk sediment is <150 µm)

3.8 Stable isotopes

3.8.1 Foraminiferal stable isotopes as palaeoceanographic tracers

The most frequently occurring stable oxygen isotopes on this planet are ^{16}O (99.6 %) and ^{18}O (0.2 %), while ^{12}C (98.9 %) and ^{13}C (1.1 %) represent the most frequent stable carbon isotopes (e.g., Ravelo and Hillaire-Marcel, 2007). The fractionation of isotopes follows thermodynamic principles. During evaporation, higher percentages of the "lighter" oxygen isotope ^{16}O are extracted from the sea, consequently, sea water is enriched in the "heavier" ^{18}O (Fig. 17). During the decay of organic matter in the sediment, mainly the "lighter" carbon isotope ^{12}C is released, thus, bottom waters become enriched in ^{12}C. Accordingly, ocean circulations may be tracked by the stable carbon isotope composition because, e.g., "old" deep water masses can be identified by high ^{12}C concentrations in bottom waters. Calcareous benthic foraminifera (like all shell-bearing marine organisms) incorporate the stable isotope composition of the surrounding water when precipitating their calcite shells. Hence, the stable isotope composition of calcareous marine organisms reflects ecological conditions, including circulation patterns, which can be utilised in palaeoceanography, interpreting stable isotope values in fossil taxa. Therefore, stable oxygen and carbon isotope ratios of marine carbonates were calculated:

$$\delta^{18}O\ [‰] = \frac{^{18}O/^{16}O_{sample} - {}^{18}O/^{16}O_{standard}}{^{18}O/^{16}O_{standard}} * 1000 \qquad (2)$$

$$\delta^{13}C\ [‰] = \frac{^{13}C/^{12}C_{sample} - {}^{13}C/^{12}C_{standard}}{^{13}C/^{12}C_{standard}} * 1000 \qquad (3)$$

Hence, the stable isotope ratios are the relation of the stable isotope composition of a given sample to a certain standard (e.g., Ravelo and Hillaire-Marcel, 2007). Broadly used standards for carbonate and water samples are Vienna Pee Dee Belemnite (VPDB) based on belemnites from the Cretaceous Pee Dee formation and Vienna Standard Mean Ocean Water (VSMOW), respectively (e.g., Ravelo and Hillaire-Marcel, 2007).

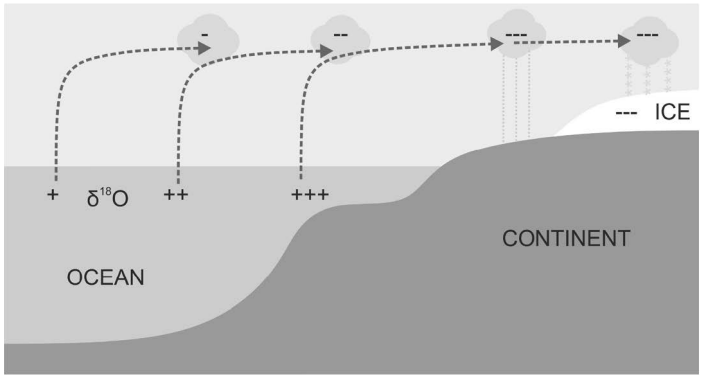

Fig. 17: Fractionation of stable oxygen isotopes. With increasing latitude, the ocean is enriched with the "heavier" oxygen isotope ^{18}O because during evaporation the "lighter" isotope ^{16}O is preferably removed from sea water. Precipitation at high latitudes and successive snow accumulation leads to low stable oxygen ratios ($\delta^{18}O$) in glaciers. The more water is "bound" in glaciers the higher the $\delta^{18}O$ values in the ocean (e.g., during glacial periods).

As the fractionation of stable oxygen isotopes is temperature dependent, $\delta^{18}O$ ratios have been used for palaeo-temperature reconstructions since the 1950s (e.g., Emiliani, 1955; Epstein et al., 1953). A major influence of salinity on $\delta^{18}O$ values has been discovered later (e.g., Rohling and Bigg, 1998). Due to the high freshwater input derived from meltwater on the one hand and brine release during sea ice formation on the other hand, salinity-induced changes in the foraminiferal $\delta^{18}O$ composition are especially relevant in Arctic waters (e.g., Mackensen and Nam, 2014; Mackensen and Schmiedl, 2016; Rasmussen and Thomsen, 2014). When comparing stable oxygen isotope values, various factors influencing the $\delta^{18}O$ composition have to be taken into account, including the pH-value of the sea water, the global ice volume (sea water becomes enriched in ^{18}O with increasing ice volume; Fig. 17), ontogenetic effects (the test size of a foraminifera has a significant influence on stable isotope ratios; e.g., Hillaire-Marcel et al., 2004) and so-called vital effects (species-dependent offset from sea water equilibrium due to metabolic processes; e.g., Ravelo and Hillaire-Marcel, 2007; Rohling and Cooke, 2003).

Apart from the above-mentioned applications, stable oxygen isotopes have widely been used to create a stratigraphic framework for sediment cores dating back several millennia because foraminiferal $\delta^{18}O$ ratios respond to orbital cycles. Correspondingly, so-called $\delta^{18}O$ stacks have been used, e.g., the "classical" *SPECMAP stack* based on planktic foraminifera (Imrie et al., 1984), or more recently the *LR04 stack* combining benthic foraminiferal $\delta^{18}O$ records (Lisiecki and Raymo, 2005).

As already outlined, stable carbon isotopes in bottom waters are tied to the decay of organic material and correspondingly also to the organic matter flux. The stable carbon isotope composition in organic matter is influenced by fractionation processes during photosynthesis by phytoplankton. Further, $\delta^{13}C$ at the sea surface is affected by the ocean–atmosphere exchange and related fractionation between CO_2 and dissolved inorganic carbon (DIC; e.g., Mackensen, 2008 and references therein). The stable isotope composition of epibenthic foraminifera reflects the stable carbon isotope ratio of DIC ($\delta^{13}C_{DIC}$) in bottom water, while endobenthic species are rather influenced by pore water $\delta^{13}C_{DIC}$. The former may reflect the degree of ventilation in bottom waters as shown for the eastern Mediterranean Sea (Schmiedl et al., 2010), while the latter is mainly affected by the remineralization of organic material in the sediment (e.g., Schmiedl and Mackensen, 2006 and references therein). Hence, $\delta^{13}C$ in (endobenthic) foraminiferal shells may be used as productivity proxy.

The fractionation of stable carbon isotopes may also be affected by various factors apart from organic matter fluxes: methane seeps at the sea floor as well as a methanotrophic diet of the foraminifera lower the $\delta^{13}C$ ratio in their shells (e.g., Consolaro et al., 2015; Mackensen, 2008; Sztybor and Rasmussen, 2017). Also the carbonate saturation in the sea water affects the stable carbon isotope composition of the foraminiferal test

(e.g., Mackensen, 2008). Large offsets between stable carbon isotope ratios in benthic foraminifera and $\delta^{13}C_{DIC}$ values in bottom or pore waters and respective corrections for $\delta^{13}C$-vital effects have been discussed (e.g., Grossman, 1987; Mackensen et al., 2000; Wefer and Berger, 1991). However, just recently Schmittner et al. (2017) analysed a huge data set of surface sediment and water samples concluding that a one-to-one relationship of $\delta^{13}C_{DIC}$ in bottom waters and $\delta^{13}C$ of epibenthic foraminifera (*Cibicides* spp.) may for the most part be reliable. In general, the relationship between foraminiferal $\delta^{13}C$ and $\delta^{13}C_{DIC}$ is very complex. Therefore, no corrections for a disequilibrium are considered in most studies, e.g., from the Svalbard area (Klitgaard Kristensen et al., 2013; Rasmussen et al., 2012).

Various studies show that the offset between the stable carbon isotope ratios in epi- and endobenthic foraminiferal tests ($\Delta\delta^{13}C$) is a valuable productivity proxy (Mackensen et al., 2000, 2017; Mackensen and Schmiedl, 2016; Milker et al., 2012; Schmiedl and Mackensen, 2006). This can be inferred because it has been shown that $\delta^{13}C$ values in endobenthic species are mainly affected by variabilities of the organic matter flux and subsequent decay during a stable oxygenation of the bottom waters and consequently stable $\delta^{13}C$ values in epibenthic species (Schmiedl and Mackensen, 2006). Just recently, Mackensen et al. (2017) illustrated that especially the offset between stable carbon isotopes of the epibenthic species *Cibicides lobatulus* and the endobenthic species *Nonionellina labradorica* exhibits a considerable correlation to the flux of marine organic carbon. Those authors even propose to use $\Delta\delta^{13}C$ values of the latter two species as “quantitative productivity proxy”.

3.8.2 Stable carbon and oxygen isotope measurements – methodological remarks

For all three studies of this thesis, stable carbon and oxygen isotopes measurements were carried out on 2–8 tests (test size: 150–500 µm) of the epibenthic foraminifera *Cibicides lobatulus* and the endobenthic foraminifera *Nonionellina labradorica*. Additionally, stable isotopes in tests of the planktic foraminifera *Neogloboquadrina pachyderma* (sinistral) from sediment core *GeoB10810-1* were measured for manuscript III. All measurements were performed at MARUM (Bremen) applying a Finnigan MAT 251™ mass spectrometer with a Kiel I carbonate preparation device, apart from a number of samples from sediment core *GeoB10817-4*, which were measured at ZMT (Leibniz Centre for Tropical Marine Ecology) in Bremen, using a Finnigan MAT 253™ gas isotope ratio mass spectrometer with a Kiel IV automated carbonate preparation device. Standard deviations of the inhouse standard (Solnhofen limestone) ranged between 0.02 and 0.03 ‰ for $\delta^{13}C$ and between 0.03 and 0.06 ‰ for $\delta^{18}O$. All stable oxygen isotope values were corrected for global ice volume following Waelbroeck et al. (2002). Due to a disequilibrium of the stable oxygen isotope ratios of benthic foraminifera compared with bottom and pore water, respectively, the former were further corrected for a so-called vital effect with +0.64 ‰ for *C. lobatulus* (Shackleton, 1974) and -0.2 ‰ for *N. labradorica* (Duplessy et al., 2005). Corrections for a $\delta^{13}C$-vital effect were not applied (as discussed in chapter 3.8.1). In the case studies of this thesis, mainly the offsets between $\delta^{13}C$ values of *C. lobatulus* and *N. labradorica* are discussed, hence, corrections would rather change the magnitude than the general patterns.

3.9 Biomarkers

3.9.1 The use of organic molecules as environmental proxies

The use of organic molecular compounds in sediments as environmental proxies (biomarkers) is very common since the late 1980s (Belt et al., 2007; Brassell et al., 1986; Volkman et al., 1993). A widely used example are long-chain alkenones produced by haptophytes like coccolithophores (marine calcareous algae), especially by the ubiquitous *Emiliania huxleyi* (Meyers, 1997). These carbon ketones (with 37 carbon atoms) are found in almost all marine sediments (Eglinton and Eglinton, 2008), but are also abundant in some lake sediments (e.g., D'Andrea et al., 2006, 2011; D'Andrea and Huang, 2005). They appear with two ($C_{37:2}$), three ($C_{37:3}$) and four double-bounds ($C_{37:4}$). The amount of $C_{37:3}$ and $C_{37:4}$ in relation to $C_{37:2}$ is temperature-dependent, i.e., this ratio increases with temperature (Eglinton and Eglinton, 2008). As coccolithophores dwell in the photic surface layer, alkenones record temperatures of the sea surface. Hence, the ratio (alkenone undersaturation index U_{37}^{K}) has been established as sea surface temperature (SST) proxy (Brassell et al., 1986), while it has been simplified later on excluding $C_{37:4}$ ($U_{37}^{K'}$ index), as $C_{37:4}$ rarely appears at temperatures >15 °C (Prahl and Wakeham, 1987). At high latitudes the application of U_{37}^{K} is a better SST proxy because of a sufficient amount of $C_{37:4}$ alkenones as recommended just recently (Filippova et al., 2016). The U_{37}^{K} index is calculated as follows (Brassell et al., 1986):

$$U_{37}^{K} = \frac{[C_{37:2}] - [C_{37:4}]}{[C_{37:2}] + [C_{37:3}] + [C_{37:4}]} \qquad (4)$$

Based on the $U_{37}^{K'}$ index (U_{37}^{K} index), various equations to calculate SSTs have been proposed (e.g., Müller et al., 1998; Prahl and Wakeham, 1987). In manuscript I (chapter 5), the following equation has been used, based on the formula suggested by Müller et al. (1998) because it yielded most realistic results:

$$U_{37}^{K} = 0.033 * \mathrm{T}\,[°\mathrm{C}] + 0.044 \quad (5)$$

The $U_{37}^{K'}$ index, used in the original equation (based on a core-top study; 60 °N–60 °S), was replaced by the U_{37}^{K} index (standard error: ±1.5 °C).

The appearance of further phytoplankton organisms (e.g., dinoflagellates, diatoms) has been traced extracting sterols out of sediment samples: e.g., 4-methyl sterol (dinosterol) is produced by most dinoflagellates (Volkman et al., 1993), while 24-methyl sterol (brassicasterol) can be produced by diatoms and other algae but also by some plants (Volkman, 1986). Therefore, these organic molecules have been used as phytoplankton biomarkers (Fahl and Stein, 1999).

During recent years, the C_{25} monounsaturated hydrocarbon (IP_{25}) has been applied in numerous studies as proxy for sea ice distribution (e.g., Belt et al., 2007; Belt and Müller, 2013; Berben et al., 2014; Cabedo-Sanz et al., 2013; Fahl and Stein, 2012; Hörner et al., 2016; Müller et al., 2009, 2011, 2012; Müller and Stein, 2014; Smik et al., 2016; Stein et al., 2012, 2017). The use of this proxy is based on the assumption that IP_{25} is exclusively produced by diatoms that live in sea ice (e.g., *Haslea* spp.; Belt et al., 2007). However, the application of IP_{25} as sea ice proxy is limited: the lack of IP_{25} may be connected to the absence of sea ice or to a very thick sea ice cover that prevents any algal growth (Fig. 18). Therefore, Müller et al. (2011) developed the so-called phytoplankton-IP_{25} index (PIP_{25}) including also information from phytoplankton by using brassicasterol or dinosterol concentrations (Fig. 18), which is calculated as follows:

$$PIP_{25} = \frac{[IP_{25}]}{[IP_{25}]+([phytoplankton\ marker]*c)} \qquad (6)$$

Because the concentration of the respective biomarkers significantly differs, sometimes in the order of several magnitudes, a balance factor *c* has been introduced (Müller et al., 2011):

$$c = \frac{mean\ [IP_{25}]}{mean\ [phytoplankton\ biomarker]} \qquad (7)$$

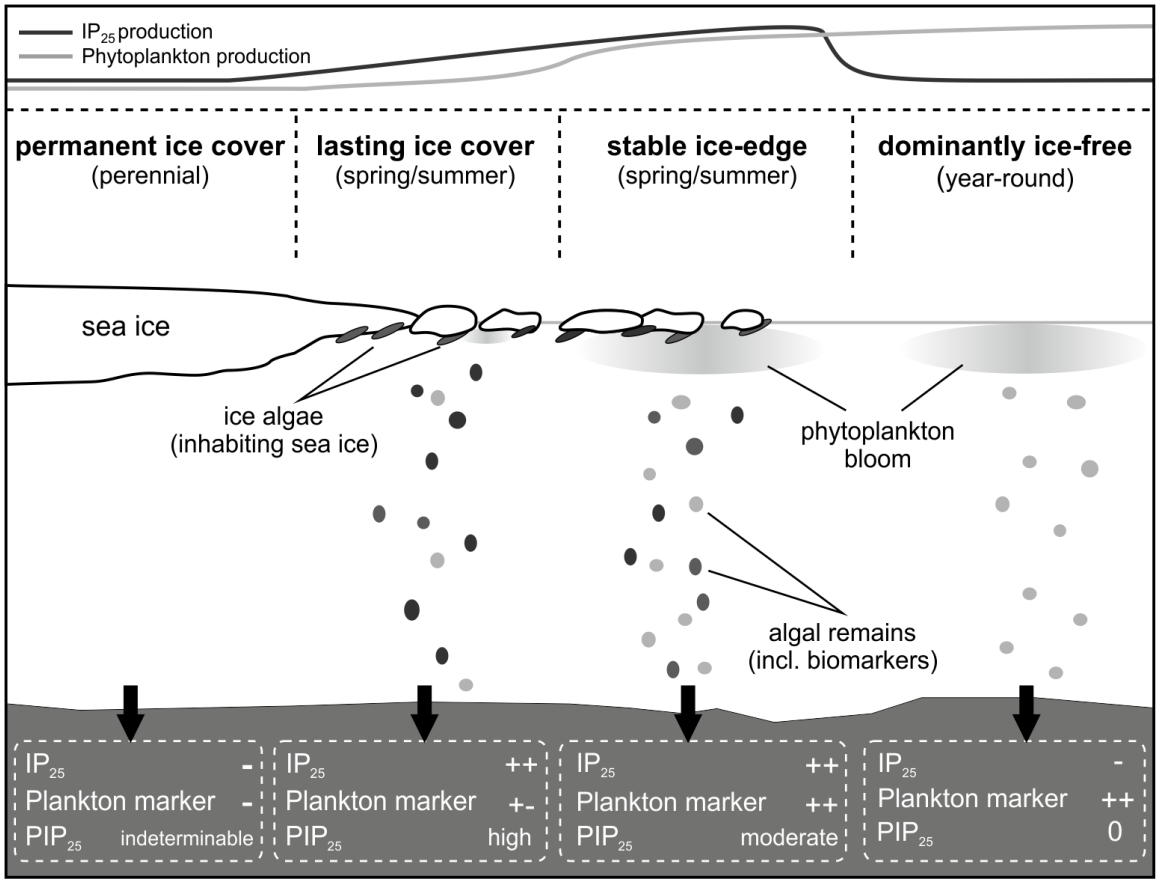

Fig. 18: The combination of IP_{25} and phytoplankton biomarkers as PIP_{25} index. Neither IP_{25} nor phytoplankton biomarkers: permanent sea ice cover (PIP_{25} indeterminable). High IP_{25}, but moderate phytoplankton biomarker concentration: extended sea ice cover (PIP_{25} >>0.7). High IP_{25} as well as phytoplankton biomarker concentration: seasonal sea ice or sea ice edge (PIP_{25} = 0.5–0.7). Low IP_{25}, but high phytoplankton biomarker concentration: reduced sea ice (PIP_{25} = 0.3–0.5). No IP_{25}, but high phytoplankton biomarker concentration: open water (PIP_{25} = 0). Sketch modified after Müller et al., (2011).

3.9.2 Sample processing for biomarker analyses

For biomarker analyses, selected samples from all three sediment cores were dried and homogenised (by grinding). The content of total organic carbon (TOC) was determined with a ELTRA™ Analyser (using 100 µg of sediment). In sediment core *GeoB10817-4*, alkenones were analysed applying the Accelerated Solvent Extractor DIONEX™, ASE 200. Samples (2 g of sediment) were processed for 15 min at 100 °C and 1,000 psi using dichloromethane and methanol (99:1, v/v) as solvent. Compounds were separated by open column chromatography (SiO_2) using *n*-hexane and dichloromethane (1:1, v/v), and dichloromethane. The alkenone composition was determined with an Agilent™ 7890 gas chromatograph based on retention time and by comparison with an external standard (from *Emiliania huxleyi* cultures with known growth temperature). Replicate analyses yielded an analytical error of <0.4 °C.

In all three sediment cores, the phytoplankton biomarkers brassicasterol (24-methylcholesta-5,22E-dien-3β-O-Si(CH_3)$_3$) and dinosterol (4α,23,24-trimethyl-5α-cholest-22E-en-3β-O-Si(CH_3)$_3$) as well as the sea ice biomarker IP_{25} were analysed. Selected samples (3 g of sediment solved in dichloromethane:methanol; 2:1, v/v) were ultrasonicated for 15 min with a Sonorex Super RK 510 at 35 khz to extract the biomarkers. Prior to analytical treatment, the internal standards 7-hexylnonadecane (0.076 µg), squalene (2.4 µg) and cholest-5-en-3β-ol-D_6 (10 µg) were used to quantify IP_{25} and sterols, respectively. Hydrocarbon and sterol fractions were separated by open column chromatography with *n*-hexane (5 ml) and *n*-hexane:ethylacetate (6 ml; 5:1, v/v), respectively. The sterol fraction was silylated at 60 °C for two hours with 500 ml bis-trimethylsilyl-trifluoroacet-amide. Gas chromatography and mass spectrometry applying an Agilent 7890B GC™ and an Agilent 5977A™ Extractor MSD with Performance Turbo Pump were used for the IP_{25} and sterol analyses (detection limit for IP_{25}: 0.005 ng μL^{-1}; Kovats Index for IP_{25}: 2086; retention indices for brassicasterol and dinosterol, normalised to cholest-5-en-3β-ol-D_6: 1.018 and 1.091, respectively). IP_{25} was quantified using the ratio of molecular ions of IP_{25} (*m/z* 350) and of the standard 7-hexylnonadecane (*m/z* 266), while sterols were quantified using the ratio of molecular ions of brassicasterol (*m/z* 470) or dinosterol (*m/z* 500) and of cholesterol-D_6 (*m/z* 464), respectively. The quantification of IP_{25} and of sterols are described in detail by Fahl and Stein (2012). Accumulation rates of all biomarkers were calculated following Ehrmann and Thiede (1985).

The phytoplankton-IP_{25} index (Müller et al., 2011) was estimated for all three sediment cores applying both phytoplankton biomarkers brassicasterol and dinosterol, apart from sediment core *GeoB10817-4* where only brassicasterol was used.

4 Overview of own research studies and author contributions

This dissertation consists of three stand-alone manuscripts that constitute the main body of the cumulative thesis. In the following, a brief overview about the major results and the contributions of all participants are given.

Manuscript I:

Atlantic Water advection vs. glacier dynamics in northern Spitsbergen since early deglaciation

Martin Bartels, Jürgen Titschack, Kirsten Fahl, Rüdiger Stein, Marit-Solveig Seidenkrantz, Claude Hillaire-Marcel, Dierk Hebbeln

(published in *Climate of the Past*, 2017; https://doi.org/10.5194/cp-13-1717-2017)

In the first manuscript, palaeoceanographic conditions and glacier responses during the deglacial period are compared with the late Holocene. Multi-proxy data (including benthic faunal assemblages, IRD, stable carbon and oxygen isotopes, grain sizes and biomarkers) illustrate that the (bottom water) inflow of relatively warm AW at the northern Spitsbergen margin contributed to the destabilization of the glaciers during the deglaciation. No glacier advances were detected during the YD when AW penetrated intermediate waters for the first time. The early Holocene was characterized by warmer temperatures than today possibly comparable to the future global warming. In contrast to the deglaciation, glaciers likely advanced despite an ongoing influence of AW during the late Holocene.

Author contributions:

M. Bartels and D. Hebbeln designed the study. M. Bartels was responsible for the sample processing, including wet and dry sieving, as well as pre-selecting of foraminifera, which was partly done by student assistants under his guidance. M. Bartels performed the faunal analyses. M.-S. Seidenkrantz revised the identification of the foraminiferal species and contributed to their interpretation. J. Titschack and M. Bartels performed the particle size measurements and respective pre-treatments with the help of a student assistant. J. Titschack carried out the CT analyses as well as respective data processing. K. Fahl analysed the biomarkers. J. Titschack created the base maps in Fig. 19b and c. M. Bartels designed the figures and interpreted all data. D. Hebbeln, C. Hillaire-Marcel and R. Stein contributed to the discussion of the data. M. Bartels prepared the manuscript with contributions from all co-authors.

Manuscript II:

Wahlenbergfjord (Svalbard): A glacier-proximal fjord suitable to reflect regional hydrographic variability during Holocene?

Martin Bartels, Jürgen Titschack, Kirsten Fahl, Rüdiger Stein, Dierk Hebbeln

(in preparation for submission)

The second manuscript unveils that even a remote glacier-proximal fjord reflects regional hydrographic changes of the Svalbard area and beyond. Based on benthic foraminiferal, IRD, stable carbon and oxygen isotope and biomarker analyses, data show a high discharge of meltwater and a significant influence of AW

in the Wahlenbergfjord during the summer insolation maximum in the early Holocene. A rapid oceanographic shift is evident during the mid-Holocene, when Arctic Water gained influence. Similar to the Woodfjord, advancing glaciers are likely in the Wahlenbergfjord during the late Holocene although an increasing AW inflow is recognisable.

Author contributions:
M. Bartels and D. Hebbeln designed the study. M. Bartels was responsible for the sample processing, including wet and dry sieving, as well as pre-selecting of foraminifera, which was partly done by student assistants under his guidance. M. Bartels performed the faunal analyses. K. Fahl carried out the biomarker analyses. J. Titschack created the base maps in Fig. 28, performed CT analyses and processed the respective data. M. Bartels designed the figures and interpreted all data. D. Hebbeln and R. Stein contributed to the discussion of the data. M. Bartels prepared the manuscript with contributions from D. Hebbeln.

Manuscript III:
Sedimentation off northwestern Spitsbergen since the deglaciation controlled by meltwater plumes and competing Atlantic and Arctic waters
Martin Bartels, Jana Schröder, Kirsten Fahl, Rüdiger Stein, Dierk Hebbeln
(in preparation)

In the third manuscript, the palaeoceanography of the Kongsfjord Trough (northwestern Spitsbergen) during the deglaciation based on benthic foraminiferal assemblages, IRD records and geochemical analyses (stable carbon and oxygen isotopes and sea ice biomarker) is evaluated and compared to previous studies from the Svalbard area indicating an early AW intrusion, which contributed to glacier retreats. Furthermore, the comparison with a nearby sediment core, situated closer to the coast, revealed partly significant differences, e.g., in palaeoproductivity, during the Holocene, which may be connected to the more distal positon of the investigated sediment core.

Author contributions:
M. Bartels and D. Hebbeln designed the study. J. Schröder processed the samples, including wet and dry sieving as well as pre-selecting of foraminifera advised by M. Bartels. M. Bartels and J. Schröder performed the faunal analyses. K. Fahl carried out the biomarker analyses. M. Bartels created the figures and interpreted all data. D. Hebbeln and R. Stein contributed to the discussion of the data. M. Bartels prepared the manuscript with contributions from D. Hebbeln.

5 Atlantic Water advection vs. glacier dynamics in northern Spitsbergen since early deglaciation (Manuscript I)

Martin Bartels[1], Jürgen Titschack[1,2], Kirsten Fahl[3], Rüdiger Stein[3], Marit-Solveig Seidenkrantz[4], Claude Hillaire-Marcel[5], Dierk Hebbeln[1]

[1]MARUM – Center for Marine Environmental Sciences, University of Bremen, 28359 Bremen, Germany
[2]SaM – Senckenberg am Meer, Marine Research Department, 26382 Wilhelmshaven, Germany
[3]Alfred Wegener Institute for Polar and Marine Research, 27568 Bremerhaven, Germany
[4]Centre for Past Climate Studies and Arctic Research Centre, Department of Geoscience, Aarhus University, 8000 Aarhus C, Denmark
[5]GEOTOP – Université du Québec à Montréal, Montreal, H3C 3P8, Canada

(published in *Climate of the Past*, 2017; https://doi.org/10.5194/cp-13-1717-2017)

Abstract

Atlantic Water (AW) advection plays an important role in climatic, oceanographic and environmental conditions in the eastern Arctic. Situated along the only deep connection between the Atlantic and the Arctic oceans, the Svalbard Archipelago is an ideal location to reconstruct the past AW advection history and document its linkage with local glacier dynamics, as illustrated in the present study of a 275 cm long sedimentary record from Woodfjorden (northern Spitsbergen; water depth: 171 m) spanning the last ~15,500 years. Sedimentological, micropalaeontological and geochemical analyses were used to reconstruct changes in marine environmental conditions, sea ice cover and glacier activity. Data illustrate a partial break-up of the Svalbard–Barents Sea Ice Sheet from Heinrich Stadial 1 onwards (until ~14.6 ka). During the Bølling–Allerød (~14.6–12.7 ka), AW penetrated as a bottom water mass into the fjord system and contributed significantly to the destabilization of local glaciers. During the Younger Dryas (~12.7–11.7 ka), it intruded into intermediate waters while evidence for a glacier advance is lacking. A short-term deepening of the halocline occurred at the very end of this interval. During the early Holocene (~11.7–7.8 ka), mild conditions led to glacier retreat, a reduced sea ice cover and increasing sea surface temperatures, with a brief interruption during the Preboreal Oscillation (~11.1–10.8 ka). Due to a ~6,000-years gap, the mid-Holocene is not recorded in this sediment core. During the late Holocene (~1.8–0.4 ka), a slightly reduced AW inflow and lower sea surface temperatures compared to the early Holocene are reconstructed. Glaciers, which previously retreated to the shallower inner parts of the Woodfjorden system, likely advanced during the late Holocene. In particular, topographic control in concert with the reduced summer insolation partly decoupled glacier dynamics from AW advection during this recent interval.

5.1 Introduction

In the context of the ongoing global warming, the Arctic is gaining increasing attention from the scientific community and the general public (e.g., IPCC, 2014; Masson-Delmotte et al., 2013). This is primarily motivated by extreme events like the 2012 sea ice minimum, the declining summer sea ice cover of recent decades (Stroeve et al., 2012) and the significant contribution of melting Arctic glaciers to the rising global sea level (e.g., Alley et al., 2005; Gregory and Huybrechts, 2006; IPCC, 2014; Overpeck et al., 2006). The Arctic is extremely sensitive to climatic changes and due to various feedback mechanisms, it is warming twice as fast as the global mean – a phenomenon commonly called the Arctic amplification (Serreze and Barry, 2011). These drastic changes in the Arctic also likely have far-reaching impacts. Several studies draw a connection to climate phenomena (especially severe winters) at lower latitudes (e.g., Cohen, 2016; Cohen et al., 2014; Kug et al., 2015; Mori et al., 2014; Overland et al., 2015; Overland, 2015), although, causal linkages between these concurrent events are open to discussion (e.g., McCusker et al., 2016; Meleshko et al., 2016; Overland et al., 2016).

While various studies suggest that these recent climate changes are induced by human activities (e.g., Abram et al., 2016; IPCC, 2014), it still remains unclear to which extent natural mechanisms may be involved. Instrumental climate data rarely cover more than the last century; sea ice observations using satellites did not even start before late 1978 (Stroeve et al., 2012). Hence, data reaching far beyond these instrumental time series are needed to assess the full range of natural environmental variability, especially the linkage between oceanic current changes and glacier instability. Sedimentary records covering centuries and millennia offer such archives of natural climate variations during pre-industrial times, i.e., without any significant anthropogenic impact. Also in the geological past, the Arctic has experienced periods of warming when ice shelves broke up and glaciers melted dramatically. The transition from the Pleistocene to the early Holocene, and especially the Holocene Thermal Maximum (HTM), when enhanced northward advection of Atlantic Water (AW; e.g., Sarnthein et al., 2003) and maximum insolation were recorded at high northern latitudes (Berger and Loutre, 1991), may help demonstrate ocean–glacier interactions under a fast warming trend, possibly comparable to the ongoing global warming.

Today, the advection of warm ocean currents is a main contributor to basal glacier melting in both hemispheres, which eventually leads to global sea level rise (e.g., Cook et al., 2016; Luckman et al., 2015; Straneo et al., 2010). Being situated at the only deep-sea gateway that connects the Arctic Ocean with the North Atlantic, the Svalbard Archipelago is an ideal location to investigate changes in the inflow of relatively warm AW into the Arctic Ocean and its influence on the sea ice regime, regional glacier activity and climatic conditions. This passage – the Fram Strait – is a major gateway for heat advection to high northern latitudes as well as for sea ice export from the Arctic towards lower latitudes. The majority of Arctic sea ice (~90 %; Rudels, 2009) and about 50% of its total freshwater (during the time period 1979–2001; Serreze et al., 2006) are exported through Fram Strait. More recent studies report an increasing liquid freshwater export of almost 4 % but decreasing sea ice export of ~17 % for the time period 2000–2010 compared to the previous 2 decades (e.g., Haine et al., 2015). Due to circulation of the northernmost branch of the North Atlantic Current along its western slope, Svalbard is bathed by warmer waters than any other Arctic location (Fig. 19a, b), providing the area with a relatively mild climate. In the present study, we chose a site at the mouth of Woodfjorden

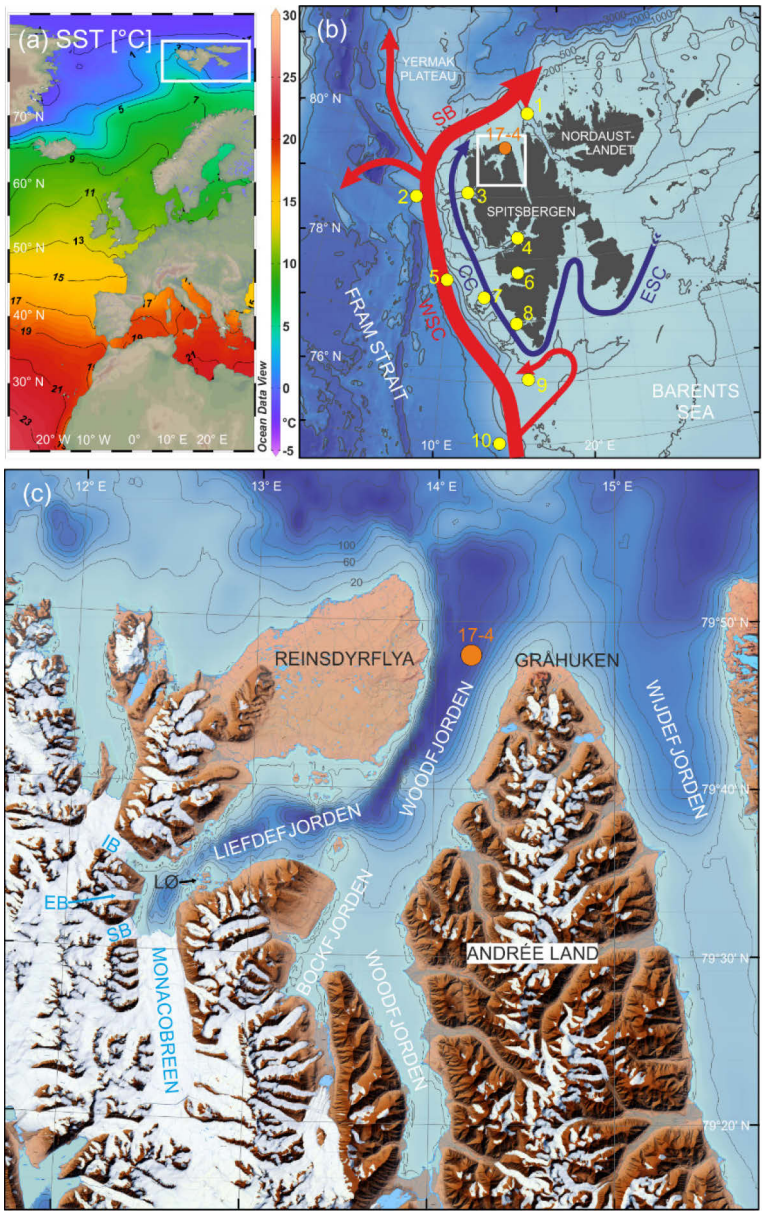

Fig. 19: (a) Average annual (1955–2012) sea surface temperatures (SSTs) of the North Atlantic (World Ocean Atlas/Ocean Data View; Locarnini et al., 2013; Schlitzer, 2015) White rectangle: Svalbard area as shown in (b). (b) Main ocean currents in the Svalbard area. Red arrows: Atlantic Water (WSC: West Spitsbergen Current; SB: Svalbard Branch). Blue arrows: Arctic Water (ESC: East Spitsbergen Current; CC: coastal current). The orange dot marks the study location (GeoB10*817-4*). Yellow dots mark other core sites mentioned in the text: 1. NP94-51 (Jernas et al., 2013; Koç et al., 2002; Ślubowska-Woldengen et al., 2007; Ślubowska et al., 2005); 2. MSM5/5-712-1 (Müller et al., 2012; Spielhagen et al., 2011; Werner et al., 2011, 2013, 2014); 3. NP05-11-21 (Jernas et al., 2013; Rasmussen et al., 2014b; Skirbekk et al., 2010); 4. JM98-845 (Rasmussen et al., 2012); 5. MD99-2304 (Hald et al., 2004); 6. MD99-2305 (Hald et al., 2004); 7. JM02-440 (Ślubowska-Woldengen et al., 2007); 8. HR3 (Majewski et al., 2009); 9. JM02-460 (Rasmussen et al., 2007); 10. 23258 (Sarnthein et al., 2003). White rectangle: study area as shown in (c). (c) Woodfjorden area with eponymous fjord and adjacent fjords. EB: Emmabreen; IB: Idabreen; SB: Seligerbreen; LØ: Lernerøyane. The orange dot marks the study location (GeoB10*817-4*). The bathymetric metadata and digital terrain model data products in (b) and (c) were derived from the EMODnet Bathymetry portal (http://emodnet-bathymetry.eu/). Topographic data in (c): © Norwegian Polar Institute (Norwegian Polar Institute, 2014).

(Fig. 19c), located at the northern margin of Svalbard where the main branch of AW enters the Arctic Ocean, for the documentation of ocean–ice interactions from deglacial times to the present. In this fjord system, which is fed today by tidewater glaciers, enhanced sedimentation rates offer a high temporal resolution.

During the Late Glacial Maximum (~21–18 ka; Svendsen et al., 2004), Svalbard´s glaciers and ice caps were part of the Svalbard–Barents Sea Ice Sheet. This grounded ice sheet covered the entire Barents Sea and expanded as far as the shelf break of Svalbard (Landvik et al., 1998). It must have been connected to the Fennoscandian Ice Sheet during the Last Glacial Maximum (Hughes et al., 2016; Landvik et al., 1998; Svendsen et al., 2004). Woodfjorden and its trough constituted one of the main northern gateways for fast flowing ice streams that drained the northwestern sector of these ice sheets during the Last Glacial Maximum (Hormes et al., 2013; Ottesen et al., 2007). Whereas the Holocene and in part the late Weichselian have been relatively well documented off (south) western Svalbard (Hald et al., 2004; Jernas et al., 2013; Majewski et al., 2009; Rasmussen et al., 2007, 2012, 2014c; Sarnthein et al., 2003; Skirbekk et al., 2010; Ślubowska-Woldengen et al., 2007; Werner et

al., 2011), palaeoceanographic records from northern Svalbard (Chauhan et al., 2014, 2015; Koç et al., 2002; Kubischta et al., 2011; Ślubowska et al., 2005) are still scarce (Fig. 19b). The present study aims to fill this gap, by compiling multi-proxy data, in particular, physical properties of the sediment, the faunal distribution and geochemical composition of benthic foraminifera, and biomarkers. Additionally, we generated a high-resolution record of ice-rafted debris (IRD) based on computer tomography. This set of proxies offers the opportunity to reconstruct the influence of AW in surface, intermediate and bottom waters, environmental conditions in surface waters and at the bottom water–sediment interface (including sea ice coverage and primary and export productivity), and glacier activity. Additionally, the study site is located at the transition zone from a glacier-influenced fjord milieu to an open ocean setting; therefore, very sensitive glacier responses to minor changes in oceanic forcing are expected.

5.2 Regional setting

The amount of AW entering the Arctic Ocean is primarily influenced by altering atmospheric pressure gradients and respective circulation patterns, i.e., the North Atlantic Oscillation (NAO) and the Arctic Oscillation (AO). Positive states of the NAO and the AO enhance AW advection, reduce the sea ice coverage and, hence, increase the salinity in the Arctic Ocean, while a negative NAO and AO decrease the AW inflow but foster the sea ice cover and the freshwater content (Rudels, 2009). AW is transported towards the Arctic Ocean by the West Spitsbergen Current (WSC; Fig. 19b). This current follows the western shelf break of the Barents Sea (the core of the WSC mainly appears between the 300 and 1000 m isobaths; e.g., Saloranta and Svendsen, 2001), continuing northward into the eastern Fram Strait (Rudels, 2009) where it sinks and flows below a colder and fresher surface water mass around 78° N (Johannessen, 1986; Manley, 1995). Therefore, heat loss to the atmosphere decreases as the warm AW core deepens (Beszczynska-Möller et al., 2011; Walczowski, 2013). Subsequently, the current is divided when a branch recirculates westward into the Fram Strait between 78 and 80° N (e.g., Hattermann et al., 2016; Schauer et al., 2004; Fig. 19b), merging with the cold and relatively fresh East Greenland Current that flows southward along the continental shelf of East Greenland (Rudels, 2009). At the northwestern shelf break of Spitsbergen, the WSC is separated into two branches that enter the Arctic Ocean (Fig. 19b). One branch circuits around the Yermak Plateau along its western slope flowing eastward into the Arctic Ocean (Yermak Branch). The second branch, namely the Svalbard Branch, crosses the southern Yermak Plateau and follows the northern shelf of Svalbard (Aagaard et al., 1987). Although the volume transport of the Svalbard Branch is smaller than that of the Yermak Branch (~1.8 Sv and ~4.9 Sv (Sverdrup), respectively; 1 Sv = 10^6 m^3 s^{-1}; Beszczynska-Möller et al., 2012) the former transports slightly warmer water than the latter (Beszczynska-Möller et al., 2012; Schauer et al., 2004).Therefore, the Svalbard Branch is considered as the most important route for warm, saline AW into the Arctic Ocean (Manley, 1995; Saloranta and Haugan, 2001). The volume transport of the WSC differs seasonally with highest values in winter and lowest in summer (Beszczynska-Möller et al., 2012). Additionally, the current is less stratified in winter caused by cooling in the Nordic Seas and current velocities are higher due to stronger wind forcing compared to the summer situation (von Appen et al., 2016). Atlantic-

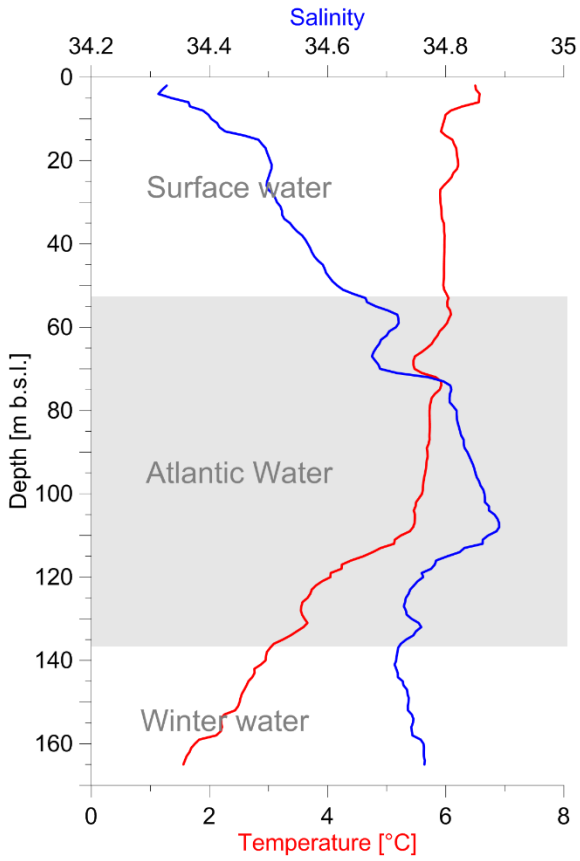

Fig. 20: Temperature and salinity against depth (in metres below sea level, m b.s.l.) at station MSM02/03-666-3 (same location as the studied sediment core GeoB10817-4; see sect. 5.3) derived during cruise MSM02/03 applying a Sea-Bird CTD sensor as described in the cruise report (Lherminier et al., 2009). The profile illustrates subsurface Atlantic Water inflow at the core site (grey shading), framed by less saline surface water on top and colder winter water at the bottom. winter water forms locally by convection processes during autumn–winter (Cottier et al., 2010). Temperature (>3 °C) and salinity boundaries (>34.65) following Cottier et al. (2005).

derived waters advected by the WSC are divided from colder and fresher Arctic waters (i.e., transported by the northern extension of the East Spitsbergen Current; Fig. 19b; Loeng, 1991; Skogseth et al., 2005) by the Arctic (Coastal) Front on the western and northern shelves of Svalbard (Walczowski, 2013). Thus, AW is only able to enter Svalbard´s shelf and fjords when surmounting this front. Barotropic instabilities seem to be the major mechanisms allowing AW to cross this temperature–salinity front (Cottier et al., 2005; Saloranta and Svendsen, 2001; Teigen et al., 2010). Especially during winter, wind-induced upwelling also significantly promotes AW advection across the Arctic (Coastal) Front (Cottier et al., 2005, 2007). In Woodfjorden, inflowing Atlantic-derived waters are stratified during summer – framed by a fresher surface water layer and a deeper colder water mass resulting from fall to winter vertical mixing processes (see illustrations of seasonal water mass distributions in a "typical" Svalbard fjord in Cottier et al., 2010), as illustrated by hydrographic data obtained during cruise MSM02/03 with RV *Maria S. Merian*, in August 2006 (Fig. 20).

The Woodfjorden system in northern Spitsbergen, the main island of the Svalbard Archipelago, includes the eponymous main fjord and the two tributary fjords Bockfjorden and Liefdefjorden (Fig. 19c). At present, only the latter is fed by four tidewater glaciers: Monacobreen and Seligerbreen (*-breen* means "glacier" in Norwegian), which form one joint glacier front, and the two smaller glaciers Emmabreen and Idabreen (Fig. 19c). Monacobreen is the 10th largest outlet glacier on Svalbard (Hagen et al., 1993). Meltwater from these glaciers contributes to the cold, relatively low-salinity surface water layer in the fjord (Fig. 20). Today, almost 60 % of Svalbard´s landmasses are glaciated (Hagen et al., 1993; Kohler et al., 2007). These almost 34,000 km^2 glaciers and ice caps represent 4.6 % of all glaciated areas on Earth (Radić et al., 2014). Calving of Svalbard´s tidewater glaciers causes a total mass loss of 5.0–8.4 km^3 yr^{-1} contributing ~2 % (0.02 mm yr^{-1}) to the annual global sea level rise (Błaszczyk et al., 2009).

5.3 Material and Methods

The 275 cm long sediment core GeoB10817-4 used in this study was retrieved at the mouth of Woodfjorden (N Spitsbergen; 79.80° N, 14.20° E; water depth 171 m; Fig. 19c) during cruise MSM02/03 in 2006

(Lherminier et al., 2009). Working halves were sampled with 10 ml syringes for microfossil analyses and grain size measurements at 5 cm intervals, as well as for biomarker analyses at a lower resolution at selected depths.

5.3.1 Computer tomography

Archive halves of the sediment core GeoB10817-4 were scanned using a Toshiba Aquilion 64™ computer tomograph (CT) at the hospital Klinikum Bremen-Mitte, with an x-ray source voltage of 120 kV and a current of 600 mA. The CT image stacks have a resolution of 0.35 mm in the x- and y-directions and 0.5 mm resolution in the z-direction (0.3 mm reconstruction unit). Images were reconstructed using Toshiba's patented helical cone beam reconstruction technique. The CT data obtained were processed using the ZIB edition of the Amira software (version 2016.25; Stalling et al., 2005). Within Amira, the CT scans of the core sections were merged and core liners, including about 2 mm of the core rims, were removed from the data set. All clasts > ~1 mm and bioturbation traces were quantified in each reconstruction slice with the "Segmentation Editor" (threshold segmentation) and the "Material Statistics" module. The threshold values used were >1,500 for lithic clasts, 601–1,499 for matrix sediment, 1–600 for bioturbation traces (open voids within the sediment that were filled by air and/or water were included), and <1 for the surrounding air and water. With the "Connected Components" module, the individual clasts were separated and subsequently analysed with the "Shape Analysis" module for their parameterization. The determined clast length was further used for a clast size analysis. Therefore, every clast within an interval of 167 CT slices (corresponding to a ~5 cm core interval) was considered and the obtained result was written to the depth of the central slice position. The analysing interval was moved slice by slice. The final results (unit: vol. % of all segmented clasts) were exported in a spreadsheet. Additionally, the x-ray density of the matrix sediment was evaluated by calculating the mean value and its standard deviation of the matrix sediment per slice (measured in Hounsfield units (HU); the matrix sediment segmentation was reduced by two voxels to exclude potential marginal artefacts).

5.3.2 AMS radiocarbon measurements

The chronostratigraphy of core GeoB10817-4 is based on 11 accelerator mass spectrometry (AMS) radiocarbon measurements from either mixed benthic foraminifera or *N. labradorica* tests, achieved at the CologneAMS, facility of the University of Cologne, or at the ETH of Zürich, respectively (Table 1). Radiocarbon ages were converted into calibrated years before present (before 1950 CE) using the radiocarbon calibration software CALIB 7.1 (calib.qub.ac.uk/calib/) and the Marine13 calibration curve (Reimer et al., 2013). Reservoir ages may have changed in the past, especially at high northern latitudes as well as during the Younger Dryas (YD) and during Heinrich Stadial 1 (Austin et al., 1995, 2011; Bard et al., 1994; Hanslik et al., 2010; Waelbroeck et al., 2001). However, as no information about palaeo-reservoir ages is available for the Svalbard area (see also Ślubowska-Woldengen et al., 2007) we applied an averaged regional reservoir age correction ($\Delta R = 98 \pm 37$ years), based on six ΔR values from the Svalbard region (Mangerud, 1972; Mangerud and Gulliksen, 1975; Olsson, 1980) derived from the Marine Reservoir Correction Database (calib.qub.ac.uk/marine/).

Table 1: AMS radiocarbon measurements and calibrated ages applying the Marine13 calibration curve (Reimer et al., 2013) and an averaged regional ΔR = 98±37 years (calib.qub.ac.uk). All measurements, apart from the measurements at 2.5 and 270.5 cm (CologneAMS, University of Cologne), were carried out at ETH Zürich. Median ages (in bold) were used for the age-depth model.

Lab ID	Depth	Dated material	^{14}C age		cal. age (2σ) [a BP]		
	[cm]		[a]	±	Min	Max	**Median**
COL2571.1.1	2.5	Mixed benthic foram.	879	31	307	496	**420**
ETH-58439	27.5	Mixed benthic foraminifera	2,155	45	1,499	1,795	**1,630**
ETH-61277	57.5	*N. labradorica*	7,845	65	8,035	8,360	**8,216**
ETH-64606	67	*N. labradorica*	8,815	60	9,217	9,519	**9,384**
ETH-61278	77	*N. labradorica*	9,395	75	9,846	10,339	**10,114**
ETH-61279	122	*N. labradorica*	9,980	75	10,613	11,082	**10,837**
ETH-61280	157	*N. labradorica*	10,230	75	10,873	11,306	**11,127**
ETH-58440	182.5	Mixed benthic foraminifera	10,710	70	11,445	12,276	**11,918**
ETH-64607	212	*N. labradorica*	11,120	80	12,283	12,726	**12,559**
ETH-58441	237	Mixed benthic foraminifera	11,810	70	13,000	13,363	**13,197**
ETH-64608	257	Mixed benthic foraminifera	11,610*	120		age reversal	
COL2572.1.1	270.5	Mixed benthic foraminifera	13,391	53	15,167	15,648	**15,391**

*The radiocarbon age from 257 cm was excluded from the age–depth model (as discussed in sect. 5.4.2).

5.3.3 Grain size measurements

Grain size measurements were performed in the Grain Size Lab at MARUM, University of Bremen with a Beckman Coulter laser diffraction particle size analyser LS 13320™. Prior to these measurements, the terrigenous sediment fractions were isolated by removing organic carbon, calcium carbonate, and biogenic opal by boiling the samples (in about 200 ml water) with 10 ml of H_2O_2 (35 %; until the reaction stopped), 10 ml of HCl (10 %; 1 min) and 6 g of NaOH pellets (10 min), respectively. After each step the samples were diluted (dilution factor: >25). Finally, remaining aggregates were destroyed prior to the measurements by boiling the samples with ~0.3 g of tetrasodium diphosphate decahydrate ($Na_4P_2O_7$ * $10H_2O$; 3 min; see McGregor et al., 2009). Sample preparation and measurements were carried out with deionized, degassed and filtered water (filter mesh size: 0.2 µm) to reduce the potential influence of gas bubbles or particles within the water. Results consist of grain size distributions within a 0.04 to 2,000 µm range, divided into 116 size classes. The calculation of the grain sizes relies on the Fraunhofer diffraction theory and the polarization intensity differential scattering (PIDS) for particles from 0.4 to 2,000 µm and from 0.04 to 0.4 µm, respectively. Reproducibility is checked regularly through replicate analyses of three internal glass-bead standards. It is better than ±0.7 µm for the mean and ±0.6 µm for the median grain size (1σ). The average standard deviation integrated over all size classes is better than ±4 vol. % (note that the standard deviation of the individual size classes is not distributed uniformly). All provided statistic values are based on geometric statistics.

Sediment grains larger than 310 µm have not been detected by the laser diffraction particle size analyser although coarser sand particles and even gravels are detected within the sieved samples of the microfossil analysis as well as within the CT clast size analyses (see sect. 5.3.4 and sect. 5.4.1; Fig. 21a). This bias results from the very small sample volume (~0.5 ml) for the particle size analysis. However, taking into account that

>98 wt. % of the dried bulk sediment is <150 µm (with the exception of four samples with 3, 4, 6 and 12 wt. % >150 µm fraction; Bartels, unpublished data), the observed grain size patterns of the siliciclastic fraction are considered as reliable.

5.3.4 Microfossil analyses

Bulk sediment samples were washed through a 63 µm sieve. The coarse fraction was dried and sieved through 100 µm and 150 µm meshes. Faunal analyses were carried out on two fractions: 100–150 µm and >150 µm (Fig. A1 in the Appendix). Counts from both fractions were summed up (i.e., >100 µm) for the discussion below. Samples with high numbers of foraminifera were split with a microsplitter. Wherever possible, 200–300 benthic foraminifera were counted in each fraction of every sample to obtain statistically robust results (Murray, 2006; Patterson and Fishbein, 1989). In addition, three replicates of an un-split as well as of a split sample were counted (each split was counted four times, including the initially counted sample). Statistical calculations reveal a standard error of 3.52 and 2.95 %, respectively. Most benthic foraminifera were identified to species level except for agglutinants, which were mainly identified to genera level due to their poorer preservation. The majority of calcareous benthic foraminifera are well preserved, but several specimens show indications of dissolution or transport. Small fragments were not counted since these specimens might be allochthonous. Distinct *Stainforthia* and *Buccella* morphotypes were lumped together as *Stainforthia loeblichi* s.l. and *Buccella frigida* s.l., respectively, because in each case possibly two species (*S. loeblichi* s.s. and *S. concava* as well as *B. frigida* s.s. and *B. tenerrima*, respectively) could not be distinguished definitely. Hyaline and agglutinating species that could not be identified are summarized as Rotaliina and Textulariina, respectively. Only few planktonic foraminifera were present in the material. As post-mortem degradation might be the main reason for the distribution of arenaceous taxa (Murray, 2006), percentages of calcareous benthic species were calculated excluding agglutinants to avoid these taphonomic effects.

Accumulation rates of benthic foraminifera were calculated following the equation of Ehrmann & Thiede (1985):

$$\mathrm{ARBF} = \mathrm{LSR} * \rho * \mathrm{BFN}, \quad (8)$$

where ARBF is the accumulation rate of benthic foraminifera [individuals cm^{-2} ka^{-1}], LSR the linear sedimentation rate [cm ka^{-1}], ρ the density of dry sediment [g cm^{-3}] and BFN the benthic foraminifera number (per gram dry sediment) [individuals g^{-1}].

5.3.5 Stable isotope measurements

Stable carbon and oxygen isotopes were measured at ZMT (Leibniz Centre for Tropical Marine Ecology) in Bremen, using a Finnigan MAT 253™ gas isotope ratio mass spectrometer with a Kiel IV automated carbonate preparation device (standard deviations of house standard: 0.02 ‰ for $\delta^{13}C$ and 0.06 ‰ for $\delta^{18}O$), and at MARUM (Bremen) using a Finnigan MAT 251™ mass spectrometer with a Kiel I carbonate preparation device (standard deviations of house standard: 0.02 ‰ for $\delta^{13}C$ and 0.03 ‰ for $\delta^{18}O$). The measurements were performed on two to eight tests (test size: 150–500 µm) of the epibenthic foraminifera *Cibicides lobatulus* (Ahrens et al., 1997; Dubicka et al., 2015) and the endobenthic foraminifera *Nonionellina*

labradorica (Ahrens et al., 1997; Alve and Bernhard, 1995; Loubere and Rayray, 2016) for bottom water and pore water signals, respectively. Stable oxygen isotope values were corrected for a global ice volume effect (Waelbroeck et al., 2002) and adjusted for vital effects: +0.64 ‰ for *C. lobatulus* (Shackleton, 1974) and -0.2 ‰ for *N. labradorica* (Duplessy et al., 2005).

5.3.6 Biomarker analyses

Selected dried sediment samples were homogenized and used for geochemical analyses. For the determination of the total organic carbon (TOC) content using an ELTRA™ analyser, 100 µg of sediment were used. Alkenone analyses, carried out to reconstruct sea surface temperatures (SSTs), were extracted using 2 g of sediment with an accelerated solvent extractor (DIONEX™, ASE 200; 100 °C, 1,000 psi, 15 min, dichloromethane and methanol (99:1, v/v) as solvent). The separation of compounds was carried out using open column chromatography (SiO_2) using *n*-hexane, dichloromethane (1:1, v/v) and dichloromethane. The composition of alkenones was analysed using gas chromatography (Agilent™ 7890). Individual alkenone ($C_{37:4}$, $C_{37:3}$, $C_{37:2}$) identification is based on retention time and the comparison with an external standard.
The alkenone unsaturation index (U_{37}^{K}) as proxy for SST (°C) was calculated following Brassell et al. (1986) due to the presence of the $C_{37:4}$ alkenone. For calculating SST, the equation

$$U_{37}^{K'} = 0.033 * \mathrm{T}\,(°\mathrm{C}) + 0.044 \quad (9)$$

by Müller et al. (1998) – based on a global core-top calibration (60° N–60° S) – was used (replacing $U_{37}^{K'}$ using U_{37}^{K} due to the presence of the $C_{37:4}$ alkenones). This equation (Eq. 9) yielded more realistic results compared to other equations whose temperature reconstructions were much too high (e.g., Prahl and Wakeham, 1987). The standard error of the calibration is reported as ±1.5 °C. The instrument stability was continuously controlled using re-runs of an external alkenone standard (extracted from *Emiliania huxleyi* cultures with known growth temperature) during the analytical sequences. The range of the total analytical error calculated by replicate analyses is less than 0.4 °C.
The C_{25} isoprenoid lipid biomarker (IP_{25}) was analysed to document sea ice coverage (Belt et al., 2007). Brassicasterol and dinosterol have been used as phytoplankton biomarkers (see Fahl and Stein, 1999; Volkman, 1986; Volkman et al., 1993). For extraction of IP_{25} and sterols, 3 g of sediment was ultrasonicated (Sonorex Super RK 510, 35 Khz, 15 min) using dichloromethane:methanol (2:1, v/v) as solvent. For quantification, internal standards 7-hexylnonadecane (7-HND, 0.076 µg per sample for IP_{25} quantification), squalane (2.4 µg per sample) and cholest-5-en-3β-ol-D_6 (10 µg per sample for sterol quantification), were added prior to analytical treatment. Separation of the hydrocarbon and sterol fractions was carried out via open column chromatography (hydrocarbon fraction with 5 ml *n*-hexane, the sterol fraction with 6 ml *n*-hexane:ethylacetate (5:1, v/v)). The latter fraction was silylated with 500 ml BSTFA (bis-trimethylsilyl-trifluoroacet-amide) (60 °C, 2h). IP_{25} and sterols were analysed using gas chromatography and mass spectrometry. Component assignment was based on comparison of gas chromatography retention times with those of reference compounds and published mass spectra. The Kovats index calculated for IP_{25} is 2,086. The detection limit for quantification of IP_{25} (Agilent 7890B GC™, Agilent 5977A™ Extractor MSD with performance turbo pump) is 0.005 ng μL^{-1} in SIM (selected ion monitoring) mode. The retention indices for brassicasterol (as 24-methylcholesta-5,22E-dien-3β-O-Si(CH_3)$_3$) and dinosterol (as 4α,23,24-trimethyl-5α-

cholest-22E-en-3β-O-Si(CH_3)$_3$) were calculated to be 1.018 and 1.091 (normalized to cholest-5-en-3β-ol-D_6 set to be 1.000), respectively.

For the quantification of IP_{25}, its molecular ion (*m/z* 350) in relation to the abundant fragment ion *m/z* 266 of the internal standard (7-HND) was used (SIM mode). The different responses of these ions were balanced using an external calibration (Fahl and Stein, 2012). Brassicasterol and dinosterol were quantified as trimethylsilyl ethers using the molecular ions *m/z* 470 and *m/z* 500, respectively, in relation to the molecular ion *m/z* 464 of cholesterol-D_6. For more details about the quantification of IP_{25} as well as the sterols see Fahl and Stein (2012). Accumulation rates of sea ice and phytoplankton biomarkers (IP_{25} and brassicasterol, respectively) were calculated following Eq. (8) by replacing the BFN term accordingly.

For more semi-quantitative estimates of present and past sea ice coverage, Müller et al. (2011) combined the sea ice proxy IP_{25} and phytoplankton biomarkers in a phytoplankton-IP_{25} index, the so-called PIP_{25} index:

$$PIP_{25} = \frac{[IP_{25}]}{[IP_{25}]+([phytoplankton\ marker]*c)}, \quad (10)$$

with c equal to the mean IP_{25} concentration divided by the mean phytoplankton biomarker concentration.

As phytoplankton biomarker, brassicasterol was used (for further discussion of advantages and limitations of the PIP_{25} approach see Belt and Müller, 2013; Smik et al., 2016; Stein et al., 2012; Xiao et al., 2015). Following the classification scheme of Müller et al. (2011), PIP_{25} values between 0.3 and 0.5, between 0.5 and 0.7, and >>0.7 point to a reduced sea ice cover, a seasonal sea ice cover including an ice edge situation, and an extended to perennial sea ice cover, respectively.

5.4 Results

5.4.1 Core description

The sediment of core GeoB10817-4 consists of some coarse sand and gravel, with scattered pebbles (Fig. 21a) embedded in a homogeneous silty clay matrix sediment. The upper ~30 cm of the sediment core are heavily bioturbated, as illustrated by the CT scan. The interval between 31 and 54 cm is characterized by a basal erosional unconformity, weakly visible on the CT picture (Fig. 21b), and high amounts of (extra- and intra-) clasts (Fig. 21b), sand (including high quantities of foraminiferal tests), and bivalve shell fragments. Furthermore, the interval exhibits an increasing x-ray density with an enhanced standard deviation accompanied by a coarsening upward of the siliciclastic fine fraction (<63 µm; observed in the grain size analyses; Fig. A2 in the Appendix). These sedimentological features point to an allochthonous origin and a deposition by mass wasting. Consequently, this interval is excluded from the subsequent palaeoceanographic reconstructions. Below this disturbance and as deep as 140 cm, a small number of clasts are found, whereas the lower part of the core contains high amounts of coarse debris (Fig. 21a).

5.4.2 Chronology

Assuming linear sedimentation rates between dated depths (ranging between 8 and 121 cm ka^{-1}), calibrated ages have been interpolated (Fig. 21c; Table 1). The segment below the 31–54 cm interval (sect. 5.4.1) covers a time span from ~15.7 to 7.8 cal. ka, whereas the one above ranges from ~1.8 to 0.3 cal. ka (from here on, all ages are given as calibrated ages BP and data are presented exclusively against age). This indicates that the deposition of the 31–54 cm layer led to a ~6,000-year gap in the sequence, spanning a large part of the

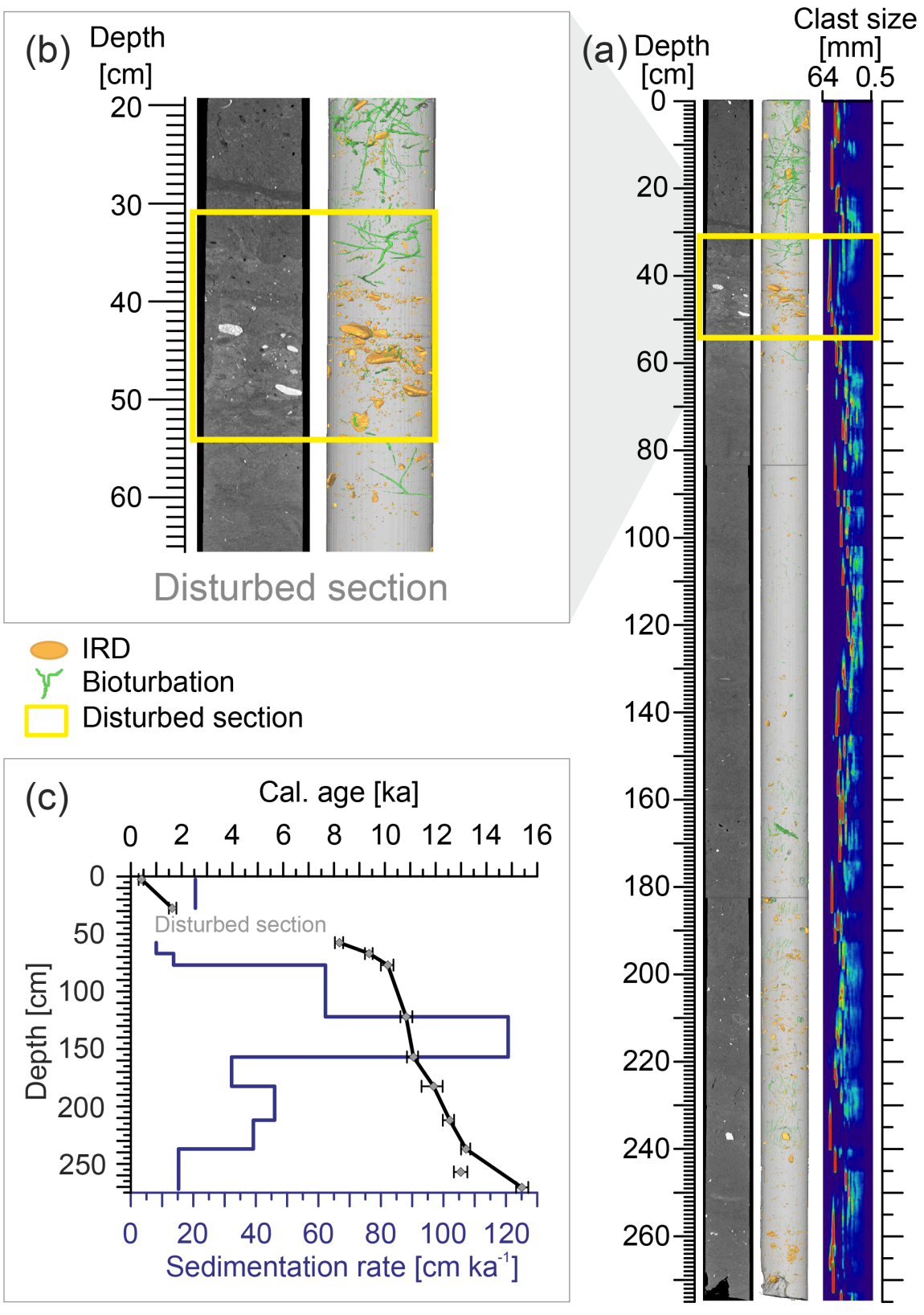

Fig. 21: (a) CT scan of the core GeoB10817-4. Left to right: orthogonal profile; interpreted image (clasts and bioturbation, see legend); clast size distribution (0–20 vol. % of clasts: blue to red, respectively). The yellow rectangle marks the disturbed section also shown in (b). (b) CT images (orthogonal and interpreted) of the disturbed section (yellow rectangle; definition of boundaries: see sect. 5.4.1 and Fig. A2 in the Appendix). (c) Age–depth plot for sediment core GeoB10817-4: The diamonds show calibrated (median) ages with error bars (Table 1); the solid black line shows linear interpolation excluding an outlier at 257 cm. The blue solid line shows corresponding sedimentation rates.

Holocene. The radiocarbon age at 257 cm depth has been excluded from the age model because it was obtained from a much smaller sample (~0.4 mg carbonate) than the overlying 237 cm deep older sample (~4.3 mg) that has been measured four times with consistent results.

5.4.3 Sedimentology

5.4.3.1 Grain sizes

Until ~13 ka, the grain size distribution of siliciclastic sediments reached a maximum of about 7 µm (mean: 4–6 µm). In the subsequent period until ~11.1 ka, a slight coarsening (max. at ~8–9 µm, mean: 6–7 µm) is observed. A further shift to coarser silt (max. at ~20 µm, mean: 8–9 µm) appeared around 10.8 ka. From ~9.4 ka on, silt around 45–50 µm shows the highest percentages (mean: 11–15 µm). In the uppermost interval of the core (~1.6–0.4 ka), a trend back to finer sediments (mean: 7–10 µm) is evident, but with a more even distribution than below the disturbed section (Fig. 22a, b).

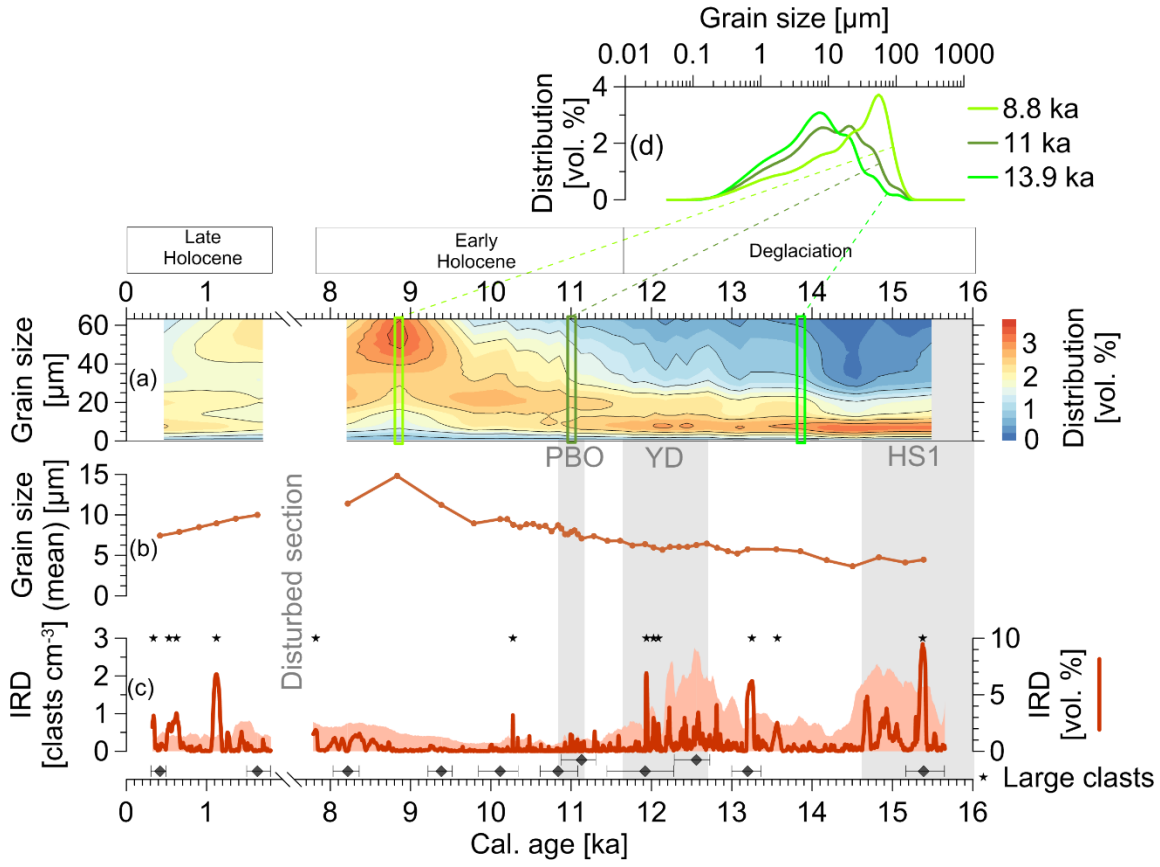

Fig. 22: (a) Grain size distribution [vol. %] of fine siliciclastic sediments (0–63 µm) derived from laser diffraction particle size analyses. Green rectangles: selected grain size distributions as shown in (d). (b) Mean grain size [µm] of siliciclastic sediments. (c) Ice-rafted debris (IRD): volume percentage (solid red line) and clasts per cubic centimetre (reddish shading) derived from CT analysis. Stars mark peaks in vol.% corresponding to single large clasts. Grey vertical shadings indicate cold periods: Preboreal Oscillation (PBO), Younger Dryas (YD) and Heinrich Stadial 1 (HS1). Dark grey diamonds: calibrated radiocarbon dated depths with error ranges. (d) Selected grain size distributions [vol. %] at ~8.8 ka (light green line), ~11 ka (dark green line) and ~13.9 ka (green line).

5.4.3.2 Ice-rafted debris

Clasts > ~1 mm detected using CT analyses (sect. 5.3.1) were considered as IRD. The interpretation of the IRD abundances is based on the volume percentages and number of clasts observed on CT scans, as the combination of these data depicts the best available IRD distribution (Fig. 21a and Fig. 22c): only a consideration of volume percentages would overestimate large clasts while the number of clasts alone would overestimate the significance of small debris. For comparison, accumulation rates of counted clasts (>500 µm; based on Ehrmann & Thiede, 1985) from sieved syringe samples are shown in the Appendix (Fig. A3) illustrating that the CT-based data offer a much more precise IRD record. CT data show that IRD is more abundant at the core bottom, containing high quantities prior to ~14.5 ka (up to 10 vol. %; up to 2.3 clasts cm^{-3}), but decrease afterwards (down to 0 % and 0.4 clasts cm^{-3}). From ~13.1 ka on, IRD amounts rise again until ~11.5 ka (max. 7 %; max. 2.8 clasts cm^{-3}). From then on, the volume percentages and number of clasts illustrate a low but continuous flux of ice-rafted material (mean: 0.2 %; 0.3 clasts cm^{-3}), and some increase particularly from ~8.5 ka on (up to 1.9 % and 0.8 clasts cm^{-3}). Above the reworked layer (from ~1.8 ka on), a further increase in the IRD content is identified especially for larger clasts (up to 7 % and 0.8 clasts cm^{-3}; Fig. 22c). Some peaks in volume percent reflect single large clasts (marked with a star in Fig. 22c).

5.4.4 Microfossil analyses

5.4.4.1 Faunal composition

Planktic foraminifera were rare or absent. Their percentages range between 0 and 2 % of the total fauna apart from one sample dated ~13 ka (~5 %). Thus, only benthic species were taken into account for calculations and interpretation. In total, 83 taxa (61 calcareous species) were identified (7–56 taxa per sample, 7–39 calcareous taxa per sample; Appendix A: Lists of benthic foraminiferal species appearing in sediment core GeoB10817-4). Calcareous species represent the major part of the benthic fauna (~80–100 %), agglutinating species occur mainly in the upper part above the reworked layer (up to ~20 %) with decreasing percentages down-core (mean: ~2 %; Fig. A4a in the Appendix).

5.4.4.2 Relative abundance and accumulation rate (flux) of benthic foraminifera

The calcareous fauna is dominated by three species: *Cassidulina reniforme* (~18–78 %, Fig. 23h), *Nonionellina labradorica* (~1–60 %, Fig. 23e) and *Elphidium clavatum* (formerly named *E. excavatum* forma *clavata*, see Darling et al., 2016; ~2–46 %, Fig. 23g), accompanied by lower percentages of *Buccella frigida* s.l. (max. ~9 %, Fig. 23c), *Cassidulina neoteretis* (max. ~23 %, Fig. 23f), *Cibicides lobatulus* (max. ~5 %, Fig. 23b), *Islandiella helenae* (max. ~10 %, Fig. 23d), *Islandiella norcrossi* (max. ~8 %, Fig. A4g in the Appendix) and *Stainforthia loeblichi* s.l. (max. ~8 %, Fig. A4i in the Appendix).

Until ~12.5 ka the accumulation rate of benthic foraminifera (ARBF) is relatively low (mean value: ~2,250 individuals (ind.) $cm^{-2}\,ka^{-1}$) subsequently slightly increasing up to a mean value of ~4,770 ind. $cm^{-2}\,ka^{-1}$. Apart from a few exceptions, the ARBF further rises from ~11.2 ka on (mean value: ~12,980 ind. $cm^{-2}\,ka^{-1}$) with peaks at ~10.8, ~10.6 and ~10.1 ka exceeding 30,000 ind. $cm^{-2}\,ka^{-1}$ (Fig. 23a). Above the disturbed section (from ~1.6 ka on), the mean ARBF reaches ~6,530 ind. $cm^{-2}\,ka^{-1}$.

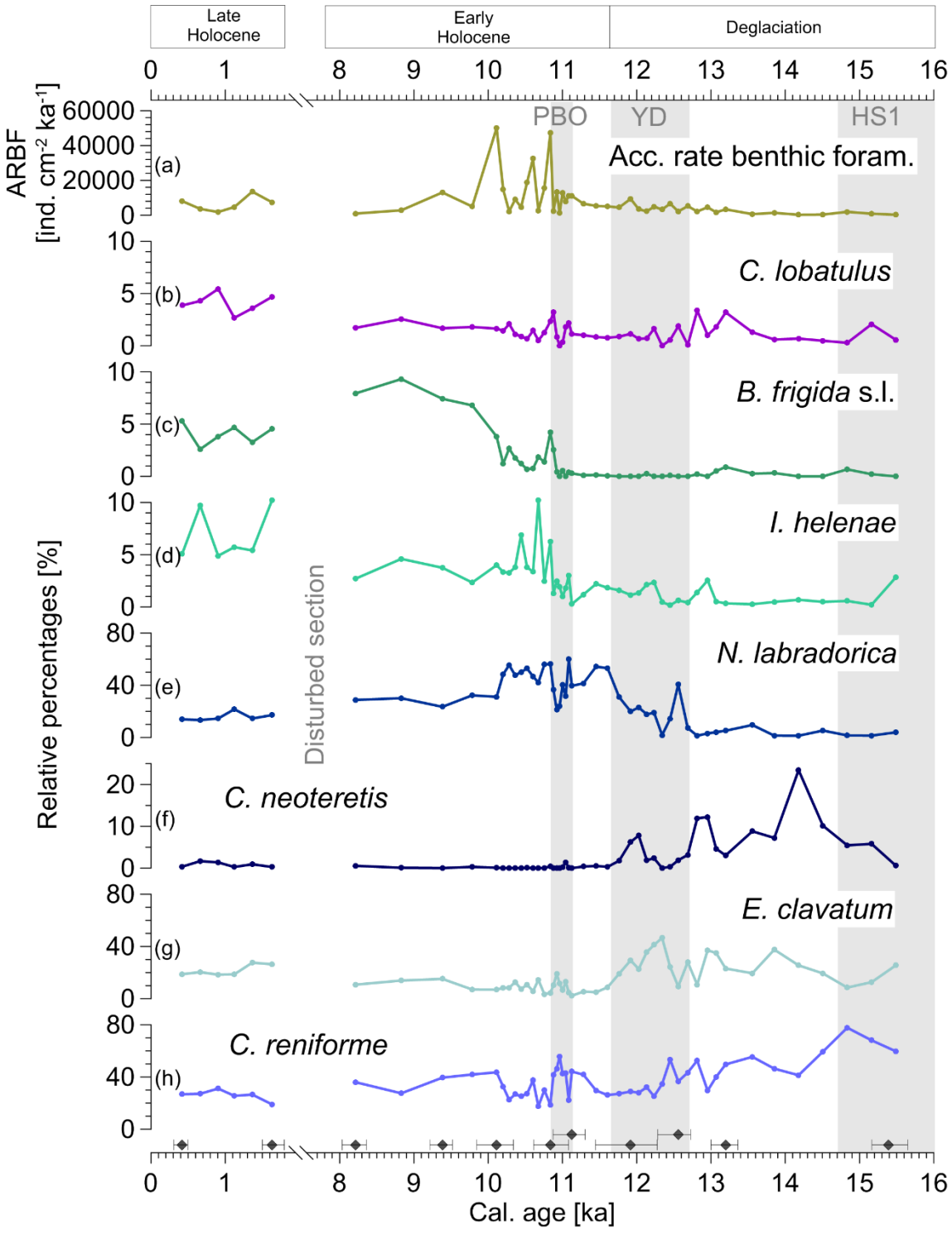

Fig. 23: (a) Accumulation rates of benthic foraminifera (ARBFs) and (b–h) relative percentages of dominant calcareous benthic foraminifera. (b) *Cibicides lobatulus*. (c) *Buccella frigida* s.l. (d) *Islandiella helenae*. (e) *Nonionellina labradorica*. (f) *Cassidulina neoteretis*. (g) *Elphidium clavatum*. (h) *Cassidulina reniforme*. Grey vertical shadings; see Fig. 22. Dark grey diamonds: calibrated radiocarbon ages with error ranges.

5.4.5 Geochemistry

5.4.5.1 Stable isotopes

Stable oxygen isotope values, corrected for vital effects and the global ice volume effect (sect. 5.3.5), increase slightly towards core top with *C. lobatulus* showing more variability and lower values than *N. labradorica* (ranging from 2.5 to 4.1 ‰ and from 3.6 to 4.4 ‰, respectively). Between ~12 and ~9 ka, $\delta^{18}O$ values of both species exhibit an enhanced offset (Fig. 24a). Stable carbon isotope values show minor variations for *C. lobatulus*, but a slight increase towards core top (0.4 to 1.6 ‰). *N. labradorica* exhibits depleted $\delta^{13}C$ values from ~11 to ~10.1 ka (down to -2.7 ‰; Fig. 24b). The $\delta^{13}C$ offset between epi- and endobenthic species ($\Delta\delta^{13}C$) varies between 1.7 and 3.7 ‰, with peak values at ~12.6, ~10.6, ~10.4 ka and ~0.4 ka (Fig. 24c).

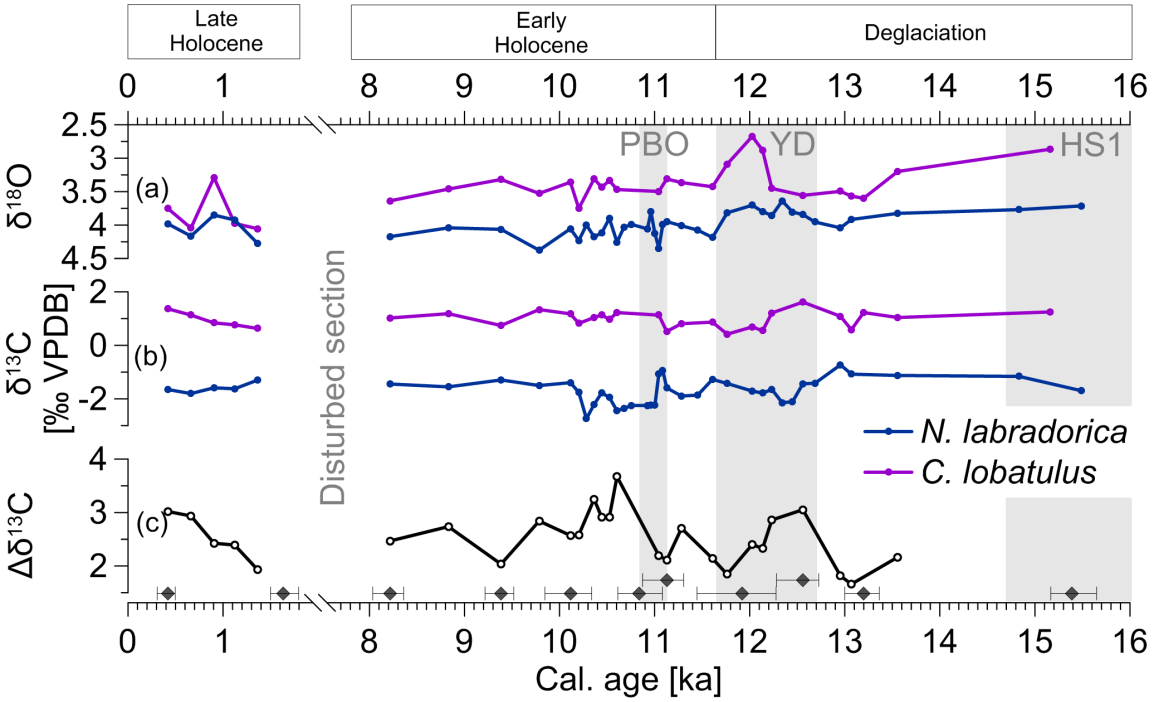

Fig. 24: (a) Stable oxygen isotopes (corrected for vital effects and the global ice effect; see sect. 5.3.5) and (b) stable carbon isotopes of the epibenthic species *Cibicides lobatulus* (purple line) vs. the endobenthic species *Nonionellina labradorica* (blue line). (c) Difference between epi- and endobenthic stable carbon isotope compositions. Grey vertical shadings; see Fig. 22. Dark grey diamonds: calibrated radiocarbon ages with error ranges.

5.4.5.2 Biomarkers

Alkenone unsaturation index (U^K_{37}) values range from 0.1 to 0.3. They yield SST values ranging from ~1 to ~7 °C. The highest temperatures were attained between ~11 and ~10 ka, whereas the lowest values are calculated prior to ~11.9 ka (Fig. 25a).

Accumulation rates of the C_{25} isoprenoid lipid biomarker (IP_{25}) range between 0.8 µg cm^{-2} ka^{-1} (~11 ka) and almost 0 µg cm^{-2} ka^{-1} (~9.4 ka; Fig. 25c). The phytoplankton-IP_{25} index (PIP_{25} index) using the phytoplankton biomarker brassicasterol (cf., Müller et al., 2011) exhibits its highest values at ~12.8 ka (~0.9) and its lowest values at ~9.4 ka (~0.1; Fig. 25b).

The accumulation rates of brassicasterol range between ~1.5 µg cm^{-2} ka^{-1} (~14.2 ka) and ~167.5 µg cm^{-2} ka^{-1} (~10.9 ka; Fig. 25d). The accumulation rate of dinosterol shows an almost parallel trend to that of brassicasterol but values are 1 magnitude lower (Fig. A5 in the Appendix).

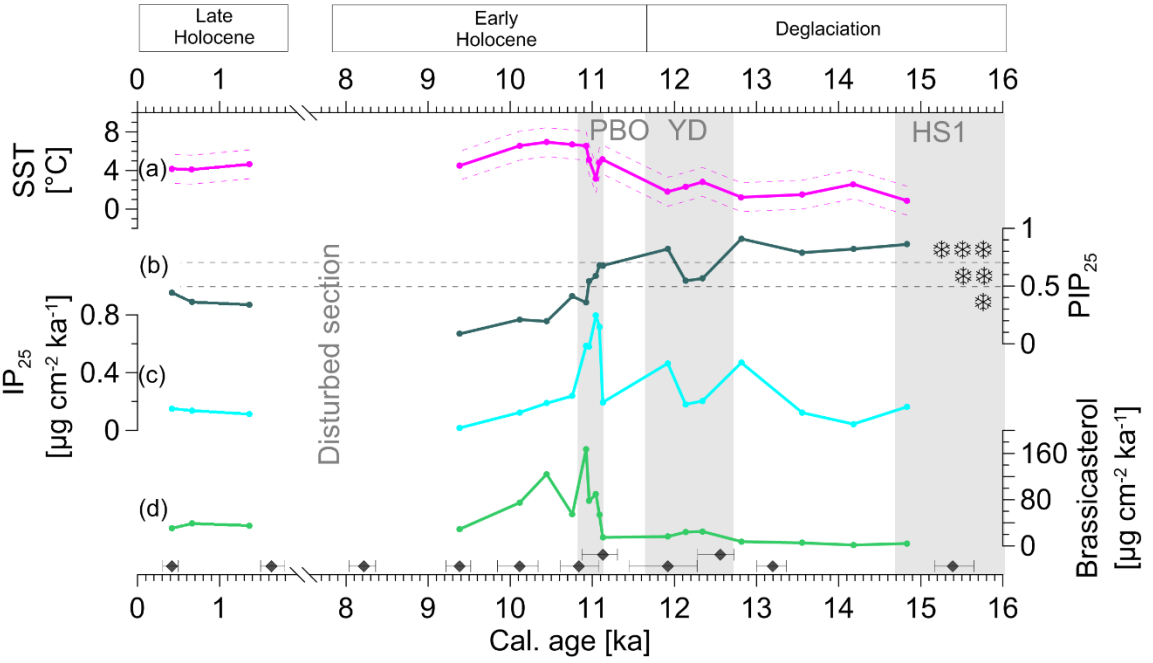

Fig. 25: (a) Sea surface temperature (SST) with standard error (±1.5 °C) derived from alkenone unsaturation index (U^K_{37}) (Brassell et al., 1986; Müller et al., 1998). (b) Phytoplankton (brassicasterol)-IP_{25} index (PIP_{25}). 0.3 to 0.5: reduced sea ice cover (❄), 0.5 to 0.7: seasonal sea ice cover (❄❄), >>0.7: extended to perennial sea ice cover (❄❄❄) (Müller et al., 2011). (c) Accumulation rate of the sea ice biomarker IP_{25}. d) Accumulation rates of phytoplankton biomarker brassicasterol. Grey vertical shadings; see Fig. 22. Dark grey diamonds: calibrated radiocarbon ages with error ranges.

5.5 Interpretation and discussion

5.5.1 Late Weichselian (until ~12.7 ka) – deglaciation in the Woodfjorden area

In the Woodfjorden area, the Heinrich Stadial 1 (until ~14.6 ka) was characterized by a very high IRD content (Fig. 26b) signifying enhanced calving of the glacier front. The increased percentages of fine siliciclastic sediments within this interval (mean: ~4–5 µm; Fig. 26a) point to some contemporaneous intensified meltwater outflows (in this study, sources of siliciclastic sediments were interpreted as terrigenous). Thus, it is assumed that parts of the Svalbard–Barents Sea Ice Sheet disintegrated during Heinrich Stadial 1 while stable oxygen isotope records of the NGRIP ice core show that atmospheric temperatures remained cold (Fig. 26g; Rasmussen et al., 2014a). Contrastingly, bottom waters might have been relatively warm and/or saline as indicated by the appearance of the benthic foraminiferal species *C. neoteretis* (Fig. 26d) as well as the high percentages (up to ~80 %) of *C. reniforme* (Fig. 23h). The occurrence of *C. neoteretis* has been connected with a strong influence of AW in bottom waters because this species is assumed to respond to a limited temperature and salinity range as well as to an enhanced food supply (Jennings et al., 2004; Jennings and Helgadottir, 1994; Mackensen et al., 1985; Rytter et al., 2002; Seidenkrantz, 1995; Seidenkrantz et al., 2013; Steinsund, 1994). *C. reniforme* also prefers saline bottom waters (Hald and Korsun, 1997; Jennings et al., 2004) and may therefore be linked to the intrusion of AW into bottom waters. The advection of AW as a subsurface or even bottom water mass during Heinrich Stadial 1 as well as during earlier Heinrich stadials,

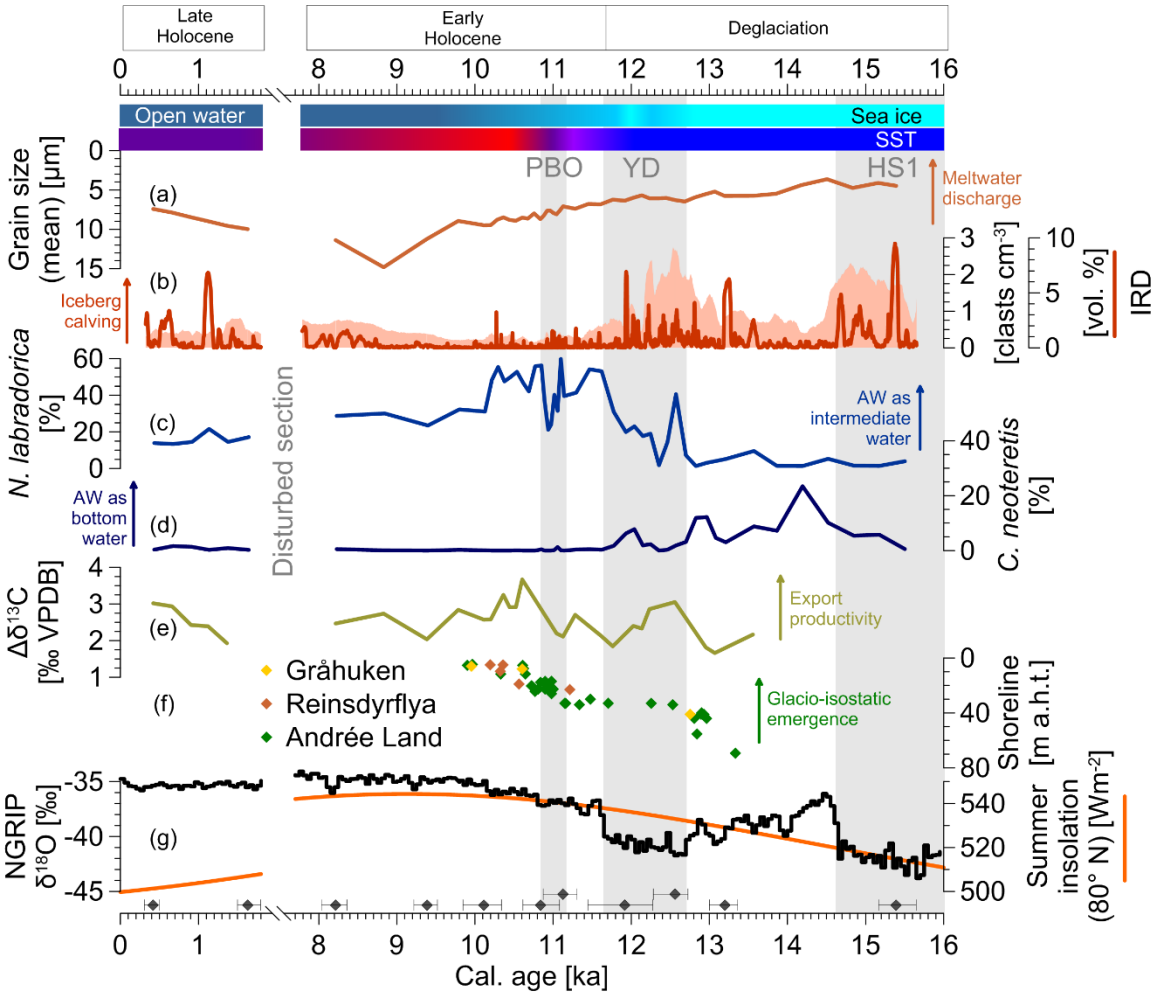

Fig. 26: The blueish horizontal bar on top symbolizes sea ice coverage based on biomarker data (PIP_{25} index). Red–blue horizontal bar symbolizes (qualitative) sea surface temperatures (red: warm, blue: cold) based on biomarker data (alkenones). (a) Mean grain size of siliciclastic (terrigenous) sediments: low values illustrate deposition of suspended sediment from meltwater plumes (note descending y-axis). (b) Volume percentage of ice-rafted debris (solid red line) and number of clasts per cubic centimetre (reddish shading) signifying glacier activity (iceberg calving). (c) Relative percentages of *N. labradorica*. High percentages: Atlantic Water intrusion into intermediate waters delivering nutrients into the photic zone. Note the almost parallel increase in export production as illustrated in (e). (d) Relative percentages of *C. neoteretis*. High percentages: Atlantic Water advection into bottom waters. (e) Offset of epi- and endobenthic $\delta^{13}C$ values indicating export productivity. (f) Radiocarbon-dated beach ridges in the Woodfjorden area (Forman et al., 2004) illustrating glacio-isostatic emergence (in metres above high tide, m a.h.t.; note descending y-axis). Colours mark different locations as indicated in the legend (locations shown in Fig. 19c). (g) Stable oxygen isotopes from NGRIP ice core (black line; Rasmussen et al., 2014a) and June–July insolation at 80° N (orange line; Berger and Loutre, 1991). Grey vertical shadings; see Fig. 22. Dark grey diamonds: calibrated radiocarbon ages with error ranges.

has already been proposed for the Svalbard area by Rasmussen et al. (2007, 2014c). Today, basal melting of tidewater glaciers in Spitsbergen from high advection rates of the relatively warm AW, is evident (Luckman et al., 2015).

Thus, during Heinrich Stadial 1, the influx of AW in the Woodfjorden area possibly contributed to the destabilization of glacier fronts. Apart from oceanic heat advection, topographic features of the relatively wide Woodfjorden system may have promoted the glacier retreat. Gump et al. (2017) reported a deglaciation of narrower fjords with higher surrounding mountains in southwestern Norway delayed more than 1000 years (see also Stokes et al., 2014).

During the Bølling interstadial (~14.6–14 ka), a continuing outflow of meltwater is expected as the grain size distribution still exhibits a peak around 7 µm (mean: ~4 µm; Fig. 22a, b and Fig. 26a). Simultaneously, the sediment shows a reddish colour (Munsell code 10R4/6) probably connected to sediment plumes loaded by glacial flour from the erosion of Devonian Old Red sandstones. Source rocks, i.e., the Wood Bay Formation, crop out at the northwestern as well as at the southeastern coast of Woodfjorden (Reinsdyrflya and Andrée Land, respectively; Fig. 19c; Harland, 1998). Melting glaciers from the former lowland may have been a potential source of these reddish sediments. This interpretation is supported by ^{10}Be ages of erratic boulders which suggest that Reinsdyrflya started to deglaciate during Heinrich Stadial 1 and became ice-free during the Bølling–Allerød (Gjermundsen et al., 2013; Hormes et al., 2013). Rasmussen and Thomsen (2013) reported on pink sediment layers derived from Devonian red beds in sediment cores from the northwestern slope of Svalbard. They interpreted those layers as deposited by meltwater plumes during interstadials. Forwick et al. (2010) also suggested that meltwater run-off connected to retreating glaciers was one possible source for fine reddish sediments deposited close to glacier fronts. Correspondingly, a glacier-proximal position is likely at our core site where tidewater glaciers may have successively waned. Percentages of *C. neoteretis* reached their maximal values during the Bølling (Fig. 26d). Almost simultaneously, this taxon peaked at the southwestern margin (Rasmussen et al., 2007) and at the northern margin of Svalbard (Ślubowska-Woldengen et al., 2007; Ślubowska et al., 2005) as well as in the Laptev Sea (off northern Siberia; Taldenkova et al., 2010) – although with considerably higher values probably deriving from a more direct influence of AW and greater water depths compared to our core location. Massive meltwater outbursts connected to the retreating glaciers possibly caused a deepening of the halocline (cf., Rasmussen and Thomsen, 2004) as the extended cold and relatively fresh surface water mass forced the more saline and thus denser AW to submerge. Accordingly, cold surface waters have been insulated from those relatively warm bottom waters enabling an extended sea ice coverage (see SST and sea ice cover; Fig. 26).

In the course of the Allerød (~14–12.7 ka), the grain size distribution shows a general trend towards slightly coarser sediment (mean: ~5.5–6 µm; Fig. 26a). The coarsening may reflect the retreat of some glaciers to more distal positions. Consequently, less fine-grained material from meltwater plumes would have reached the core location. Szczucin and Zajączkowski (2012) showed that meltwater-derived suspended particulate matter is mostly deposited within few kilometres from sources in glacier-influenced fjords of Svalbard, as mixing of meltwater with sea water induces flocculation and a subsequent suspension settling. Łącka et al. (2015) observed similar phenomena during the deglaciation of the Storfjord Trough (southern Spitsbergen). A further retreat of the glaciers is also suggested by slightly increasing munbers of (most likely ice-rafted) clasts in the core studied (Fig. 26b), indicating enhanced calving. Radiocarbon-dated beach ridges at the eastern coast of Woodfjorden (Andrée Land) point to a glacio-isostatic emergence of ~20 m (Forman et al., 2004) in the course of the Allerød (Fig. 26f). This uplift illustrates a massive retreat of the Svalbard–Barents Sea Ice Sheet, at least following Heinrich Stadial 1, as the decreasing ice sheet load caused a successive continental rebound. Despite this Allerød sea level drop, AW advection may have only been slightly reduced (if at all). The inflow of oceanic water into Woodfjorden is not restricted by a sill in a narrower sense, only on the seaward side, the peninsula Reinsdyrflya and the island Moffen are connected by a shallower ridge (~80–100 m depth; see Fig. 19c), possibly slightly decelerating the AW influx.

Towards the transition to the YD, percentages of *C. neoteretis* increased again (Fig. 26d). This trend is also in agreement with studies from the western, southwestern and northern Svalbard margin (Rasmussen et al., 2007; Ślubowska-Woldengen et al., 2007; Ślubowska et al., 2005) as well as from East Greenland (Jennings et al., 2006) although percentages of *C. neoteretis* were significantly higher at these locations during the Allerød–YD transition. The concomitant appearance of *C. neoteretis* may indicate some AW influx reaching the sea floor (e.g., Lubinski et al., 2001; Steinsund, 1994).

5.5.2 Younger Dryas (~12.7–11.7 ka) – oceanographic transitions and glacier responses

During the early YD, the benthic foraminiferal fauna was still dominated by *C. reniforme* (Fig. 23h) but percentages of *N. labradorica* rapidly increased (Fig. 26c). The latter species prefers fresh organic matter and is even able to sequester chloroplasts (Bernhard and Bowser, 1999; Cedhagen, 1991). *N. labradorica* shows maximum abundances between 1 and 2 cm sediment depth (e.g., Ahrens et al., 1997; Alve and Bernhard, 1995; Loubere and Rayray, 2016; Newton and Rowe, 1995). In general, this species is associated with glacier-distal habitats (Korsun and Hald, 1998, 2000). It commonly blooms in connection with enhanced productivity found near oceanic fronts (e.g., Rytter et al., 2002; Sheldon et al., 2016b; Steinsund, 1994). Ślubowska-Woldengen et al. (2007) concluded that rising percentages of *N. labradorica* reflect the approaching Arctic Coastal Front, which divided Atlantic (i.e., the Svalbard Branch) and Arctic waters. Studies from the northern Svalbard continental slope (Koç et al., 2002; Ślubowska et al., 2005) and from the Bellsund trough (western Spitsbergen; Ślubowska-Woldengen et al., 2007) show similar distributions of *N. labradorica* during the YD. According to reconstructions of the Svalbard–Barents Sea Ice Sheet, the Barents Sea itself was no longer covered by this ice sheet at the beginning of the YD (Hormes et al., 2013), enabling the East Spitsbergen Current to surround the Svalbard Archipelago, transporting Arctic Water to the western and northern Svalbard margins and thus causing the development of the Arctic Coastal Front. At the study site in Woodfjorden, AW may have risen in the water column, possibly detaching from the sea floor and enabling the formation of denser winter water at the bottom (see modern situation illustrated in Fig. 20). The rise of AW may have been caused by a slightly declined meltwater outflow (Fig. 22a and Fig. 26a), which no longer forced AW to submerge (see section 5.5.1), and/or by upwelling events. Modern AW intrusion into the fjords of Spitsbergen occurs intermittently (e.g., Carmack and Wassmann, 2006; Wassmann, 2015) and is amplified by wind-induced upwelling (Cottier et al., 2005, 2007). Today, easterlies are the prevailing winds at the northern margin of Svalbard (Lind and Ingvaldsen, 2012). Then, northward Ekman transport of surface waters generates (southward) upwelling of subsurface (or intermediate) AW, which subsequently is able to flood the northern shelf of Svalbard (Falk-Petersen et al., 2015; Lind and Ingvaldsen, 2012). A northward retreat of the sea ice edge even amplifies this mechanism (Falk-Petersen et al., 2015 and references therein). Comparable conditions might have occurred very frequently at the mouth of Woodfjorden during the early YD, especially because the sea ice coverage was temporarily reduced during this time interval (Fig. 25b). Due to the resultant shallower halocline, an oceanic front (i.e., the Arctic Coastal Front) formed, separating AW from Arctic Water. In the Arctic, AW is commonly associated with enhanced nutrition: nutrients are transported from deeper water masses to the surface in the North Atlantic by winter mixing. The subsequent northward advection of these nutrients promotes primary production at higher northern latitudes while Arctic-derived waters contain only low nutrient amounts (Hunt et al., 2016). Thus, the advection of AW distributes nutrients

onto the Arctic shelves, e.g., the shelves and fjords of Svalbard (Carmack and Wassmann, 2006). Therefore, the inflow of (sub)surface AW in the photic zone is interpreted as leading directly to a higher productivity (Carmack and Wassmann, 2006; Falk-Petersen et al., 2015; Sakshaug, 1997). Accordingly, nutrient advection and consequentially increasing phytoplankton blooms in spring and early summer may have resulted from such upwelling events during the early YD. High $\delta^{13}C$ offsets ($\Delta\delta^{13}C$; Fig. 26e) between the epi- (*C. lobatulus*) and the endobenthic species (*N. labradorica*) during this time interval point to enhanced remineralization rates and consequentially enhanced export production (see, e.g., Mackensen, 2008; Mackensen and Schmiedl, 2016). Therefore, $\Delta\delta^{13}C$ values are considered to be valuable palaeoproductivity proxies (Mackensen et al., 2017). Apart from a generally amplified productivity resulting from the stronger summer insolation of the YD (Fig. 26g; Berger and Loutre, 1991), as suggested by Müller and Stein (2014), the increased (export) production possibly resulted from AW incursion into the photic zone. The subsurface advection of the relatively warm AW may also have contributed to further retreat of local glaciers: maximum amounts of IRD (Fig. 26b) and increased percentages of fine-grained sediments (mean: ~6 µm; Fig. 26a) point to increased calving rates and meltwater outflow.

Following the peak appearance of *N. labradorica*, a shift in the faunal distribution is recognized around 12.4 ka: percentages of *C. reniforme* declined while those of *E. clavatum* rose (Fig. 23e, g, h). The dominance of *E. clavatum* possibly responded to comparable unstable conditions linked to sediment-laden waters and/or high-frequency IRD deposition connected to glacier melting events. *E. clavatum* is found in extreme modern environments, e.g., affected by very turbid meltwater plumes and/or relatively low salinities, where *C. reniforme* is not able to survive (Korsun and Hald, 1998, 2000; Steinsund, 1994). Also at the coast of Newfoundland, eastern Canada, a comparable faunal change occurred during a similar time period (Pearce et al., 2014). A shift from relatively stable to unstable conditions during the YD has been inferred from various studies, although this shift may have started at the earliest at ~12.3–12.2 ka (Bakke et al., 2009; Lane et al., 2013; Pearce et al., 2013). The slightly earlier inception at Woodfjorden (and off Newfoundland) may result from dating uncertainties and/or regional differences. Lane et al. (2013) showed, based on lacustrine records from Germany and Norway, that timing differences are likely connected to diverging regional conditions. Interestingly, Łącka et al, (2015) describe a contrary trend to our record with warmer intervals during the late YD in the Storfjord Trough (southern Spitsbergen). Mild summers and a strong seasonality during the YD are also reported from southern and eastern Greenland (Björck et al., 2002; Hall et al., 2008).

Cabedo-Sanz et al. (2013) report about ameliorating, sea ice-free conditions off northern Norway as early as ~11.9 ka. In our record, lower IRD deposition (Fig. 26b) along with gradually declining percentages of *E. clavatum* (Fig. 23g) are observed during the late YD (from ~12 ka on), which probably indicates a further retreat of glacier fronts into inner fjord positions with a consequential reduction in icebergs melting at the mouth of Woodfjorden. Salvigsen and Høgvard (2006) noted that several glaciers at the head of Bockfjorden, a tributary fjord of the inner Woodfjorden (Fig. 19c), were disconnected from the main fjord at the end of the YD. Prevailing fine-grained sediments (mean: ~6 µm; Fig. 26a) – presumably connected to meltwater run-off – also point to some disintegration of glaciers. Birgel and Stein (2004) assumed that a "last deglaciation event" on Svalbard occurred around 12 ka, although they proposed a concurrent stable AW advection warming surface waters. In contrast, our data indicate that the spreading of cold and low-salinity surface waters – resulting from enhanced inputs of meltwater – likely deepened the Atlantic-derived waters.

Accordingly, AW-influenced bottom waters may have resulted in the observed slightly increasing percentages of *C. neoteretis* (Fig. 26d) during the late YD (e.g., Jennings et al., 2004; Rytter et al., 2002; Steinsund, 1994). As surface waters were consequently better insulated from relatively warm AW, SSTs probably fell again while sea ice expanded (see Fig. 25a, b). However, a perennial closed sea ice cover in Woodfjorden, as suggested by Brückner and Schellmann (2003), seems unlikely as the data above show continuous deposition of IRD during the entire YD (Fig. 26b), even when maximum PIP_{25} values are observed (Fig. 25b). This leads to the inference that broken-up sea ice at least during summer enabled high productivity of sea ice diatoms and iceberg calving and dispersal. Hence, it remains unclear if *C. neoteretis* responded rather to those food pulses during summer, as proposed by Wollenburg et al. (2004), than to the presence of AW.

The retreat of glaciers during the YD as suggested by our data is further supported by studies based on radiocarbon-dated beach ridges or moraines (Mangerud and Landvik, 2007; Salvigsen and Høgvard, 2006; Salvigsen and Österholm, 1982) as well as on ^{10}Be-dated boulders (Reusche et al., 2014). They point to the absence of any YD glacier advance along the western and northern coasts of Spitsbergen. Possible contemporaneous glacier advances in several other regions of Svalbard – especially in Isfjorden (central Spitsbergen) – still remain under debate (Birgel and Stein, 2004; Boulton, 1979; Forwick, 2005; Svendsen et al., 1996). Nonetheless, YD glacier retreats have also been observed in the Disko Bay, western Greenland, where the Jakobshavn Isbræ retreated from ~12.2 ± 0.6 ka onwards (Rinterknecht et al., 2014). Rinterknecht et al. (2014) connect this retreat to warm ocean currents, which destabilized the marine terminating glacier by basal melting. A possibly ongoing deglaciation already at the onset of the YD and a further glacier retreat in the course of the YD is controversially discussed for the Scottish Highlands (Bromley et al., 2014; Small and Fabel, 2016).

5.5.3 Early Holocene (~11.7–7.8 ka) – amelioration of environmental conditions

Climatic conditions were ameliorated during the YD–early Holocene transition (starting ~11.7 ka) as summer insolation approached its maximum values (Fig. 26g; Berger and Loutre, 1991). Also the high offset between δ^{18}O values of *C. lobatulus* and *N. labradorica* (Fig. 24a) – which already started during the second half of the YD and persists during the entire early Holocene – presumably indicates increasing seasonal differences due to the contrast between high summer and low winter insolation (Fig. 26g) as suggested by Rasmussen et al. (2012) for the Isfjord. Indeed, *C. lobatulus* calcifies in summer, whereas *N. labradorica* calcifies in spring or early summer (Zajączkowski et al., 2010a). Rising $\Delta\delta^{13}$C and lower δ^{13}C values in *N. labradorica* (Fig. 24b and Fig. 26e) may indicate higher organic matter inputs deriving from enhanced primary production. High percentages of *N. labradorica* (Fig. 26c) point to a growing influence of the Arctic Coastal Front with intensified AW circulation in intermediate waters (see sect. 5.5.2). Simultaneously, declining IRD amounts suggest a significant reduction in iceberg rafting (Fig. 26b). Grain size measurements illustrate some coarsening (Fig. 26a), likely resulting from the retreat of glaciers to innermost positions in the fjords as smaller amounts of fine-grained suspended material associated with meltwater plumes reached the core location (see Szczucin and Zajączkowski, 2012).

Between ~11.1 and ~10.8 ka, a short-term shift in the faunal assemblage is recognized: percentages of *N. labradorica* dropped while those of *E. clavatum* and *C. reniforme* increased (Fig. 23e, g, h). This likely

illustrates a northward shift of the Arctic Coastal Front (away from the coast) and a consequentially stronger influence of cold and fresh Arctic waters. Also some surface cooling is indicated by rapidly decreasing SSTs (Fig. 25a). *E. clavatum* – an opportunistic species (e.g., Korsun and Hald, 2000; Newton and Rowe, 1995) – took advantage of these deteriorated conditions. Increasing percentages of *C. reniforme* may reflect the presence of some saline AW at the fjord floor as this species is reported to respond to Atlantic (Intermediate) Water, e.g., at the eastern Greenland shelf (Jennings and Helgadottir, 1994). Several studies describe simultaneous and similar faunal changes around Svalbard (Rasmussen et al., 2012, 2014c; Skirbekk et al., 2010; Ślubowska-Woldengen et al., 2007; Ślubowska et al., 2005), generally associated with the Preboreal Oscillation (PBO) cooling interval (Björck et al., 1996). Some divergence in the timing of the PBO – especially at the Hinlopen trough (Ślubowska et al., 2005) – may be due to chronological uncertainties and possibly distinct reservoir ages, as suggested by Rasmussen et al. (2014b). Different trigger mechanisms have been suggested for the PBO inception. Meltwater discharge from the disintegrating Fennoscandian Ice Sheet into the Baltic Ice Lake and subsequent drainage into the Nordic Seas have been proposed as one possible cause of the PBO cooling (Björck et al., 1996, 1997; Hald and Hagen, 1998). In contrast, Fisher et al. (2002) assumed that a single meltwater flood event from Lake Agassiz into the Arctic Ocean resulted in an expansion and thickening of sea ice as well as in fresher North Atlantic surface waters.

Despite this cooling, there is no evidence for any significant glacier re-advance in the Woodfjorden area as IRD did not change much (Fig. 26b). Grain size measurements still illustrate high but steadily decreasing fractions of fine sediments (~7–8.5 µm; Fig. 22a, d), which might reflect continuous meltwater discharge and thus further deglaciation. Nevertheless, increasing percentages of coarser sediments (~20 µm) are also observed during the PBO (Fig. 22a, d). These coarser sediments probably resulted from sea ice-rafted deposition as sediments >10 µm are interpreted as transported by sea ice (Hebbeln, 2000). During previous time intervals, enhanced percentages of this coarser fraction (~20 µm) were masked because they were diluted by high amounts of meltwater-transported finer sediment (e.g., grain size distribution at ~13.9 ka; Fig. 22d). In contrast, presumed sea ice-rafted debris is better recognizable during the PBO when the grain size distribution is less influenced by suspended sediments derived from meltwater plumes (see Fig. 22d). Sea ice biomarkers exhibit a decreasing trend indicating a moderate sea ice coverage (Fig. 25b) but peak values of IP_{25} (Fig. 25c) illustrate a high number of sea ice diatoms, which possibly characterize a sea ice edge position at the mouth of Woodfjorden. Thus, the deposition of sea ice-rafted material at the core site seems realistic. Subsequently, maximum accumulation rates of the phytoplankton marker brassicasterol (Fig. 25d) point to algal blooms in spring–summer under open water conditions that persisted throughout the early Holocene (see PIP_{25} values; Fig. 25b and Fig. 26).

At the end of the PBO, *N. labradorica* rapidly recovered (reaching up to ~50 %; Fig. 26c), while *E. clavatum* and *C. reniforme* declined in percentage (Fig. 23g, h). This faunal transition probably reflects the return of the Arctic Coastal Front in the vicinity of the core site, accompanied by rising AW intruding into intermediate water masses in the fjord (see sect. 5.5.2). This hydrographic change was likely a response to the onset of the Holocene Thermal Maximum (HTM) in Svalbard, at ~10.8 ka (Miller et al., 2010), when summer temperatures significantly exceeded modern temperatures due to the higher summer insolation (Fig. 26g; Berger and Loutre, 1991). Peaks in the ARBF, with more than 50,000 ind. cm^{-2} ka^{-1}, as well as enhanced accumulation rates of brassicaserol (Fig. 23a and Fig. 25d), indicate high food supplies. The observed increase

in $\Delta\delta^{13}C$ values (Fig. 26e) implies a high export productivity lasting until ~10.4 ka. This may be linked to the presence of AW as a subsurface or even surface water mass, hence amplifying productivity in the photic zone. The appearance of the thermophilous mussel *Mytilus edulis* at the outer part of Woodfjorden (Reinsdyrflya) supports the assumption of a surface injection of AW at least from ~10.6 ka on (9,815 ±80 ^{14}C a; Salvigsen, 2002). Several studies around Spitsbergen report about a benthic faunal pattern comparable to the record above during the HTM (Groot et al., 2014; Rasmussen et al., 2012; Skirbekk et al., 2010; Ślubowska-Woldengen et al., 2007). Ślubowska-Woldengen et al. (2008) showed that *N. labradorica* reached maximum percentages at sites influenced by the WSC or the Svalbard Branch. At the mouth of Woodfjorden, percentages of *I. helenae* (Fig. 23d) rose at the onset of the HTM. This species has been connected to sea ice algae blooms in various studies (mostly lumped with *I. norcrossi*; e.g., Steinsund, 1994). Because sea ice coverage shows a decreasing trend (see PIP_{25}; Fig. 25b), whereas alkenone-based SSTs reached peak values of ~7 °C (Fig. 25a), it seems more likely that *I. helenae* did not respond specifically to sea ice algae blooms but rather to an enhanced productivity (probably due to open waters), as already proposed by Polyak et al. (2002), Seidenkrantz (2013) and Wollenburg et al. (2004).

During the HTM, increasing SSTs (based on planktic foraminiferal assemblages) were reconstructed at the western Svalbard continental slope (Hald et al., 2004), south of Spitsbergen at Storfjorden slope (Rasmussen et al., 2014c), and at the western Barents slope (Sarnthein et al., 2003). Lacustrine records from NW Spitsbergen indicate maximum temperatures based on alkenones until ~10.5 ka (van der Bilt et al., 2016). Carbonara et al. (2016) and Rigual-Hernández et al. (2017), report about maximum concentrations of diatoms and coccoliths (mainly warm water species) and inferred a causally strengthened advection of AW during the HTM south of Spitsbergen. Thus, a significant warming in the Svalbard area occurred during this time interval, with temperatures exceeding modern temperatures (compare alkenone-based SST data in Fig. 25a with hydrographic data in Fig. 20 and in Rasmussen and Thomsen, 2014; Rasmussen et al., 2014b).

Iceberg production remained low during the HTM. From ~10.1 ka on, IRD percentages were reduced to a minimum (Fig. 26b) – although slightly increasing at around 9 ka – indicating a retreat of most glaciers to innermost fjord positions while some large tidewater glaciers (e.g., Monacobreen; Fig. 19c) stayed connected to the fjord system during the early Holocene. Radiocarbon-dated beach ridges show a contemporary drop in relative sea level almost down to the present level (Fig. 26f; Forman et al., 2004), in response to the deglaciation of Spitsbergen with the consequential rebound persisting into the HTM .

Grain size distribution during the HTM exhibits maxima around 20 µm (Fig. 22a) that may indicate relatively high fluxes of sea-ice-rafted debris. In this scenario, some winter sea ice cover would have been present, although sea ice biomarker concentration is low during the interval (see PIP_{25} minima in Fig. 25b). The PIP_{25} index is based on sea ice diatoms and is thought to respond to spring–summer conditions (Müller et al., 2011). However, a coarsening of the sediment due to stronger bottom currents cannot be excluded.

After ~10.1 ka another slight shift in the faunal distribution is recognized (Fig. 23): *N. labradorica* declined whereas *C. reniforme* rose again (Fig. 23e, h). This faunal change may be linked to a repeated northward movement of the Arctic Coastal Front away from the core site in concert with submerging AW. Following a significant peak in the ARBF at ~10.1 ka, all proxies for productivity reveal a decreasing trend (i.e., $\Delta\delta^{13}C$, accumulation rates of brassicasterol and benthic foraminifera; Fig. 26e, Fig. 25d and Fig. 23a) indicating a decreasing AW influence in the photic zone. Slightly cooler conditions have been consistently reported from

the Storfjord Trough (southern Spitsbergen) at the end of the early Holocene, probably due to a stronger influence of Arctic Water (Łącka et al., 2015).

Around 8.8 ka, a further coarsening of the sediment is observed (maximum percentages ~45–50 µm, mean: ~15 µm; Fig. 22a and Fig. 26a). This shift in the grain size distribution may indicate higher current velocities. The pronounced skewness towards coarse sediments seen in the grain size distribution point to winnowing, and/or bypass of the fine fraction (see grain size distribution at ~8.8 ka in Fig. 22d). The epibenthic species *C. lobatulus* – commonly connected to strong bottom currents (Hald and Korsun, 1997; Hansen and Knudsen, 1995; Steinsund, 1994) – displays slightly increased proportions during this time period (Fig. 23b). Higher percentages of *B. frigida* s.l. (Fig. 23c) support these findings because the species develops preferentially in coarse sediments (Steinsund, 1994). This taxon has also been connected to ice edge algal blooms (Hald and Steinsund, 1996; Steinsund, 1994). Here however, this seems unlikely; analogous to *I. helenae*, its presence rather corresponds to reduced sea ice cover conditions during spring–summer, as inferred from declining PIP_{25} values (Fig. 23c and Fig. 25b). Seidenkrantz (2013) suggested that *B. frigida* thrives right after the retreat of sea ice. Apart from the species preference for coarse sediments, the occurrence of *B. frigida* s.l. seems to be mainly controlled by the presence of open waters enabling primary production and high organic matter fluxes to the sea floor. Consistently, *B. frigida* is reported to feed on fresh particulate organic matter in the Northeast Water Polynya (northeastern Greenland; Newton and Rowe, 1995). An enhanced productivity at the mouth of Woodfjorden is indeed indicated by increasing $\Delta\delta^{13}C$ values (Fig. 26e) simultaneously matching peak percentages of *B. frigida* s.l. at around 8.8 ka (Fig. 23c).

5.5.4 Late Holocene (~1.8–0.4 ka) – aftermath of the neoglaciation

In comparison with the early Holocene, distinct differences in the benthic foraminiferal fauna mark the last ~1,400 years of our record. The faunal composition suggests frequent AW incursions, temporarily as bottom water mass: the *N. labradorica* abundance decreased to ~13–22 % (Fig. 26c), whereas *C. reniforme* exhibits percentages up to ~31 % (Fig. 23h). *C. reniforme* may indicate more saline conditions in bottom waters linked to the presence of AW at the sea floor (Hald and Korsun, 1997; Jennings et al., 2004; Jennings and Helgadottir, 1994). Enhanced percentages of the opportunistic species *E. clavatum* (up to ~28 %; Fig. 23g) point to unstable conditions, e.g., high inter-annual variability in environmental conditions. Nonetheless, *I. helenae* reached proportions comparable to those of the HTM (>5 %; Fig. 23d), reflecting still sufficient food availability. Increasing $\Delta\delta^{13}C$ values (Fig. 26e) characterize this interval, likely responding to the temporary influence of AW in subsurface waters transporting nutrients into the photic zone. Late Holocene seasonally ice-free waters (see Fig. 25b) enabled primary productivity despite lower SSTs than those inferred above for the HTM interval (~4 °C; Fig. 25a), very likely due to the decreasing summer insolation and reduced seasonal temperature contrast (Berger and Loutre, 1991; Fig. 26g). Cooling in the Fram Strait area during the late Holocene is reported at various locations and assigned reduced insolation (e.g., Hald et al., 2004; Müller et al., 2012; Rasmussen et al., 2012; Rigual-Hernández et al., 2017; Ślubowska-Woldengen et al., 2007; Werner et al., 2013). Although sea ice biomarkers suggest open waters during summer (Fig. 25b and Fig. 26), increased proportions of ~20 µm and ~50 µm grain size fractions (Fig. 22a) may imply the deposition of (winter) sea-ice-rafted debris (see sect. 5.5.3).

Parallel to this cooling, a slight increase in IRD percentages indicates enhanced glacier activity with intensified iceberg production (Fig. 26b) in the Woodfjorden area. Furrer et al. (1991) report about advances of Monacobreen into Liefdefjorden (Fig. 19c) during the Older Subatlantic (~1.2 cal. ka; 1,315 ±100 ^{14}C a), whose glacier ice front reached Lernerøyane, a small archipelago ~6 km from its modern position. Advancing glaciers have also been reported in central Spitsbergen during a similar time period (Baeten et al., 2010; Humlum et al., 2005). The growth of Monacobreen possibly responded to the neoglacial cooling trend (as described by Porter and Denton, 1967), which led to waxing of Arctic glaciers (e.g., Miller et al., 2010; Solomina et al., 2015, 2016), and is reflected in increased IRD deposition in the present study.

In contrast to conditions inferred above, some other studies state a general warming trend (Bonnet et al., 2010; D'Andrea et al., 2012; Jernas et al., 2013; Majewski et al., 2009; Spielhagen et al., 2011; Werner et al., 2011) as well as a strengthened influx of AW during the last 2 millennia in the Svalbard area (Groot et al., 2014; Rasmussen et al., 2012; Sarnthein et al., 2003; Ślubowska et al., 2005). However, as the mid-Holocene is missing in the present record (see sect. 5.4.1), we can only compare the early vs. late Holocene. As the late Holocene is marked by cooler conditions than those prevailing during the HTM, a link to the neoglaciation is assumed, but the actual trend from the mid- to the late Holocene is unknown.

5.5.5 The role of Atlantic Water in the deglaciation history of the Svalbard–Barents Sea Ice Sheet

Around the Svalbard margins, intrusion of AW is generally causally linked to the retreat of glaciers since the late Weichselian (Hormes et al., 2013; Jessen et al., 2010; Klitgaard Kristensen et al., 2013; Skirbekk et al., 2010; Ślubowska-Woldengen et al., 2007; Ślubowska et al., 2005). The subsurface inflow of AW into fjords possibly melted tidewater glaciers from underneath, as proposed by Hormes et al. (2013). Today, submarine melting of tidewater glaciers induced by warm ocean currents is observed in the Arctic, e.g., in Alaska (Bartholomaus et al., 2013; Motyka et al., 2003), Greenland (Holland et al., 2008; Inall et al., 2014; Straneo et al., 2010) and Svalbard (Luckman et al., 2015), as well as in Antarctica, i.e., on the Antarctic Peninsula (Cook et al., 2016; Padman et al., 2012; Wouters et al., 2015).

Interpreting the appearance of *C. neoteretis,* numerous studies assume that the intensification of AW inflow along the Svalbard margin occurred relatively simultaneously during the Bølling–Allerød (Klitgaard Kristensen et al., 2013; Rasmussen et al., 2007; Ślubowska et al., 2005). In the Laptev Sea, this species has been connected to Atlantic-derived water, from ~15.4 ka onwards (Taldenkova et al., 2010). AW presence is also inferred prior to ~14 ka off West Greenland (Sheldon et al., 2016a). At the margin of the Arctic Ocean, north of Svalbard, *C. neoteretis* showed high abundances from at least 24 ka onwards (Wollenburg et al., 2004). Despite the assumed intrusion of relatively warm water masses, planktic foraminifera assemblages indicate low subsurface temperatures without considerable changes far into the YD, along the W Barents slope (Sarnthein et al., 2003) and along the W-Svalbard margin (Hald et al., 2004). Thus, a subsurface to bottom inflow of relatively warm AW is assumed during the Bølling–Allerød, while surface waters remained cold.

The YD cold event has been studied extensively. This cold reversal was most likely initiated by a massive glacial lake drainage into the Arctic Ocean that reduced the Atlantic Meridional Overturning Circulation (Broecker, 2006; Broecker et al., 1989; Fahl and Stein, 2012; Murton et al., 2010; Stein et al., 2012; Tarasov and Peltier, 2005). Nonetheless, the influence of AW is seen at numerous locations around Svalbard, at least

during the early YD and possibly temporarily (e.g., Rasmussen et al., 2007; Ślubowska et al., 2005; this study, see Fig. 26c, d). A shift of the Arctic Coastal Front towards the study areas at the northern Svalbard margin characterizes the situation during the YD. The proximal position of this oceanic front is linked to an initial AW intrusion into intermediate waters of Woodfjorden providing higher food supplies (Fig. 26e) while contributing to the retreat of tidewater glaciers (Fig. 26a, b).

During the early Holocene, the Nordic Seas, the Fram Strait and Barents Sea were characterized by a high AW inflow (e.g., Bauch et al., 2001; Carbonara et al., 2016; Groot et al., 2014; Müller and Stein, 2014; Rigual-Hernández et al., 2017; Risebrobakken et al., 2011; Telesiński et al., 2015; Werner et al., 2013, 2016), coinciding with a general warming trend in the entire Svalbard region – especially after the PBO (e.g., Hald et al., 2004; Rasmussen et al., 2012; Sarnthein et al., 2003; Skirbekk et al., 2010; Ślubowska et al., 2005; this study, see Fig. 25a). This trend is in agreement with the early Holocene warming observed in the entire North Atlantic (Marchal et al., 2002).

The interruption of the warming trend during the PBO occurred almost simultaneously around Svalbard but is more pronounced in northern locations (Rasmussen et al., 2014b; Skirbekk et al., 2010; Ślubowska et al., 2005; this study, see Fig. 23 and Fig. 25) than along the (south)western margin of Svalbard (Rasmussen et al., 2012, 2014c; Ślubowska-Woldengen et al., 2007). Accordingly, it seems likely that the PBO was triggered by a vast meltwater flood from the Mackenzie River area into the Arctic Ocean (Fisher et al., 2002), than by a meltwater discharge from the Fennoscandian Ice Sheet into the Nordic Seas as assumed earlier (Björck et al., 1996). Thus, northern sites may have been more strongly affected by the resulting colder and fresher surface waters and the expansion of a thicker pack ice, which concurred to force AW to sink deeper in the water column.

Nevertheless, as discussed above, AW was present at the northern margin of Spitsbergen during the last 2 millennia, although its influx was weaker and its position possibly deeper in the water column, when compared to HTM conditions Fig. 26c). Various studies report similar oceanographic conditions during this time interval (e.g., Hald et al., 2004; Rasmussen et al., 2014b; Skirbekk et al., 2010; Ślubowska-Woldengen et al., 2007; Ślubowska et al., 2005). Contrary to the HTM and the YD, there are indications of glacier advances regardless of the AW advection during the late Holocene (Fig. 26a, b), possibly resulting from the lower summer insolation of the interval (Berger and Loutre, 1991; see Fig. 26g). Additionally, the AW incursion into Woodfjorden as a relatively deep water mass may have been of minor influence on glacier fronts as tidewater glaciers may only have been present in the shallower inner parts of the fjord system during the late Holocene (Furrer et al., 1991; Salvigsen and Høgvard, 2006). Hence, the glacier dynamics were possibly decoupled from AW advection during the late Holocene.

5.6 Conclusions

Multi-proxy analyses of sediment core GeoB10817-4 from the mouth of Woodfjorden (northern Spitsbergen) enabled us to document ocean–ice interactions since the deglaciation (since ~15,500 years) at the northern margin of Svalbard, providing insights into glacier activity as well as into bottom, intermediate and surface water conditions, including sea ice coverage.

- The deglaciation period (until ~12.7 ka; excluding the Younger Dryas) was marked by a disintegrating Svalbard–Barents Sea Ice Sheet, as illustrated by high calving rates and enhanced

meltwater inputs. Cold surface waters were covered by extensive sea ice, while early intrusions of Atlantic Water as a bottom water mass occurred (Fig. 27a).

- During the early Younger Dryas (~12.7–12.4 ka), Atlantic Water was still advected as an intermediate water mass, probably connected to a coastward shift of the Arctic Coastal Front. Its intrusion was accompanied by warmer surface waters and high iceberg melting rates, which may have been linked to the retreat of some tidewater glaciers towards the fjord heads (Fig. 27b). During the late Younger Dryas (~12.4–11.7 ka), surface waters cooled while sea ice extended and Atlantic Water temporarily penetrated into bottom waters.
- Conditions improved during the early Holocene (~11.7–7.8 ka), with an increasing subsurface Atlantic Water inflow, and were briefly interrupted during the Preboreal Oscillation. This deterioration occurred almost simultaneously around Svalbard, but was more pronounced at the northern margin of Svalbard than in the south. During the succeeding Holocene Thermal Maximum, sea surface temperatures reached their maximum surpassing modern temperatures. Productivity flourished and sea ice coverage declined. Most glaciers retreated to innermost fjord positions during this interval. Only single tidewater glaciers survived (especially Monacobreen) (Fig. 27c).
- The early vs. late Holocene depict distinct environmental conditions. Productivity gradually increased in the course of the late Holocene (~1.8–0.4 ka) while Atlantic Water temporarily sank from intermediate to bottom waters. Even though sea surface temperatures were lower than during

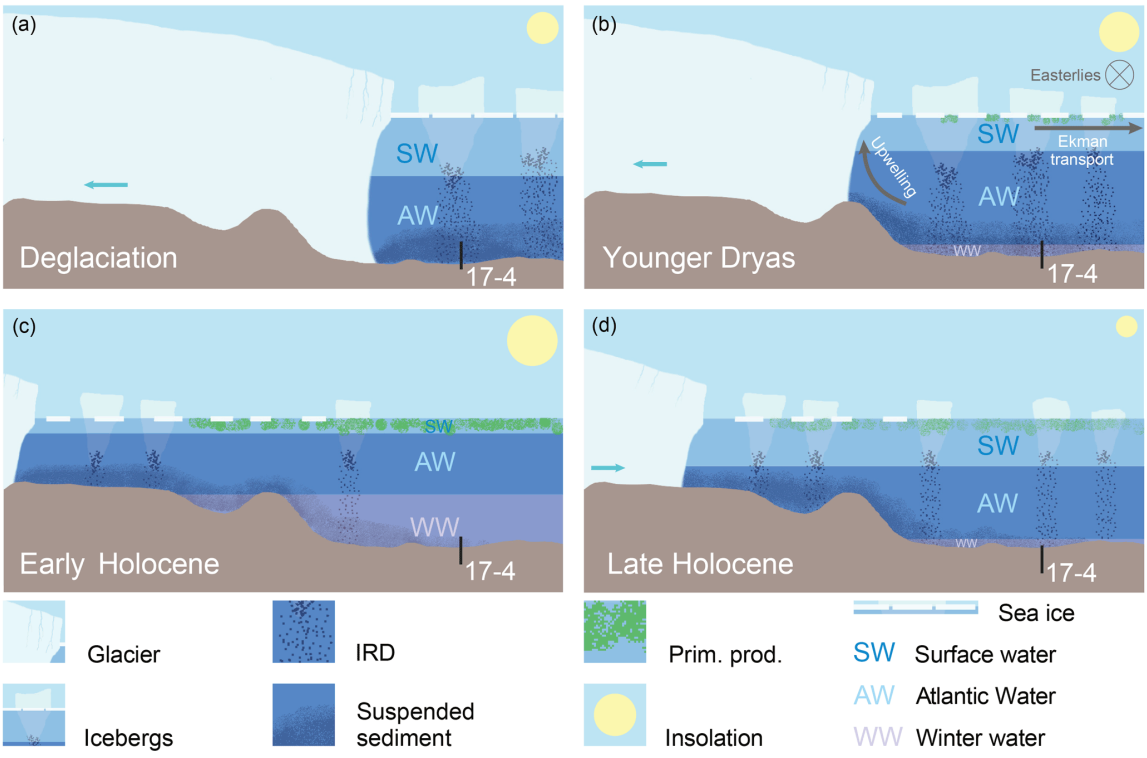

Fig. 27: Environmental conditions in Woodfjorden during (a) the deglaciation, (b) the Younger Dryas, (c) the early Holocene and (d) the late Holocene. Black bars mark the location of sediment core GeoB108*17-4*. Glacier retreats or advances are marked by turquoise arrows. Yellow circles symbolize insolation changes (Berger and Loutre, 1991). The crossed circle in (b) signifies easterlies (blowing perpendicular to the profile) triggering a northward Ekman transport of the surface waters which entailed an upwelling of intermediate waters (i.e., AW; see Lind and Ingvaldsen, 2012).

the early Holocene, sea ice coverage was reduced. High iceberg production possibly responded to some late Holocene glacier advance (neoglaciation) in response to low summer insolation (Fig. 27d).

- From the deglaciation on, the presence of Atlantic Water – in bottom as well as in intermediate waters – is connected to retreating glaciers at the northern Svalbard margin, while during the late Holocene, glaciers might have grown despite relatively constant inflow of Atlantic Water (possibly below surface).
- The Holocene Thermal Maximum includes – apart from a few differences (e.g., considerable higher summer insolation, dropping relative sea level due to the glacio-isostatic rebound) – numerous similarities to a future warming: sea surface temperatures were most likely warmer than today, resulting in a reduced sea ice coverage and consequential open waters that enabled high primary production. Already today, reduced sea ice promotes increasing phytoplankton blooms (Arrigo and van Dijken, 2011, 2015). During the Holocene Thermal Maximum, subsurface intrusion of warm Atlantic Water contributed to the melting and retreat of glaciers to inner fjord positions; a phenomenon that is also observed today, e.g., at Svalbard´s tidewater glaciers (Luckman et al., 2015). Thus, environmental conditions during the Holocene Thermal Maximum are comparable with the already ongoing global warming, at least for the Svalbard region.

Data availability

Supplement data are available on PANGAEA: https://doi.pangaea.de/10.1594/PANGAEA.882243.

Appendix A: Lists of benthic foraminiferal species appearing in sediment core GeoB10817-4

Agglutinating species

Adercotryma glomerata (Brady, 1878)
Ammodiscus sp.
Bathysiphon rufum de Folin, 1886
Bathysiphon spp.
Cribrostomoides spp.
Cuneata arctica (Brady, 1881)
Eggerella spp.
Hippocrepinella sp.
Lagenammina spp.
Miliammina spp.
Portatrochammina bipolaris Bronnimann & Whittaker, 1980
Portatrochammina karica (Shchedrina, 1946)
Portatrochammina spp.
Recurvoides turbinatus (Brady, 1881)
Reophax spp.
Spiroplectammina biformis (Parker & Jones, 1865)
Textularia earlandi Phleger, 1952
Textularia spp.
Textularia torgata Parker, 1952
Textulariina
Trochammina astrifica (Rhumbler, 1938)
Trochammina spp.

Calcareous species

Astrononion gallowayi Loeblich & Tappan, 1953
Bolivina pseudopunctata Höglund, 1947
Buccella frigida s.l. (*B. frigida* s.s. (Cushman, 1922) and *B. tenerrima* (Bandy, 1950))
Buccella spp.
Bulimina c.f. *alazanensis/rostrata*
Cassidulina neoteretis Seidenkrantz, 1995
Cassidulina reniforme Nørvang, 1945
Cassidulininae
Cibicides lobatulus (Walker & Jacob, 1798)
Cibicidinae
Cornuspira involvens (Reuss, 1850)
Cornuspira spp.
Dentalina spp.
Discorbinella araucana (d'Orbigny, 1839)
Elphidium albiumbilicatum (Weiss, 1954)
Elphidium asklundi Brotzen, 1943
Elphidium bartletti Cushman, 1933
Elphidium clavatum Cushman, 1930 (formerly named *Elphidium excavatum* (Terquem, 1875) forma *clavata* Cushman, 1930; see Darling et al., 2016)
Elphidium hallandense Brotzen, 1943
Elphidium spp.
Elphidium williamsoni Haynes, 1973
Epistominella spp.
Fissurina orbignyana Seguenza, 1862
Fissurina spp.
Glandulina ovula d'Orbigny, 1846
Globobulimina auriculata (Bailey, 1894)
Globobulimina spp.
Globobulimina turgida (Bailey, 1851)
Globulina spp.
Haynesina spp.
Islandiella helenae Feyling−Hanssen & Buzas, 1976
Islandiella islandica (Nørvang, 1945)
Islandiella norcrossi (Cushman, 1933)
Islandiella spp.
Lagena distoma Parker & Jones, 1864
Lagena laevis (Montagu, 1803)
Lagena striata (d'Orbigny)
Melonis barleeanus (Williamson, 1858)
Melonis spp.
Miliolida
Miliolinella spp.
Nodosaria spp.
Nonionella auriculata Heron-Allan & Earland, 1930
Nonionella turgida (Williamson, 1858)
Nonionellina labradorica (Dawson, 1860)
Oolina hexagona (Williamson, 1848)
Pullenia quinqueloba (Reuss, 1851)
Quinqueloculina seminula (Linné, 1758)
Quinqueloculina spp.
Quinqueloculina stalkeri Loeblich & Tappan, 1953
Robertina spp.
Rosalina spp.
Rotaliina
Stainforthia loeblichi s.l. (*S. loeblichi* s.s. (Feyling−Hanssen, 1954) and *S. concava* Höglund, 1947)
Stainforthia spp.
Trifarina angulosa (Willamson, 1858)
Trifarina fluens (Todd, 1947)
Triloculina spp.
Triloculina trihedral Loeblich & Tappan, 1953
Uvigerina mediterranea Hofker, 1932
Uvigerina spp.

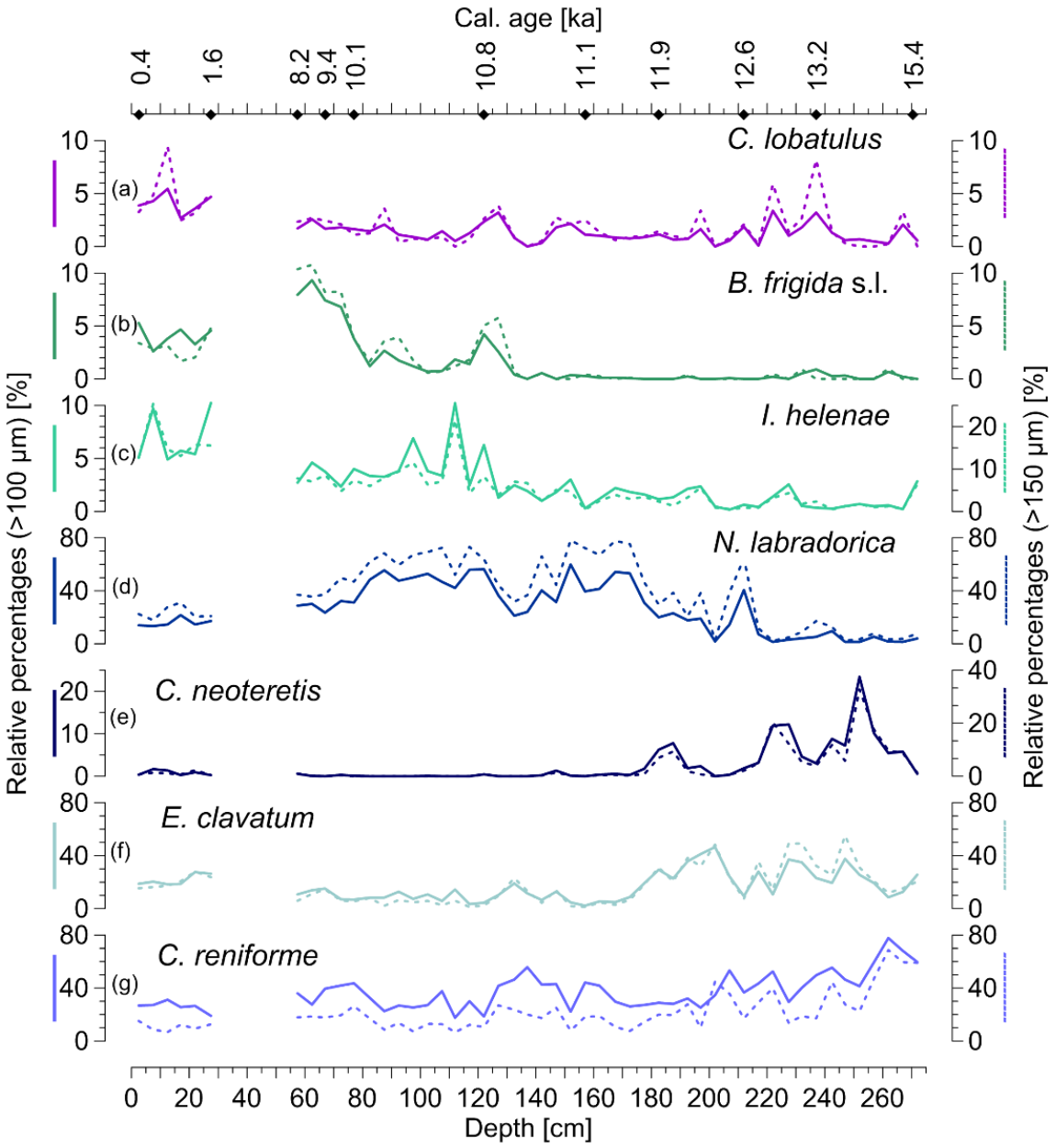

Fig. A1: Relative percentages of the dominant calcareous benthic foraminifera. Comparison of fraction >100 µm (solid lines) vs. fraction >150 µm (dashed lines). a) *Cibicides lobatulus*. b) *Buccella frigida* s.l. c) *Islandiella helenae*. d) *Nonionellina labradorica*. e) *Cassidulina neoteretis*. f) *Elphidium clavatum*. g) *Cassidulina reniforme*. Note similar pattern of the faunal distributions. The highest offset can be recognized for *N. labradorica* and *C. reniforme* because the majority of *N. labradorica* appears in the >150 µm fraction whereas the majority of *C. reniforme* appears in the >100 µm fraction. Black diamonds: calibrated radiocarbon ages.

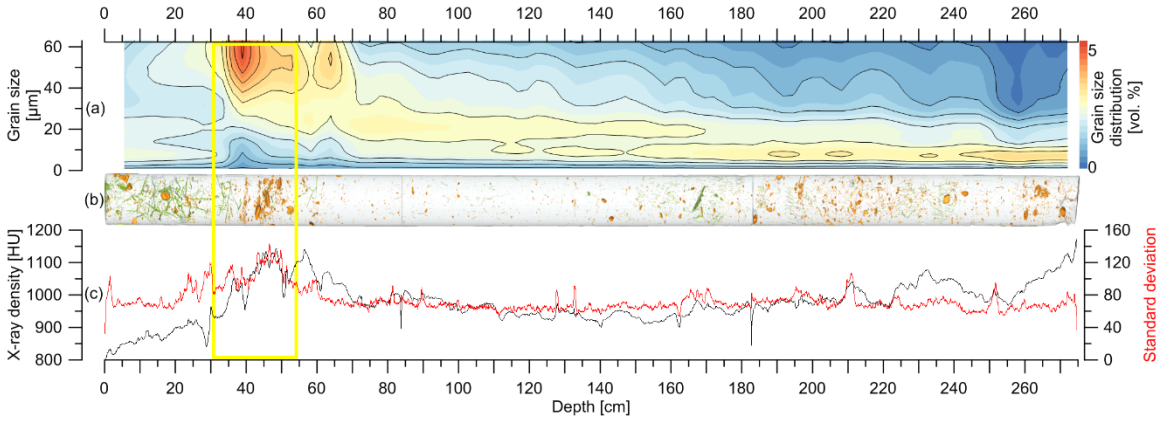

Fig. A2: a) Grain size distribution of fine siliciclastic sediments (0–63 µm). b) Interpreted CT analysis showing bioturbation (green) and clasts (orange). c) X-ray density (black line) in Hounsfield units (HU) with standard deviation (red line) derived from CT analysis. Yellow rectangle marks disturbed section. Note coarsening upwards of fine sediments (a), high accumulation of clasts (b) and increased x-ray density as well as respective standard deviation (c) in the disturbed section.

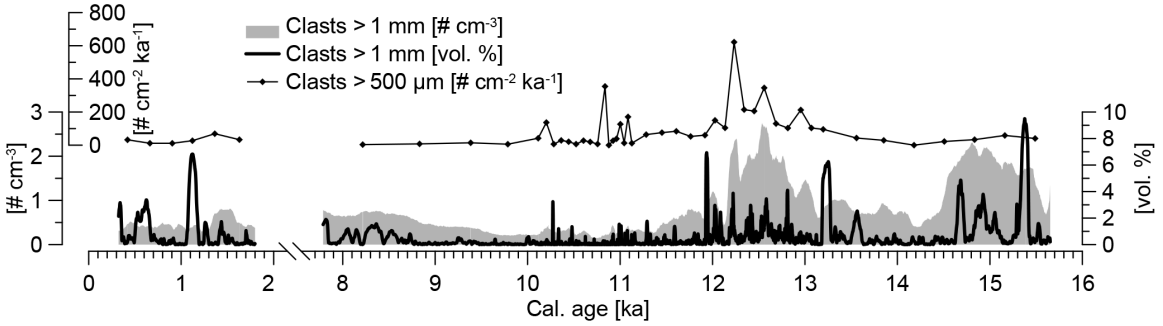

Fig. A3: Comparison of methods to determine the input of ice-rafted debris (IRD): accumulation rates (Ehrmann and Thiede, 1985) of clasts >500 µm based on count data as well as volume percentages and number of clasts (>1 mm) cm^{-3} based on CT analyses.

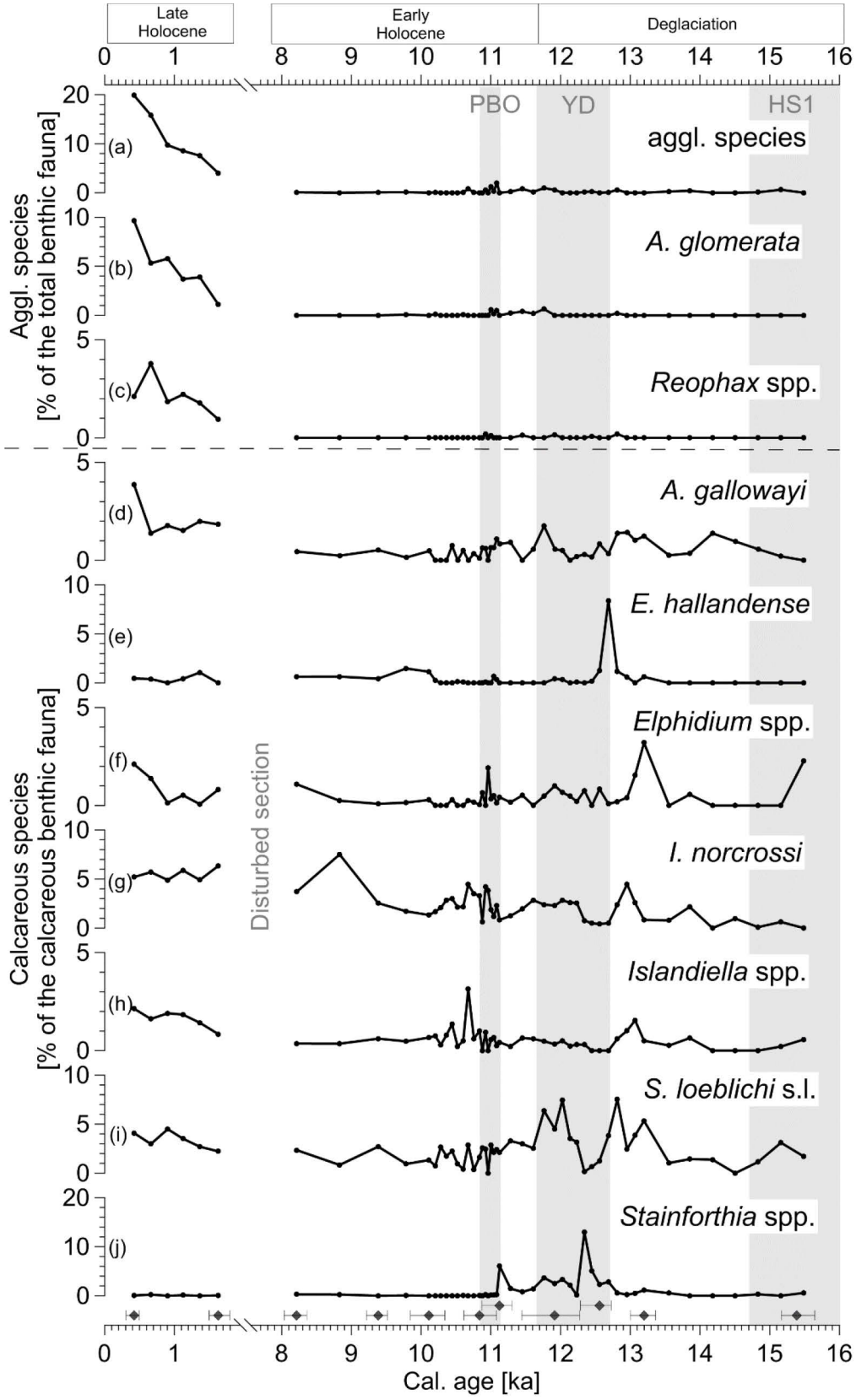

Fig. A4: Relative percentages of the total benthic foraminiferal fauna: a) sum of agglutinating species. b) *Adercotryma glomerata*. c) *Reophax* spp. Relative percentages of the calcareous benthic foraminiferal fauna: d) *Astrononion gallowayi*. e) *Elphidium hallandense*. f) *Elphidium* spp. (excluding *E. asklundi*, *E. bartletti*, *E. clavatum*, *E. hallandense*). g) *Islandiella norcrossi*. h) *Islandiella* spp. (excl. *I. helenae*, *I. islandica*, *I. norcrossi*). i) *Stainforthia loeblichi* s.l. j) *Stainforthia* spp. (excluding *S. loeblichi* s.l.). Grey vertical shadings; see Fig. 22. Dark grey diamonds: calibrated radiocarbon ages with error ranges.

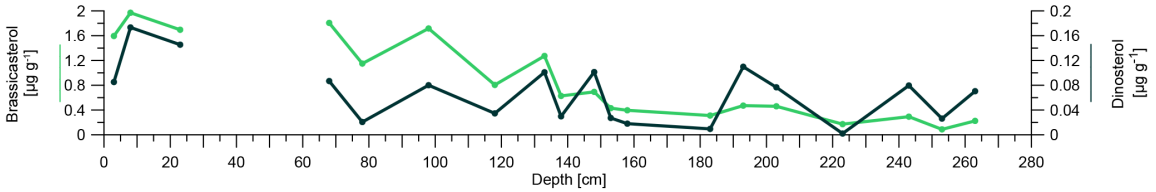

Fig. A5: Phytoplankton biomarker [µg g^{-1} sediment]: brassicasterol (light green line) and dinosterol (dark green line). Note almost parallel trend with brassicasterol showing values 1 magnitude higher than dinosterol.

Author contributions

M. Bartels and D. Hebbeln designed the study. M. Bartels performed the faunal analyses, created the figures and interpreted all data. J. Titschack created the base maps in Fig. 19 (b and c), performed the particle size measurements and CT analyses as well as respective data processing. K. Fahl carried out the biomarker analyses. M.-S. Seidenkrantz revised the identification of the foraminiferal species and contributed to their interpretation. D. Hebbeln, C. Hillaire-Marcel and R. Stein contributed significantly to the discussion of the data. M. Bartels prepared the manuscript with contributions from all co-authors.

Competing interests

The authors declare that they have no conflict of interest.

Acknowledgements

This project was supported by the Deutsche Forschungsgemeinschaft (DFG) through the International Research Training Group "Processes and impacts of climate change in the North Atlantic Ocean and the Canadian Arctic" (IRTG 1904 ArcTrain). We would like to thank the captain and crew of RV *Maria S. Merian* as well as the scientists on-board during the cruise MSM02/03 in 2006 for retrieving the samples. The following persons are acknowledged for carrying out measurements: Janet Rethemeyer, University of Cologne, and Lukas Wacker, ETH (Zürich), for radiocarbon measurements as well as Birgit Meyer and Henning Kuhnert, MARUM (Bremen), for stable isotope measurements, and Walter Luttmer, AWI (Bremerhaven), for technical assistance. Further we thank Hyunyung Boo, McGill University (Montreal), as well as Nele Lamping, Jan Unverfärth and Marco Wolsza, MARUM (Bremen), for sample processing. Sample material was provided by the GeoB repository at MARUM, Bremen. Klinikum Bremen-Mitte is gratefully acknowledged for providing their facilities for the computed tomographies. Arne-Jörn Lemke and Christian Timann, Gesundheit Nord (Bremen), are thanked for performing the CT scans and their support during the measurements. The authors also thank the Editor and two anonymous reviewers for improving the paper with comments and suggestions.

6 Wahlenbergfjord (Svalbard): A glacier-proximal fjord suitable to reflect regional hydrographic variability during Holocene? (Manuscipt II)

Martin Bartels[a], Jürgen Titschack[a], Kirsten Fahl[b], Rüdiger Stein[b], Dierk Hebbeln[a]

[a]MARUM – University of Bremen, 28359 Bremen, Germany
[b]Alfred Wegener Institute for Polar and Marine Research, 27568 Bremerhaven, Germany

(submitted to *Boreas*)

Abstract

Exceptional high sedimentation rates in Arctic fjords provide the possibility to reconstruct environmental conditions in high temporal resolution during the (pre-)Holocene. The unique geographical position of Svalbard at the intersection of Arctic and Atlantic waters offers the opportunity to estimate local (mainly glacier-related) vs. regional (hydrographic) variabilities. Sedimentological, micropalaeontological and geochemical data of a sedimentary record from the very remote, glacier-surrounded Wahlenbergfjord in eastern Svalbard provides information on glacier dynamics, palaeoceanographic and sea ice conditions during the Holocene. The present study illustrates a high meltwater discharge during the summer insolation maximum (~11.3–7.7 ka) when the intrusion of upwelled relative warm Atlantic-derived waters led to an almost open fjord situation with reduced sea ice. Around 7.7 ka, a rapid hydrographic shift is recognisable: The dominance of inflowing Atlantic-derived waters was replaced by a strengthening influence of Arctic Water reflecting regional palaeoceanographic conditions evident in the benthic foraminiferal fauna also at Svalbard´s margins. Neoglacial conditions characterised the late Holocene (~3.1–0.2 ka), when glaciers likely advanced as cold atmospheric temperatures were decoupled from the advection of relative warm intermediate waters probably caused by an extending sea ice coverage. Accordingly, our data elucidate that even a remote, glacier-proximal study site reflects rapid as well as longer-term regional changes.

6.1 Introduction

Arctic fjords have the potential to provide high-resolution climate archives for the last deglaciation and the subsequent Holocene, because of the large accumulation of mainly glacigenic sediments. The importance and value of fjords for oceanographic, biological, ecological, sedimentological and (bio)geochemical studies has been appreciated by scientists since more than a century (Syvitski et al., 1987). Fjords combine physical features of oceans with those of estuarine systems. Most Arctic fjords are covered by seasonal sea ice and fed by tidewater glaciers until today (Howe et al., 2010). Their topography controls the circulation in the fjord system influencing (and complicating) fjord processes (Inall and Gillibrand, 2010). Sedimentological and palaeoceanographic processes in fjords have been studied extensively during the last thirty years showing that sedimentation in high-latitude fjords is primarily influenced by glacier activity including the deposition of ice-rafted material and meltwater-transported sediments (Howe et al., 2010; and references therein). Amongst Arctic fjords, those in Svalbard are unique as they are exposed to milder climate conditions than any other fjords at similar latitudes by the far northward advection of relative warm Atlantic Water (AW) that also considerably affect the fjord settings directly (Cottier et al., 2010).

Although the Wahlenbergfjord in Nordaustlandet, eastern Svalbard (Fig. 28a, b), is influenced by glacier dynamics until today, substantial changes occurred in the past ~20 ka. During the Last Glacial Maximum (~21.7–18.2 ka; ~18–15 ^{14}C ka after Landvik et al., 1998), the study area was characterised by the massive Svalbard–Barents Sea Ice Sheet (SBIS) which covered the entire Barents Sea as well as the islands of the Svalbard archipelago and consequently also the Wahlenbergfjord (Landvik et al., 1998). Glacio-isostatic emergence data based on radiocarbon-dated raised beaches suggest that one major ice dome of the SBIS was located at the southwestern margin of Nordaustlandet covering the southern mouth of Hinlopen Strait (Forman et al., 2004). This assumption is supported by reconstructed ice-sheet flows using swath-bathymetry data, which illustrate that the SBIS was drained northward through the Hinlopen Strait (Dowdeswell et al., 2010) as well as eastward south of Nordaustlandet (Hogan et al., 2010a). In their ^{10}Be-based study, Hormes et al. (2011) showed that some smaller ice domes covered Nordaustlandet during the late Weichselian likely coalescing with the above mentioned major ice dome during the Last Glacial Maximum when

Fig. 28: (a) Svalbard Archipelago with (sub)surface ocean currents: relative warm Atlantic Water (red arrows) and cold Arctic Water (blue arrow). Yellow dots mark core location GeoB10831-3 of the present study and further core sites mentioned in the text. A: NP05-71 (Klitgaard Kristensen et al., 2013); B: NP94-51 (Jernas et al., 2013; Koç et al., 2002; Ślubowska-Woldengen et al., 2007; Ślubowska et al., 2005); C: GeoB10817-4 (Bartels et al., 2017); D: NP05-11-21 (Jernas et al., 2013; Rasmussen et al., 2014b; Skirbekk et al., 2010); E: MSM5/5-712-1 (Müller et al., 2012; Spielhagen et al., 2011; Werner et al., 2014, 2013, 2011); F: JM98-845 (Rasmussen et al., 2012); G: MD99-2304 (Hald et al., 2004); H: MD99-2305 (Hald et al., 2004); I: JM02-440 (Ślubowska-Woldengen et al., 2007); J: HR3 (Majewski et al., 2009); K: JM02-460 (Rasmussen et al., 2007; Rasmussen and Thomsen, 2014). Green rectangle: Study area as shown in (b). (b) Northeastern Spitsbergen and western Nordaustlandet with main ice caps Vestfonna and Austfonna surrounding Wahlenbergfjord. Locations mentioned in the text are indicated (see legend). Yellow dots mark studied core location GeoB10831-3 as well as core sites GeoB10817-4 (Bartels et al., 2017) and NP94-51 (Jernas et al., 2013; Koç et al., 2002; Ślubowska-Woldengen et al., 2007; Ślubowska et al., 2005). Green dots mark CTD stations of hydrographic profile (shown in (c)). The bathymetric metadata and Digital Terrain Model data products in (a) and (b) have been derived from the EMODnet Bathymetry portal (http://emodnet-bathymetry.eu/). Topographic data in (b): © Norwegian Polar Institute (Norwegian Polar Institute, 2014). (c) Salinity profile of the Hinlopen Strait/Wahlenbergfjord transect (green dashed line in (b)). Station 739-1 is located at the core site GeoB10831-3. Hydrographic data were measured during cruise MSM02/03 in August 2006 utilising a Sea Bird CTD sensor (for methodological details see cruise report; Lherminier et al., 2009). Interpolated profile created with Ocean Data View (Schlitzer, 2015). Assumed boundaries for Atlantic Water are marked with a white contour line (salinity = 34.65; Cottier et al., 2005).

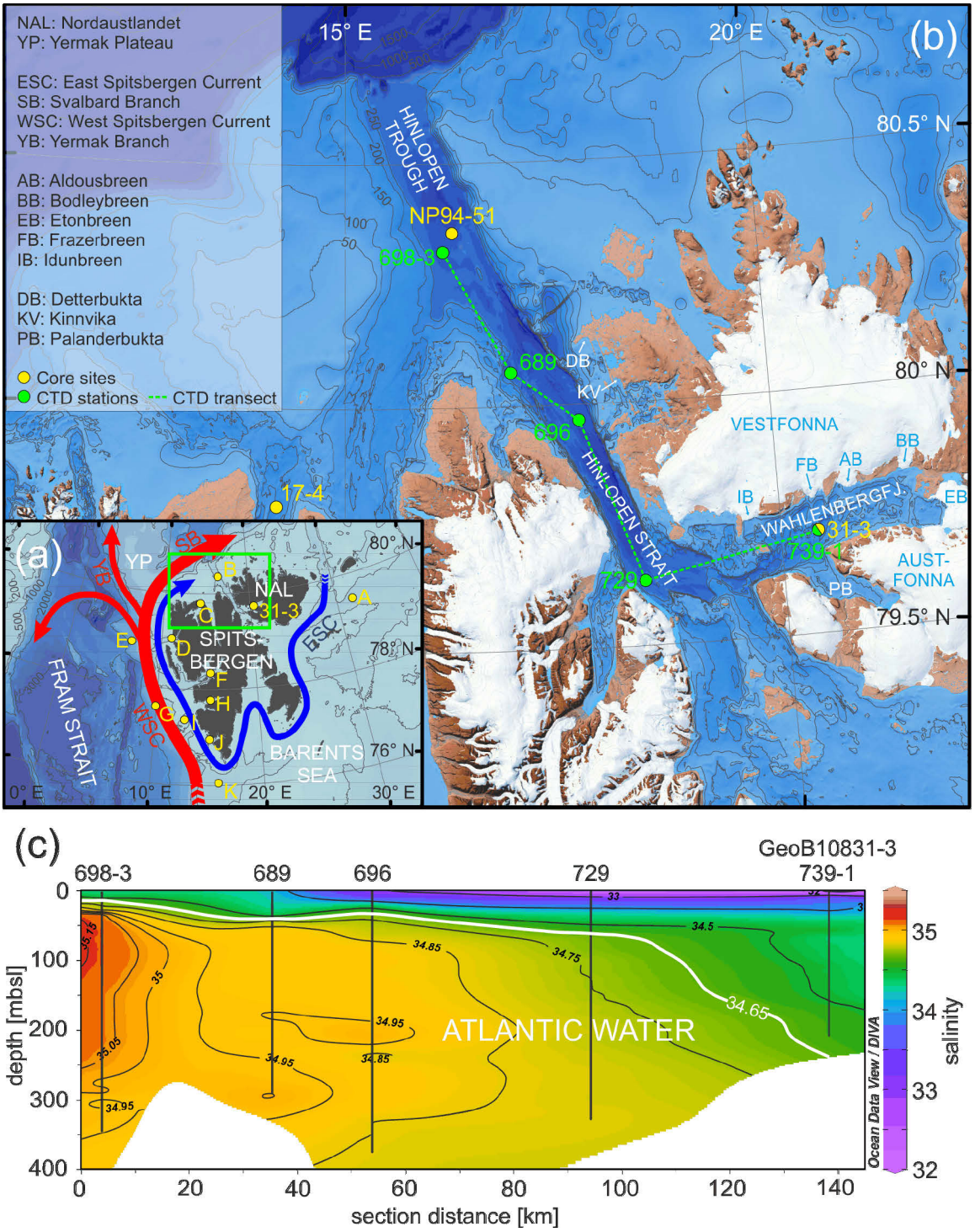

Wahlenbergfjord was one of the main ice stream pathways draining those ice domes (Flink et al., 2017). Accordingly, the Wahlenbergfjord was ice-filled until the onset of the Holocene (Flink et al., 2017). Palaeoceanographic changes during the Holocene have been documented for the continental slopes and fjords of the southern, western and northern Svalbard margin as well as for the troughs further east of the archipelago. The entire region has been directly affected by AW advection (e.g., Bartels et al., 2017; Klitgaard Kristensen et al., 2013; Kubischta et al., 2010; Łącka et al., 2015; Lubinski et al., 2001; Rasmussen et al., 2007, 2012; Skirbekk et al., 2010; Ślubowska-Woldengen et al., 2007; Ślubowska et al., 2005).

The present study investigates the Holocene palaeoenvironmental development within the remote Wahlenbergfjord. We especially focused on (i) how the major climatic and oceanographic changes were reflected in this remote fjord, today located more than hundred kilometres away from the main route of relative warm AW influencing the region (Fig. 28a), and (ii) the effect of the interplay between the Atlantic and Arctic waters and the numerous tidewater glaciers surrounding the fjord on the local environment through time. Therefore, we evaluated benthic foraminifera assemblage data combined with sediment properties and geochemical tracers to gain information on the regional development of the water masses, the sea ice coverage and the local glacier dynamics.

6.2 Physical setting

6.2.1 Oceanography

Relative warm and saline AW is transported to high northern latitudes by the Norwegian Atlantic Current continuing as the West Spitsbergen Current (Rudels, 2009; Fig. 28a). The West Spitsbergen Current follows the western continental margin of Spitsbergen as it is topographically steered (Saloranta and Svendsen, 2001). Due to the presence of fresher surface waters deriving from melting sea ice and glaciers (e.g., in the fjords of western Spitsbergen), AW submerges at 78 °N (Johannessen, 1986; Manley, 1995). Successively, the West Spitsbergen Current is divided north-west of Spitsbergen into the northward flowing Yermak Branch and the Svalbard Branch (Fig. 28a). The Svalbard Branch crosses the Yermak Plateau and follows the northern continental slope of Svalbard (Aagaard et al., 1987). As relative fresh and cold surface waters insulate the warmer AW core from heat loss to the atmosphere, the Svalbard Branch is considered to be most important for heat advection into the Arctic Ocean (Manley, 1995; Saloranta and Haugan, 2001). A southward intrusion of submerged Atlantic-derived waters into Hinlopen Strait is evident in the salinity profile of the Hinlopen–Wahlenbergfjord transect (Fig. 28c; based on hydrographic data retrieved during RV Maria S. Merian cruise MSM02/03 in August 2006; Lherminier et al., 2009). If remnants of AW reach into Wahlenbergfjord today cannot be proven by the presented hydrographic data showing lower salinities in the fjord compared with the Hinlopen Strait. However, Atlantic-derived waters probably mix with cold, probably fresher local (winter) waters and/or with northward flowing Arctic waters from the northern Barents Sea, which possibly enter the fjord via the southern Hinlopen Strait.

6.2.2 Wahlenbergfjord – local setting

The west–east orientated Wahlenbergfjord is the biggest fjord of Nordaustlandet, the second largest island of the Svalbard archipelago (Fig. 28a, b). The Wahlenbergfjord system consist of the eponymous fjord and the tributary Palanderbukta (Fig. 28b). The ~50 km long Wahlenbergfjord itself is up to ~290 m deep in the outer part, whereas the inner part is much shallower (Flink et al., 2017). The bedrock sill at the fjord´s mouth is interrupted by a ~200 m deep passage to the Hinlopen Strait, which divides Nordaustlandet from Spitsbergen. Major parts of Nordaustlandet are covered by two large ice caps (Vestfonna and Austfonna) whose outlet glaciers drain into the Wahlenbergfjord system (Fig. 28b). Accordingly, this fjord system is influenced by tidewater glaciers until today (e.g., Idunbreen, Frazerbreen, Aldousbreen, Bodleybreen, Etonbreen). During the last decades, those tidewater glaciers – especially at the north coast of the Wahlenbergfjord – were partly retreating (Braun et al., 2011). Large portions of the coasts exhibit bare rocks, mainly outcrops of the Pre-

Cambrian–Ordovician *Hekla Hoek* complex (e.g., Flood et al., 1969; Harland et al., 1966; Ohta, 1982) as well as Carboniferous and Permian sediments including dolomites and limestones (e.g. Lauritzen, 1981). Accordingly, glacigenic sediments (meltwater-transported suspended glacier flour as well as ice-rafted detritus) are most likely eroded remnants from those rock formations.

6.3 Material and Methods

This study is based on the 575 cm long sediment core GeoB10831-3 which was retrieved from the Wahlenbergfjord (Nordaustlandet; 79.71 °N, 20.43 °E; Fig. 28a, b) from 217 m water depth during RV *Maria S. Merian* cruise MSM02/03 in August 2006 (Lherminier et al., 2009). Archive halves of the sediment core were scanned by a computer tomograph (CT) at the hospital *Klinikum Bremen-Mitte*. All clasts > ~1 mm were quantified (volume percentages and number of clasts per cm^3). Running means of those data have been calculated, which were considered every 5 cm when plotted against age. For methodological details of the CT analyses see Bartels et al. (2017). For microfossil and stable oxygen and carbon isotope analyses, working halves of the sediment core were sampled with 10 ml syringes in 20 cm and 5 cm intervals, respectively. Bulk samples were washed through a 63 µm sieve. The remnants were dried before they were sieved trough 150 µm and 500 µm meshes.

In each microfossil sample at least 200–300 foraminifera from the >150 µm fraction were counted to obtain representative assemblages (Patterson and Fishbein, 1989), using a micro-splitter if the number of foraminifera was higher. Only four samples contain less than 200 foraminifera; one sample (depth: 83 cm) was discarded from faunal analyses due to a very low number of specimens (<50). Where possible, benthic foraminifera were identified at species level. While agglutinating species exhibit a lower preservation potential, most calcareous benthic foraminifera show no indications of dissolution or transport. To avoid any taphonomic error, only calcareous taxa have been taken into account for calculating relative percentages (contributions of agglutinants are low with ~0–16 % of the total benthic foraminiferal fauna decreasing down-core). Morphotypes of the calcareous benthic foraminifera species *Stainforthia loeblichi* s.s. and *S. concava* as well as *Buccella frigida* s.s. and *B. tenerrima* were not distinguished and are grouped as *S. loeblichi* s.l. and *B. frigida* s.l., respectively. Where hyaline could not be identified, they were summarized as Rotaliina. Benthic foraminiferal accumulation rates (BFAR; excluding agglutinants) were determined following Ehrmann & Thiede (1985). A Principle Component Analysis (PCA) of the calcareous fauna (considering species above 1 %) was performed (covariance mode) to identify dominant faunal assemblages and their respective developments through time with the software *PAST* (PAleontological STatistics) version 3.16 (Hammer et al., 2001).

AMS radiocarbon measurements of mixed benthic foraminifera (~1.4–12.2 mg carbonate) in seven samples were carried out at *Cologne AMS*, University of Cologne, and at ETH in Zürich (Table 2). All samples were measured twice apart from the samples at 0.5 and 571.5 cm depth. The age–depth model for core GeoB10831-3 was created using the Bayesian software *BACON* (Blaauw and Christen, 2011) based on *R* (R Development Core Team, 2011). The *Marine13* calibration curve (Reimer et al., 2013) and an averaged regional reservoir age correction $\Delta R = 98 \pm 37$ years were applied (averaging six ΔR values from the marine reservoir database on http:/calib.org/marine/; Mangerud, 1972; Mangerud and Gulliksen, 1975; Olsson, 1980). All radiocarbon measurements (including non-averaged double measurements) were used to create the

age–depth model (Table 2). Default priors of *BACON* were used apart from the settings for error estimation. Those parameters (Student´s-t distribution) were set at t.a = 9 and t.b = 10 (default: 3 and 4, respectively) to receive a less smoothed age–depth model that includes all calibrated radiocarbon ages. From here on, ages are given as calibrated ages (ka = thousand years before 1950 CE).

Table 2: AMS radiocarbon measurements of mixed benthic foraminifera and calibrated ages applying the Marine13 calibration curve (Reimer et al., 2013) and an averaged regional ΔR = 98±37 years (calib.qub.ac.uk/marine/). Measurements were carried out at *Cologne AMS*, University of Cologne and at ETH Zürich. All depths are median depths of syringe-samples with 1 cm radii. Age–depth model developed with *BACON* (Blaauw and Christen, 2011). Calendar ages given in the text are weighted mean values (wmean) provided by *BACON*.

Lab ID	depth	^{14}C age		cal. age [a BP]			
	[cm]	[a]	±	min	max	median	**wmean**
COL2576.1.1	0.5	620	28	-66	295	199	**178**
ETH-61281.1.1	61.5	2,288	86	1,943	2,306	2,130	**2,130**
ETH-61281.2.1	61.5	2,852	69				
ETH-61282.1.1	107.5	3,312	73	2,920	3,249	3,089	**3,088**
ETH-61282.2.1	107.5	3,,224	77				
ETH-58453.1.1	137.5	4,994	71	4,922	5,405	5,112	**5,153**
ETH-58453.2.1	137.5	5,547	90				
ETH-61283.5.1	372.5	7,642	72	7,923	8,178	8,043	**8,049**
ETH-61283.6.1	372.5	7,651	78				
ETH-58454.1.1	477.5	8,830	80	9,248	9,504	9,394	**9,390**
ETH-58454.2.1	477.5	8,655	77				
COL2577.1.1	571.5	10,385	38	11,115	11,562	11,283	**11,298**

Stable carbon and oxygen isotopes measurements were carried out on the carbonate shells of the epibenthic foraminifera *Cibicides lobatulus* and the endobenthic foraminifera *Nonionellina labradorica* (4–10 individuals from each species; 150–500 µm in size) at MARUM in Bremen employing the Finnigan MAT 251 gas isotope ratio mass spectrometer with a Kiel I automated carbonate preparation device (standard deviation of in-house standard: 0.03 ‰ for $\delta^{13}C$ and 0.04 ‰ for $\delta^{18}O$). Stable oxygen isotope data were corrected for the global ice volume effect (Waelbroeck et al., 2002) and vital effects of the benthic species: +0.64 ‰ for *C. lobatulus* (Shackleton, 1974) and -0.2 ‰ for *N. labradorica* (Duplessy et al., 2005).

Homogenised, dried sediment samples from selected depths were geochemically analysed. For the estimation of sea ice coverage, the C_{25} isoprenoid lipid biomarker (IP_{25}) was analysed (see Belt et al., 2007). Additionally, the phytoplankton biomarkers brassicasterol and dinosterol have been examined (as described in Fahl and Stein, 1999; Volkman, 1986; Volkman et al., 1993). About 3 g of sediment were ultrasonicated for extraction of IP_{25} and sterols. The latter were analysed by gas chromatography/mass spectrometry using internal standards for quantification. For methodological details of the biomarker analyses see Fahl and Stein (2012) and Bartels et al. (2017). Accumulation rates of biomarkers (IP_{25}, brassicasterol and dinosterol) were calculated following Ehrmann & Thiede (1985). Phytoplankton-IP_{25} indices have been computed after Müller et al. (2011) using brassicasterol (P_BIP_{25}) and dinosterol (P_DIP_{25}) as phytoplankton biomarkers, respectively.

6.4 Results

6.4.1 Lithology

The upper ~450 cm of sediment core GeoB10831-3 consist of almost homogenous olive grey (Munsell code 5Y4/1) silty clay with several black flames and mottles whereas an oxidised brownish layer is evident in the upper centimetre. From ~450 cm downwards, the sediment is grading from brownish grey (5YR4/1) to pale brown (5YR5/2) while black mottles are still recognisable.

Clasts > ~1 mm detected by the CT analyses were considered as ice-rafted. Apart from several single larger clasts randomly distributed over the entire core length, the highest amounts of ice-rafted debris (IRD) appear in the upper 90 cm (up to 4.7 clasts cm^{-3} and up to 10 vol. %, respectively; Fig. 29). High volume percentages of clasts mainly derive from single large clasts (see peaks in vol. % and clasts in CT image/processed CT data; Fig. 29). The CT identified clasts in the interval between ~370–410 cm, which most likely derive from pyritized traces of bioturbation (processed CT data in Fig. 29).

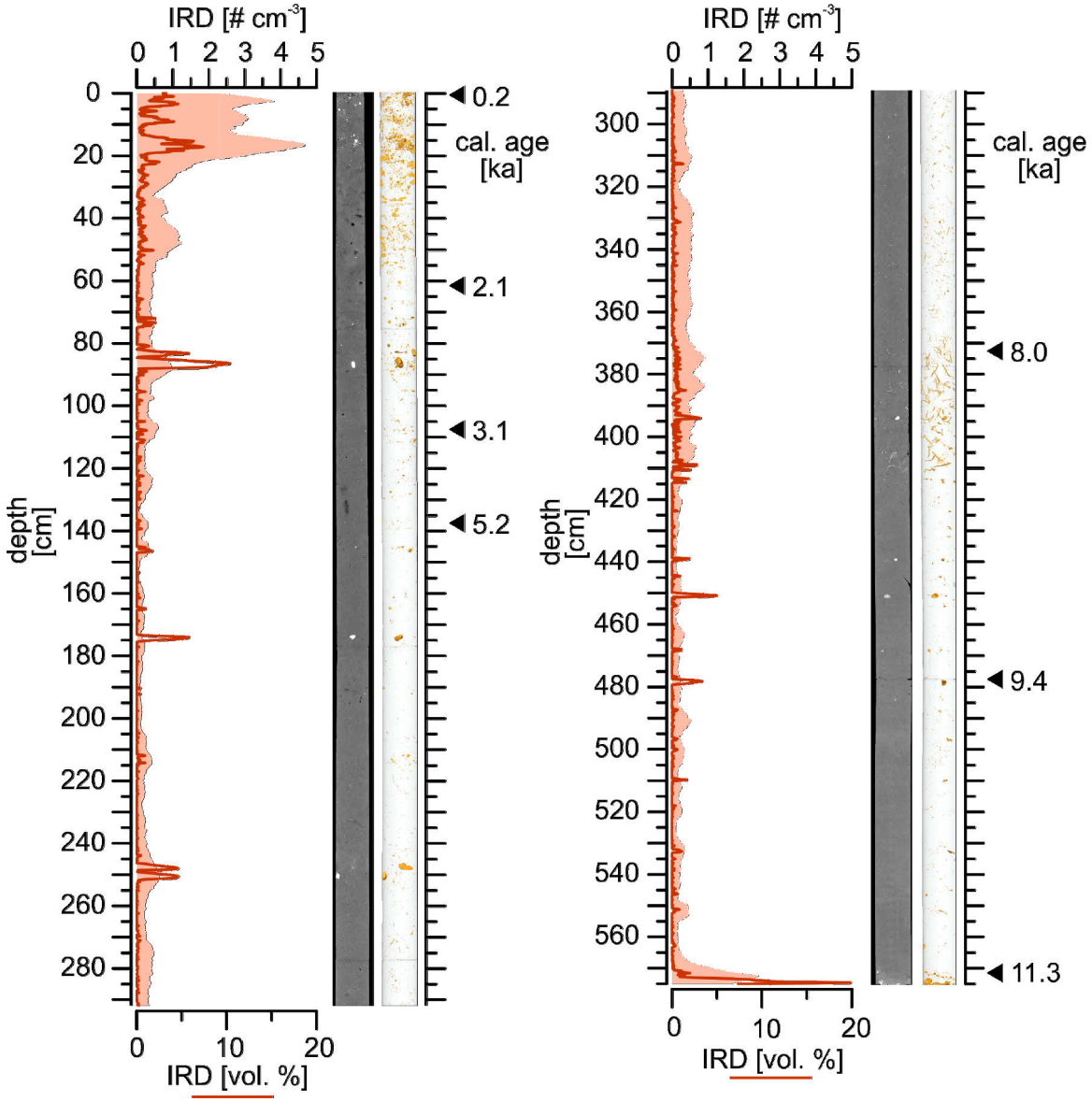

Fig. 29: IRD content: clasts > ~1 mm per cm^3 (reddish shadings) and volume percentages of clasts (red line) as derived from CT analyses. CT image (orthogonal slice, left) and processed CT data (right) showing clasts (orange), with calibrated radiocarbon dating points (triangles; see Table 2) on the right y-axis.

6.4.2 Chronology

Sediment core GeoB10831-3 covers a time span from 11.3–0.2 ka (Table 2; Fig. 30). Sedimentation rates are comparably high in the lower part of the core (142.5–571.5 cm; 11.3–5.3 ka) ranging from 48 to 84 cm ka^{-1} (mean: 74 cm ka^{-1}), while they are considerably lower in the upper part (0.5–137.5 cm; mean: 34 cm ka^{-1}; Fig. 30). The lowest sedimentation rates (~13 cm ka^{-1}) were determined between 112–127.5 cm (4.5–3.3 ka). In the latter interval, an unconformity (e.g., a hiatus) is not evident, but cannot be excluded; sediment texture is homogenous and an erosive horizon is not recognisable in the CT image (Fig. 29).

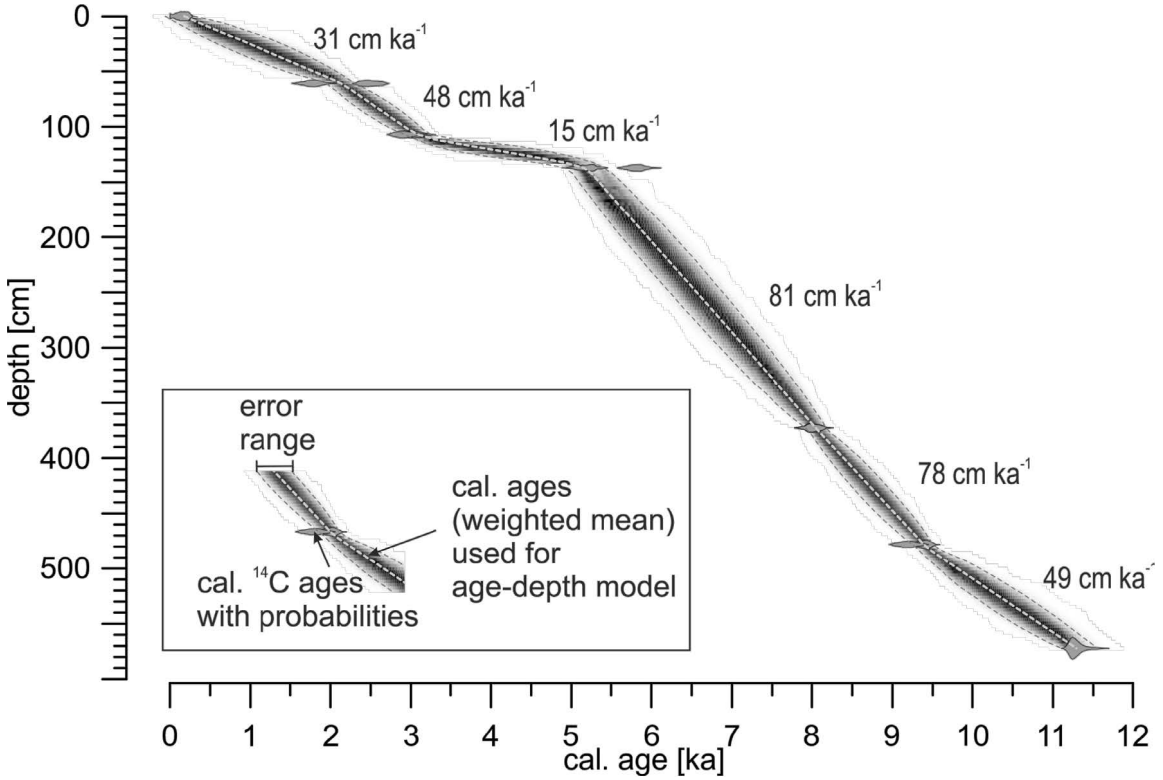

Fig. 30: Age–depth model developed with *BACON* (Blaauw and Christen, 2011) applying the *Marine13* calibration curve (Reimer et al., 2013) and a regional reservoir correction ΔR = 98 ±37 years (calib.qub.ac.uk/marine/): Light grey dashed curve shows weighted mean ages; shadings show error ranges (Table 2); grey shapes mark calibrated radiocarbon measurements including probability ranges (not provided in Table 2). Numbers at curve give mean sedimentation rates between radiocarbon-dated depths derived from *BACON*.

6.4.3 Microfossil analysis

The benthic foraminiferal fauna is composed of 52 calcareous taxa (10–28 calcareous taxa per sample). Until ~5.4 ka, the BFAR shows highest values ranging between ~750 and ~5,930 individuals cm^{-2} ka^{-1} (Fig. 31f). Subsequently, the BFAR is declining (~110–2,190 individuals cm^{-2} ka^{-1}; Fig. 31f). *Cassidulina reniforme* (~1–51 %; Fig. 31a), *Nonionellina labradorica* (~4–59 %; Fig. 31b) and *Elphidium clavatum* (~1–78 %; Fig. 31c) dominate the benthic fauna. Further abundant species are *Buccella frigida* s.l. (~1–16 %; Fig. 31d), *Cibicides lobatulus* (~2–57 %; Fig. 31e), *Islandiella helenae* (~1–19 %; not shown) and *Melonis barleeanus* (~0–12 %; not shown).

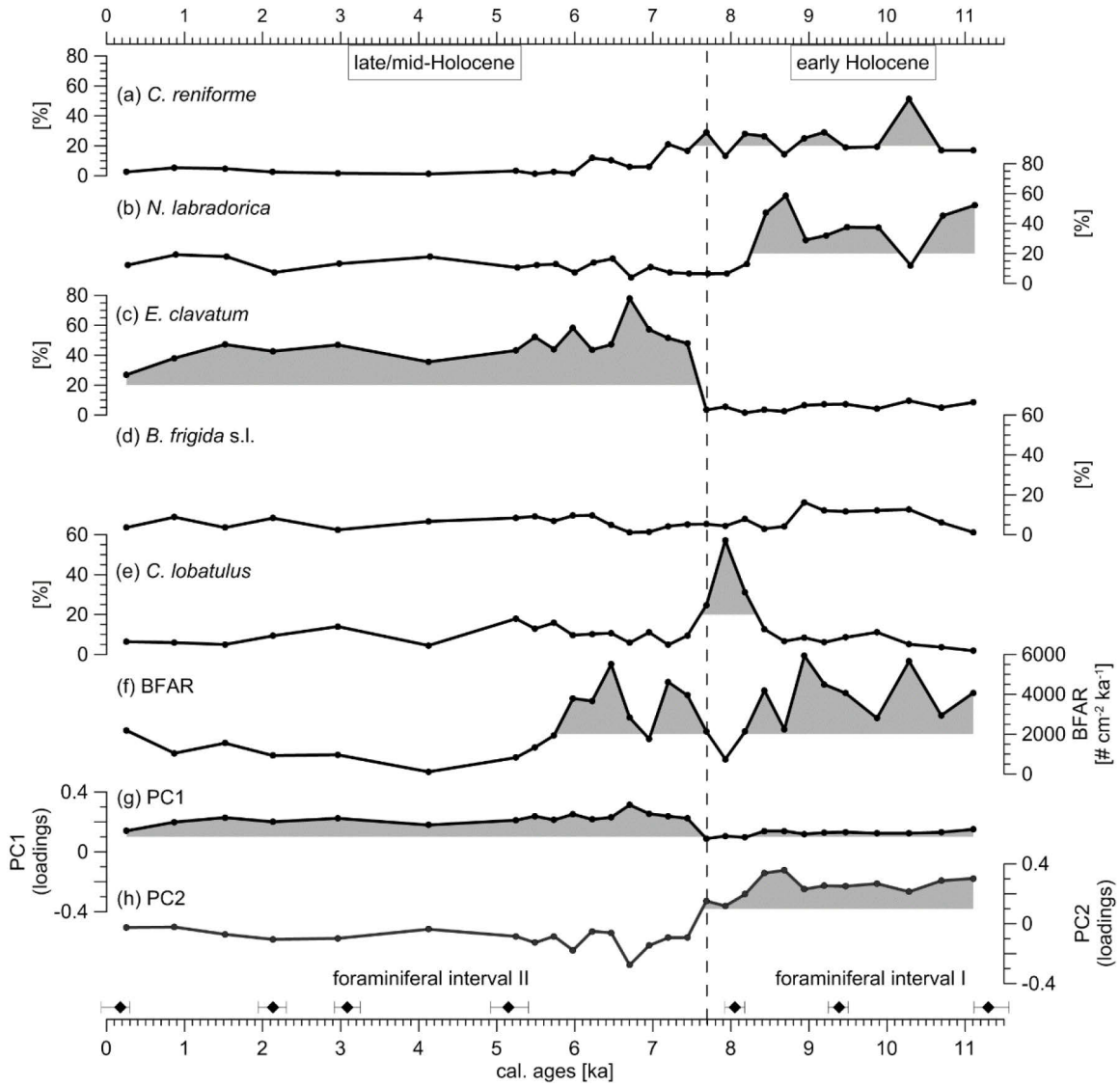

Fig. 31: Calcareous benthic foraminifera fauna: relative percentages of *Cassidulina reniforme* (a), *Nonionellina labradorica* (b), *Elphidium clavatum* (c), *Buccella frigida* s.l. (d), *Cibicides lobatulus* (e). (f) Benthic foraminiferal accumulation rate (BFAR). Principle Component Analyses (PCA): Distribution of principle components PC1 (g) and PC2 (h) over time (loadings). Dashed line marks boundary between foraminiferal intervals I (early Holocene) and II (late/mid-Holocene) based on the distribution of foraminiferal assemblages (principle components). Diamonds show calibrated radiocarbon dating points with error ranges (Table 2).

The PCA of the calcareous benthic foraminiferal fauna yielded two principle components (assemblages; PC1 and PC2) describing ~86.1 % of the variance. The major part of the fauna is covered by PC1 (~60.8 %), which is dominated by *E. clavatum* (from here on, named "*E. clavatum* assemblage"; Table 3). PC2 explains ~25.2 % of the faunal variance and is dominated by *N. labradorica*, while *C. reniforme* is an associated species (from here on, named "*N. labradorica* assemblage"; Table 3). Faunal intervals were defined regarding the major appearances of the faunal assemblages: Faunal interval I (~11.3–7.7 ka) was dominated by the *N. labradorica* assemblage (Fig. 31h). The subsequent faunal interval II (~7.7–0.2 ka) was dominated by the *E. clavatum* assemblage, although the influence of the *N. labradorica* assemblage is slightly increasing at the end of this interval (Fig. 31g, h).

Table 3: Scores and variance of the Principle Component Analyses (PCA). Scores show the relevance of dominating and associated species with respect to the corresponding assemblage (principle component).

Scores	Principle component 1 (*E. clavatum* assemblage)	Principle component 2 (*N. labradorica* assemblage)
B. frigida s.l.	0.07	0.09
C. reniforme	0.28	**0.56**
C. lobatulus	0.27	0.14
E. clavatum	**1.66**	-0.61
I. helenae	0.14	0.07
N. labradorica	0.60	**0.91**
Variance [%]	60.8	25.2

6.4.4 Stable carbon and oxygen isotopes

Stable oxygen isotopes (corrected for vital and global ice volume effect) of the epibenthic foraminifera *C. lobatulus* show an increasing trend until 4.9 ka and less variation afterwards. While $\delta^{18}O$ values of *C. lobatulus* range from 3.2 to 4.5 ‰, stable oxygen isotope ratios of the endobenthic foraminifera *N. labradorica* exhibit slightly less variability apart from a few peaks ranging between 3.2 to 4.3 ‰. Before ~6.5 ka, a higher offset of epi- and endobenthic $\delta^{18}O$ values is indicated compared to the following time interval (Fig. 32a).

Stable carbon isotopes show no significant trend during the entire record; neither for *C. lobatulus* (-0.1 to 1.6 ‰) nor for *N. labradorica* (-4 to -1 ‰) whose variability is much higher (Fig. 32b). The offset between the epi- and the endobenthic stable carbon isotope ratios ($\Delta\delta^{13}C = \delta^{13}C_{C.\ lobatulus} - \delta^{13}C_{N.\ labradorica}$) is high (up to 4.7 ‰) until ~8 ka, around 3.3 ka (max. 3.8 ‰, however, marked by only one data point) and during the last 1000 years (max. 4.3 ‰) but relatively low from ~6.8 to ~3.8 ka (1.9 to 3.5 ‰) as well as from ~3.1 to ~1 ka (mainly below 3 ‰; Fig. 32c).

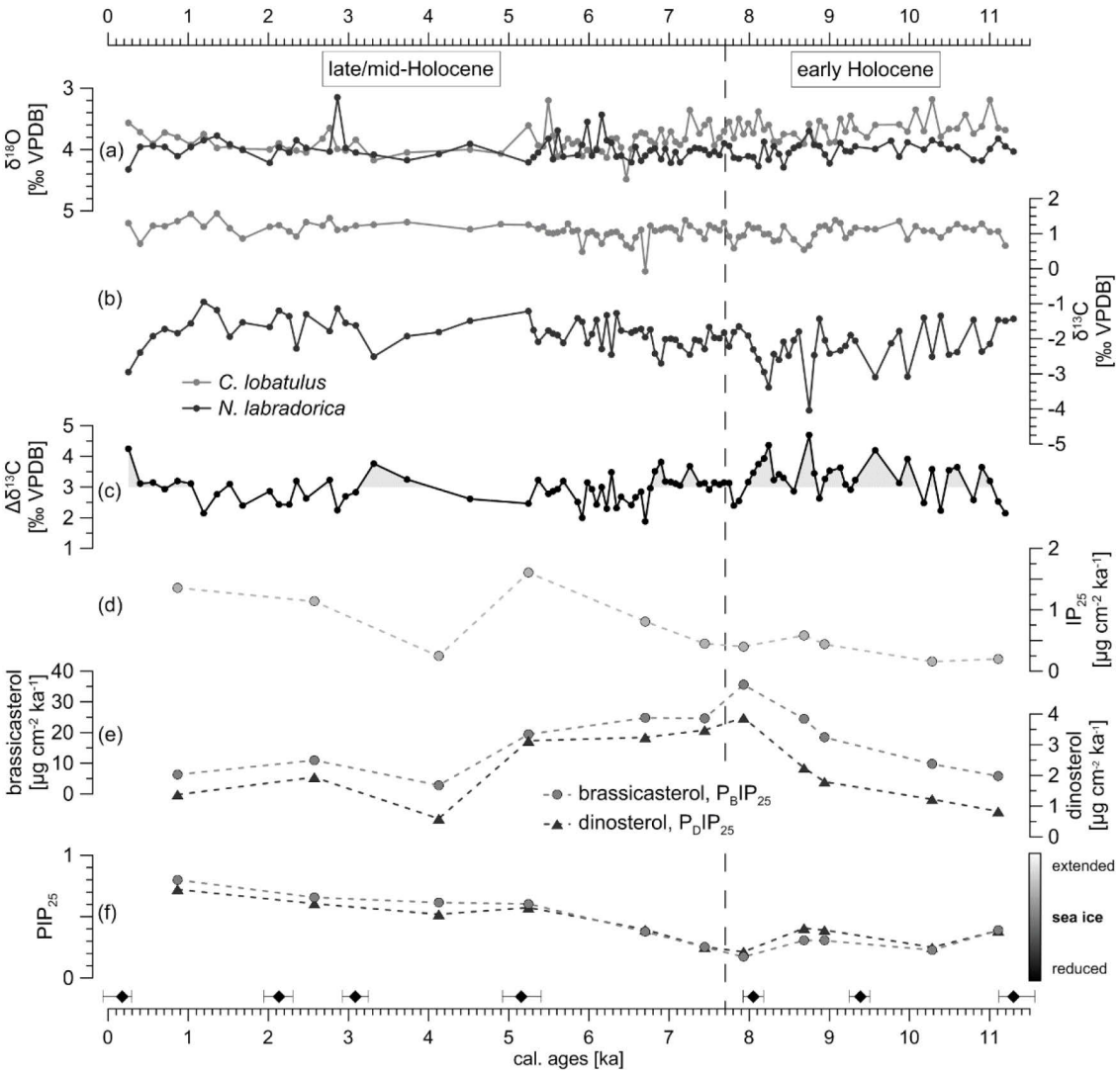

Fig. 32: Stable oxygen isotopes (corrected for global ice volume and vital effects; (a)) and stable carbon isotopes (b) derived from shells of the epibenthic foraminiferal species *C. lobatulus* (light grey lines) and the endobenthic foraminiferal species *N. labradorica* (dark grey lines). (c) Offset between epi- and endobenthic stable carbon isotopes (*C. lobatulus – N. labradorica*). (d) Accumulation rates of sea ice biomarkers (IP_{25}). (e) Accumulation rates of phytoplankton biomarkers brassicasterol (light grey dots) and dinosterol (dark grey triangles). (f) Phytoplankton-IP_{25} indices P_BIP_{25} (light grey dots) and P_DIP_{25} (dark grey triangles) illustrating the sea ice cover ranging from a reduced to an extended coverage. Dashed line marks boundary between the early and the late/mid-Holocene, respectively (see Fig. 31). Diamonds show calibrated radiocarbon dating points with error ranges (Table 2).

6.4.5 Biomarkers

Accumulation rates of both phytoplankton biomarkers exhibit a parallel trend peaking between ~7.9–5.2 ka (Fig. 32e). Brassicasterol (~2.8–35.6 µg cm^{-2} ka^{-1}) attained ten times higher values than dinosterol (~0.6–3.9 µg cm^{-2} ka^{-1}). Accumulation rates of sea ice biomarkers IP_{25} range from ~0.2 to ~1.6 µg cm^{-2} ka^{-1}, while highest values were reached at ~5.2 ka (Fig. 32d). Phytoplankton-IP_{25} indices P_BIP_{25} (using brassicasterol) and P_DIP_{25} (using dinosterol) show almost similar values (~0.2–0.8 and ~0.2–0.7, respectively). Until ~5.2 ka, both PIP_{25} indices range from ~0.2 to ~0.4, while afterwards, values up to ~0.8 were reached (Fig. 32f). The scatter plot in Fig. 33, showing the amount of IP_{25} in relation to phytoplankton biomarkers per gram total organic carbon (TOC), exhibits low IP_{25} values before ~7.7 ka while both phytoplankton biomarkers varied.

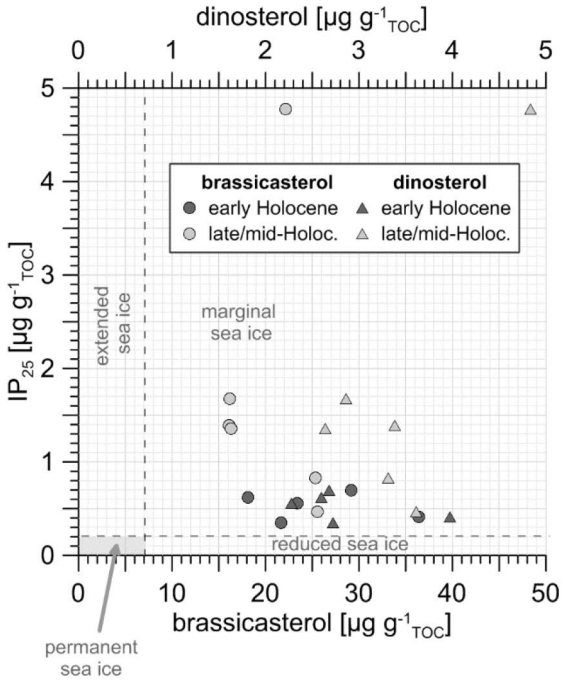

Fig. 33: Scatter plot showing sea ice biomarker (IP_{25} in µg per g TOC) against the phytoplankton biomarkers (in µg per g TOC) dinosterol (triangles) and brassicasterol (dots) during the early (>7.7 ka; dark grey) and late/mid-Holocene (<7.7 ka; light grey), respectively.

In contrast, higher IP_{25} values were observed after ~7.7 ka with a range of brassicasterol and dinosterol values similar to the previous interval. Peak IP_{25} and dinosterol amounts were reached at ~0.9 ka (Fig. 33).

6.5 Holocene palaeoceanographic evolution of the Wahlenbergfjord and glacier responses

The observed faunal intervals (Fig. 31g, h) allow the division of the record into the early Holocene (faunal interval I; ~11.3–7.7 ka) and the late/mid-Holocene (faunal interval II; ~7.7–0.2 ka). Due to significant changes in the BFAR and the IRD record it is reasonable to further subdivide the latter interval into the mid- (~7.7–5.2 ka) and the late Holocene (~5.2–0.2 ka; Fig. 34).

6.5.1 Early Holocene

The early Holocene (from ~11.3 ka on) in the Wahlenbergfjord area was dominated by the *N. labradorica* assemblage (Fig. 34a). The dominating species of the latter assemblage commonly lives around two to three centimetres below the bottom water–sediment interface (Alve and Bernhard, 1995; Loubere and Rayray, 2016) and feeds on fresh organic matter (Cedhagen, 1991). As this species preferentially responds to enhanced productivity at oceanic fronts, high percentages of *N. labradorica* (Fig. 31b) presumably indicate the formation of such a front in the Wahlenbergfjord (e.g., Rytter et al., 2002; Sheldon et al., 2016b; Steinsund, 1994). The corresponding high productivity is also reflected in the simultaneously high offset between epi- and endobenthic stable carbon ratios ($\Delta\delta^{13}C$; Fig. 34b), which has been proposed to be a valuable proxies for palaeo-productivity (Mackensen et al., 2017). The formation of such an oceanic front was likely caused by wind-induced upwelling of intermediate waters triggered by down-fjord blowing katabatic winds typical for Arctic fjords (Cottier et al., 2010). Due to the consequential deflection of surface waters by Ekman transport to the right (towards the northern shore), intermediate waters may have been upwelled south of the main wind-driven westward surface water transport (Cottier et al., 2010; Inall and Gillibrand, 2010). With sustained wind forcing it is possible that intermediate waters reached the surface forming an oceanic front (Cottier et al., 2010; Fig. 35a). Pawłowska et al. (2017) just recently emphasised the significant impact of Coriolis force-driven hydrodynamics, which led to different benthic foraminiferal faunas and sedimentation regimes at the northern part compared with the southern part of a west–east orientated fjord in southern Spitsbergen (Hornsund). While the northern part was mainly influenced by glacier-related sedimentation, the southern part was rather affected by advected water masses from the shelf.

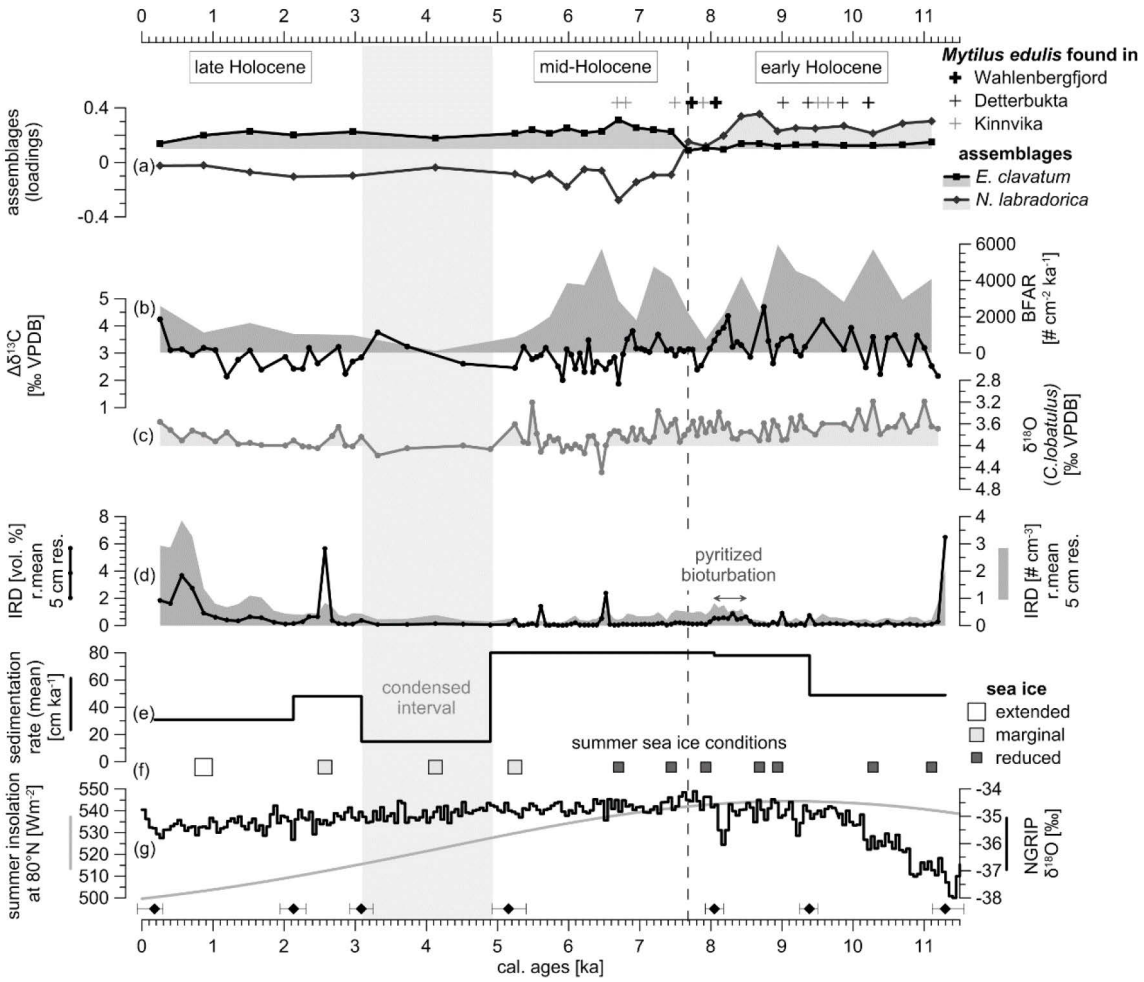

Fig. 34: (a) Distribution of foraminiferal assemblages (PCA loadings). Crosses: Appearance of the thermophilous blue mussel (*Mytilus edulis*) in northern Nordaustlandet and Wahlenbergfjord (locations see legend and Fig. 28a; Blake, 2006; Salvigsen, 2002). (b) Benthic foraminiferal accumulation rate (BFAR; shadings) and offset between epi- and endobenthic foraminiferal stable carbon isotopes (*C. lobatulus – N. labradorica*; black line). (c) Epibenthic foraminiferal stable oxygen isotopes. (d) Ice-rafted debris (IRD = clast > ~1 mm) derived from CT analyses (running mean, 5 cm resolution): volume percentages of clasts (line) and number of clasts per cm^3 (shadings). (e) Mean sedimentation rate based on *BACON* age–depth model (see also Fig. 30). (f) Symbols show reduced, marginal and extended summer sea ice conditions, respectively (based on P_BIP_{25} and IP_{25}/phytoplankton biomarker relations; see Fig. 32f and Fig. 33). (g) June–July insolation at 80 °N (grey line; Berger and Loutre, 1991) and stable oxygen isotopes from Greenland ice core NGRIP (black line; Rasmussen et al., 2014a). Dashed line marks boundary of time intervals based on the distribution of foraminiferal assemblages (see Fig. 31). Grey vertical shading indicates interval of condensed sediment. Diamonds show calibrated radiocarbon dating points with error ranges (Table 2).

During the early Holocene, intermediate waters in the Wahlenbergfjord were possibly remnants of Atlantic-derived waters. The southward advection of AW into the adjacent Hinlopen Strait may have been generated by intense wind-induced upwelling events at the northern Svalbard shelf like it has been reported from the western Spitsbergen shelf today (Cottier et al., 2007). Lind and Ingvaldsen (2012) reported that prevalent easterlies north of Svalbard support the upwelling of AW onto the northern shelf. This would enable a strengthened AW inflow into the Hinlopen Strait. Due to the interrupted sill at the Wahlenbergfjord´s mouth, a ~200 m deep passage connects the Hinlopen Strait with the Wahlenbergfjord allowing AW to enter the fjord (Fig. 28b). At high latitudes, productivity is promoted by the influx of AW as it transports nutrients that can only be consumed when entering the photic zone (e.g., Carmack and Wassmann, 2006; Falk-Petersen et al., 2015; Sakshaug, 1997). High amounts of marine organic matter in surface sediment samples from the eastern

Fram Strait (Birgel and Stein, 2004) may either derive from nutrients advected by AW, directly fostering primary production, or from the high flux of biogenic material, which is expected at the summer sea ice margin (Hebbeln and Wefer, 1991). Both scenarios would support the assumption that AW inflow is triggering enhanced productivity, as the seasonal melting of sea ice and the consequential position of the sea ice margin are also controlled by the inflow of warm AW west of Svalbard (e.g., Aagaard and Carmack, 1989; Untersteiner, 1988). An enhanced productivity at the study site during the early Holocene is also reflected in maximum BFAR (almost 6,000 individuals cm^{-2} ka^{-1}; Fig. 34b). The concurrent appearance of *B. frigida* s.l. (Fig. 31d) is most likely linked to this general productivity increase as *Buccella* spp. has been found at locations with high fresh and labile organic matter input (Polyak et al., 2002; Seidenkrantz, 2013). Parallel increasing percentages of *B. frigida* s.l. with high $\Delta\delta^{13}C$ values have likewise been recognised in a fjord of northern Spitsbergen during a similar time interval (Bartels et al., 2017). Skirbekk et al. (2010) also linked the abundant appearance of *Buccella* spp. at the northwestern Spitsbergen margin during the early Holocene to enhanced productivity. However, apart from the presence of AW and/or an oceanic front, a high productivity could likewise be connected to an increased nutrient supply by meltwater input. Indeed, Calleja et al. (2017) observed phytoplankton blooms in a glacier-proximal setting during spring, the main calcification time of *N. labradorica* (Zajączkowski et al., 2010b).

Nevertheless, Salvigsen (2002) and Blake (2006) reported about the appearance of the thermophilous blue mussel (*Mytilus edulis*) at the head of the Wahlenbergfjord at ~8.1 ka (7,700 ±150 uncorrected ^{14}C years BP) and ~7.7 ka (7,370 ±20 uncorrected ^{14}C years BP), respectively (Fig. 34a). Those bivalves have been linked to the influence of relative warm AW at the sea surface (Blake, 2006; Hansen et al., 2011; Salvigsen, 2002). As proposed above, persistent upwelling possibly allowed Atlantic-derived waters to reach the surface layer. In fjords of northwestern Nordaustlandet (Detterbukta and Kinnvika; see Fig. 28b for locations) *M. edulis* findings documented the inflow of surface AW already from ~10.2 ka onwards (9490 ±20 uncorrected ^{14}C years BP) until ~6.7 ka (6,335 ±25 uncorrected ^{14}C years BP; Blake, 2006; Fig. 34a). The earlier start and the longer time span of AW advection documented for the northern part of Nordaustlandet compared to the Wahlenbergfjord may be caused by the vicinity of the main branch of AW (the Svalbard Branch; Fig. 28a, b) to those northern shelf sites. However, due to glacier erosion and different outcrop situations, the Wahlenbergfjord *M. edulis* record might be incomplete and thus a continuous inflow of Atlantic-derived waters into the fjord during the entire early Holocene cannot be excluded. Nonetheless, it is also possible that the appearance of the blue mussel was linked to the higher summer insolation (Fig. 34g), which warmed the shallow waters at the fjord coasts as suggested by Ślubowska et al. (2005).

Depleted oxygen isotope ratios of *C. lobatulus* (Fig. 34c) in the early Holocene may reflect relatively warm bottom waters triggered by increased summer insolation (Berger and Loutre, 1991; Fig. 34g) causing relatively mild climatic conditions in Svalbard related to the Holocene Thermal Maximum (e.g., Miller et al., 2010b). However, as *C. lobatulus* calcifies in summer and *N. labradorica* in spring (Zajączkowski et al., 2010), the comparable high offset between the $\delta^{18}O$ ratios of *C. lobatulus* and *N. labradorica* (Fig. 32a) may be an effect of reduced summer salinities caused by increased meltwater supply from summer surface melting of the glaciers due to the high insolation reaching the deeper part of the fjord by sediment-laden, dense meltwater plumes.

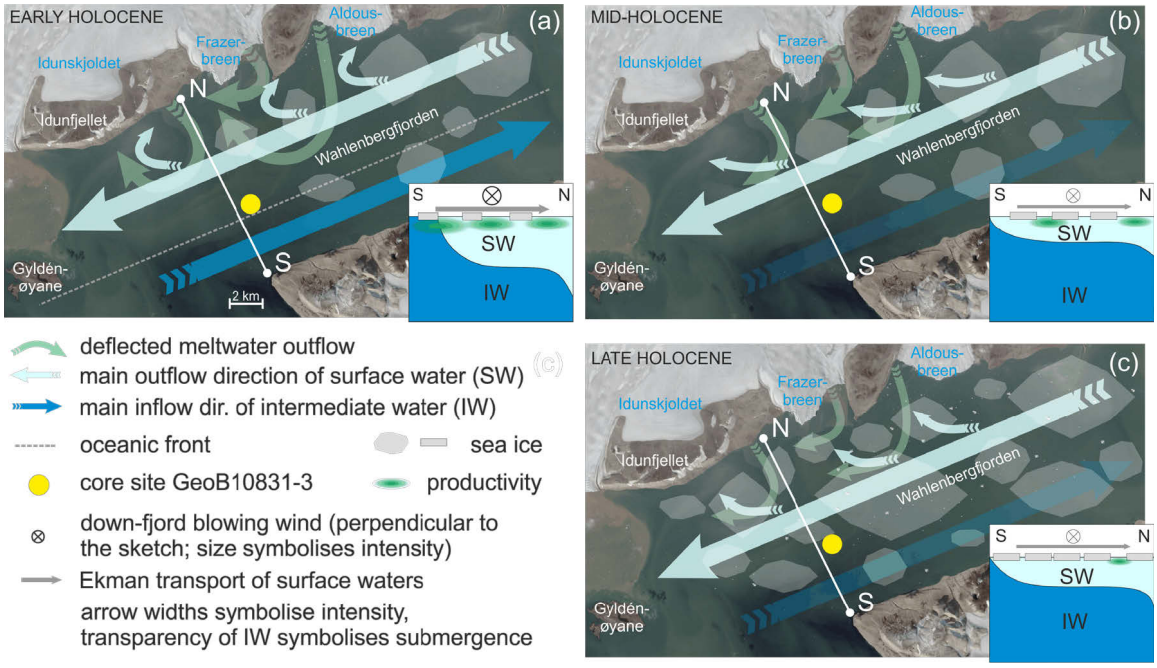

Fig. 35: Modern satellite images showing sediment plumes and recent positions of glacier fronts in the Wahlenbergfjord with assumed circulation, sea ice cover and iceberg rafting during the early (a), the mid- (b) and the late Holocene (c). Inserts symbolise cross-fjord profiles (S–N) with simplified distributions of water masses and wind-induced upwelling of intermediate waters due to Ekman transport of surface waters (after Cottier et al., 2010) as well as sea ice and productivity.
USGS Landsat picture: © Norwegian Polar Institute (http://toposvalbard.npolar.no/).

The reasons for comparable low amounts of ice-rafted material found in the early Holocene Wahlenbergfjord sediments (Fig. 34d) are probably twofold. Risen summer insolation probably increased the surface melting on the glaciers resulting in enhanced meltwater production and in a very high accumulation of fine-grained sediments within the fjord (especially from 9.4 ka onwards with up to almost 80 cm ka^{-1}; Fig. 34e, g) that masked the coarse IRD flux. In addition, during the mild early Holocene conditions, summer sea surface temperatures partly reaching 8–10 °C (indicated by *M. edulis* findings as discussed in Hansen et al., 2011) may have contributed to reduce the number of glaciers entering the fjord directly as tidewater glaciers and thus causing a diminished IRD input. Those comparably warm surface temperatures most likely resulted in a reduced sea ice cover during summer (Fig. 35a), which is also reflected in the sea ice biomarker data exhibiting lowest IP_{25} values during the early Holocene (Fig. 32d and Fig. 33). The trend of increasing phytoplankton biomarker data (dinosterol and brassicasterol; Fig. 32e and Fig. 33) in the course of the early Holocene also points to temporarily open water conditions during summer. Furthermore, the enhanced seasonality, caused by the maximal summer insolation during this time interval (Fig. 34g) and reflected in the mentioned offset between the oxygen isotope ratios of *C. lobatulus* and *N. labradorica* (Fig. 32c; see Rasmussen et al., 2012), probably contributed to relatively warm surface waters and consequential reduced sea ice coverage during summer. Open water conditions may also have been caused by katabatic winds like it was assumed at the northern Barents Sea margin during previous glacial periods (e.g., during MIS 6; Knies et al., 1999; Kremer et al., 2018).

The transition to the mid-Holocene is marked by the most prominent shift in the composition of the benthic foraminiferal fauna. The percentages of *B. frigida* s.l. declined already around 9 ka (Fig. 31d), followed by those of *N. labradorica* that diminished between 8.4 and 8.2 ka (Fig. 31b), parallel to a decrease in the $\Delta\delta^{13}C$

values suggesting a declining productivity (Fig. 34a, b). At ~7.9 ka, when sea ice proxies suggest a reduced sea ice cover (Fig. 32f and Fig. 34f), maximum percentages of *C. lobatulus* (Fig. 31e) in one individual sample might reflect strong bottom currents as assumed in various studies (Hald and Korsun, 1997; Hansen and Knudsen, 1995; Korsun and Hald, 1998; Steinsund, 1994). However, those percentages should be interpreted cautiously as they are based on only 91 specimens.

6.5.2 Mid-Holocene

From ~7.7 ka on, the *E. clavatum* assemblage dominated the benthic foraminiferal fauna (Fig. 34a). A similar faunal shift and/or a rapid increase of *E. clavatum* percentages is reported from the western, northern and eastern Svalbard margins (e.g., Hald et al., 2004; Klitgaard Kristensen et al., 2013; Kubischta et al., 2011; Rasmussen et al., 2012; Skirbekk et al., 2010; Ślubowska et al., 2005; locations: see Fig. 28a), as well as from the Franz Victoria Trough (east of Nordaustlandet; Duplessy et al., 2001). In modern faunas, *E. clavatum* is mainly found in the upper centimetre of the sediment but it can migrate down to 8 cm below the sediment surface depending on the food availability (Hunt and Corliss, 1993; Linke and Lutze, 1993). In Arctic regions, it primarily appears in cold waters <1 °C and within a wide salinity range of ~32.5–35 (Hald et al., 1994). Around Svalbard this relates predominantly to Arctic Water as defined by Cottier et al. (2005). Therefore, the shift to a dominance of *E. clavatum* may be connected to an increasing influence of Arctic Water replacing AW as previously suggested by various studies (Klitgaard Kristensen et al., 2013; Rasmussen et al., 2012; Skirbekk et al., 2010). Thus, a decreasing advection of AW probably allowed Arctic Water to enter the Wahlenbergfjord through Hinlopen Strait. Enriched $\delta^{18}O$ values of *C. lobatulus*, from ~6.5 ka onwards, support the assumption of cold Arctic-derived waters (Fig. 34c) as Arctic Water is colder than AW while salinities do not necessarily diverge (see definition of water masses in Cottier et al., 2005 and Loeng, 1991). While the BFAR stayed rather unchanged (Fig. 34b) and phytoplankton biomarkers exhibit peak values between ~7.9 and ~5.2 ka (Fig. 32e) a decreased productivity cannot be expected before ~6.8 ka when $\Delta\delta^{13}C$ values (Fig. 34b) declined. Arctic Water is assumed to be less nutrient-rich compared to AW (Hunt et al., 2016), but despite a possible dominating influence of Arctic Water in the fjord the enhanced productivity may have derived from a strong meltwater run-off (see maximum sedimentation rates; Fig. 34e) delivering high amounts of nutrients as reported from a glacier front in the Kongsfjord (western Spitsbergen; Calleja et al., 2017). At ~6.7 ka, reduced down-fjord winds may have lowered the upwelling of intermediate waters, consequently productivity decreased (reflected in the lowest values of the *N. labradorica* assemblage and decreased $\Delta\delta^{13}C$ values; Fig. 34a, b). Katabatic winds likely weakened because of the declined elevation of the ice caps (see emergence of the continental land masses reflecting shrinking ice loads in Forman et al., 2004) resulting in less steep slopes at the fjord coasts. Modelling studies of katabatic flow dynamics in Greenland show that katabatic winds are topographically-steered and mainly amplified by the steep coastal margins of the Greenland Ice Sheet (Heinemann and Klein, 2002; Klein and Heinemann, 2002).

The IRD content remained low during the mid-Holocene, apart from peaks deriving from single large clasts (Fig. 29 and Fig. 34d). Coarse particles were probably still diluted by the high accumulation of fine-grained, meltwater-derived sediments (comparable to the early Holocene; Fig. 34e). Thus, the reduced AW advection may have allowed the glaciers to grow, however, without reaching a size resulting in a considerable increase of IRD deposition within the fjord. Although bearing in mind the low temporal resolution, the PIP_{25} indices

suggest a trend towards a continuously expanding sea ice cover throughout the mid-Holocene (Fig. 34f), while the sea ice biomarker IP_{25} reached its peak value around 5.2 ka at the transition to the late Holocene (Fig. 32d). Nevertheless, phytoplankton biomarkers still exhibit high values (Fig. 32e) indicating an enhanced primary production and suggesting rather a sea ice edge situation at the core site, which provided favourable conditions for both, sea ice diatoms and phytoplankton thriving in open waters.

6.5.3 Late Holocene

The timespan ~5.2–3.1 ka was characterised by a rapid reduction of the sedimentation rate (Fig. 34e) that might indicate a hiatus between the calibrated radiocarbon ages at ~5.2 and ~3.1 ka (see Fig. 30). Gaps in mid-Holocene records from the Svalbard region are reported e.g., from the Woodfjord, northern Spitsbergen, as well as from the Storfjord, south of Spitsbergen, even though spanning different time spans (e.g., Bartels et al., 2017; Rasmussen and Thomsen, 2014). Thus, erosional events are likely in Svalbard´s fjord basins during the Holocene, especially in glacier-proximal settings like the studied site. Although a rapid decline of the meltwater outflow is an alternative explanation for the abrupt decline of the sedimentation rate, some probability of the presence of a hiatus and the very low number of data points in this interval preclude any meaningful interpretation of this section.

The most prominent signal in the late Holocene part of the Wahlenbergfjord sedimentary record is the increase in IRD since the Subboreal–Subatlantic transition (~3.1–2.4 ka; Fig. 34d). Werner et al. (2011) linked increasing IRD deposition at the western Spitsbergen margin to the Neoglaciation, although they recognised that high calving rates indicated by IRD may have various reasons ranging from retreating glaciers after intensive summer melting to advancing glaciers during cooler conditions with higher snow accumulation. However, reports about local glacier advances in central Spitsbergen at ~3 ka (2800–2900 ^{14}C years BP) and again at ~2.5 ka (2,400–2,500 ^{14}C years BP; Svendsen and Mangerud, 1997) point to waxing glaciers as the main reason for the increase in IRD deposition (Fig. 34d and Fig. 35c). These glacier advances are most likely caused by atmospheric cooling at the end of the Subboreal, as indicated, e.g., by $\delta^{18}O$ values from the Greenland NGRIP ice core (Fig. 34g; Rasmussen et al., 2014a), by data from peats and permafrost soils on Spitsbergen (e.g., Humlum, 2005; Humlum et al., 2003; Jaworski, 2016), and by evidence that solar activity has been reduced around 2.7 ka contributing to a cooling in both hemispheres (van Geel et al., 1999, 2000). Advancing glaciers possibly have been fed by high snow accumulation triggered by the proposed enhanced humidity in northern Europe (Wanner et al., 2008) like it has been supposed for some events during the late Weichselian, when open waters in the Greenland–Iceland–Norwegian seas might have acted as a moisture source promoting the growth of the SBIS (Hebbeln et al., 1994). Colder conditions in the Wahlenbergfjord during the late Holocene are also suggested by increasing values of the PIP_{25} indices pointing to an extending sea ice cover, although the record is based only on a few data points (Fig. 34f and Fig. 35c). Additionally, IP_{25} and dinosterol (vs. total organic carbon) show highest values at ~0.9 ka (Fig. 33) supporting an expanded sea ice coverage at the core site. During the last millennium, an extended sea ice cover is also reported from the eastern Fram Strait (Müller et al., 2012). Interestingly, the micropaleontological data from the Wahlenbergfjord rather indicate a warming. The benthic foraminiferal faunal distribution during the Subatlantic – especially during the last two millennia – exhibits a gradual decrease of the dominating *E. clavatum* assemblage (Fig. 34a). Such a pattern has also been observed from the western and northern

margins of Svalbard (Jernas et al., 2013; Ślubowska et al., 2005) as well as from the western Barents Sea, south of Spitsbergen (Wilson et al., 2011). This faunal change has been connected to ameliorating conditions due to a stronger AW advection (e.g., Jernas et al., 2013) in line with reports about a correspondent strengthening AW influence in the Nordic Seas during the last 3,000 years (Dylmer et al., 2013). And indeed, in addition to the faunal shift, slightly depleted $\delta^{18}O$ values of *C. lobatulus* (Fig. 34c) possibly point to warmer bottom waters in the Wahlenbergfjord, also reflecting a stronger influence of Atlantic-derived waters. However, despite probably ameliorated conditions in the bottom waters, productivity as reflected by the BFAR (Fig. 34b) remained well below early and mid-Holocene levels possibly controlled by the extension of sea ice (Fig. 34f). Jernas et al. (2013) assumed that such discrepancies are caused by a decoupling of atmospheric cooling and enhanced subsurface AW advection possibly facilitated by the extended sea ice cover.

6.6 Local vs. regional palaeoenvironmental information derived from a proximal fjord setting

Glacier-proximal, over-deepened fjord settings not directly linked to the open ocean can be assumed to be merely recorders of local then of regional conditions. However, the benthic foraminiferal record from the Wahlenbergfjord illustrates that at such a setting not only local but also distinct regional palaeoenvironmental signals are recorded. Especially, the faunal shift at the onset of the mid-Holocene (at ~7.7 ka; Fig. 31 and Fig. 34a), when the abundance of *E. clavatum* (and the respective assemblage) rapidly increased, is reflected in records from the entire Svalbard region (Fig. 36) and even farther east at the western margin of Franz Josef Land (Duplessy et al., 2001; Hald et al., 2004; Klitgaard Kristensen et al., 2013; Kubischta et al., 2011; Rasmussen et al., 2012; Skirbekk et al., 2010; Ślubowska-Woldengen et al., 2007). All studies around Svalbard show a parallel decrease of *N. labradorica* (Fig. 36), which usually is connected to retreating oceanic fronts and/or decreasing AW influence along with the associated productivity drop (Rasmussen et al., 2012; Ślubowska et al., 2005). Only at the easternmost sites (west of Franz Josef Land), *N. labradorica* (as well as *Buccella* spp.) had its major appearance just starting synchronously with the increase of *E. clavatum* what has been linked to an approaching sea ice edge and a related productivity increase (Duplessy et al., 2001; Klitgaard Kristensen et al., 2013). However, the rapidly rising dominance of *E. clavatum* probably indicates a regional hydrographic shift affecting all locations at the north(western) Barents Sea margin. A likely trigger for these faunal changes is an assumed weakening of the AMOC that affected the North Atlantic at ~7 ka (Solignac et al., 2004). For around 7.7 ka, Sarnthein et al. (2003) documented a (sub-)sea surface temperature drop of ~3 °C at the western Barents shelf, which was likely linked to a weakening of the West Spitsbergen Current (Fig. 36f). In lake sediments from northwestern Spitsbergen a temperature drop of even ~6 °C is recorded between ~7.8 and ~7 ka, which has been connected to a stronger influence of Arctic Water and expanding sea ice (van der Bilt et al., 2016). At the western Svalbard margin, a cooling of AW and re-advancing glaciers are dated to the same time interval (7.6 ±0.1 ka; Jessen et al., 2010) when also Hald et al. (2007) documented a stronger presence of Arctic Water in the Svalbard region. Timing discrepancies on a centennial scale between some of these observations may be caused by age model uncertainties. However, an earlier onset of this cooling trend with increasing latitude and greater distance from the West Spitsbergen Current, respectively, is also possible.

Among the various benthic foraminiferal assemblage data, highest percentages of *E. clavatum* were observed in Isfjord and in Wahlenbergfjord (Rasmussen et al., 2012; this study; Fig. 36a, d) which possibly is linked to the relatively glacier-proximal fjord-settings appreciated by *E. clavatum* (e.g., Korsun and Hald, 1998, 2000). In addition, the benthic foraminiferal distributions in these fjords show further similarities: At the transition between the dominances of *N. labradorica* and *E. clavatum* a short-term increase of *C. lobatulus* is observed. This similarity may suggest that the high percentage of *C. lobatulus* in our record should not be discarded despite the small number of specimens in that sample (Fig. 31f). Rasmussen et al. (2012) linked this faunal shift to strong currents and mixing due to a stronger influx of AW that may have been cooled by mixing with Arctic waters. Thus, a smooth transition from a dominating AW influence to an increasing Arctic Water influence is likely at both study sites. Contrastingly, in the Storfjord Trough (south of Svalbard) a continuous inflow of AW is assumed (Łącka et al., 2015; Rasmussen et al., 2007). Seeing the regional pattern in the benthic foraminiferal assemblages around Svalbard (Fig. 36) underlines the potential of glacier-proximal, over-deepened fjord settings not directly linked to the open ocean to record regional environmental changes in addition to local glacier-influenced conditions. With respect to partly extraordinary high sediment accumulation rates observed in Arctic fjords with strong glacier influences (up to 1 m a^{-1} or even 13 m a^{-1} in fjords of Svalbard and Alaska, respectively; Howe et al., 2010 and references therein), even remote fjord settings can offer exceptional palaeoarchives of regional palaeoenvironmental conditions with very high temporal resolutions.

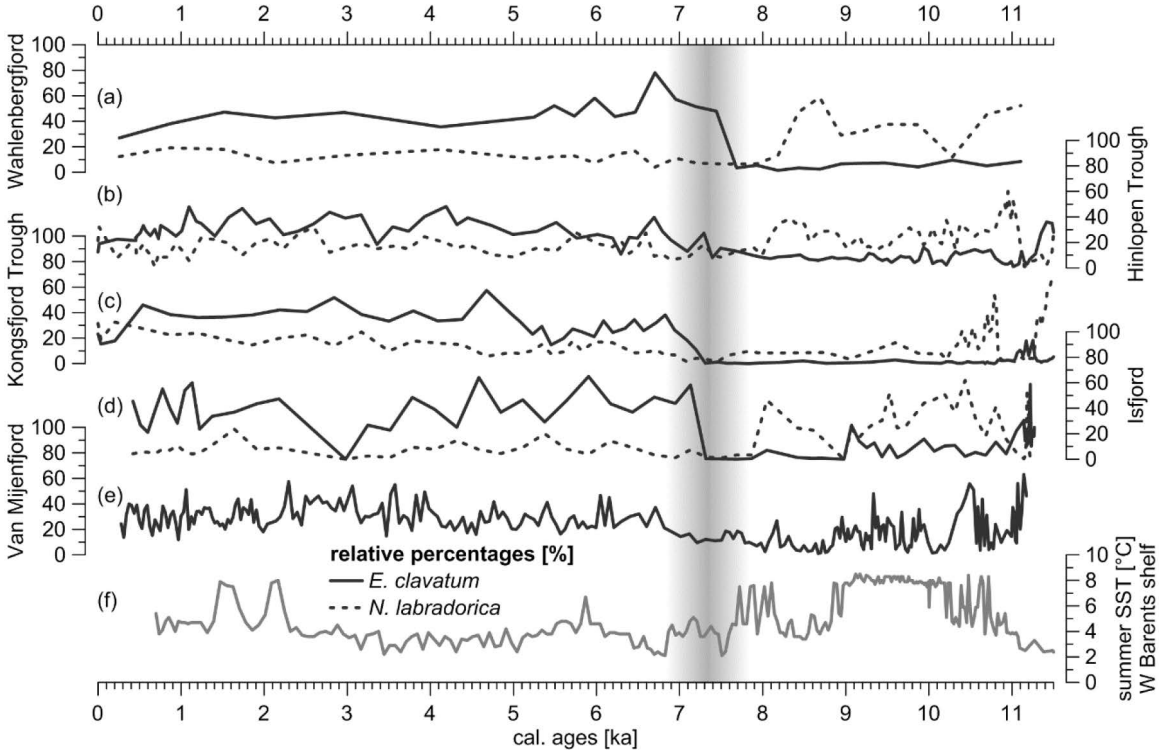

Fig. 36: Comparison of percentages of *E. clavatum* (solid lines) and *N. labradorica* (dashed lines) in the Svalbard area: (a) Wahlenbergfjord (GeoB10831-3; this study). (b) Hinlopen Trough (NP94-51; Ślubowska et al., 2005). (c) Kongsfjord Trough (NP05-11-21; Skirbekk et al., 2010). (d) Isfjord (JM98-845; Rasmussen et al., 2012). (e) Van Mijenfjord (MD99-2305; Hald et al., 2004). Core locations (a)–(e): see Fig. 28a. (f) Summer (sub-)sea surface temperatures at the western Barents shelf (23258; Sarnthein et al., 2003). Graded shading marks time span of faunal shift including the timing discrepancies between the records.

6.7 Conclusions

Micropalaeontological, sedimentological and geochemical investigations of sediment core GeoB10831-3 – retrieved from the Wahlenbergfjord (Nordaustlandet) – revealed Holocene climatic and hydrographic variabilities and glacier responses.

During the summer insolation maximum in the course of the early Holocene (~11.3–7.7 ka), high amounts of meltwater were discharged from melting glaciers into the fjord and relative warm AW-influenced intermediate waters were advected and upwelled, both offering a high productivity.

At ~7.7 ka, a rapid hydrographic shift is reflected in the foraminiferal fauna: Arctic Water replaced the dominant influence of AW possibly triggered by a weakened AMOC.

An extending sea ice cover probably caused a decoupling of atmospheric and hydrographic conditions during the Subatlantic (~3.1–0.2 ka): while glaciers probably expanded due to the decreased summer insolation and resulting colder atmospheric temperatures, bottom waters warmed possibly affected by the re-advection of AW.

Surprisingly, regional environmental/climatic patterns are reflected in the fauna at our core site (see Fig. 36) despite the remote and glacier-proximal location of the studied fjord. Accordingly, AW advection as important driver of the regional environmental setting does not only affect coasts and fjords along the Svalbard margin, but also remote over-deepened fjords with the respective topographic prerequisites (i.e., a deep connection at its mouth). Due to the very high sediment accumulation those fjord records offer very high temporal resolutions, which should be explored in further detail to resolve even short-term climate variations during the deglaciation and the early Holocene.

Acknowledgements

This project was supported by the *Deutsche Forschungsgemeinschaft* (DFG) through the International Research Training Group "Processes and impacts of climate change in the North Atlantic Ocean and the Canadian Arctic" (IRTG 1904 *ArcTrain*). For retrieving the samples during the cruise MSM02/03 in 2006, the captain and the crew as well as the scientists on RV *Maria S. Merian* are acknowledged. We also thank the following for the performance of measurements: Janet Rethemeyer, University of Cologne, and Lukas Wacker, ETH (Zürich), for radiocarbon measurements as well as Birgit Meyer and Henning Kuhnert, MARUM (Bremen), for stable isotope measurements, and Walter Luttmer, AWI (Bremerhaven), for technical assistance. We are grateful that Christian Haas, Christian Rintisch, Anna-Lena Rugen and Jan Unverfärth, MARUM (Bremen), processed the samples. Tilia Breckenfeld is thanked for her contribution to the discussion of hydrographic data. Sample material was provided by the GeoB repository at MARUM, Bremen. We thank the Klinikum Bremen-Mitte who provided their facilities for the performed computed tomographies. Arne-Jörn Lemke and Christian Timann, Gesundheit Nord (Bremen), are acknowledged for performing the CT scans and their support during the measurements.

7 Sedimentation off northwestern Spitsbergen since the deglaciation controlled by meltwater plumes and competing Atlantic and Arctic waters (Manuscript III)

Martin Bartels[1], Jana Schröder[1], Kirsten Fahl[2], Rüdiger Stein[2], Dierk Hebbeln[1]

[1]MARUM – University of Bremen, Bremen, 28359, Germany
[2]Alfred Wegener Institute for Polar and Marine Research, Bremerhaven, 27568, Germany

(in preparation)

Abstract

The Kongsfjord Trough (northwestern Spitsbergen) is an ideal location to examine the interplay between Atlantic and Arctic waters in the past as it is crossed by the oceanic front separating these water masses on the western Spitsbergen shelf. Furthermore, the trough was one of the main pathways for ice streams draining the Svalbard–Barents Sea Ice Sheet, which covered the Svalbard Archipelago during the last glaciation. Data of sediment core GeoB10810-1 add the palaeoceanographic evolution during this time period, illustrating that bottom water intrusion of relatively warm Atlantic Water, starting before 14,800 years ago, had a major impact on glacier retreat during the deglaciation. In the following, rather instable environmental conditions prevailed that also continued when the Arctic Coastal Front was established well before the Younger Dryas (~12,900–11,700 years ago) and an ice-free Barents Sea allowed for the advection of Arctic waters by the East Spitsbergen Current. A continuous meltwater discharge until ~10,300 years ago illustrates that melting was the dominant process during the disintegration of the ice sheet over northwestern Spitsbergen compared to glacier calving and iceberg release. A comparison of the GeoB10810-1 data with the Holocene palaeoceanographic record of core NP05-11-21 also from the Kongsfjord Trough but from a site closer to the coast reveals differences especially regarding the palaeoproductivity information pointing to a reduced productivity at the near-coastal site for the early Holocene probably caused by the presence of turbid meltwater plumes.

7.1 Introduction

The Svalbard–Barents Sea Ice Sheet covered the entire Barents Sea including the islands of the Svalbard Archipelago during the Last Glacial Maximum (LGM; ~21,700–18,200 years ago; Landvik et al., 1998) comprising several ice domes. One major ice dome covered northwestern Spitsbergen (the main island of the Svalbard Archipelago) probably with altitudes of >1,350 m above sea level (Gjermundsen et al., 2013). This northwestern tip of the Svalbard–Barents Sea Ice Sheet had a major drainage through the Kongsfjord–Krossfjord system and the Kongsfjord Trough, which connects the Kongsfjord and its adjacent fjords across the western Spitsbergen shelf with the open Fram Strait (Fig. 37b, c; Henriksen et al., 2014; Landvik et al., 2005; Ottesen et al., 2007). Advances and successive retreats of those outlet glaciers are evident in the sea floor morphology, where terminal, recessional and so-called De Geer moraines were left behind (e.g., Streuff et al., 2015). The examination of sediment cores from the Kongsfjord Trough revealed the history of deglaciation from a sedimentological point of view (Landvik et al., 2005). Accordingly, the Kongsfjord Trough was deglaciated by ~16.6 ka, when the glacier front was located at the mouth of the Kongsfjord–Krossfjord system (Henriksen et al., 2014).

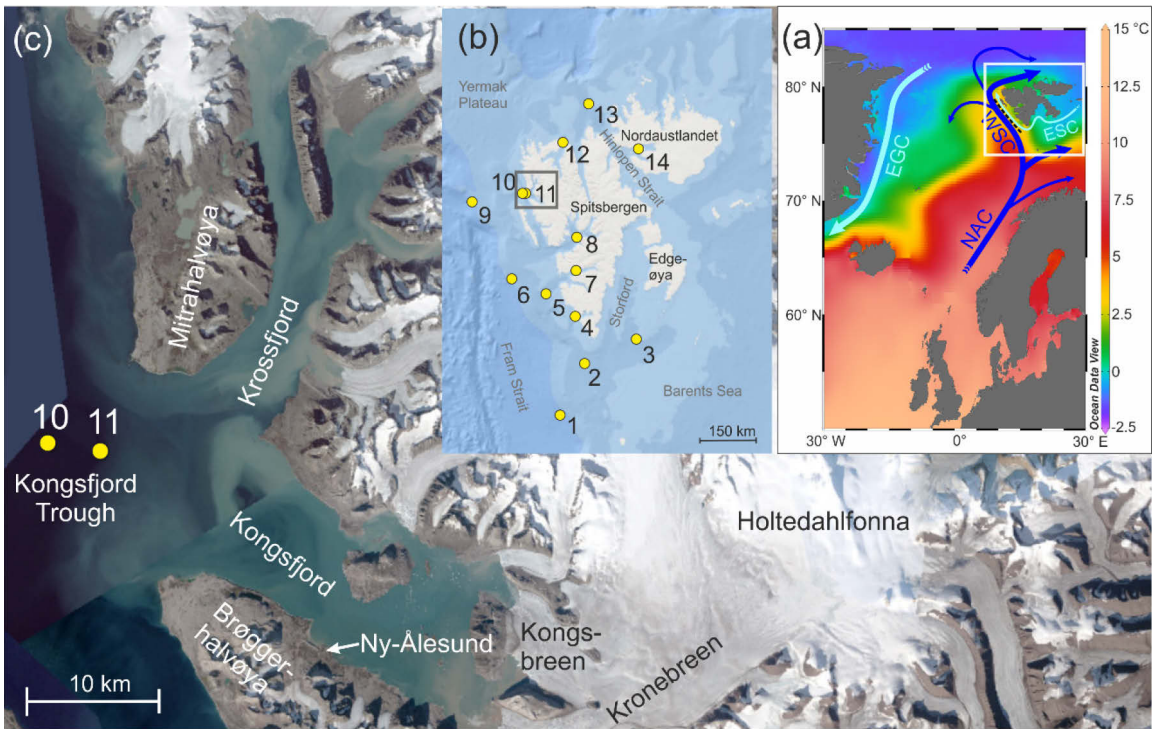

Fig. 37: (a) Average annual sea surface temperatures of the North Atlantic (1955–2012; World Ocean Atlas/Ocean Data View; Locarnini et al., 2013; Schlitzer, 2015). Dark blue arrows symbolise pathways of relatively warm (sub-)surface waters (NAC: North Atlantic Current, WSC: West Spitsbergen Current) of Atlantic origin; light blue arrows symbolise pathways of cold (sub-)surface waters (EGC: East Greenland Current, ESC: East Spitsbergen Current) of Arctic origin. Dashed line symbolises modern position of the Arctic Coastal Front. White rectangle marks the study area as shown in (b). (b) Map of the Svalbard Archipelago including the main island Spitsbergen with sites of palaeoceanographic studies indicated: 1. Sarnthein et al. (2003); 2. Rasmussen et al. (2007), Rasmussen and Thomsen (2014); 3. Łącka et al. (2015); 4. Majewski et al. (2009); 5. Rasmussen et al. (2007); 6. Hald et al. (2004); 7. Hald et al. (2004); 8. Rasmussen et al. (2012); 9. Müller et al. (2012), Müller and Stein (2014), Spielhagen et al. (2011), Werner et al. (2013, 2014); 10. this study; 11. Jernas et al. (2013), Rasmussen et al. (2014), Skirbekk et al. (2010); 12. Bartels et al. (2017); 13. Jernas et al. (2013), Koç et al. (2002), Ślubowska-Woldengen et al. (2007), Ślubowska et al. (2005); 14. Bartels et al. (in prep.). Grey rectangle marks study area as shown in (c). Basemap created with *ArcGIS online* (http://www.arcgis.com). (c) Satellite image of the Kongsfjord system with tributary fjords and glaciers during summer. Yellow dots mark core sites GeoB10810-1 (10) and NP05-11-21 (11). USGS Landsat picture: © Norwegian Polar Institute (http://toposvalbard.npolar.no/).

Today, the area is predominantly affected by the northernmost extension of the North Atlantic Current advecting heat to higher latitudes (Fig. 37a). Those relatively warm ocean waters are able to enter the fjord system seasonally, e.g., by wind-induced upwelling (Cottier et al., 2005, 2007), subsequently largely contributing to the calving of the glacier fronts. Luckman et al. (2015) observed that comparable warm Atlantic-derived waters contributed to the destabilization and calving at modern glacier fronts, e.g., of Kronebreen at the head of Kongsfjord (see Fig. 37c for locations). The variability of those currents and respective glacier responses in the Kongsfjord Trough next to the mouth of this fjord system were examined for the last ~12,000 years (Fig. 37b, c; Rasmussen et al., 2014b; Skirbekk et al., 2010). However, palaeoceanographic reconstructions covering the time span between the onset of the ice sheet retreat and the beginning of the Holocene are still lacking. Our study aims to add this missing piece to the puzzle, further elucidating differences in palaeoenvironmental responses to a littoral setting compared with a more distal location. Situated only a few kilometres further offshore as the study site NP05-11-21 (Rasmussen et al., 2014b; Skirbekk et al., 2010), the sediment core investigated in the present study is well suited to answer if the proximity to the coast has a significant impact on the palaeoenvironment of such a glacimarine trough setting.

7.2 Regional setting

7.2.1 Modern oceanography

The Arctic Ocean and especially its intermediate water masses mainly consist of Atlantic-derived waters (Rudels, 2009; Rudels et al., 1994). This relatively warm and saline Atlantic Water (AW) is transported by the West Spitsbergen Current (WSC) to high northern latitudes which eventually enters the Arctic Ocean at the northern margin of Svalbard (e.g., Rudels, 2009; Fig. 37a). The topographical steered WSC follows the western shelf break of Spitsbergen (Saloranta and Svendsen, 2001). Here, the Arctic Coastal Front separates Atlantic-derived waters on its seaward side from colder and fresher Arctic coastal waters, i.e., the Coastal Current, on its landward side (Saloranta and Svendsen, 2001). The Coastal Current is the extension of the East Spitsbergen Current, which transports cold and fresh Arctic Water along the shelf of Edgeøya into the Storfjord (Loeng, 1991; Fig. 37a, b). Subsequently, the East Spitsbergen Current continues as the warmer and less saline Coastal Current surrounding the southern tip of Spitsbergen (Skogseth et al., 2005) from where it flows northward on the western shelf of Spitsbergen (Loeng, 1991). These geotropically flowing Arctic waters on the western Spitsbergen shelf restrict the intrusion of AW into the fjords. Atlantic-derived waters can only enter the fjords during barotropic instabilities, which occur particularly in summer. In addition, wind-induced transport of AW seems to be one of the most important factors of seasonal AW advection into the fjords (Sundfjord et al., 2017). Cottier et al. (2007) reported strong northerly wind-generated upwelling events during winter that enabled AW to flood the western Spitsbergen shelf and to enter the Kongsfjord–Krossfjord system preventing the formation of winter sea ice. After intruding into the fjord, AW mixes with the colder and less saline coastal waters resulting in Transformed Atlantic Water (Cottier et al., 2005; Howe et al., 2003). These water masses are usually covered by fresher Surface Water deriving from glacier melt (salinities ranging from <28–34; Cottier et al., 2005). At the shelf break, the inflow of those brackish meltwater-derived surface waters forces the WSC to submerge around 78 °N, only a few kilometres south of

the Kongsfjord Trough, from where it continues its northward flow as a subsurface current (Johannessen, 1986; Manley, 1995).

7.2.2 The Kongsfjord–Krossfjord system

The Kongsfjord–Krossfjord system consist of the two eponymous fjords Kongsfjord and Krossfjord with several smaller tributary fjords and bights (Fig. 37c). The fjord system extends into the Kongsfjord Trough connecting the fjord waters with shelf waters from the western Spitsbergen shelf (Svendsen et al., 2002; Trusel et al., 2010). The exchange of fjord and shelf waters between the Kongsfjord Trough and the Kongsfjord–Krossfjord system is not restricted by a sill at the joined fjord mouth (Howe et al., 2003; Trusel et al., 2010). Due to the seasonal inflow of comparably warm of AW, the Kongsfjord is almost perennially ice-free. The fjord hosts Ny-Ålesund, one of the northernmost year-round inhabited (research) towns.

Kongsfjord, Krossfjord and most of the tributary fjords and bights are fed by tidewater glaciers. The former is particularly influenced by the Kongsbreen and the Kronebreen (Fig. 37c). Kronebreen is with 690 km^2 the sixth largest outlet glacier in Svalbard draining the second largest ice cap in Spitsbergen: Holtedalfonna (1,375 km^2; Hagen et al., 1993; Fig. 37c). Bedrock erosion by Kronebreen and its tributary glaciers contributed to a sediment deposition at the head of the Kongsfjord of 1,400 t km^{-2} a^{-1} between 1984 and 2009 (Trusel et al., 2010). During the late Weichselian, the Kongsfjord Trough was filled by an ice stream which flew through Krossfjord and Kongsfjord (Gjermundsen et al., 2013; Henriksen et al., 2014; Landvik et al., 2005) draining a massive ice dome that covered northwestern Spitsbergen (Gjermundsen et al., 2013). Consequential glacial erosion carved deep basins in the fjords exceeding 300 m water depth (Howe et al., 2003).

7.3 Material and Methods

Sediment core GeoB10810-1 was retrieved from 348 m water depth in the Kongsfjord Trough (northwestern Spitsbergen; 79.0535 °N, 10.9002 °E; Fig. 37b, c) during cruise MSM02/03 with RV *Maria S. Merian* in August 2006 (Lherminier et al., 2009). The study is based on material from this 752 cm long core, which was sampled with 10 ml syringes for the analyses of microfossils, ice-rafted debris (IRD), stable isotopes and biomarkers.

Dried bulk samples were washed through a 63 µm sieve and dry-sieved trough 150 µm and 250 µm meshes. Remnants of each fraction were weighted. For microfossil as well as IRD analyses, the sediment core was sampled in 20 cm intervals, while for stable isotope analyses every five centimetres samples were taken. In each sample at least 200–300 foraminifera/clasts were counted (as recommended by Patterson and Fishbein, 1989), using a microsplitter if the number of foraminifera/clasts was higher. Only three samples contain less than 200 foraminifera, whereas ten samples comprise less than 200 clasts. The faunal analysis was performed on the >150 µm fraction, while clasts >250 µm are considered as ice-rafted. Whereas planktic foraminifera were combined as one group, benthic foraminifera were mostly identified at species level. The species groups *Stainforthia loeblichi* s.l. and *Buccella frigida* s.l. contain different morphotypes of the calcareous benthic species *Stainforthia loeblichi* s.s. and *Stainforthia concava* as well as *Buccella frigida* s.s. and *Buccella tenerrima*, respectively, which could not be differentiated. Not identified hyaline species were assembled as Rotaliina. The majority of calcareous benthic foraminifera were well preserved without any

indications of dissolution or transport. A carbonate saturation in the Kongsfjord Trough could be illustrated by chemical measurements during cruise MSM02/03 (Teichert et al., 2014). Contrastingly, agglutinating benthic foraminifera show a lower preservation potential. Therefore, only percentages of the calcareous fauna were calculated. Additionally, percentages of planktic foraminifera (in relation to the total fauna) were computed.

AMS radiocarbon measurements of bivalves, mixed benthic foraminifera or the endobenthic foraminifera *N. labradorica* from eight core depths were performed at ETH in Zürich (Table 4). Apart from one sample in 628 cm depth, double measurements were carried out. At two depths (402.5 and 507 cm) additional measurements were carried out at graphitized samples. The Bayesian software *BACON* (Blaauw and Christen, 2011) based on *R* (R Development Core Team, 2011) was used to create an age–depth model for core GeoB10810-1 applying the *Marine13* calibration curve (Reimer et al., 2013) and an averaged regional reservoir age correction ΔR = 98 ±37 years averaging six ΔR values (calib.qub.ac.uk/marine/; Mangerud, 1972; Mangerud and Gulliksen, 1975; Olsson, 1980). Double (and triple) measurements were not averaged, but all raw data were implied in the age–depth model. Apart from the settings for the Student´s-t distribution (for error estimation) default priors of *BACON* were applied. The Student´s-t distribution was set at t.a = 9 and t.b = 10 (instead of t.a = 3 and t.b = 4) to receive a less smoothed age–depth model involving all calibrated radiocarbon ages. Calendar ages for the samples above the youngest (7 cm) and below the oldest radiocarbon measurement (722 cm) were interpolated linearly assuming the same sedimentation rates as below and above, respectively.

Table 4: AMS radiocarbon measurements (sediment core GeoB10810-1) and calibrated ages applying the *Marine13* calibration curve (Reimer et al., 2013) and an averaged regional ΔR = 98 ±37 years (see calib.qub.ac.uk/marine/). All measurements carried out at ETH Zürich. Age–depth model developed with *BACON* (Blaauw and Christen, 2011). Calendar ages given in the text are weighted mean values (wmean).

Lab ID	depth	dated material	^{14}C age		cal. age [a BP]			
	[cm]		[a]	±	min	max	median	**wmean**
ETH-72002.1.1	7	mixed benthic foraminifera	1,881	53	1,295	1,518	1,402	**1,407**
ETH-72002.2.1	7	mixed benthic foraminifera (replicate)	1,981	49				
ETH-64604.1.1	61.5	*N. labradorica*	3,473	57	2,973	3,310	3,142	**3,143**
ETH-64604.2.1	61.5	*N. labradorica* (replicate)	3,308	64				
ETH-72003.1.1	103	*N. labradorica*	4,568	55	4,454	4,782	4,613	**4,618**
ETH-72003.2.1	103	*N. labradorica* (replicate)	4,524	55				
ETH-72004.1.1	283	*N. labradorica*	9,835	72	9,671	10,604	10,315	**10,280**
ETH-72004.2.1	283	*N. labradorica* (replicate)	10,443	76				
ETH-72005.5.1	402.5	*N. labradorica* (graphitized)	10,466	26				
ETH-72005.1.1	402.5	*N. labradorica*	10,565	98	11,224	11,604	11,387	**11,403**
ETH-72005.2.1	402.5	*N. labradorica* (replicate)	9,800	74				
ETH-72006.5.1	507	*N. labradorica* (graphitized)	10,917	27				
ETH-72006.1.1	507	*N. labradorica*	10,978	77	12,289	12,593	12,464	**12,459**
ETH-72006.2.1	507	*N. labradorica* (replicate)	10,966	78				
ETH-72007.1.1	627.5	mixed benth. foram.	measurement failed					
ETH-72007.2.1	627.5	mixed benth. foram.	12,570	94	13,705	14,139	13,930	**13,931**
ETH-64605.1.1	722	bivalves	12,716	97	14,709	15,185	14,999	**14,988**
ETH-64605.2.1	722	bivalves (replicate)	12,724	107				

Stable oxygen and carbon isotopes from four to ten carbonate shells (>150 µm) of the planktic foraminifera *Neogloboquadrina pachyderma* (sinistral), the epibenthic foraminifera *Cibicides lobatulus* and the endobenthic foraminifera *Nonionellina labradorica* were measured at MARUM in Bremen using a Finnigan MAT 251 gas isotope ratio mass spectrometer with a Kiel I automated carbonate preparation device (standard deviation of house standard: 0.03 ‰ for $\delta^{13}C$ and 0.05 ‰ for $\delta^{18}O$). Stable oxygen isotope measurements were corrected for the global ice volume (Waelbroeck et al., 2002) and, additionally, for vital effects of the benthic species (*C. lobatulus*: +0.64 ‰; Shackleton, 1974; *N. labradorica*: -0.2 ‰; Duplessy et al., 2005).
Biomarker analyses were carried out in selected depths using homogenised, dried sediment samples. The C_{25} isoprenoid lipid biomarker (IP_{25}) as well as brassicasterol and dinosterol were analysed to reconstruct sea ice coverage (cf., Belt et al., 2007) and phytoplankton activity (cf., Fahl and Stein, 1999; Volkman, 1986; Volkman et al., 1993), respectively. For biomarker extraction, ~3 g of sediment were ultrasonicated and analysed by gas chromatography/mass spectrometry using internal standards for quantification. Methodological details of the biomarker analyses are described in Fahl and Stein (2012) and Bartels et al. (2017). Phytoplankton-IP_{25} indices (P_BIP_{25} and P_DIP_{25}) have been calculated using the phytoplankton biomarkers brassicasterol and dinosterol, respectively (following Müller et al., 2011).
Accumulation rates of fine and coarse sediment fractions, ice-rafted debris, sea ice and phytoplankton biomarkers as well as of foraminifera were calculated according to a formula developed by Ehrmann & Thiede (1985).

7.4 Results

7.4.1 Core description

The olive grey sediment of core GeoB10810-1 contains sandy, clayey silt with several alterations. The upper three centimetres exhibit a brownish colour, while the ~262 cm below show dark mottles and strong traces of bioturbation. Between 513 and 536 cm the clayey silt is grading from olive grey to red-brown with black mottles. Around 536 cm the sediment has a lighter colour. From 580 cm on, the sediment is getting more brownish downwards with several black mottles. Big dropstones were found at 15, 37, 127, 232, 258, 267, 324, 345, 364, 388, 435 and 740–742 cm (see also Fig. 39a) while intact bivalve shells and shell fragments appeared at 121, 145, 182, 201, 224, 280 and 258 cm. Between 514–540 cm a long vertical bioturbation trace of a mussel is evident.

7.4.2 Chronology

Sediment core GeoB10810-1 covers a time span from ~15.3–1.3 ka (Fig. 38). Sedimentation rates of the lower part of the core (282–747.5 cm; until ~10.3 ka) were high with ~93.2 cm ka^{-1} on average, compared to the upper part with lower sedimentation rates (2.5–282 cm; mean: ~31.1 cm ka^{-1}). At ~11.2 ka (377.5 cm) highest sedimentation rates were calculated (~111.6 cm ka^{-1}) whereas the minimum value was attained at ~3.6 ka (73 cm; ~27.7 cm ka^{-1}).

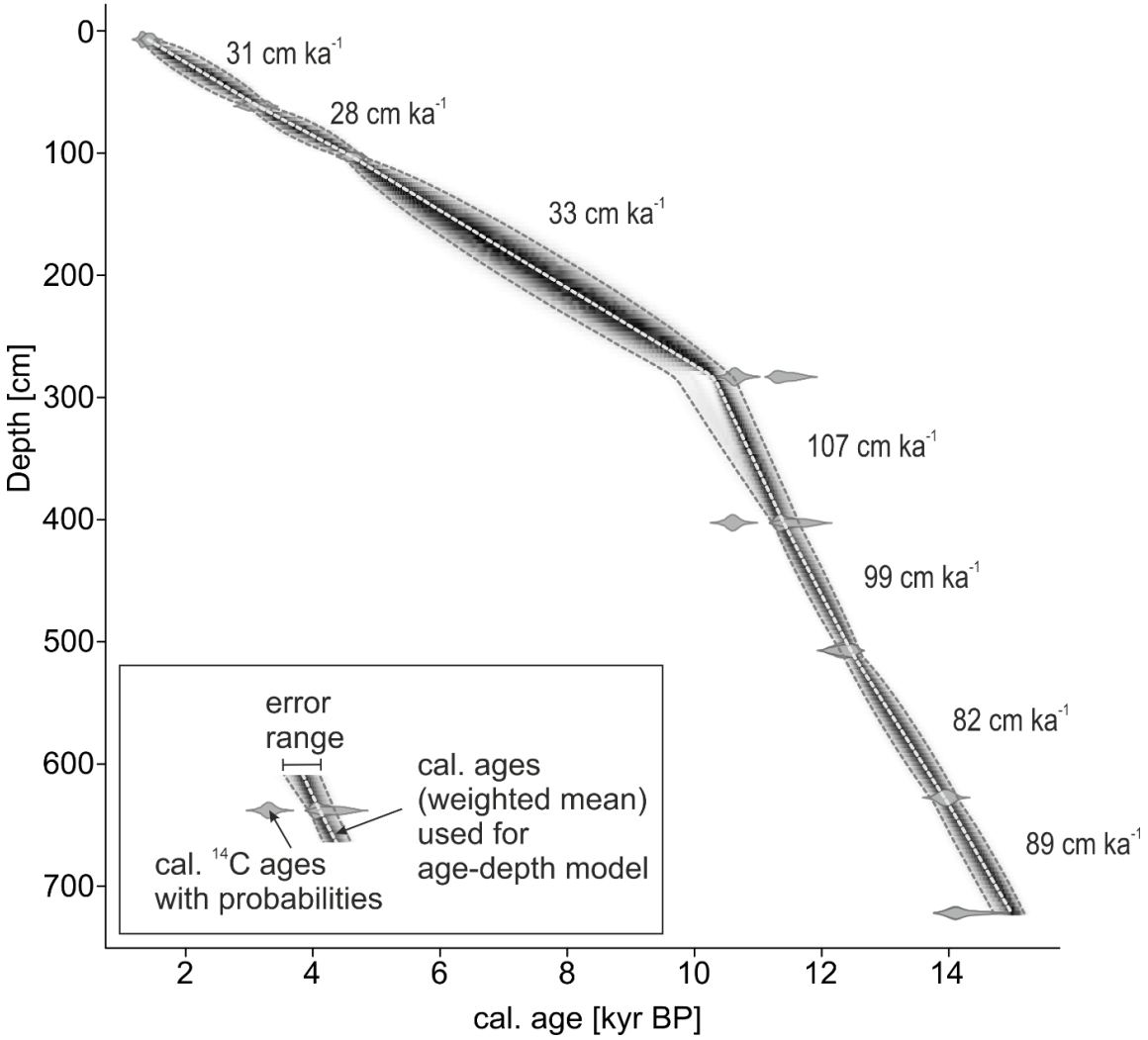

Fig. 38: Age–depth model for sediment core GeoB10810-1 from the northwestern Spitsbergen shelf based on Bayesian age estimation with *BACON* (Blaauw and Christen, 2011). The *Marine13* calibration curve (Reimer et al., 2013) and a regional reservoir correction (ΔR) of 98 ±37 years (calib.qub.ac.uk/marine/; see sect. 7.3) were used. For calibrated ages with error ranges refer to Table 4. Numbers at curves give averaged sedimentation rates between radiocarbon-dated depths.

7.4.3 Sedimentology

7.4.3.1 Ice-rafted debris (IRD)

Clasts >250 µm were considered as ice-rafted. The highest numbers of IRD were counted between ~15.2–12.2 ka reaching peak accumulation rates of ~23,990 clasts cm^{-2} ka^{-1}. After a reduced accumulation of ice-rafted clasts between ~12–11.6 ka, a slightly increase of the IRD flux can be recognized during the interval ~11–10.7 ka reaching values between ~5,430–7,610 clasts cm^{-2} ka^{-1}. Subsequently, accumulation rates of IRD never exceeded ~6,390 clasts cm^{-2} ka^{-1} (Fig. 39a).

7.4.3.2 Grainsizes

Percentages of the fine fraction (<63 µm) constitute up to ~99.3 % of the dry sediment (~22.4–121.7 g cm^{-2} ka^{-1}). Between ~10.4 and ~10.2 ka, accumulation rates of fine sediments decreased rapidly dropping from ~105.4 g cm^{-2} ka^{-1} to ~35.2 g cm^{-2} ka^{-1} (Fig. 39b). Accumulation rates of the coarse sediment fraction (>63 µm) range between ~0.6–29.3 g cm^{-2} ka^{-1} (mean: ~4.9 g cm^{-2} ka^{-1}). The highest amounts of this grainsize fraction appeared in the two lowermost samples of the core (at ~15.3 and ~15.2 ka; Fig. 39b) exceeding

~17 % of the dry sediment. The accumulation rate of the sediment fraction >150 µm varies between ~0.2–20.7 g cm^{-2} ka^{-1} (mean: ~2.1 g cm^{-2} ka^{-1}). From ~15.1 to ~13.7 ka, the coarser grainsizes exhibit several peaks (maxima at ~14.4 and ~14.3 ka). Subsequently, accumulation rates of the sediment fraction >150 µm remained low apart from the interval ~11.1–10.8 ka when values increased up to ~8.1 g cm^{-2} ka^{-1} (Fig. 39b).

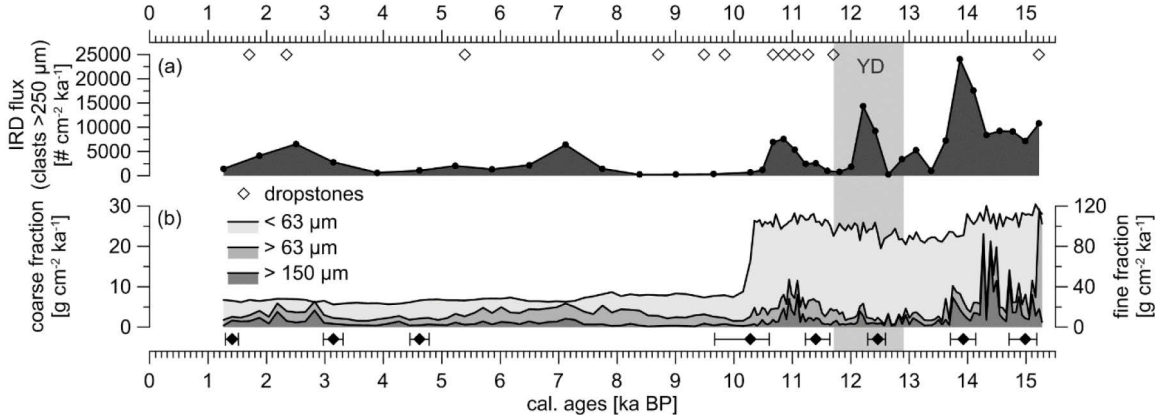

Fig. 39: (a) Accumulation rate of ice-rafted debris (IRD; clasts >250 µm) in sediment core GeoB10810-1 from the northwestern Spitsbergen shelf. Open diamonds show appearance of large dropstones (see sect. 7.4.1). (b) Accumulation rates of fine (<63 µm) and coarse sediment fraction (>63 µm and >150 µm). Black diamonds show calibrated ages with error ranges (Table 4).

7.4.4 Microfossil analysis

Apart from single peaks (max. ~16 % of the total fauna), planktic foraminifera were rare or even absent (mean: ~2 % of the total foraminifera fauna; Fig. 40j). Agglutinants also occurred only sporadic (~0–3 % of the total benthic fauna). Hereafter, relative percentages of the calcareous fauna are given for the most common benthic foraminifera species: *Cassidulina reniforme* (~0–61 %; Fig. 40b), *Elphidium clavatum* (~1–52 %; Fig. 40c) and *Nonionellina labradorica* (~0–63 %; Fig. 40d) dominated the benthic fauna, while *Cassidulina neoteretis* exhibits high percentages from ~15 to ~12.6 ka (max. ~53 %; Fig. 40a). Further abundant species are *Buccella frigida* s.l. (max. ~27 %; Fig. 40e), *Cibicides lobatulus* (max. ~17 %; Fig. 40f), *Elphidium bartletti* (max. ~7 %; Fig. 40g), *Islandiella helenae* (max. ~13 %; Fig. 40h), *Islandiella norcrossi* (max. ~12 %; Fig. 40i) and *Melonis barleeanus* (max. ~12 %; not shown). In total, 41 calcareous and 4 agglutinating taxa could be identified (7–20 taxa per sample). Until ~12.2 ka, the accumulation rate of benthic foraminifera (including agglutinating species) shows relatively low values between ~1,770 and ~8,760 individuals cm^{-2} ka^{-1}. Subsequently, the benthic foraminifera flux is increasing up to ~52,230 ind. cm^{-2} ka^{-1} at ~7.1 ka. From then on, accumulation rates are declining down to the minimum at the uppermost sample (~940 ind. cm^{-2} ka^{-1} at ~1.3 ka; Fig. 40k).

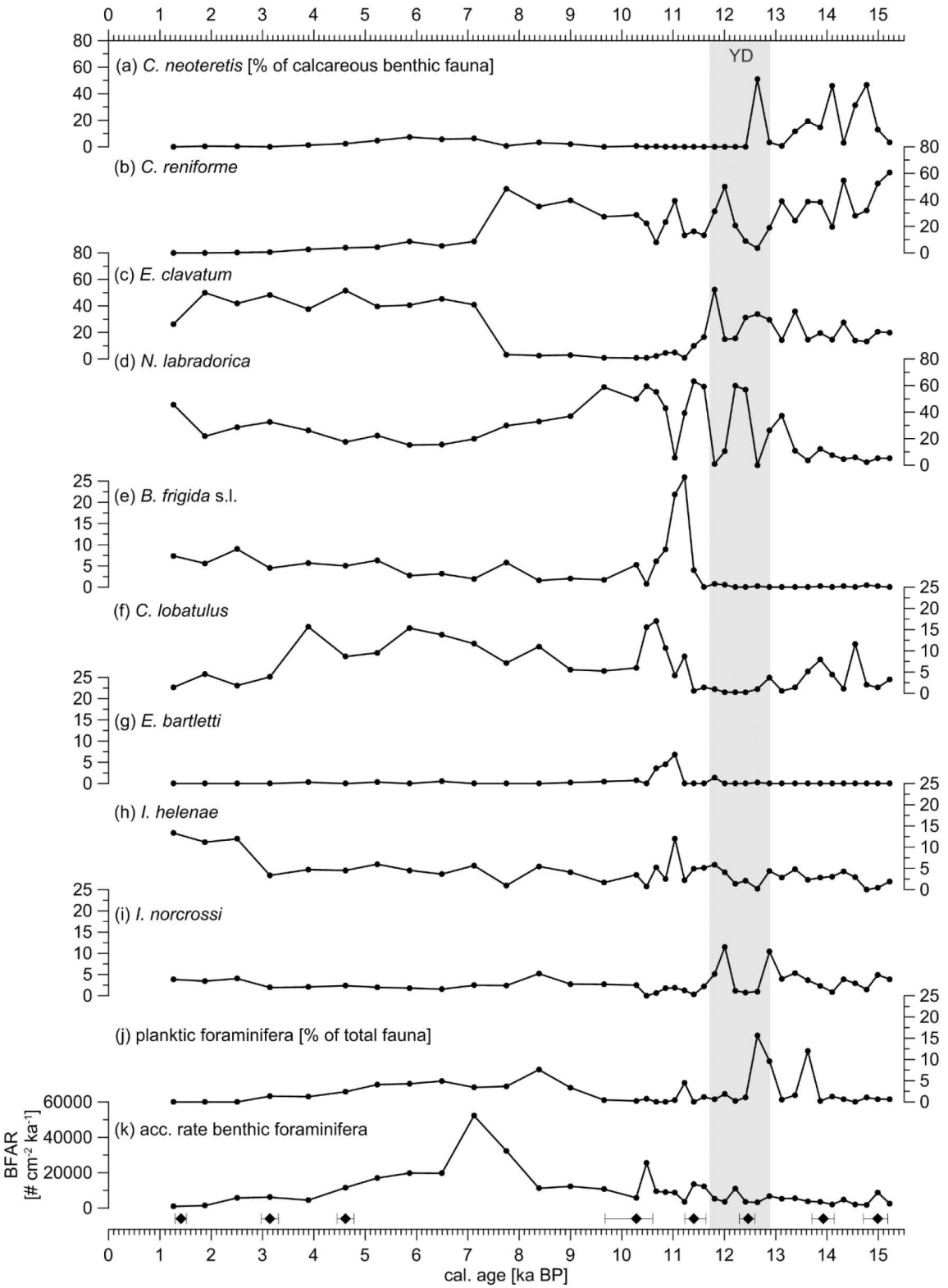

Fig. 40: (a–i) Relative percentages (in relation to the calcareous benthic fauna) of the dominant benthic species in sediment core GeoB10810-1 from the northwestern Spitsbergen shelf: (a) *Cassidulina neoteretis*, (b) *Cassidulina reniforme*, (c) *Elphidium clavatum*, (d) *Nonionellina labradorica*, (e) *Buccella frigida* s.l., (f) *Cibicides lobatulus*, (g) *Elphidium bartletti*, (h) *Islandiella helenae*, (i) *Islandiella norcrossi*. (j) Relative percentages (in relation to the total foraminifera fauna) of planktic foraminifera. (k) accumulation rate of benthic foraminifera (BFAR; including agglutinants). Grey bar marks duration of Younger Dryas. Black diamonds show calibrated ages with error ranges (Table 4).

7.4.5 Geochemistry

7.4.5.1 Stable carbon and oxygen isotopes

Ratios of planktic foraminiferal stable oxygen isotopes (measured at tests of *N. pachyderma* sin.) show a very high variability between ~13.6 and ~12.6 ka, ranging between ~1.7 and ~3.4 ‰. Subsequently, less variable values were achieved fluctuating around a mean of ~3 ‰ (Fig. 41a). Benthic foraminiferal stable oxygen ratios also exhibit a high variability during until ~11.3 ka, with values of the epibenthic species *C. lobatulus* (~1.9 to ~3.6 ‰) oscillating stronger than those of the endobenthic species *N. labradorica* (~3.2 to ~4.2 ‰). Until ~8.2 ka, the $\delta^{18}O$ values of the two benthic species had a large offset, whereas they show almost similar values afterwards, slightly exceeding the mean (~3.5 ‰ and ~3.8 ‰, respectively; Fig. 41a).

Planktic foraminiferal stable carbon isotope ratios show a slightly increasing trend from ~10.5 ka on ranging from ~-0.4 to ~0.8 ‰, while epibenthic foraminiferal $\delta^{13}C$ values exhibit almost no trend ranging from ~0.5 to ~1.5 ‰. The variability of endobenthic foraminiferal $\delta^{13}C$ values is comparably larger with significant lower ratios ranging from ~-0.6 to ~-2.8 ‰ (Fig. 41b). The offset between the epi- and the endobenthic stable carbonate ratios ($\Delta\delta^{13}C_{C.lob\text{-}N.lab}$) ranges between ~3.7 ‰ and ~1.9 ‰, while highest values were reached during the period ~10.9–3.1 ka (Fig. 41c).

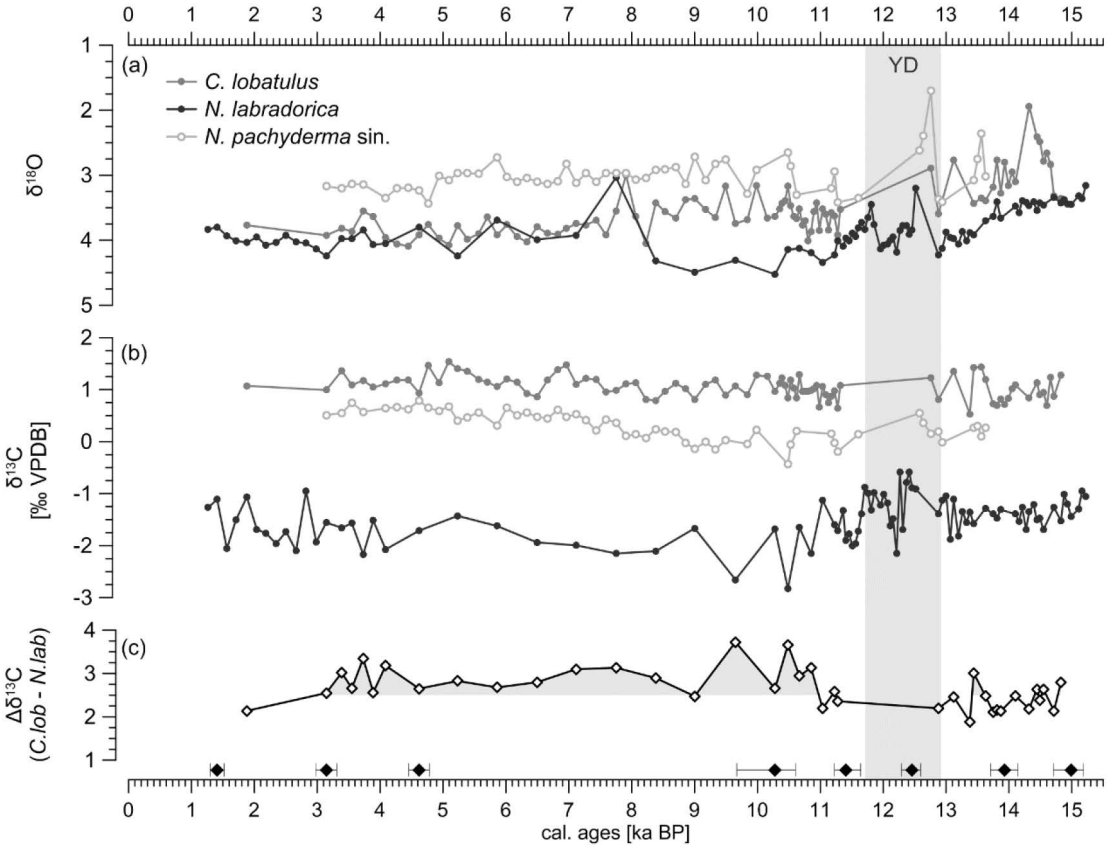

Fig. 41: (a) Planktic (*N. pachyderma* sin.), epi- (*C. lobatulus*) and endobenthic (*N. labradorica*) foraminiferal stable oxygen isotopes corrected for vital effects (only benthic) and global ice volume (see sect. 7.3) in sediment core GeoB10810-1 from the northwestern Spitsbergen shelf. (b) Planktic, epi- and endobenthic foraminiferal stable carbon isotopes. (c) Offset between epi- and endobenthic foraminiferal stable carbon isotopes ($\Delta\delta^{13}C_{C.lob\text{-}N.lab}$). Black diamonds show calibrated ages with error ranges (Table 4).

7.4.5.2 Biomarkers

Highest accumulation rates of the sea ice biomarker IP_{25} (~0.5 µg cm^{-2} ka^{-1}) were reached at ~13.6 and ~12.6 ka gradually decreasing since then. At ~9.7 and ~7.1 ka, values dropped to almost 0 µg cm^{-2} ka^{-1} (Fig. 42a). Both phytoplankton biomarkers show a parallel trend to each other ranging from ~2.4 to ~27.3 µg cm^{-2} ka^{-1} (brassicasterol) and from ~0.9 to ~6 µg cm^{-2} ka^{-1} (dinosterol), while maxima were reached at 11 ka (Fig. 42b). Respective phytoplankton–IP_{25} indices using brassicasterol and dinosterol as phytoplankton marker, also exhibit a parallel trend with similar sea ice reconstructions for each PIP_{25} index regarding the threshold values of Müller et al. (2011). Only one data point (at 14.8 ka) shows a higher offset implying different interpretations (P_BIP_{25} = 0.6, seasonal sea ice cover; P_DIP_{25} = 0.4, reduced sea ice cover; Fig. 42c). For simplicity, we only refer to P_BIP_{25} in the following discussion.

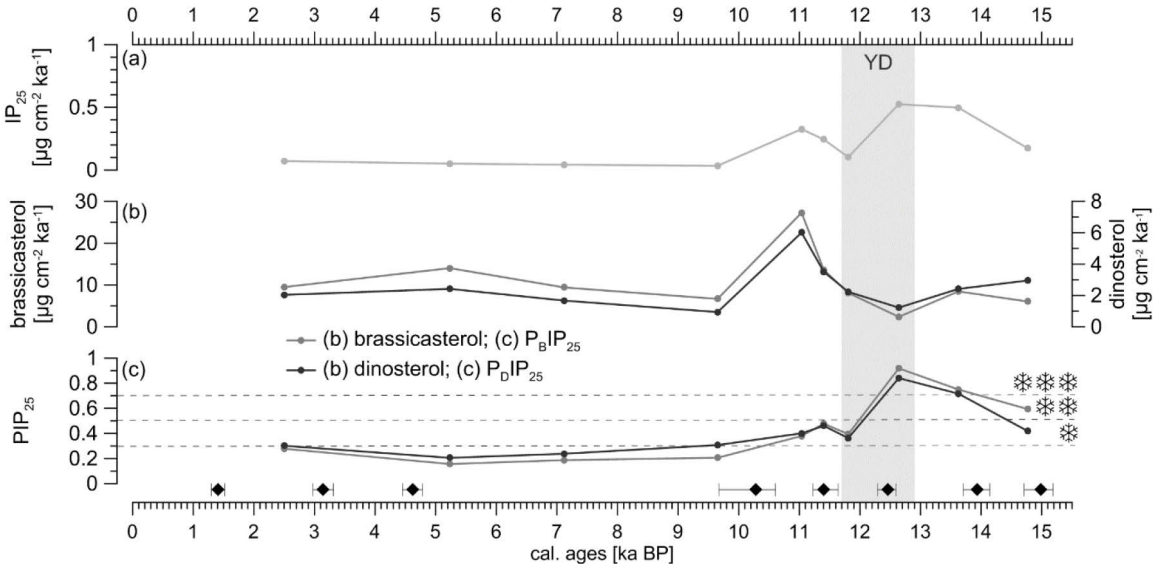

Fig. 42: Accumulation rates of (a) the sea ice biomarker IP_{25} and (b) the phytoplankton biomarkers brassicasterol and dinosterol in sediment core GeoB10810-1 from the northwestern Spitsbergen shelf. (c) Phytoplankton–IP_{25} indices using brassicasterol (P_BIP_{25}) and dinosterol (P_DIP_{25}) as phytoplankton biomarkers, respectively. Thresholds for reduced (❄; 0.3–0.5), seasonal (❄❄; 0.5–0.7) and extended sea ice cover (❄❄❄; >0.7) after Müller et al. (2011). Black diamonds show calibrated ages with error ranges (Table 4).

7.5 Discussion

Previous studies examined the retreat of the Svalbard–Barents Sea Ice Sheet in the Kongsfjord Trough (Henriksen et al., 2014; Landvik et al., 2005) and its palaeoceanography during the subsequent Holocene (Rasmussen et al., 2014b; Skirbekk et al., 2010). However, our data add an important time interval shedding light on the palaeoceanography during the deglaciation of the trough. Additionally, the studied core site GeoB10810-1 is situated farer offshore than sediment core NP05-11-21 (Rasmussen et al., 2014b; Skirbekk et al., 2010; Fig. 37) and, therefore, expected to record even small-scale hydrographic variabilities, while it may be less affected by influences from land.

7.5.1 The deglaciation at the northwestern Spitsbergen margin

The deposition of a diamicton before ~16.5 ±0.3 ka in sediment cores from the Kongsfjord Trough as well as a distinct moraine a few kilometres to the east of our core location indicates that the trough has been deglaciated more than thousand years prior to the oldest date in sediment core GeoB10810-1 (Henriksen et

al., 2014; Landvik et al., 2005). These oldest sediments in core GeoB10810-1 are marked by maximum inputs of IRD between ~15.3 and ~10.5 ka (Fig. 43a), which likely illustrate enhanced iceberg calving linked to the ongoing disintegration of the Svalbard–Barents Sea Ice Sheet. During this period, the IRD flux shows three distinct peaks at 13.8 ka, at 12.2 ka and at 10.8 ka (Fig. 43a) with the latter having also been recorded by Skirbekk et al. (2010; Fig. 44g). Probably these IRD peaks represent periods of enhanced iceberg calving driven by a pulsed deglaciation with surge-like glacier outbursts. IRD records from other parts of the Svalbard archipelago also show a pulsed IRD signal during the deglaciation (Klitgaard Kristensen et al., 2013; Łącka et al., 2015; Rasmussen et al., 2007; Ślubowska-Woldengen et al., 2007; Ślubowska et al., 2005), however, which usually show a different temporal pattern pointing to a local triggering of such surge-like glacier outbursts. Only the last IRD peak in core GeoB10810-1 at 10.8 ka, fitting in the time interval of the Preboreal Oscillation (Björck et al., 1996), seems to be mirrored in almost all these records indicating a more regional effect of this climatic oscillation (see below).

The correlation of the accumulation rates of coarse-grained sediment and of IRD suggests that major parts of the sediment >63 µm were ice-rafted as well (Fig. 43a), which is in line with process studies showing that sinking lithogenic particles >40 µm in the waters off Svalbard are provided mostly by ice-rafting (Hebbeln, 2000). At the same time, very high accumulation rates of fine-grained (<63 µm) sediments (Fig. 43b) indicate massive meltwater outflow most likely also connected to the retreat of the ice sheet, thereby documenting a proximal but continuously retreating glacier front, obviously not affected by the major IRD deposition events mentioned above. Thus, our record documents persistent deglacial conditions, which reached far into the early Holocene enduring until ~10.3 ka (Fig. 43a, b) as also observed by Skirbekk et al. (2010). Thus, around 10 ka the major deglaciation of northern Spitsbergen providing enormous amounts of meltwater might have come to an end, followed by a period with a much more balanced setting with precipitation onto the glaciers and melting of the glaciers being roughly on a similar level. The dramatic shift in the accumulation rate of fine-grained material compared to the more gradual change in the coarser, most likely ice-rafted fractions indicates that glacier melting and meltwater production was a much more prominent process of the deglaciation than ice export by calving and iceberg production. Abrupt drops in sedimentation rates around 10 ka also have been documented from other fjords and troughs of southern, western and northern Spitsbergen (Bartels et al., 2017; Groot et al., 2014; Łącka et al., 2015) highlighting a contemporaneous end of the fast deglaciation around Spitsbergen in line with observations from coastal settings (e.g., Forman, 1990; Forman et al., 2004; Lehman and Forman, 1992).

On the ocean side, the advection of AW affecting the bottom waters at site GeoB10810-1 is indicated by rather high percentages of *C. neoteretis* from ~14.8 ka onwards (Fig. 43e) as this species is commonly linked to stable salinities and, thus, (chilled) AW at the bottom (Jennings et al., 2004; Rytter et al., 2002; Seidenkrantz, 1995; Seidenkrantz et al., 2013; Steinsund, 1994). Accordingly, Atlantic-derived bottom waters were possibly able to advect onto the western Spitsbergen shelf and enter the Kongsfjord–Krossfjord system as early as ~14.8 ka where they may have contributed to the retreat of the outlet glaciers that drained the Svalbard–Barents Sea Ice Sheet as it also can be observed today (Luckman et al., 2015). Further to the north in the Hinlopen Trough, a comparable increase in the relative contribution of *C. neoteretis* has been observed to occur slightly later around ~14.3 ka (Ślubowska et al., 2005) possibly reflecting the time-transgressive northward penetration of AW during the deglaciation.

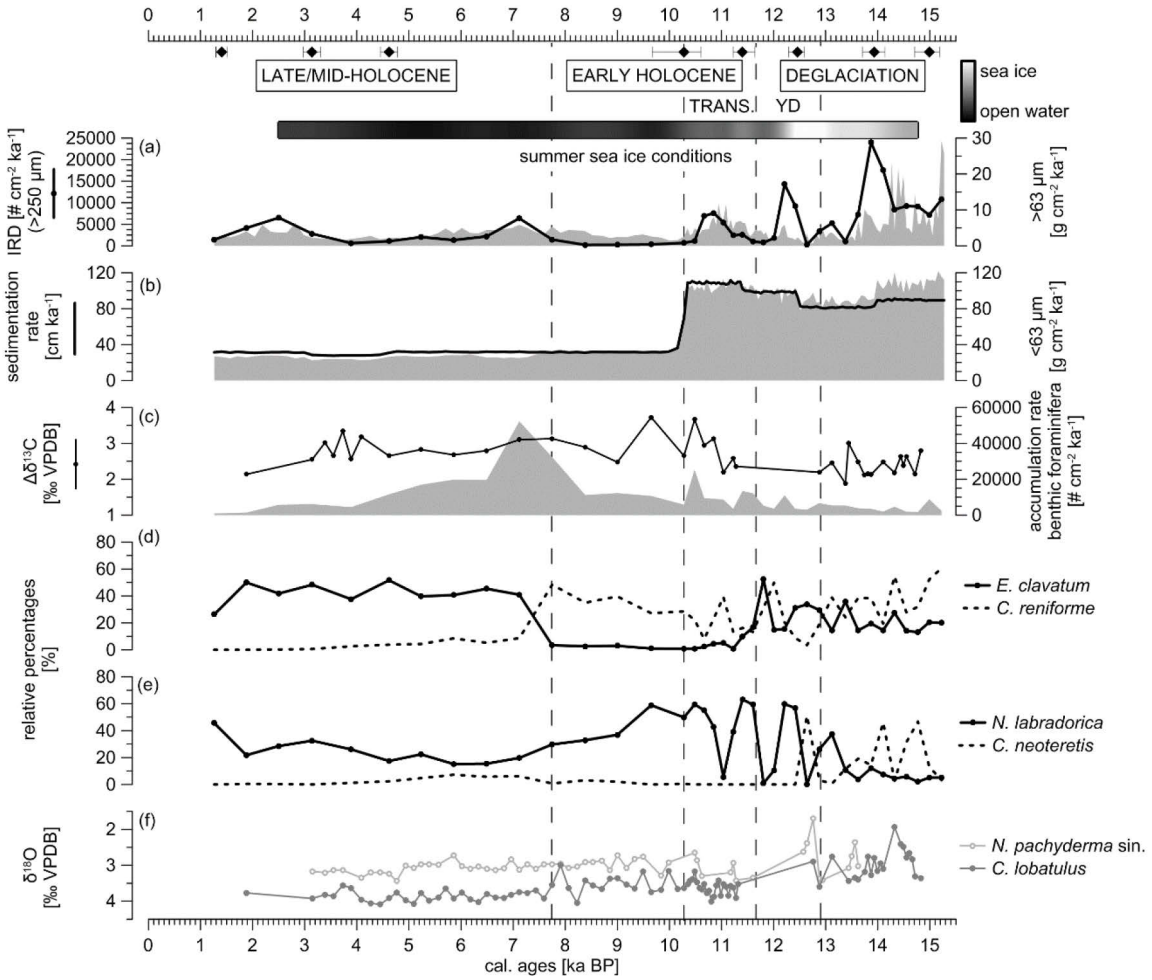

Fig. 43: Overview of selected palaeoenvironmental proxies provided by sediment core GeoB10810-1 from the northwestern Spitsbergen shelf: (a) Summer sea ice conditions based on P_BIP_{25} (see Fig. 42c) ranging from open fjord conditions (black) to an extended sea ice cover (white); accumulation rate of ice-rafted debris (IRD; clasts >250 µm; line) and of coarse-grained sediment (>63 µm; shading). (b) Sedimentation rate (line) and accumulation rate of fine-grained sediment (<63 µm; shading). (c) Offset of epi- and endobenthic foraminiferal carbon isotopes (line) and accumulation rate of benthic foraminifera (shading). (d) Relative percentages of *E. clavatum* (solid line) and of *C. reniforme* (dashed line). (e) Relative percentages of *N. labradorica* (solid line) and of *C. neoteretis* (dashed line). (f) Stable oxygen isotopes of the planktic foraminifera *N. pachyderma* sin. (light grey line) and the epibenthic foraminifera *C. lobatulus* (dark grey line). Black diamonds show calibrated ages with error ranges (Table 4). Dashed vertical lines mark time intervals "deglaciation", "early Holocene" and "late/mid-Holocene" as well as subdivisions "Younger Dryas" (YD) and "YD–early Holocene transition" (TRANS.).

Hormes et al. (2013) suggested a rapid deglaciation of the inner Kongsfjord Trough between ~14.4 and ~14.1 ka fitting to high coarse fraction accumulation rates in core GeoB10810-1 (Fig. 43a) that might reflect such a fast retreat. In addition, at the same time extremely low $\delta^{18}O$ values of *C. lobatulus* point to reduced salinities that probably result from dense sediment-laden meltwater plumes reaching down to the sea floor. Contemporary variations in the benthic foraminifera fauna, when for this short period *C. reniforme* and *E. clavatum* partly replaced *C. neoteretis,* can be interpreted to reflect such rather variable, instable conditions as the conjunctly appearance of *C. reniforme* and *E. clavatum* is commonly associated with harsh conditions, e.g., in glacier-proximal environments (e.g., Hald and Korsun, 1997; Hansen and Knudsen, 1995; Korsun and Hald, 1998).

From ~14 ka on, when the Barents Sea was already largely ice-free, those ice sheets covering Svalbard and Franz Josef Land (an archipelago east of Svalbard) were separated (Hughes et al., 2016) enabling Arctic

Water to enter the Barents Sea and flow around Svalbard. At around 13.4 ka rising percentages of *N. labradorica* (Fig. 43e) point to a first significant increase in the advection of AW in intermediate waters probably contributing to the establishment of the Arctic Coastal Front dividing AW and Arctic waters in proximity of the core site and, thus, triggering productivity as reflected in a smooth but recognisable increase in the accumulation of benthic foraminifera in relation to increased percentages of *N. labradorica* (Fig. 43c, e). The presence of this species has been related to glacier-distal locations and to enhanced productivity in various modern (sub-)Arctic shelf settings (Hald and Korsun, 1997; Rytter et al., 2002; Steinsund, 1994). A productivity increase is also indicated by simultaneously rising $\Delta\delta^{13}C$ values (Fig. 43c). The offset between epi- and endobenthic $\delta^{13}C$ values ($\Delta\delta^{13}C_{C.lob\text{-}N.lab}$) is assumed to act as a palaeoproductivity proxy (Mackensen et al., 2017) because low endobenthic $\delta^{13}C_{N.lab}$ values (reflecting a pore water signal) point to high remineralization rates in the sediment and, thus, to an enhanced export productivity. At the onset of the Younger Dryas (YD), AW advection in intermediate waters was probably reduced leading to a weakening of the front and a subsequent decrease in productivity as documented by a shift in the benthic foraminifera fauna when *C. neoteretis* largely replaced *N. labradorica* (Fig. 43e) that can also be observed in the Hinlopen Trough record of Ślubowska et al. (2005). Very low planktic foraminifera $\delta^{18}O$ values combined with ~1.2 ‰ higher epibenthic $\delta^{18}O$ values in core GeoB10810-1 (Fig. 43f) point to a strong stratification of the water column at this time. A massive discharge of meltwater into the Arctic Ocean has been proposed as a trigger for the YD (e.g., Murton et al., 2010). This freshwater outburst may have forced AW to sink in the Kongsfjord Trough where the low planktic $\delta^{18}O$ values possibly reflect such a freshening of the surface waters like it has been observed in the Nordic Seas (e.g., Bauch et al., 2001; Telesiński et al., 2014, 2015) and on the southeastern Greenland shelf (Jennings et al., 2006). Simultaneously, sea ice may have expanded to its maximum extension due to these fresher surface waters as indicated by the sea ice proxies (Fig. 43a). Similar sea ice conditions were reported for ~12.8–12.6 ka from the eastern Fram Strait ~90 km west of our core location (Müller and Stein, 2014). Although the PIP_{25} indices in sediment core GeoB10810-1 fit such nearby records, it has to be noted that the GeoB10810-1 PIP_{25} data should be interpreted cautiously as those sea ice proxies are based on comparable low amounts of the sea ice diatom biomarker IP_{25} (maximal ~0.5 µg cm^{-2} ka^{-1}). Especially, as planktic foraminifera exhibit peak percentages at the onset of the YD (~16 % of the total foraminiferal fauna; Fig. 40j), thus, not supporting a perennial sea ice coverage at this site.

In the following, the YD was marked by rather variable conditions with short-term peaks in the flux of IRD, in the relative importance of various species of benthic foraminifera, and in the sea ice cover (Fig. 43). Similar variable conditions during the YD have been observed all along the Svalbard margins from the Storfjord up to the Hinlopen Trough (Bartels et al., 2017; Łącka et al., 2015; Ślubowska-Woldengen et al., 2007; Ślubowska et al., 2005). More detailed comparisons of the individual wiggles between these records are hampered by the resolution of the available age–depth models. Rather instable conditons during the YD were also reported from western Greenland, where glaciers partly advanced before rapidly retreating in the mid-YD (Hogan et al., 2016; Jennings et al., 2014; Ó Cofaigh et al., 2013; Rinterknecht et al., 2014).

Off northwestern Spitsbergen such variable conditions lasted well into the early Holocene until ~10.3 ka, when the end of the fast deglaciation of Spitsbergen as documented in the drastic drop in sedimentation rates coincided with the establishment of much more stable environmental conditions in the Kongsfjord Trough in the early Holocene (Fig. 43b). During this YD–early Holocene transition phase, the appearance of new

benthic foraminifera species such as *B. frigida* s.l. and *E. bartletti* and peak abundances of *I. helenae* (Fig. 40e, g, h) point to ameliorating conditions heralding the onset of the Holocene as these species have been linked with improved productivity conditions (Polyak et al., 2002; Seidenkrantz, 2013). Indeed, enhanced productivity during this time is indicated by increasing benthic foraminifera accumulation rates and by high $\Delta\delta^{13}C$ values (Fig. 43c) as well as by high accumulation rates of the phytoplankton biomarkers (Fig. 42b). This increase in productivity is probably triggered by the approaching Arctic Coastal Front pushed shoreward by an increasing advection of AW that also results in a reduction of the sea ice cover (Fig. 43a) bringing the core site close to the sea ice margin where productivity often is enhanced (e.g., Hebbeln and Wefer, 1991). Enhanced percentages of *C. lobatulus* (Fig. 40f), a species that has been connected to strong bottom currents (e.g., Altenbach et al., 1999; Hald and Korsun, 1997; Hansen and Knudsen, 1995; Korsun and Hald, 1998; Steinsund, 1994), are an additional indicator pointing to a stronger advection of AW.

Interestingly, the benthic foraminifera accumulation rates in core GeoB10810-1 are higher during this period as those reconstructed for the near-by core NP05-11-21 (Fig. 37c and Fig. 44f; Skirbekk et al., 2010) although for our core only individuals >150 µm have been counted compared to >100 µm specimens counted in the other core and in spite of a similar qualitative shift in the faunal composition pointing towards higher productivity in core NP05-11-21 (Fig. 44). This distinct difference might be related to the still ongoing final deglaciation of northwestern Spitsbergen marked by very high sedimentation rates in the Kongsfjord Trough cores, with even higher rates of >150 cm ka^{-1} in site NP05-11-21 that is closer to the coast compared to core GeoB10810-1 with 107 cm ka^{-1}. With most of the delivered material being rather fine (Fig. 39), an (at least seasonal) presence of turbid meltwater plumes close to the sea surface can be assumed that still hampered local productivity (which was well below mid-Holocene levels). In such a scenario, productivity would increase with increasing distance from the fjord as it is reflected in the benthic foraminifera accumulation rates of the two cores (Fig. 44f).

A prominent event during this period is the Preboreal Oscillation (as described by Björck et al., 1996), a short-term cooling event around 11 ka that is recorded at many sites around Svalbard (Bartels et al., 2017; Rasmussen et al., 2012, 2014c; Skirbekk et al., 2010; Ślubowska-Woldengen et al., 2007; Ślubowska et al., 2005) and marked by a distinct minimum in the relative percentages of *N. labradorica* (Fig. 44a) and a peak in the IRD flux (Fig. 44g). This faunal shift may be connected to a retreat of the Arctic Coastal Front and a stronger influence of Arctic Water advected by the Coastal Current. At both sites, increasing percentages of *C. reniforme* (Fig. 44d; Skirbekk et al., 2010) suggest cold but saline bottom waters (Mackensen et al., 1985; Polyak et al., 2002; Sejrup and Guilbault, 1980). Consistently, enriched epibenthic and planktic $\delta^{18}O$ values are evident in our record between ~11.3 and ~10.8 ka (Fig. 43f), which may be linked to a cooling of bottom and surface waters, respectively, like it has been reported from core site NP05-11-21 (Rasmussen et al., 2014b). Enhanced ice-rafting at the same time might result from a temporarily enhanced iceberg production. Ślubowska-Woldengen et al. (2007) linked comparable "late" IRD peaks to the final break-up of the Svalbard–Barents Sea Ice Sheet. However, enhanced calving may have been caused by glacier advances as this IRD peak correlates with the cooling during the Preboreal Oscillation.

7.5.2 The Holocene in the Kongsfjord Trough

7.5.2.1 Early Holocene (~10.3–7.2 ka)

The early Holocene dominance of *C. reniforme* and *N. labradorica* and the absence of *E. excavatum* in accordance with the lowest IRD input of the entire record point to the warmest conditions of the last ~15.3 ka recorded off northwestern Spitsbergen likely corresponding to the Holocene Climate Optimum (Fig. 44; Skirbekk et al., 2010). Whereas the divergent pattern of higher (lower) relative contributions of the mostly larger *N. labadorica* (smaller *C. reniforme*) in core GeoB10810-1 (NP35-11-21) probably can be explained by the grain size effect resulting from counting the >150 µm (>100 µm) fraction, higher percentages of *Buccella* spp. and higher benthic foraminifera accumulation rates in core NP05-11-21 indicate a higher productivity at the site closer to the coast (Fig. 44). This might be triggered by strongest AW advection during this time pushing the Arctic Coastal Front far onto the shelf as, e.g., also indicated by the highest fluxes of planktic foraminifera at the near coastal site (Rasmussen et al., 2014b). However, also at near-by site GeoB10810-1 the benthic foraminifera accumulation rates and especially the $\Delta\delta^{13}C$ values point to moderate to high productivities combined with ice-free conditions (Fig. 43a, c). Large seasonal contrasts can be assumed during the early Holocene reflected by an enhanced offset of benthic foraminiferal stable oxygen isotopes (Rasmussen et al., 2012): high $\delta^{18}O$ values of *N. labradorica* may indicate cold bottom waters in spring, while relatively lower $\delta^{18}O$ values of *C. lobatulus* may reflect warmer bottom waters and/or lower salinities linked to meltwater plumes during summer (see Zajączkowski et al., 2010a).

7.5.2.2 Mid-Holocene (~7.2–4.7 ka)

The early to mid-Holocene transition is marked by a prominent faunal shift, namely the replacement of *C. reniforme* and *N. labradorica* by *E. clavatum* (Fig. 43d, e and Fig. 44), which is recognisable in almost the entire Svalbard region (Duplessy et al., 2001; Hald et al., 2004; Klitgaard Kristensen et al., 2013; Rasmussen et al., 2012) even reaching into remote fjords in central Svalbard (Bartels et al., in prep.). This regional faunal shift probably reflects a growing influence of Arctic Water due to a diminishing AW influx. Consistently, slightly increasing $\delta^{18}O$ values of *C. lobatulus* point to colder bottom waters (see also Rasmussen et al., 2014b). The concomitant increase in the $\delta^{18}O$ values of *N. labradorica*, reaching the same level as the *C. lobatulus* $\delta^{18}O$ values probably reflects more stable bottom water conditions with less seasonal differences as assumed for the Early Holocene. Also for the mid-Holocene, high accumulation rates of benthic foraminifera at both core sites in the Kongsfjord Trough and slightly enhanced $\Delta\delta^{13}C$ values at core location GeoB10810-1 indicate still a high productivity (Fig. 43f and Fig. 44c). However, a slightly increased IRD flux in core GeoB10810-1 (>250µm) that is not recorded in the coarser IRD fraction analysed for core NP05-11-21 (Fig. 44g) points to already slightly deteriorating conditions following the Holocene Climate Optimum. Although this presumed cooling had no impact on the sea ice coverage in the Kongsfjord Trough (Fig. 43a), it might have allowed some Svalbard glaciers to grow and to produce an increasing number of icebergs increasing the IRD input.

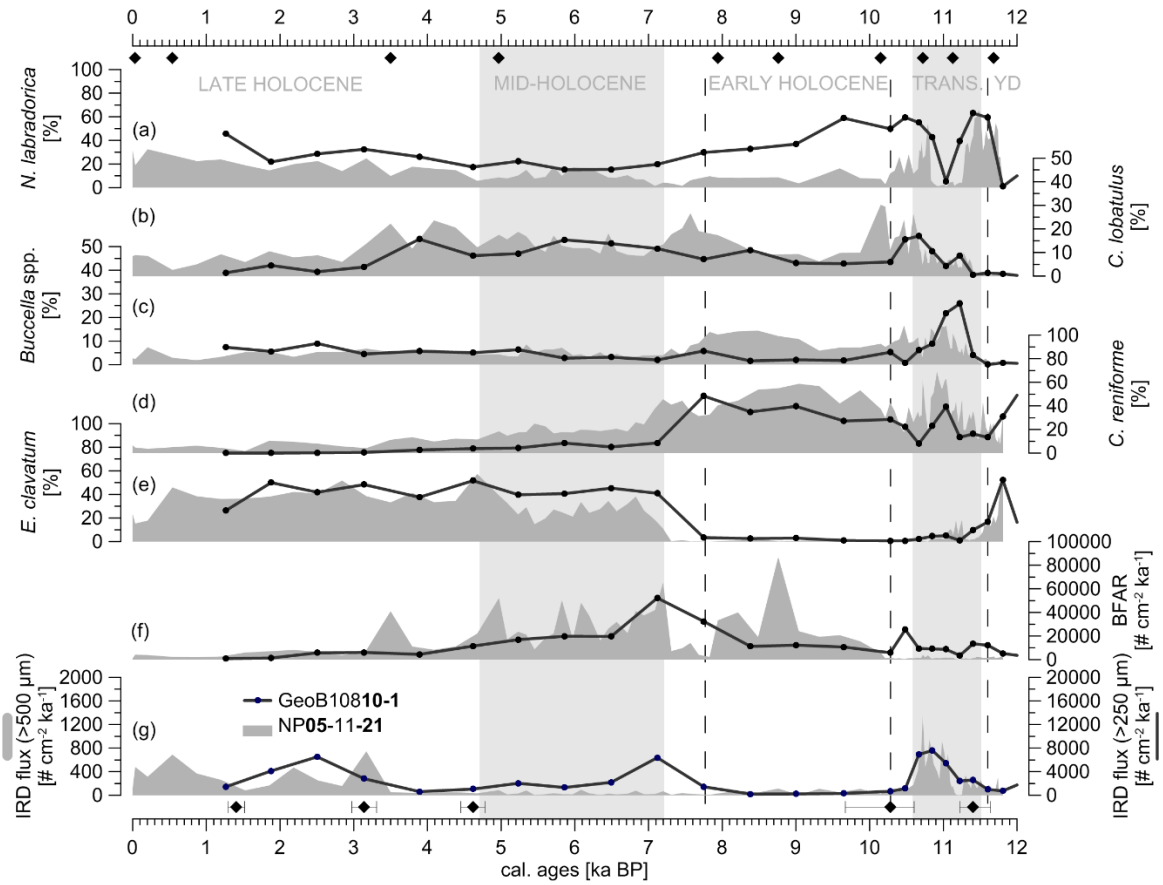

Fig. 44: Comparison of relative percentages of dominant benthic foraminifera (a–e) and accumulation rates of benthic foraminifera (f) and of ice-rafted debris (g) in sediment cores GeoB10810-1 (lines; this study) and NP05-11-21 (shadings; Skirbekk et al., 2010), both collected from the Kongsfjord Trough in different distance from the coast. Relative percentages of (a) *Nonionellina labradorica*, (b) *Cibicides lobatulus*, (c) *Buccella* spp., (d) *Cassidulina reniforme*, (e) *Elphidium clavatum* (*E. excavatum* in Skirbekk et al., 2010); accumulation rates of (f) benthic foraminifera (BFAR) and of (g) ice-rafted clasts (IRD fluxes) >250 µm (this study) and >500 µm (Skirbekk et al., 2010). Light grey and white backgrounds mark time intervals "Younger Dryas" (YD), "Holocene transition" (TRANS.), "early Holocene", "mid-Holocene" and "late Holocene" as defined in Skirbekk et al. (2010). Dashed vertical lines mark time intervals as defined in Fig. 43. Diamonds at upper x-axis show calibrated ages for sediment core NP05-11-21 , diamonds at lower x-axis show calibrated ages with error ranges for sediment core GeoB10810-1 (Table 4).

7.5.2.3 Late Holocene (<4.7 ka)

During the late Holocene, increasing glacier activity in the Kongsfjord–Krossfjord system is evident in both records: From ~3.2 ka on, the accumulation rate of IRD increased significantly (Fig. 44g). The enhanced deposition of ice-rafted material is probably connected to glacier advances during the so-called neoglaciation (Porter and Denton, 1967). Van der Bilt et al. (2015) reported glacier advances on Mitrahalvøya (a peninsula separating the Krossfjord from the Fram Strait; see Fig. 37c) during roughly the same period. Especially between ~1.7 and ~1 ka, glacier advances have been observed at various locations on Spitsbergen (e.g., Humlum et al., 2005; Røthe et al., 2015; Svendsen and Mangerud, 1997; de Wet et al., 2017). The link of the increased IRD flux to the neoglaciation and, thus, to a cooling resulting in advancing glaciers highlights the difference to the deglaciation record, when the decaying glaciers predominantly resulted in the increased input of fine material most likely delivered by meltwater plumes (Fig. 39). Interestingly, the higher glacier activity in the hinterland and the resulting deposition of IRD in the Kongsfjord Trough did not significantly affect the dominant foraminiferal fauna (Fig. 40). Hence, stable hydrographic conditions continuing since the

mid-Holocene can be assumed: The persistent dominance of *E. clavatum* points to a strong Arctic Water but weak AW influence (Fig. 43d and Fig. 44e).

7.6 Conclusions

The examination of benthic foraminiferal assemblages, stable carbon and oxygen isotopes, biomarkers and sediment properties of sediment core GeoB10810-1 enabled us to reconstruct the palaeoceanography of the Kongsfjord Trough since the deglaciation. We compared our results with the close-by but closer to the coast collected Holocene record of core NP05-11-21 (Rasmussen et al., 2014b; Skirbekk et al., 2010).

At both sites, deglacial conditions persisted until the early Holocene (~10.3 ka), when the supply of considerable amounts of glacigenic sediment from glaciers in the hinterland ceased. The dominance of fine-grained sediment accumulation over the IRD flux until ~10.3 ka illustrates that meltwater discharge was a more important process during the deglaciation of northwestern Spitsbergen as iceberg production commonly associated with the transport of coarse IRD. The early inflow of AW affecting the sea floor in the Kongsfjord Trough, starting already at ~14.8 ka, contributed significantly to the retreat of the outlet glaciers of the Svalbard–Barents Sea Ice Sheet. The YD, triggered by a massive freshwater input into the Arctic Ocean, was characterized by complex and very variable palaeoceanographic conditions. During the subsequent YD/early Holocene transition, productivity increased, especially at the more distal core site GeoB10810-1, were turbid meltwater plumes had less influence than at core location NP05-11-21 situated closer to the coast. A short-term cooling (the Preboreal Oscillation) is recognisable in both records. A further increasing productivity is observed during the early Holocene when data of both cores, but particularly of core NP05-11-21, reveal ameliorated conditions probably triggered by the Holocene Climate Optimum. At the onset of the mid-Holocene, a dramatic shift in the benthic foraminiferal fauna found in the entire Svalbard region revealed that the Arctic waters increased in importance in relation to AW. During the late Holocene, the intensifying glacier activity had no considerable influence on the palaeoenvironment of the Kongsfjord Trough. The comparison of the coastal-proximal sediment core NP05-11-21 and the more distal site GeoB10810-1 revealed that a distance of a few kilometres results in (although small-scale) different environmental conditions, that can support the reconstruction of the palaeoenvironment, as, e.g., shown for the reduced productivity in the setting closer to the coast probably caused by enhanced turbidity due to sediment-laden meltwater plumes.

Acknowledgements

This project was supported by the *Deutsche Forschungsgemeinschaft* (DFG) through the International Research Training Group "Processes and impacts of climate change in the North Atlantic Ocean and the Canadian Arctic" (IRTG 1904 *ArcTrain*). The captain and the crew as well as the scientists on board the RV *Maria S. Merian* during the cruise MSM02/03 in 2006 are thanked for retrieving the samples. For the performance radiocarbon measurements, we are grateful to Lukas Wacker at ETH in Zürich. Birgit Meyer and Henning Kuhnert at MARUM in Bremen are thanked for stable isotope measurements. Further, Anna-Lena Rugen (MARUM, Bremen) and Walter Luttmer (AWI, Bremerhaven) were acknowledged for sample processing and technical assistance. Sample material was provided by the GeoB repository at MARUM, Bremen.

8 Synthesis

Palaeoceanographic analyses of sedimentary records retrieved at one trough and two fjords from northwestern and northern Spitsbergen as well as from western Nordaustlandet, respectively, revealed the palaeoceanography and the ocean–ice interactions during the Holocene and beyond. The case studies of this thesis added some further pieces to the puzzle of the palaeoceanography in the (Norwegian) Arctic during the past ~15,000 years.

The **deglaciation** in the Svalbard area was characterized by the disintegration of the Svalbard–Barents Sea Ice Sheet, which is reflected by high amounts of IRD at the core sites in northwestern and northern Spitsbergen (Kongsfjord Trough and Woodfjord, respectively; Fig. 45a, b). The retreat of the ice sheet was most likely triggered by a strengthened inflow of the West Spitsbergen Current (WSC) transporting relatively warm AW along the north(-western) Svalbard margin and entering the bottom waters of the fjords and troughs (Fig. 46a). Intruding AW in bottom waters, especially in the Kongsfjord Trough, is illustrated by risen percentages of *C. neoteretis* (Fig. 45a, b), a benthic foraminiferal species commonly associated with those water masses (e.g., Seidenkrantz, 1995; Seidenkrantz et al., 2013; Steinsund, 1994). High percentages of *E. clavatum* (Fig. 45a, b) indicate the glacier-proximal setting at the sample sites as this species usually flourishes next to glacier fronts at high latitudes (e.g., Korsun and Hald, 1998, 2000). Accordingly, outflow glaciers of the Svalbard–Barents Sea Ice Sheet terminated close to the investigated core locations in the Kongsfjord Trough and at the mouth of the Woodfjord (Fig. 46a). Deglacial conditions persisted far into the Holocene signified by high sedimentation rates and the enhanced accumulation of meltwater-derived fine-grained sediments until ~10 ka at the north(-western) Spitsbergen margin (see chapters 5 and 7) and even until 5.2 ka in the Wahlenbergfjord (see chapter 6), which was filled with a glacier until 11.3 ka (Flink et al., 2017). Accordingly, glacier melting can be considered as the dominant process during deglaciation compared to glacier calving.

At the Kongsfjord Trough, an oceanic front developed separating the WSC from the East Spitsbergen Current (ESC; Fig. 46b) developed around the onset of the **Younger Dryas** (~12,900–11,700 years ago), denoted by increasing percentages of *N. labradorica* (Fig. 45a, b), whose appearance is assumed to be linked to high productivity at oceanic fronts (e.g., Hald and Korsun, 1997). Subsequently, AW was possibly forced to sink down again temporary at the Kongsfjord Trough and in the Woodfjord caused by high amounts of brackish water occupying Arctic surface waters linked to the meltwater outburst that triggered the YD cold spell (e.g., Murton et al., 2010). This hydrographic shift is most pronounced in the record from the Kongsfjord Trough illustrated by peak percentages of *C. neoteretis* (Fig. 45a) and a negative planktic $\delta^{18}O$ excursion (*N. pachyderma* sin.; see chapter 7). High IRD amounts in both sediment cores from north(-western) Spitsbergen (Fig. 45a, b) point to a persisting glacier activity, rather illustrating a further retreat than YD glacier advances because a continuing discharge of meltwater-derived fine-grained sediments is recognisable in both records (see chapters 5 and 7). The core sites at the north(-western) Spitsbergen margin were still located close to the glacier front during the YD (see Fig. 46b), indicated also by increased percentages of *E. clavatum* (Fig. 45a, b). Data of the studied Spitsbergen core locations revealed highly variable environmental conditions during the YD suggesting a more complex setting in the Svalbard area than the proposed bipartite YD stadial in the more southerly North Atlantic (e.g., Bakke et al., 2009).

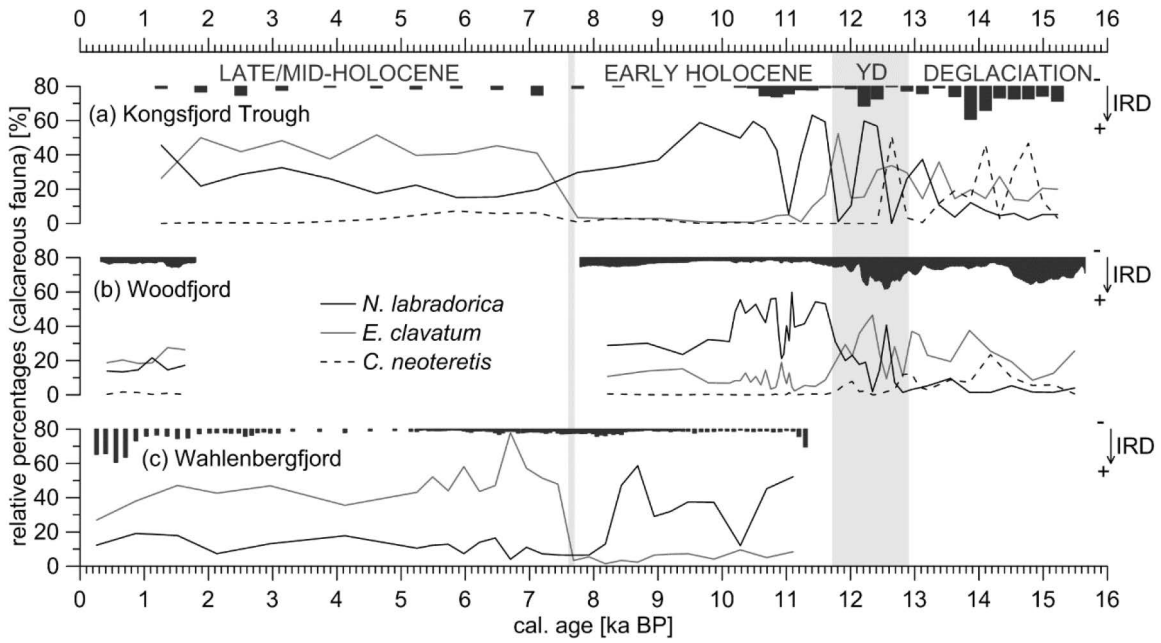

Fig. 45: Compilation of relative abundances (in relation to the calcareous benthic foraminiferal fauna) of selected benthic foraminifera species from the three study sites: *N. labradorica* (solid black line), *E. clavatum* (solid grey line) and *C. neoteretis* (dashed black line) as well as qualitative records of ice-rafted debris (IRD; bar plots; note descending y-axis) at the core sites in (a) the Kongsfjord Trough (GeoB10810-1; northwestern Spitsbergen; chapter 7), (b) the Woodfjord (GeoB10817-4; northern Spitsbergen; chapter 5) and (c) the Wahlenbergfjord (GeoB10831-3; Nordaustlandet; chapter 6). Grey vertical bars mark time interval of Younger Dryas (YD) and early–mid-Holocene transition.

Deteriorating environmental conditions occurred almost parallel at various locations along the Svalbard margins around 11,000 years ago (especially reflected in declining *N. labradorica* percentages), although probably not in the Wahlenbergfjord record (Fig. 45). However, a sea ice edge close to the north(-western) Svalbard margin during this time period (the so-called Preboreal Oscillation; Björck et al., 1996) resulted in an enhanced productivity signified by phytoplankton biomarkers and increased percentages of benthic foraminifera associated with the input of organic matter (e.g., *Buccella* spp.; see chapters 5 and 7). In some areas around Spitsbergen, including the Kongsfjord Trough, the Preboreal Osciallation was characterized by an enhanced IRD deposition, which might have been connected to glacier advances.

During the subsequent part of the **early Holocene** (<10,000 years ago), when summer insolation reached its maximum (Berger and Loutre, 1991), glaciers on Svalbard retreated to innermost fjord positions terminating at the fjord heads or even on land. Accordingly, IRD deposition was reduced at all three study sites (Fig. 45). This time period was characterized by a strong AW advection even penetrating remote fjords like the Wahlenbergfjord (Fig. 46c), where oceanic fronts developed. High productivity along these oceanic fronts is indicated by an abundant appearance of *N. labradorica* in the studied sediment cores (Fig. 45) as well as by high $\Delta\delta^{13}C$ values (offset between $\delta^{13}C$ ratios of *N. labradorica* and *C. lobatulus*; see chapters 5, 6 and 7), a valuable proxy for export productivity (Mackensen et al., 2017). Compared with the Woodfjord, AW inflow was longer lasting in the Kongsfjord Trough (Fig. 45a), which is situated only a few kilometres north of the latitude where AW submerges under fresher surface waters during modern times (Johannessen, 1986; Manley, 1995). In the Wahlenbergfjord, the development of an oceanic front was largely influenced by local wind-induced upwelling.

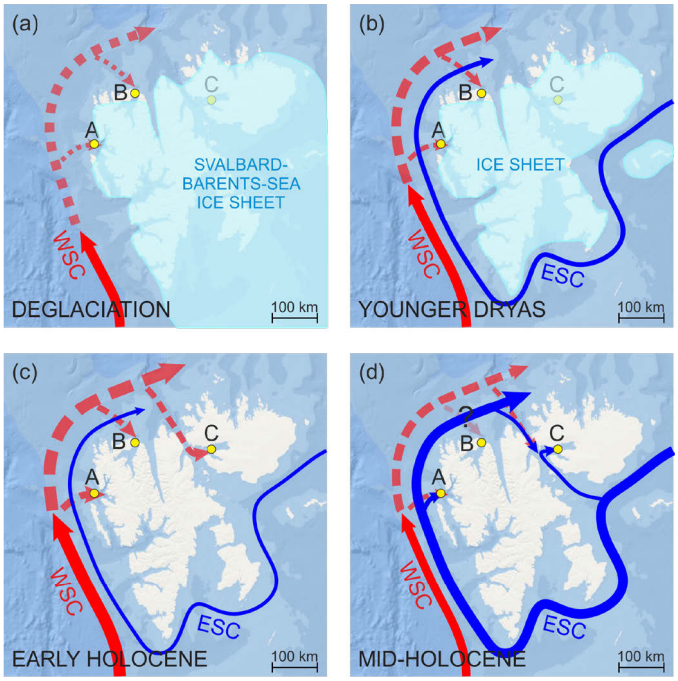

Fig. 46: Palaeoceanography in the Svalbard area. (a) Deglaciation: West Spitsbergen Current (WSC) submerged (stippled line) and affected bottom waters. (b) Younger Dryas: an oceanic front developed separating WSC and East Spitsbergen Current (ESC). (c) Early Holocene: strong inflow of WSC. (d) Mid-Holocene: weakening of WSC, strong influence of ESC. Core sites: (A) GeoB10810-1 in the Kongsfjord Trough (chapter 7); (B) GeoB10817-4 in the Woodfjord (chapter 5); (C) GeoB10831-3 in the Wahlenbergfjord (chapter 6). Ice sheet extension based on reconstructions by Hormes et al. (2013). Basemap created with ArcGIS online (http://www.arcgis.com).

At the transition to the **mid-Holocene** (around 7,700 years ago), significant hydrographic changes are suggested by a rapid shift in the benthic foraminiferal fauna, namely by the replacement of *N. labradorica* and *C. reniforme* by *E. clavatum*. This shift is recognisable in numerous records from the Svalbard area, including the studied sediment cores in the Kongsfjord Trough and even in the remote Wahlenbergfjord (Fig. 45a, c). While this time period is not documented in the sedimentary archive from the Woodfjord, further records from the Svalbard region (Rasmussen et al., 2012) imply a weakening of the WSC and a stronger influence of Arctic waters (e.g., the ESC; Fig. 46d). It is remarkable that this regional hydrographic change is reflected in the sediments of a very remote and glacier-proximal fjord like the Wahlenbergfjord in Nordaustlandet.

Advances of some glaciers in Svalbard during the **late Holocene** are reported in various publications (e.g., Humlum et al., 2005; Svendsen and Mangerud, 1997). Increasing amounts of IRD at the investigated study sites may be connected to these growing glaciers (Fig. 45). Lower atmospheric temperatures induced by the decreased summer insolation (Berger and Loutre, 1991) during the late Holocene probably triggered the waxing of those glaciers. Slightly increasing percentages of *N. labradorica* at all investigated core locations point to a strengthened AW inflow in the fjords and troughs (Fig. 45). Why glaciers advanced despite the advection of those relatively warm waters, may be explained by an extended sea ice cover (like sea ice biomarkers in the Wahlenbergfjord suggest; see chapter 6) decoupling the cold atmosphere from relatively warm ocean currents (as assumed by Jernas et al., 2013). During the late Holocene, most glaciers terminated in the shallower inner basins of the fjords, thus, it is also possible that AW, primarily encountered in intermediate waters, was not able to reach the glacier fronts.

In retrospect, the open questions compiled in chapter 1.4 could be answered with the case studies of this thesis: (a) AW advection had a significant influence on the disintegration of the Svalbard–Barents Sea Ice Sheet and the retreat of its outlet glaciers during the deglaciation, not only at the northern Svalbard margin (see chapters 5 and 7). While the inflow of AW contributed to the melting of glaciers during the latter time period, some glaciers in Svalbard were able to advance despite a strengthened AW influx during the late Holocene (as discussed above and in chapters 5, 6 and 7). (b) Regional hydrographic fluctuations could be

traced even in a remote glacier-proximal fjord setting like the Wahlenbergfjord. At least during the early Holocene, AW entered the latter fjord in Nordaustlandet. (c) Also in the Kongsfjord Trough, the bottom water inflow of AW contributed to the deglaciation of the glaciated hinterland in northwestern Spitsbergen. Interestingly, palaeoenvironmental conditions (especially productivity) diverged between two study sites only a few kilometres away from each other, however, with different distances to the coast (see chapter 7).

The three case studies comprising this thesis elucidated that the advection of relatively warm water masses contributed significantly to the disintegration of the Svalbard–Barents Sea Ice Sheet, evidenced by the ongoing deglaciation after a considerable advection of AW began. Thus, once triggered, the shrinking of the glaciers and ice sheets lasted thousands of years, despite a variable intensity of the AW influx. This phenomenon might be transferred to currently retreating ice shelves on Antarctica, where glacier melting has been linked to relatively warm ocean currents (e.g., Christianson et al., 2016; Cook et al., 2016; Padman et al., 2012; Wouters et al., 2015). However, the results of those case studies further illustrate that such interactions might be very complex as, e.g., late Holocene glaciers probably advanced despite the influx of AW, which possibly was caused by an extended sea ice coverage insulating the cold atmosphere from warmer ocean currents. Accordingly, the presently declining sea ice cover might enhance a further melting of tidewater glaciers in the Arctic. The reflexion of regional signals in a very remote Arctic fjord setting illustrates that even those locations are vulnerable in the context of the ongoing global warming.

9 Outlook

While answering those questions discussed in the previous chapter, new open questions and research gaps arose, which will be addressed in the following. Although many studies examined the modern distribution of AW along the western and northern Svalbard margins (Cottier et al., 2005; Fahrbach et al., 2001; Hattermann et al., 2016; Koenig et al., 2017; Pérez-Hernández et al., 2017; Saloranta and Haugan, 2001; Saloranta and Svendsen, 2001; Schauer et al., 2004), detailed hydrographic surveys of most Svalbard´s fjords are still lacking. Therefore, CTD transects down the fjords, e.g., the Woodfjord or the Wahlenbergfjord, are required, especially with respect to palaeoceanographic reconstructions compared with modern hydrographic conditions.

Those surveys could be combined with transects of sediment cores, ideally hitting the basal till to trace the onset of marine sedimentation and, thus, to reconstruct the history of glacier retreats during the deglaciation. Radiocarbon measurements from samples at the junction from basal till to glacimarine sediments would complete bathymetric studies, which estimated the disintegration of the ice sheets based on morphological features (Baeten et al., 2010; Dowdeswell et al., 2010; Flink et al., 2017; Forwick and Vorren, 2010; Henriksen et al., 2014; Hogan et al., 2010b; Landvik et al., 2005; Ottesen et al., 2007), as well as studies based on cosmogenic radionuclides and on radiocarbon-dated beach ridges (Brückner and Schellmann, 2003; Forman et al., 2004; Gjermundsen et al., 2013; Hormes et al., 2011, 2013; Lehman and Forman, 1992; Salvigsen and Österholm, 1982).

The analyses of biomarkers in the framework of this thesis showed that the use of brassicasterol and dinosterol (as phytoplankton markers), IP_{25} and PIP_{25} (for sea ice reconstructions) as well as of alkenones (for SST estimations) are powerful tools when applied to Arctic fjord environments. Accordingly, it may be valuable to study those geochemical tracers in higher resolution in specific time periods, e.g., during the YD or the Preboreal Oscillation. Fjord sediments usually contain only few or no planktic foraminifera. Thus, further proxies for surface conditions could be examined: Diatoms and dinoflagellates may provide information about surface conditions, including the sea ice distribution (e.g., Bonnet et al., 2010; Koç et al., 2002; Sha et al., 2014; de Vernal et al., 2013), which possibly could complement the biomarker-based surface water reconstructions in the case studies of this thesis.

Source areas of coarse-grained IRD may be assessable when analyzing the mineralogy of the grains (e.g., by x-ray diffraction or microprobes). Those methods were possibly applicable at coarse sand grains and/or at larger dropstones, which were found in the inspected sediment cores. However, the geology of the investigated fjords is very complex (e.g., Dallmann, 1999; Harland, 1998) making the estimation of IRD provenances very difficult. The continuous downcore analysis of IRD based on computer tomography (CT) proved to be a very useful and precise tool providing much more exact data on glacier activity than the commonly used method of counting coarse grains in distinct samples. Thus, the application of CT scans is highly recommended for future investigations of sediment cores from Polar regions.

For the estimation of the palaeoenvironment based on benthic foraminiferal assemblages detailed knowledge about their habitat preferences is required. Although a number of studies investigated modern foraminiferal fjord faunas in (sub-)Arctic environments (e.g., Hald and Korsun, 1997; Hansen and Knudsen, 1995; Jennings and Helgadottir, 1994; Korsun and Hald, 1998, 2000), further work would be valuable, especially regarding the dominant Arctic fjord species *C. neoteretis*, *C. reniforme*, *E. clavatum* and *N. labradorica.* “Living”

(stained) and dead specimens of those species should be sampled in surface sediments during different seasons and compared to CTD data (i.e., temperature and salinity), total organic carbon measurements, stable carbon and oxygen isotopes as well as pH-values of sea water, sedimentation rates and probably also submarine light penetration data. The almost perennial accessibility to some Svalbard fjords fulfils a prerequisite for such studies.

Due to the high number of local palaeoenvironmental studies from the Svalbard area it would be valuable to combine those records applying statistical approaches and assess the palaeoceanographic evolution of this entire region, like it has been done for sea surface temperatures of the (northern) North Atlantic (Hald et al., 2007; Marchal et al., 2002). An extensive compilation of proxy data from the Svalbard area (and beyond) and their implementation into new model setups may be helpful for an approximation to the "bigger picture" of the palaeoceanographic development in the region. Marine archives may further be combined with terrestrial and lacustrine records. The broad spectrum of methodologic approaches and different proxies might complicate such a comparison, but the reconstruction of AW advection (based on various data sets, e.g., biomarkers, trace elements, stable isotopes, benthic or planktic foraminifera assemblages), seems to be a suitable candidate for the first step. Nowadays, AW is a major contributor for heat advection to high northern latitudes, which predominantly controls (winter) sea ice coverage. Compiling numerous proxy data from the Svalbard area may be extended beyond the regional framework and be compared with data from the entire North Atlantic and/or the Arctic Ocean. Such a broader overview might elucidate the importance of the Arctic Amplification throughout the past ~15,000 years adding more detailed and continuous data of this time period to previously modelled time slices of the last three million years (see Miller et al., 2010a). Furthermore, rather process orientated than chronological studies are achievable if various local records from a larger area are combined, e.g., focusing on trigger mechanisms for certain climatic events like the Preboreal Oscillation. As this latter cooling event is reflected in many palaeorecords from the Svalbard region, it might act as an example of very rapid climate shifts under (Holocene) climatic optimum conditions.

References

Aagaard, K. and Carmack, E. C.: The role of sea ice and other fresh water in the Arctic circulation, J. Geophys. Res., 94(1), 14,414-485,498, doi:10.1029/JC094iC10p14485, 1989.

Aagaard, K., Foldvik, A. and Hillman, S. R.: The West Spitsbergen Current: Disposition and water mass transformation, J. Geophys. Res., 92(C4), 3778–3784, doi:10.1029/JC092iC04p03778, 1987.

Abram, N. J., McGregor, H. V., Tierney, J. E., Evans, M. N., McKay, N. P., Kaufman, D. S., Thirumalai, K., Martrat, B., Goosse, H., Phipps, S. J., Steig, E. J., Kilbourne, K. H., Saenger, C. P., Zinke, J., Leduc, G., Addison, J. A., Mortyn, P. G., Seidenkrantz, M.-S., Sicre, M.-A., Selvaraj, K., Filipsson, H. L., Neukom, R., Gergis, J., Curran, M. A. J. and Gunten, L. von: Early onset of industrial-era warming across the oceans and continents, Nature, 536(7617), 411–418, doi:10.1038/nature19082, 2016.

Ahrens, M. J., Graf, G. and Altenbach, A. V.: Spatial and temporal distribution patterns of benthic foraminifera in the Northeast Water Polynya, Greenland, J. Mar. Syst., 10, 445–465, 1997.

Alley, R. B.: The Younger Dryas cold interval as viewed from central Greenland, Quat. Sci. Rev., 19(1–5), 213–226, doi:10.1016/S0277-3791(99)00062-1, 2000.

Alley, R. B., Clark, P. U., Huybrechts, P. and Joughin, I.: Ice-Sheet and Sea-Level Changes, Science, 310(5747), 456–460, doi:10.1126/science.1114613, 2005.

Altenbach, A. V., Pflaumann, U., Schiebel, R., Thies, A., Timm, S. and Trauth, M.: Scaling percentages and distributional patterns of benthic Foraminifera with flux rates of organic carbon, J. Foraminifer. Res., 29(3), 173–185 [online] Available from: http://jfr.geoscienceworld.org/content/29/3/173.abstract, 1999.

Alve, E. and Bernhard, J. M.: Vertical migratory response of benthic foraminifera to controlled oxygen concentrations in an experimental mesocosm, Mar. Ecol. Prog. Ser., 116, 137–151, 1995.

André, A., Weiner, A., Quillévéré, F., Aurahs, R., Morard, R., Douady, C. J., de Garidel-Thoron, T., Escarguel, G., de Vargas, C. and Kucera, M.: The cryptic and the apparent reversed: lack of genetic differentiation within the morphologically diverse plexus of the planktonic foraminifer Globigerinoides sacculifer, Paleobiology, 39(1), 21–39, doi:10.1666/0094-8373-39.1.21, 2013.

von Appen, W.-J., Schauer, U., Hattermann, T. and Beszczynska-Möller, A.: Seasonal Cycle of Mesoscale Instability of the West Spitsbergen Current, J. Phys. Oceanogr., 46, 1231–1254, doi:10.1175/JPO-D-15-0184.1, 2016.

Arrigo, K. R. and van Dijken, G. L.: Secular trends in Arctic Ocean net primary production, J. Geophys. Res., 116(C9), 60–70, doi:10.1029/2011JC007151, 2011.

Arrigo, K. R. and van Dijken, G. L.: Continued increases in Arctic Ocean primary production, Prog. Oceanogr., 136, 60–70, doi:10.1016/j.pocean.2015.05.002, 2015.

Austin, W. E. N., Bard, E., Hunt, J. B., Kroon, D. and Peacock, J. D.: The ^{14}C Age of the Icelandic Vedde Ash: Implications for Younger Dryas Marine Reservoir Age Corrections, Radiocarbon, 37(1), 53–62, doi:10.1017/S0033822200014788, 1995.

Austin, W. E. N., Telford, R. J., Ninnemann, U. S., Brown, L., Wilson, L. J., Small, D. P. and Bryant, C. L.: North Atlantic reservoir ages linked to high Younger Dryas atmospheric radiocarbon concentrations, Glob. Planet. Change, 79(3–4), 226–233, doi:10.1016/j.gloplacha.2011.06.011, 2011.

Axford, Y., Losee, S., Briner, J. P., Francis, D. R., Langdon, P. G. and Walker, I. R.: Holocene temperature

history at the western Greenland Ice Sheet margin reconstructed from lake sediments, Quat. Sci. Rev., 59, 87–100, doi:10.1016/j.quascirev.2012.10.024, 2013.

Badding, M. E., Briner, J. P. and Kaufman, D. S.: ^{10}Be ages of late Pleistocene deglaciation and Neoglaciation in the north-central Brooks Range, Arctic Alaska, J. Quat. Sci., 28(1), 95–102, doi:10.1002/jqs.2596, 2013.

Baeten, N. J., Forwick, M., Vogt, C. and Vorren, T. O.: Late Weichselian and Holocene sedimentary environments and glacial activity in Billefjorden, Svalbard, in Fjord Systems and Archives, vol. 344, edited by W. E. N. Austin, M. Forwick, and M. Paetzel, pp. 207–223, Geological Society, London., 2010.

Bakke, J., Lie, Ø., Heegaard, E., Dokken, T., Haug, G. H., Birks, H. H., Dulski, P. and Nilsen, T.: Rapid oceanic and atmospheric changes during the Younger Dryas cold period, Nat. Geosci., 2(3), 202–205, doi:10.1038/ngeo439, 2009.

Balascio, N. L., D'Andrea, W. J., Gjerde, M. and Bakke, J.: Hydroclimate variability of High Arctic Svalbard during the Holocene inferred from hydrogen isotopes of leaf waxes, Quat. Sci. Rev., 1–11, doi:10.1016/j.quascirev.2016.11.036, 2016.

Bard, E., Arnold, M., Mangerud, J., Paterne, M., Labeyrie, L., Duprat, J., Mélières, M.-A., Sønstegaard, E. and Duplessy, J. C.: The North Atlantic atmosphere-sea surface ^{14}C gradient during the Younger Dryas climatic event, Earth Planet. Sci. Lett., 126(4), 275–287, doi:10.1016/0012-821X(94)90112-0, 1994.

Bartels, M., Titschack, J., Fahl, K., Stein, R., Seidenkrantz, M.-S., Hillaire-Marcel, C. and Hebbeln, D.: Atlantic Water advection vs. glacier dynamics in northern Spitsbergen since early deglaciation, Clim. Past, 13(12), 1717–1749, doi:10.5194/cp-13-1717-2017, 2017.

Bartels, M., Titschack, J., Fahl, K., Stein, R. and Hebbeln, D.: Wahlenbergfjord (Svalbard): A glacier-surrounded fjord suitable to reflect regional hydrographic variability during Holocene?, submitted to Boreas.

Bartholomaus, T. C., Larsen, C. F. and O'Neel, S.: Does calving matter? Evidence for significant submarine melt, Earth Planet. Sci. Lett., 380, 21–30, doi:10.1016/j.epsl.2013.08.014, 2013.

Bauch, H. A., Erlenkeuser, H., Spielhagen, R. F., Struck, U., Matthiessen, J., Thiede, J. and Heinemeier, J.: A multiproxy reconstruction of the evolution of deep and surface waters in the subarctic Nordic seas over the last 30,000 yr, Quat. Sci. Rev., 20(4), 659–678, doi:10.1016/S0277-3791(00)00098-6, 2001.

Belt, S. T. and Müller, J.: The Arctic sea ice biomarker IP_{25}: A review of current understanding, recommendations for future research and applications in palaeo sea ice reconstructions, Quat. Sci. Rev., 79, 9–25, doi:10.1016/j.quascirev.2012.12.001, 2013.

Belt, S. T., Massé, G., Rowland, S. J., Poulin, M., Michel, C. and LeBlanc, B.: A novel chemical fossil of palaeo sea ice: IP_{25}, Org. Geochem., 38(1), 16–27, doi:10.1016/j.orggeochem.2006.09.013, 2007.

Berben, S. M. P., Husum, K., Cabedo-Sanz, P. and Belt, S. T.: Holocene sub-centennial evolution of Atlantic water inflow and sea ice distribution in the western Barents Sea, Clim. Past, 10(1), 181–198, doi:10.5194/cp-10-181-2014, 2014.

Berger, A. and Loutre, M. F.: Insolation values for the climate of the last 10 million years, Quat. Sci. Rev., 10(4), 297–317, doi:10.1016/0277-3791(91)90033-Q, 1991.

Berger, W. H.: The younger dryas cold spell—a quest for causes, Palaeogeogr. Palaeoclimatol. Palaeoecol., 89, 219–237, doi:10.1016/0921-8181(90)90018-8, 1990.

Berger, W. H., Bonneau, M.-C. and Parker, F. L.: Foraminifera on the deep-sea floor: lysocline and dissolution rate, Oceanol. Acta, 5(2), 249–258, 1982.

Bernhard, J. M. and Bowser, S. S.: Benthic foraminifera of dysoxic sediments: chloroplast sequestration and functional morphology, Earth-Science Rev., 46(1–4), 149–165, doi:10.1016/S0012-8252(99)00017-3, 1999.

Beszczynska-Möller, A., Woodgate, R., Lee, C., Melling, H. and Karcher, M.: A Synthesis of Exchanges Through the Main Oceanic Gateways to the Arctic Ocean, Oceanography, 24(3), 82–99, doi:10.5670/oceanog.2011.59, 2011.

Beszczynska-Möller, A., Fahrbach, E., Schauer, U. and Hansen, E.: Variability in Atlantic water temperature and transport at the entrance to the Arctic Ocean, 1997–2010, ICES J. Mar. Sci., 69(5), 852–863, doi:10.1093/icesjms/fss056, 2012.

van der Bilt, W. G. M., Bakke, J., Vasskog, K., D'Andrea, W. J., Bradley, R. S. and Ólafsdóttir, S.: Reconstruction of glacier variability from lake sediments reveals dynamic Holocene climate in Svalbard, Quat. Sci. Rev., 126, 201–218, doi:10.1016/j.quascirev.2015.09.003, 2015.

van der Bilt, W. G. M., D'Andrea, W. J., Bakke, J., Balascio, N. L., Werner, J. P., Gjerde, M. and Bradley, R. S.: Alkenone-based reconstructions reveal four-phase Holocene temperature evolution for High Arctic Svalbard, Quat. Sci. Rev., in press, doi:10.1016/j.quascirev.2016.10.006, 2016.

van der Bilt, W. G. M., Lane, C. S. and Bakke, J.: Ultra-distal Kamchatkan ash on Arctic Svalbard: Towards hemispheric cryptotephra correlation, Quat. Sci. Rev., 1–6, doi:10.1016/j.quascirev.2017.04.007, 2017.

Birgel, D. and Stein, R.: Northern Fram Strait and Yermak Plateau: distribution, variability and burial of organic carbon and paleoenvironmental implications, in The Organic Carbon Cycle in the Arctic Ocean, edited by R. Stein and R. W. Macdonald, pp. 279–294, Springer, Berlin., 2004.

Björck, S., Kromer, B., Johnsen, S., Bennike, O., Hammarlund, D., Lemdahl, G., Possnert, G., Rasmussen, T. L., Wohlfarth, B., Hammer, C. U. and Spurk, M.: Synchronized Terrestrial-Atmospheric Deglacial Records Around the North Atlantic, Science, 274(5290), 1155–1160, doi:10.1126/science.274.5290.1155, 1996.

Björck, S., Rundgren, M., Ingólfsson, Ó. and Funder, S.: The Preboreal oscillation around the Nordic Seas: terrestrial and lacustrine responses, J. Quat. Sci., 12(6), 455–465, doi:10.1002/(SICI)1099-1417(199711/12)12:6<455::AID-JQS316>3.0.CO;2-S, 1997.

Björck, S., Bennike, O., Rosén, P., Andresen, C. S., Bohncke, S., Kaas, E. and Conley, D.: Anomalously mild Younger Dryas summer conditions in southern Greenland, Geology, 30(5), 427–430, doi:10.1130/0091-7613(2002)030<0427:AMYDSC>2.0.CO;2, 2002.

Björck, S., Koç, N. and Skog, G.: Consistently large marine reservoir ages in the Norwegian Sea during the Last Deglaciation, Quat. Sci. Rev., 22(5–7), 429–435, doi:10.1016/S0277-3791(03)00002-7, 2003.

Blaauw, M. and Christen, J. A.: Flexible Paleoclimate Age-Depth Models Using an Autoregressive Gamma Process, Bayesian Anal., 6(3), 457–474, doi:10.1214/11-BA618, 2011.

Blake, W.: Occurrence of the *Mytilus edulis* complex on Nordaustlandet, Svalbard: radiocarbon ages and

climatic implications, Polar Res., 25(2), 123–137, doi:10.1111/j.1751-8369.2006.tb00028.x, 2006.

Błaszczyk, M., Jania, J. A. and Hagen, J. O.: Tidewater glaciers of Svalbard: Recent changes and estimates of calving fluxes, Polish Polar Res., 30(2), 85–142, 2009.

Boersma, A.: Foraminifera, in Introduction to Marine Micropaleontology, edited by B. U. Haq and A. Boersma., 1998.

Bond, G., Showers, W., Cheseby, M., Lotti, R., Almasi, P., DeMenocal, P., Priore, P., Cullen, H., Hajdas, I. and Bonani, G.: A Pervasive Millennial-Scale Cycle in North Atlantic Holocene and Glacial Climates, Science, 278(5341), 1257–1266, doi:10.1126/science.278.5341.1257, 1997.

Bondevik, S., Mangerud, J., Birks, H. H., Gulliksen, S. and Reimer, P. J.: Changes in North Atlantic Radiocarbon Reservoir Ages During the Allerød and Younger Dryas, Science, 312(5779), 1514–1517, doi:10.1126/science.1123300, 2006.

Bonnet, S., de Vernal, A., Hillaire-Marcel, C., Radi, T. and Husum, K.: Variability of sea-surface temperature and sea-ice cover in the Fram Strait over the last two millennia, Mar. Micropaleontol., 74(3–4), 59–74, doi:10.1016/j.marmicro.2009.12.001, 2010.

Bornhold, B. D., Jay, C. V., McConnaughey, R., Rathwell, G., Rhynas, K. and Collins, W.: Walrus foraging marks on the seafloor in Bristol Bay, Alaska: A reconnaissance survey, Geo-Marine Lett., 25(5), 293–299, doi:10.1007/s00367-004-0205-y, 2005.

Boulton, G.: Glacial history of the Spitsbergen archipelago and the problem of a Barents Shelf ice sheet, Boreas, 8, 31–57, doi:10.1111/j.1502-3885.1979.tb00429.x, 1979.

Bradley, R. S. and England, J. H.: The Younger Dryas and the Sea of Ancient Ice, Quat. Res., 70(1), 1–10, doi:10.1016/j.yqres.2008.03.002, 2008.

Brassell, S. C., Eglinton, G., Marlowe, I. T., Pflaumann, U. and Sarnthein, M.: Molecular stratigraphy: a new tool for climatic assessment, Nature, 320(6058), 129–133, doi:10.1038/320129a0, 1986.

Braun, M., Pohjola, V. A., Pettersson, R., Möller, M., Finkelnburg, R., Falk, U., Scherer, D. and Schneider, C.: Changes of glacier frontal positions of Vestfonna (Nordaustlandet, Svalbard), Geogr. Ann. Ser. A, Phys. Geogr., 93(4), 301–310, doi:10.1111/j.1468-0459.2011.00437.x, 2011.

Broecker, W. S.: Was the Younger Dryas triggered by a flood?, Science, 312(5777), 1146–1148, doi:10.1126/science.1123253, 2006.

Broecker, W. S., Kennett, J. P., Flower, B. P., Teller, J. T., Trumbore, S., Bonani, G. and Wolfli, W.: Routing of meltwater from the Laurentide Ice Sheet during the Younger Dryas cold episode, Nature, 341, 318–321, doi:10.1038/341318a0, 1989.

Bromley, G. R., Putnam, A. E., Rademaker, K. M., Lowell, T. V, Schaefer, J. M., Hall, B., Winckler, G., Birkel, S. D. and Borns, H. W.: Younger Dryas deglaciation of Scotland driven by warming summers, Proc. Natl. Acad. Sci. USA, 111(17), 6215–6219, doi:10.1073/pnas.1321122111, 2014.

Brückner, H. and Schellmann, G.: Late Pleistocene and Holocene Shorelines of Andréeland, Spitsbergen (Svalbard) - Geomorphological Evidence and Palaeo-Oceanographic Significance, J. Coast. Res., 19(4), 971–982 [online] Available from: http://www.jstor.org/stable/4299241, 2003.

Cabedo-Sanz, P., Belt, S. T., Knies, J. and Husum, K.: Identification of contrasting seasonal sea ice conditions during the Younger Dryas, Quat. Sci. Rev., 79, 74–86, doi:10.1016/j.quascirev.2012.10.028, 2013.

Calleja, M. L., Kerherv, P., Bourgeois, S., Kędra, M., Leynaert, A., Devred, E., Babin, M. and Morata, N.:

Effects of increase glacier discharge on phytoplankton bloom dynamics and pelagic geochemistry in a high Arctic fjord, Prog. Oceanogr., 159, 195–210, doi:10.1016/j.pocean.2017.07.005, 2017.

Carbonara, K., Mezgec, K., Varagona, G., Musco, M. E., Lucchi, R. G., Villa, G., Morigi, C., Melis, R. and Caffau, M.: Palaeoclimatic changes in Kveithola, Svalbard, during the Late Pleistocene deglaciation and Holocene: Evidences from microfossil and sedimentary records, Palaeogeogr. Palaeoclimatol. Palaeoecol., 463, 136–149, doi:10.1016/j.palaeo.2016.10.003, 2016.

Carmack, E. and Wassmann, P.: Food webs and physical-biological coupling on pan-Arctic shelves: Unifying concepts and comprehensive perspectives, Prog. Oceanogr., 71(2–4), 446–477, doi:10.1016/j.pocean.2006.10.004, 2006.

Cedhagen, T.: Retention of chloroplasts and bathymetric distribution in the Sublittoral Foraminiferan *Nonionellina Labradorica*, Ophelia, 33(1), 17–30, doi:10.1080/00785326.1991.10429739, 1991.

Chauhan, T., Rasmussen, T. L., Noormets, R., Jakobsson, M. and Hogan, K. A.: Glacial history and paleoceanography of the southern Yermak Plateau since 132 ka BP, Quat. Sci. Rev., 92, 155–169, doi:10.1016/j.quascirev.2013.10.023, 2014.

Chauhan, T., Rasmussen, T. L. and Noormets, R.: Palaeoceanography of the Barents Sea continental margin, north of Nordaustlandet, Svalbard, during the last 74 ka, Boreas, 45(1), 76–99, doi:10.1111/bor.12135, 2015.

Christianson, K., Bushuk, M., Dutrieux, P., Parizek, B. R., Joughin, I. R., Alley, R. B., Shean, D. E., Abrahamsen, E. P., Anandakrishnan, S., Heywood, K. J., Kim, T., Lee, S. H., Nicholls, K., Stanton, T., Truffer, M., Webber, B. G. M., Jenkins, A., Jacobs, S., Bindschadler, R. and Holland, D. M.: Sensitivity of Pine Island Glacier to observed ocean forcing, Geophys. Res. Lett., 43(20), 10,817-10,825, doi:10.1002/2016GL070500, 2016.

Cohen, J.: An observational analysis: Tropical relative to Arctic influence on midlatitude weather in the era of Arctic amplification, Geophys. Res. Lett., 43(10), 5287–5294, doi:10.1002/2016GL069102, 2016.

Cohen, J., Screen, J. A., Furtado, J. C., Barlow, M., Whittleston, D., Coumou, D., Francis, J., Dethloff, K., Entekhabi, D., Overland, J. and Jones, J.: Recent Arctic amplification and extreme mid-latitude weather, Nat. Geosci., 7(August), 627–637, doi:10.1038/ngeo2234, 2014a.

Cohen, J., Screen, J. A., Furtado, J. C., Barlow, M., Whittleston, D., Coumou, D., Francis, J., Dethloff, K., Entekhabi, D., Overland, J. and Jones, J.: Recent Arctic amplification and extreme mid-latitude weather, Nat. Geosci., 7(9), 627–637, doi:10.1038/ngeo2234, 2014b.

Consolaro, C., Rasmussen, T. L., Panieri, G., Mienert, J., Bünz, S. and Sztybor, K.: Carbon isotope ($\delta^{13}C$) excursions suggest times of major methane release during the last 14 kyr in Fram Strait, the deep-water gateway to the Arctic, Clim. Past, 11(4), 669–685, doi:10.5194/cp-11-669-2015, 2015.

Cook, A. J., Holland, P. R., Meredith, M. P., Murray, T., Luckman, A. and Vaughan, D. G.: Ocean forcing of glacier retreat in the western Antarctic Peninsula, Science, 353(6296), 283–286, doi:10.1126/science.aae0017, 2016.

Cottier, F., Tverberg, V., Inall, M., Svendsen, H., Nilsen, F. and Griffiths, C.: Water mass modification in an Arctic fjord through cross-shelf exchange: The seasonal hydrography of Kongsfjorden, Svalbard, J. Geophys. Res., 110(C12), C12005, doi:10.1029/2004JC002757, 2005.

Cottier, F. R., Nilsen, F., Inall, M. E., Gerland, S., Tverberg, V. and Svendsen, H.: Wintertime warming of an Arctic shelf in response to large-scale atmospheric circulation, Geophys. Res. Lett., 34(10), L10607, doi:10.1029/2007GL029948, 2007.

Cottier, F. R., Nilsen, F., Skogseth, R., Tverberg, V., Skarðhamar, J. and Svendsen, H.: Arctic fjords: a review of the oceanographic environment and dominant physical processes, in Fjord Systems and Archives, vol. 344, edited by J. A. Howe, W. E. N. Austin, M. Forwick, and M. Paetzel, pp. 35–50, Geological Society, London., 2010.

Cowan, E. A. and Powell, R. D.: Suspended sediment transport and deposition of cyclically interlaminated sediment in a temperate glacial fjord, Alaska, U.S.S, Glacimarine Enviornments Process. Sediments. Geol. Soc. Spec. Publ., 53(November 2008), 1689–1699, doi:10.1017/CBO9781107415324.004, 1990.

Cowan, E. A., Cai, J., Powell, R. D., Clark, J. D. and Pitcher, J. N.: Temperate Glacimarine Varves: An Example from Disenchantment Bay, Southern Alaska Ellen, J. Sediment. Res., 67(3), 536–549, 1997.

D'Andrea, W. J. and Huang, Y.: Long chain alkenones in Greenland lake sediments: Low $\delta^{13}C$ values and exceptional abundance, Org. Geochem., 36(9), 1234–1241, doi:10.1016/j.orggeochem.2005.05.001, 2005.

D'Andrea, W. J., Lage, M., Martiny, J. B. H., Laatsch, A. D., Amaral-Zettler, L. A., Sogin, M. L. and Huang, Y.: Alkenone producers inferred from well-preserved 18S rDNA in Greenland lake sediments, J. Geophys. Res. Biogeosciences, 111(3), 1–8, doi:10.1029/2005JG000121, 2006.

D'Andrea, W. J., Huang, Y., Fritz, S. C. and Anderson, N. J.: Abrupt Holocene climate change as an important factor for human migration in West Greenland, Proc. Natl. Acad. Sci., 108(24), 9765–9769, doi:10.1073/pnas.1101708108, 2011.

D'Andrea, W. J., Vaillencourt, D. A., Balascio, N. L., Werner, A., Roof, S. R., Retelle, M. and Bradley, R. S.: Mild Little Ice Age and unprecedented recent warmth in an 1800 year lake sediment record from Svalbard, Geology, 40(11), 1007–1010, doi:10.1130/G33365.1, 2012.

Dallmann, W.: Lithostratigraphic Lexicon of Svalbard, Norsk Polarinstitutt, Tromsø., 1999.

Darby, D. A., Ortiz, J. D., Grosch, C. E. and Lund, S. P.: 1,500-year cycle in the Arctic Oscillation identified in Holocene Arctic sea-ice drift, Nat. Geosci., 5(12), 897–900, doi:10.1038/ngeo1629, 2012.

Darling, K. F., Schweizer, M., Knudsen, K. L., Evans, K. M., Bird, C., Roberts, A., Filipsson, H. L., Kim, J.-H., Gudmundsson, G., Wade, C. M., Sayer, M. D. J. and Austin, W. E. N.: The genetic diversity, phylogeography and morphology of Elphidiidae (Foraminifera) in the Northeast Atlantic, Mar. Micropaleontol., 129, 1–23, doi:10.1016/j.marmicro.2016.09.001, 2016.

Davis, J. C.: Statistics and Data Analysis in Geology, 3rd ed., Wiley, New York., 2003.

Delworth, T. and Dixon, K.: Implications of the recent trend in the Arctic/North Atlantic oscillation for the North Atlantic thermohaline circulation, J. Clim., 13(21), 3721–3727, doi:10.1175/1520-0442(2000)013<3721:IOTRTI>2.0.CO;2, 2000.

Deser, C.: On the teleconnectivity of the "Arctic Oscillation" Geophys. Res. Lett., 27(6), 779–782, doi:10.1029/1999GL010945, 2000.

Dowdeswell, J. A., Elverhøi, A. and Spielhagen, R.: Glacimarine sedimentary processes and facies on the

Polar North Atlantic margins, Quat. Sci. Rev., 17(1–3), 243–272, doi:10.1016/S0277-3791(97)00071-1, 1998.

Dowdeswell, J. A., Whittington, R. J., Jennings, A. E., Andrews, J. T., Mackensen, A. and Marienfeld, P.: An origin for laminated glacimarine sediments through sea-ice build-up and suppressed iceberg rafting, Sedimentology, 47(3), 557–576, doi:10.1046/j.1365-3091.2000.00306.x, 2000.

Dowdeswell, J. A., Hogan, K. A., Evans, J., Noormets, R., Cofaigh, C. O. and Ottesen, D.: Past ice-sheet flow east of Svalbard inferred from streamlined subglacial landforms, Geology, 38(2), 163–166, doi:10.1130/G30621.1, 2010.

Dubicka, Z., Złotnik, M. and Borszcz, T.: Test morphology as a function of behavioral strategies — Inferences from benthic foraminifera, Mar. Micropaleontol., 116, 38–49, doi:10.1016/j.marmicro.2015.01.003, 2015.

Duplessy, J. C., Ivanova, E., Murdmaa, I., Paterne, M. and Labeyrie, L.: Holocene paleoceanography of the northern Barents Sea and variations of the northward heat transport by the Atlantic Ocean, Boreas, 30(1), 1–16, doi:10.1111/j.1502-3885.2001.tb00984.x, 2001.

Duplessy, J. C., Cortijo, E., Ivanova, E., Khusid, T., Labeyrie, L., Levitan, M., Murdmaa, I. and Paterne, M.: Paleoceanography of the Barents Sea during the Holocene, Paleoceanography, 20(4), PA4004, doi:10.1029/2004PA001116, 2005.

Dylmer, C. V., Giraudeau, J., Eynaud, F., Husum, K. and de Vernal, A.: Northward advection of Atlantic water in the eastern Nordic Seas over the last 3000 yr, Clim. Past, 9(4), 1505–1518, doi:10.5194/cp-9-1505-2013, 2013.

Eglinton, T. I. and Eglinton, G.: Molecular proxies for paleoclimatology, Earth Planet. Sci. Lett., 275(1–2), 1–16, doi:10.1016/j.epsl.2008.07.012, 2008.

Ehrmann, W. and Thiede, J.: History of Mezozoic and Cenozoic sediment fluxes to the North Atlantic Ocean, Contrib. to Sedimentol., 15, 1–109, 1985.

Eiríksson, J., Larsen, G., Knudsen, K. L., Heinemeier, J. and Símonarson, L. A.: Marine reservoir age variability and water mass distribution in the Iceland Sea, Quat. Sci. Rev., 23(20–22 SPEC. ISS.), 2247–2268, doi:10.1016/j.quascirev.2004.08.002, 2004.

Elverhøi, A., Andersen, E. S., Dokken, T., Hebbeln, D., Spielhagen, R. F., Svendsen, J. I., Sorflaten, M., Rornes, A., Hald, M. and Forsberg, C. F.: The Growth and Decay of the Late Weichselian Ice Sheet in Westrn Svalbard and Adjacent Areas Based on Provence Studies of Marine Sediments, Quat. Res., 303–316, 1995.

Elverhøi, A., Dowdeswell, J. A., Funder, S., Mangerud, J. and Stein, R.: Glacial and oceanic history of the polar north atlantic margins: An overview, Quat. Sci. Rev., 17(1–3), 1–10, doi:10.1016/S0277-3791(97)00073-5, 1998.

Emiliani, C.: Pleistocene Temperatures, J. Geol., 63(6), 538–578, 1955.

Epstein, S., Buchsbaum, R., Lowenstam, H. A. and Urey, H. C.: Revised Carbonate-Water Isotopic Temperature Scale, Geol. Soc. Am. Bull., 64, 1315–1325, doi:10.1130/0016-7606(1953)64, 1953.

Ezat, M. M., Rasmussen, T. L. and Groeneveld, J.: Persistent intermediate water warming during cold stadials in the southeastern Nordic seas during the past 65 k.y., Geology, 42(8), 663–666, doi:10.1130/G35579.1, 2014.

Fahl, K. and Stein, R.: Biomarkers as organic-carbon-source and environmental indicators in the late quaternary Arctic Ocean: Problems and perspectives, Mar. Chem., 63(3–4), 293–309, doi:10.1016/S0304-4203(98)00068-1, 1999.

Fahl, K. and Stein, R.: Modern seasonal variability and deglacial/Holocene change of central Arctic Ocean sea-ice cover: New insights from biomarker proxy records, Earth Planet. Sci. Lett., 351–352, 123–133, doi:10.1016/j.epsl.2012.07.009, 2012.

Fahrbach, E., Meincke, J., Østerhus, S., Rohardt, G., Schauer, U., Tverberg, V. and Verduin, J.: Direct measurements of volume transports through Fram Strait, Polar Res., 20(2), 217–224, 2001.

Falk-Petersen, S., Pavlov, V., Berge, J., Cottier, F., Kovacs, K. M. and Lydersen, C.: At the rainbow's end: high productivity fueled by winter upwelling along an Arctic shelf, Polar Biol., 38(1), 5–11, doi:10.1007/s00300-014-1482-1, 2015.

Fiedel, S. J.: The mysterious onset of the Younger Dryas, Quat. Int., 242(2), 262–266, doi:10.1016/j.quaint.2011.02.044, 2011.

Filippova, A., Kienast, M., Frank, M. and Schneider, R. R.: Alkenone paleothermometry in the North Atlantic: A review and synthesis of surface sediment data and calibrations, Geochemistry, Geophys. Geosystems, 17, 1370–1382, doi:10.1002/2015GC006106, 2016.

Firestone, R. B., West, A., Kennett, J. P., Becker, L., Bunch, T. E., Revay, Z. S., Schultz, P. H., Belgya, T., Kennett, D. J., Erlandson, J. M., Dickenson, O. J., Goodyear, A. C., Harris, R. S., Howard, G. A., Kloosterman, J. B., Lechler, P., Mayewski, P. A., Montgomery, J., Poreda, R., Darrah, T., Hee, S. S. Q., Smith, A. R., Stich, A., Topping, W., Wittke, J. H. and Wolbach, W. S.: Evidence for an extraterrestrial impact 12,900 years ago that contributed to the megafaunal extinctions and the Younger Dryas cooling., Proc. Natl. Acad. Sci. U. S. A., 104(41), 16016–16021, doi:10.1073/pnas.0706977104, 2007.

Fisher, T. G., Smith, D. G. and Andrews, J. T.: Preboreal oscillation caused by a glacial Lake Agassiz flood, Quat. Sci. Rev., 21(8–9), 873–878, doi:10.1016/S0277-3791(01)00148-2, 2002.

Flink, A. E., Noormets, R., Fransner, O., Hogan, K. A., Regan, M., Jakobsson, M., O´Regan, M. and Jakobsson, M.: Past ice flow in Wahlenbergfjorden and its implications for late Quaternary ice sheet dynamics in northeastern Svalbard, Quat. Sci. Rev., 163, 162–179, doi:10.1016/j.quascirev.2017.03.021, 2017.

Flood, B., Gee, D. G., Hjelle, A., Siggerud, T. and Winsnes, T. S.: Skrifter Nr. 146 - The geology of Nordaustlandet, northern and central parts, Norsk Polarinstitutt, Oslo., 1969.

Fontanier, C., Jorissen, F. J., Lansard, B., Mouret, A., Buscail, R., Schmidt, S., Kerhervé, P., Buron, F., Zaragosi, S., Hunault, G., Ernoult, E., Artero, C., Anschutz, P. and Rabouille, C.: Live foraminifera from the open slope between Grand Rhône and Petit Rhône Canyons (Gulf of Lions, NW Mediterranean), Deep Sea Res. Part I Oceanogr. Res. Pap., 55(11), 1532–1553, doi:10.1016/j.dsr.2008.07.003, 2008.

Forman, S. L.: Post-glacial relative sea-level history of northwestern Spitsbergen , Svalbard, Geol. Soc. Am. Bull., 102(November), 1580–1590, 1990.

Forman, S. L., Lubinski, D. J., Ingólfsson, Ó., Zeeberg, J. J., Snyder, J. A., Siegert, M. J. and Matishov, G. G.: A review of postglacial emergence on Svalbard, Franz Josef Land and Novaya Zemlya, northern

Eurasia, Quat. Sci. Rev., 23(11–13), 1391–1434, doi:10.1016/j.quascirev.2003.12.007, 2004.

Forwick, M.: Sedimentary processes and palaeoenvironments in Spitsbergen fjords, University of Tromsø, 2005.

Forwick, M. and Vorren, T. O.: Late Weichselian and Holocene sedimentary environments and ice rafting in Isfjorden, Spitsbergen, Palaeogeogr. Palaeoclimatol. Palaeoecol., 280(1–2), 258–274, doi:10.1016/j.palaeo.2009.06.026, 2009.

Forwick, M. and Vorren, T. O.: Stratigraphy and deglaciation of the Isfjorden area, Spitsbergen, Nor. Geol. Tidsskr., 90(4), 163–179, 2010.

Forwick, M., Vorren, T. O., Hald, M., Korsun, S., Roh, Y., Vogt, C. and Yoo, K.-C.: Spatial and temporal influence of glaciers and rivers on the sedimentary environment in Sassenfjorden and Tempelfjorden, Spitsbergen, in Fjord Systems and Archives, vol. 344, edited by J. A. Howe, W. E. N. Austin, M. Forwick, and M. Paetzel, pp. 163–193, Geological Society, London., 2010.

Fransner, O., Noormets, R., Flink, A. E., Hogan, K. A. and Jakobsson, M.: Glacial landforms and their implications for glacier dynamics in Rijpfjorden and Duvefjorden, northern Nordaustlandet, Svalbard, J. Quat. Sci., 32(3), 437–455, doi:10.1002/jqs.2938, 2017.

Furrer, G., Stapfer, A. and Glaser, U.: Zur nacheiszeitlichen Gletschergeschichte des Liefdefjords (Spitzbergen) (Ergebnisse der Geowissenschaftlichen Spitzbergenexpedition 1990), Geogr. Helv., 46(4), 147–155, doi:10.5194/gh-46-147-1991, 1991.

van Geel, B., Raspopov, O. M., Renssen, H., van der Plicht, J., Dergachev, V. A. and Meijer, H. A. J.: The role of solar forcing upon climate change, Quat. Sci. Rev., 18(3), 331–338, doi:10.1016/S0277-3791(98)00088-2, 1999.

van Geel, B., Heusser, C. J., Renssen, H. and Schuurmans, C. J. E.: Climatic change in Chile at around 2700 BP and global evidence for solar forcing: a hypothesis, The Holocene, 10(5), 659–664, doi:10.1191/09596830094908, 2000.

Gjermundsen, E. F., Briner, J. P., Akçar, N., Salvigsen, O., Kubik, P., Gantert, N. and Hormes, A.: Late Weichselian local ice dome configuration and chronology in Northwestern Svalbard: early thinning, late retreat, Quat. Sci. Rev., 72, 112–127, doi:10.1016/j.quascirev.2013.04.006, 2013.

Gjermundsen, E. F., Briner, J. P., Akçar, N., Foros, J., Kubik, P. W., Salvigsen, O. and Hormes, A.: Minimal erosion of Arctic alpine topography during late Quaternary glaciation, Nat. Geosci., 8(10), 789–792, doi:10.1038/ngeo2524, 2015.

Gregory, J. M. and Huybrechts, P.: Ice-sheet contributions to future sea-level change, Philos. Trans. R. Soc. A Math. Phys. Eng. Sci., 364(1844), 1709–1732, doi:10.1098/rsta.2006.1796, 2006.

Gregory, J. M., Huybrechts, P. and Raper, S. C. B.: Threatened loss of the Greenland ice-sheet, Nature, 428(April), 2513–2513, doi:10.1038/nature02512, 2004.

Groot, D. E., Aagaard-Sørensen, S. and Husum, K.: Reconstruction of Atlantic water variability during the Holocene in the western Barents Sea, Clim. Past, 10(1), 51–62, doi:10.5194/cp-10-51-2014, 2014.

Grossman, E. L.: Stable isotopes in modern benthic foraminifera; a study of vital effect, J. Foraminifer. Res., 17(1), 48–61, doi:10.2113/gsjfr.17.1.48, 1987.

Gump, D. J., Briner, J. P., Mangerud, J. and Svendsen, J. I.: Deglaciation of Boknafjorden, south-western Norway, J. Quat. Sci., 32(1), 80–90, doi:10.1002/jqs.2925, 2017.

Sen Gupta, B. K.: Introduction to modern foraminifera, in Modern Foraminifera, edited by B. K. Sen Gupta, pp. 3–6, Kluver Academic Publishers, New York., 2003.

Hagen, J. O., Listøl, O., Roland, E. and Jørgensen, T.: Glacier Atlas of Svalbard and Jan Mayen, edited by A. Brekke, Norsk Polarinstitutt, Oslo., 1993.

Haine, T. W. N., Curry, B., Gerdes, R., Hansen, E., Karcher, M., Lee, C., Rudels, B., Spreen, G., Steur, L. De, Stewart, K. D. and Woodgate, R.: Arctic freshwater export: Status, mechanisms, and prospects, Glob. Planet. Change, 125, 13–35, doi:10.1016/j.gloplacha.2014.11.013, 2015.

Hald, M. and Hagen, S.: Early Preboreal cooling in the Nordic seas region triggered by meltwater, Geology, 26(7), 615–618, doi:10.1130/0091-7613(1998)026<0615:EPCITN>2.3.CO, 1998.

Hald, M. and Korsun, S.: Distribution of modern benthic foraminifera from fjords of Svalbard, European Arctic, J. Foraminifer. Res., 27(2), 101–122, doi:10.2113/gsjfr.27.2.101, 1997.

Hald, M. and Steinsund, P. I.: Benthic foraminifera and carbonate dissolution in the surface sediments of the Barents and Kara Sea, in Surface Sediment Composition and Sedimentary Processes in the Central Arctic and along the Eurasian Continental Margin, edited by R. Stein, G. I. Ivanov, M. A. Levitan, and K. Fahl, pp. 285–307, Bremerhaven., 1996.

Hald, M., Steinsund, P. I., Dokken, T., Korsun, S., Polyak, L. and Aspeli, R.: Recent and Late Quaternary distribution of *Elphidium excavatum* f. *clavatum* in Arctic Seas, in Late Cenozoic benthic foraminifera: Taxonomy, Ecology and Stratigraphy, vol. 32, edited by H. P. Sejrup and K. L. Knudsen, pp. 141–153, Cushman Foundation for Foraminiferal Research., 1994.

Hald, M., Ebbesen, H., Forwick, M., Godtliebsen, F., Khomenko, L., Korsun, S., Ringstad Olsen, L. and Vorren, T. O.: Holocene paleoceanography and glacial history of the West Spitsbergen area, Euro-Arctic margin, Quat. Sci. Rev., 23(20–22), 2075–2088, doi:10.1016/j.quascirev.2004.08.006, 2004.

Hald, M., Andersson, C., Ebbesen, H., Jansen, E., Klitgaard-Kristensen, D., Risebrobakken, B., Salomonsen, G. R., Sarnthein, M., Sejrup, H. P. and Telford, R. J.: Variations in temperature and extent of Atlantic Water in the northern North Atlantic during the Holocene, Quat. Sci. Rev., 26(25–28), 3423–3440, doi:10.1016/j.quascirev.2007.10.005, 2007.

Hall, B., Baroni, C., Denton, G., Kelly, M. A. and Lowell, T.: Relative sea-level change, Kjove Land, Scoresby Sund, East Greenland: implications for seasonality in Younger Dryas time, Quat. Sci. Rev., 27(25–26), 2283–2291, doi:10.1016/j.quascirev.2008.08.001, 2008.

Hammer, Ø., Harper, D. A. T. and Ryan, P. D.: PAST: Paleontological statistics software package for education and data analysis, Palaeontol. Electron., 4(1), 1–9, 2001.

Hansen, A. and Knudsen, K. L.: Recent foraminiferal distribution in Freemansundet and early Holocene stratigraphy on Edgeoya, Svalbard, Polar Res., 14(2), 215–238, doi:10.1111/j.1751-8369.1995.tb00690.x, 1995.

Hansen, H. J.: Shell construction in modern calcareous Foraminifera, in Modern Foraminifera, edited by B. K. Sen Gupta, pp. 57–70, Kluver Academic Publishers, New York., 2003.

Hansen, J., Hanken, N. M., Nielsen, J. K., Nielsen, J. K. and Thomsen, E.: Late Pleistocene and Holocene distribution of *Mytilus edulis* in the Barents Sea region and its palaeoclimatic implications, J. Biogeogr., 38(6), 1197–1212, doi:10.1111/j.1365-2699.2010.02473.x, 2011.

Hanslik, D., Jakobsson, M., Backman, J., Björck, S., Sellén, E., O'Regan, M., Fornaciari, E. and Skog, G.:

Quaternary Arctic Ocean sea ice variations and radiocarbon reservoir age corrections, Quat. Sci. Rev., 29(25–26), 3430–3441, doi:10.1016/j.quascirev.2010.06.011, 2010.

Harland, W. B.: The Geology of Svalbard, Memoir 17., Geological Society, London., 1998.

Harland, W. B., Wallis, R. H. and Gayer, R. A.: A Revision of the Lower Hecla Hoek Succession in Central North Spitsbergen and Correlation Elsewhere, Geol. Mag., 103(1), 70–97, doi:10.1017/S0016756800050433, 1966.

Hass, H. C.: A method to reduce the influence of ice-rafted debris on a grain size record from northern Fram Strait, Arctic Ocean, Polar Res., 21(2), 299–306 [online] Available from: http://www.polarresearch.net/index.php/polar/article/view/6491, 2002.

Hattermann, T., Isachsen, P. E., von Appen, W.-J. J., Albretsen, J. and Sundfjord, A.: Eddy-driven recirculation of Atlantic Water in Fram Strait, Geophys. Res. Lett., 43, 3406–3414, doi:10.1002/2016GL068323, 2016.

Hebbeln, D.: Flux of ice-rafted detritus from sea ice in the Fram Strait, Deep Sea Res. Part II Top. Stud. Oceanogr., 47(9–11), 1773–1790, doi:10.1016/S0967-0645(00)00006-0, 2000.

Hebbeln, D. and Wefer, G.: Effects of ice coverage and ice-rafted material on sedimentation in the Fram Strait, Nature, 350, 409–411, doi:10.1038/350409a0, 1991.

Hebbeln, D., Dokken, T., Andersen, E. S., Hald, M. and Elverhøi, A.: Moisture supply for northern ice-sheet growth during the Last Glacial Maximum, Nature, 370(6488), 357–360, doi:10.1038/370357a0, 1994.

Hebbeln, D., Henrich, R. and Baumann, K.-H.: Paleoceanography of the Last Interglacial/Glacial Cycle in the Polar North Atlantic, Quat. Sci. Rev., 17(1–3), 125–153, doi:10.1016/S0277-3791(97)00067-X, 1998.

Heinemann, G. and Klein, T.: Modelling and observations of the katabatic flow dynamics over Greenland, Tellus A, 54(5), 542–554, doi:10.1034/j.1600-0870.2002.201401.x, 2002.

Heinrich, H.: Origin and Consequences of Cyclic Ice Rafting in the Northeast Atlantic Ocean During the Past 130,000 Years, Quat. Res., 29(2), 142–152, doi:10.1016/0033-5894(88)90057-9, 1988.

Henriksen, M., Alexanderson, H., Landvik, J. Y., Linge, H. and Peterson, G.: Dynamics and retreat of the Late Weichselian Kongsfjorden ice stream, NW Svalbard, Quat. Sci. Rev., 92, 235–245, doi:10.1016/j.quascirev.2013.10.035, 2014.

Hillaire-Marcel, C., de Vernal, A., Polyak, L. and Darby, D.: Size-dependent isotopic composition of planktic foraminifers from Chukchi Sea vs. NW Atlantic sediments—implications for the Holocene paleoceanography of the western Arctic, Quat. Sci. Rev., 23(3–4), 245–260, doi:10.1016/j.quascirev.2003.08.006, 2004.

van Hoesel, A., Hoek, W. Z., Pennock, G. M. and Drury, M. R.: The Younger Dryas impact hypothesis: a critical review, Quat. Sci. Rev., 83, 95–114, doi:10.1016/j.quascirev.2013.10.033, 2014.

Hogan, K. A., Dowdeswell, J. A., Noormets, R., Evans, J. and Ó Cofaigh, C.: Evidence for full-glacial flow and retreat of the Late Weichselian Ice Sheet from the waters around Kong Karls Land, eastern Svalbard, Quat. Sci. Rev., 29(25–26), 3563–3582, doi:10.1016/j.quascirev.2010.05.026, 2010a.

Hogan, K. A., Dowdeswell, J. A., Noormets, R., Evans, J., Ó Cofaigh, C. and Jakobsson, M.: Submarine landforms and ice-sheet flow in the Kvitøya Trough, northwestern Barents Sea, Quat. Sci. Rev.,

29(25–26), 3545–3562, doi:10.1016/j.quascirev.2010.08.015, 2010b.

Hogan, K. A., Ó Cofaigh, C., Jennings, A. E., Dowdeswell, J. A. and Hiemstra, J. F.: Deglaciation of a major palaeo-ice stream in Disko Trough, West Greenland, Quat. Sci. Rev., 147, 5–26, doi:10.1016/j.quascirev.2016.01.018, 2016.

Hogan, K. A., Dowdeswell, J. A., Hillenbrand, C.-D., Ehrmann, W., Noormets, R. and Wacker, L.: Subglacial sediment pathways and deglacial chronology of the northern Barents Sea Ice Sheet, Boreas, 1–22, doi:10.1111/bor.12248, 2017.

Holbourn, A., Henderson, A. S. and MacLeod, N.: Atlas of Benthic Foraminifera, Wiley Blackwell, London., 2013.

Holland, D. M., Thomas, R. H., de Young, B., Ribergaard, M. H. and Lyberth, B.: Acceleration of Jakobshavn Isbræ triggered by warm subsurface ocean waters, Nat. Geosci., 1(10), 659–664, doi:10.1038/ngeo316, 2008.

Hormes, A., Akçar, N. and Kubik, P. W.: Cosmogenic radionuclide dating indicates ice-sheet configuration during MIS 2 on Nordaustlandet, Svalbard, Boreas, 40(4), 636–649, doi:10.1111/j.1502-3885.2011.00215.x, 2011.

Hormes, A., Gjermundsen, E. F. and Rasmussen, T. L.: From mountain top to the deep sea – Deglaciation in 4D of the northwestern Barents Sea ice sheet, Quat. Sci. Rev., 75, 78–99, doi:10.1016/j.quascirev.2013.04.009, 2013.

Hörner, T., Stein, R., Fahl, K. and Birgel, D.: Post-glacial variability of sea ice cover, river run-off and biological production in the western Laptev Sea (Arctic Ocean) – A high-resolution biomarker study, Quat. Sci. Rev., 143, 133–149, doi:10.1016/j.quascirev.2016.04.011, 2016.

Howe, J. A., Moreton, S. G., Morri, C. and Morris, P.: Multibeam bathymetry and the depositional environments of Kongsfjorden and Krossjorden, western Spitzbergen, Svalbard, Polar Res., 22(2), 301–316 [online] Available from: http://eprints.gla.ac.uk/257/, 2003.

Howe, J. A., Austin, W. E. N., Forwick, M., Paetzel, M., Harland, R. and Cage, A. G.: Fjord systems and archives: a review, in Fjord Systems and Archives, vol. 344, edited by W. E. N. Austin, M. Forwick, and M. Paetzel, pp. 5–15, Geological Society, London., 2010.

Hughes, A. L. C., Gyllencreutz, R., Lohne, Ø. S., Mangerud, J. and Svendsen, J. I.: The last Eurasian ice sheets - a chronological database and time-slice reconstruction, DATED-1, Boreas, 45(1), 1–45, doi:10.1111/bor.12142, 2016.

Humlum, O.: Holocene permafrost aggradation in Svalbard, in Cryospheric Systems: Glaciers and Permafrost, edited by C. Harris and J. B. Murton, pp. 11–130, Geological Society, London., 2005.

Humlum, O., Instanes, A. and Sollid, J. L.: Permafrost in Svalbard: a review of research history, climatic background and engineering challenges, Polar Res., 22(2), 191–215, doi:10.3402/polar.v22i2.6455, 2003.

Humlum, O., Elberling, B., Hormes, A., Fjordheim, K., Hansen, O. H. and Heinemeier, J.: Late-Holocene glacier growth in Svalbard, documented by subglacial relict vegetation and living soil microbes, The Holocene, 15(3), 396–407, doi:10.1191/0959683605hl817rp, 2005.

Hunt, A. S. and Corliss, B. H.: Distribution and microhabitats of living (stained) benthic foraminifera from the Canadian Arctic Archipelago, Mar. Micropaleontol., 20(3–4), 321–345, doi:10.1016/0377-

8398(93)90041-U, 1993.

Hunt, G. L., Drinkwater, K. F., Arrigo, K., Berge, J., Daly, K. L., Danielson, S., Daase, M., Hop, H., Isla, E., Karnovsky, N., Laidre, K., Mueter, F. J., Murphy, E. J., Renaud, P. E., Smith, W. O., Trathan, P., Turner, J. and Wolf-Gladrow, D.: Advection in polar and sub-polar environments: Impacts on high latitude marine ecosystems, Prog. Oceanogr., 149, 40–81, doi:10.1016/j.pocean.2016.10.004, 2016.

Hurrell, J. W.: Decadal Trends in the North Atlantic Oscillation: Regional Temperatures and Precipitation, Science, 269(5224), 676–679, doi:10.1126/science.269.5224.676, 1995.

Hurrell, J. W., Kushnir, Y., Ottersen, G. and Visbeck, M.: An overview of the North Atlantic Oscillation, in The North Atlantic Oscillation: Climatic Significance and Environmental Impact, pp. 1–35, American Geophysical Union., 2003.

Imrie, J., Hays, J. D., Martinson, D. G., McIntyre, A., Mix, A. C., Morley, J. J., Pisias, N. G., Prell, W. L. and Shackleton, N. J.: The orbital theory of Pleistocene climate: Support from a revised chronology of the marine $\delta^{18}O$ record, in Milankovitch and Climate, Part 1, edited by A. Berger, pp. 269–305, Springer, New York. [online] Available from: http://epic.awi.de/41839/1/Imbrie-etal_1984.pdf, 1984.

Inall, M. E. and Gillibrand, P. A.: The physics of mid-latitude fjords: a review, in Fjord Systems and Archives, vol. 344, edited by J. Howe, W. E. N. Austin, M. Forwick, and M. Paetzel, pp. 17–33, Geological Society, London., 2010.

Inall, M. E., Murray, T., Cottier, F. R., Scharrer, K., Boyd, T. J., Heywood, K. J. and Bevan, S. L.: Oceanic heat delivery via Kangerdlugssuaq Fjord to the south-east Greenland ice sheet, J. Geophys. Res. Ocean., 119(2), 631–645, doi:10.1002/2013JC009295, 2014.

IPCC: Contribution of Working Groups I, II and III to the Fifth Assessment Report of the Intergovernmental Panel on Climate Change, edited by R. K. Pachauri and L. A. Meyer, IPCC, Geneva., 2014.

Isaksson, E., Hermanson, M., Hicks, S., Igarashi, M., Kamiyama, K., Moore, J., Motoyama, H., Muir, D., Pohjola, V., Vaikmäe, R., van de Wal, R. S. . and Watanabe, O.: Ice cores from Svalbard—useful archives of past climate and pollution history, Phys. Chem. Earth, 28(28–32), 1217–1228, doi:10.1016/j.pce.2003.08.053, 2003.

Jackson, R., Carlson, A. E., Hillaire-Marcel, C., Wacker, L., Vogt, C. and Kucera, M.: Asynchronous instability of the North American-Arctic and Greenland ice sheets during the last deglaciation, Quat. Sci. Rev., 164, 140–153, doi:10.1016/j.quascirev.2017.03.020, 2017.

Jaworski, T.: The morphology of peat bog surfaces on Hermansenøya, NW Svalbard, Polar Sci., 11, 83–95, doi:10.1016/j.polar.2016.11.006, 2016.

Jennings, A. E. and Helgadottir, G.: Foraminiferal Assemblages From the Fjords and Shelf of Eastern Greenland, J. Foraminifer. Res., 24(2), 123–144, doi:10.2113/gsjfr.24.2.123, 1994.

Jennings, A. E., Weiner, N. J., Helgadottir, G. and Andrews, J. T.: Modern foraminiferal faunas of the southwestern to northern Iceland Shelf: Oceanographic and environmental controls, J. Foraminifer. Res., 34(3), 180–207, doi:10.2113/34.3.180, 2004.

Jennings, A. E., Hald, M., Smith, M. and Andrews, J. T.: Freshwater forcing from the Greenland Ice Sheet during the Younger Dryas: Evidence from southeastern Greenland shelf cores, Quat. Sci. Rev., 25(3–4), 282–298, doi:10.1016/j.quascirev.2005.04.006, 2006.

Jennings, A. E., Walton, M. E., Ó Cofaigh, C., Kilfeather, A., Andrews, J. T., Ortiz, J. D., De Vernal, A. and Dowdeswell, J. A.: Paleoenvironments during Younger Dryas-Early Holocene retreat of the Greenland Ice Sheet from outer Disko Trough, central west Greenland, J. Quat. Sci., 29(1), 27–40, doi:10.1002/jqs.2652, 2014.

Jernas, P., Klitgaard Kristensen, D., Husum, K., Wilson, L. and Koç, N.: Palaeoenvironmental changes of the last two millennia on the western and northern Svalbard shelf, Boreas, 42(1), 236–255, doi:10.1111/j.1502-3885.2012.00293.x, 2013.

Jessen, S. P., Rasmussen, T. L., Nielsen, T. and Solheim, A.: A new Late Weichselian and Holocene marine chronology for the western Svalbard slope 30,000–0 cal years BP, Quat. Sci. Rev., 29(9–10), 1301–1312, doi:10.1016/j.quascirev.2010.02.020, 2010.

Johannessen, O. M.: Brief overview of the physical oceanography, in The Nordic Seas, edited by B. G. Hurdle, pp. 103–127, Springer, New York., 1986.

Jonkers, L., Prins, M. A., Moros, M., Weltje, G. J., Troelstra, S. R. and Brummer, G.-J. A.: Temporal offsets between surface temperature, ice-rafting and bottom flow speed proxies in the glacial (MIS 3) northern North Atlantic, Quat. Sci. Rev., 48, 43–53, doi:10.1016/j.quascirev.2012.06.006, 2012.

Jonkers, L., Barker, S., Hall, I. R. and Prins, M. A.: Correcting for the influence of ice-rafted detritus on grain size-based paleocurrent speed estimates, Paleoceanography, 30(10), 1347–1357, doi:10.1002/2015PA002830, 2015.

Jorissen, F. J., de Stigter, H. C. and Widmark, J. G. V.: A conceptual model explaining benthic foraminiferal microhabitats, Mar. Micropaleontol., 26(1–4), 3–15, doi:10.1016/0377-8398(95)00047-X, 1995.

Jorissen, F. J., Fontanier, C. and Thomas, E.: Paleoceanographical Proxies Based on Deep-Sea Benthic Foraminiferal Assemblage Characteristics, in Developments in Marine Geology - Proxis in Late Cenozoic Paleoceanography, vol. 1, edited by C. Hillaire-Marcel and A. de Vernal, pp. 263–325, Elsevier B.V., 2007.

Klein, T. and Heinemann, G.: Interaction of katabatic winds and mesocyclones near the eastern coast of Greenland, Meteorol. Appl., 9(4), 407–422, doi:10.1017/S1350482702004036, 2002.

Klitgaard Kristensen, D., Rasmussen, T. L. and Koç, N.: Palaeoceanographic changes in the northern Barents Sea during the last 16000 years - new constraints on the last deglaciation of the Svalbard-Barents Sea Ice Sheet, Boreas, 42(3), 798–813, doi:10.1111/j.1502-3885.2012.00307.x, 2013.

Knies, J., Vogt, C. and Stein, R.: Late Quaternary growth and decay of the Svalbard/Barents Sea ice sheet and paleoceanographic evolution in the adjacent Arctic Ocean, Geo-Marine Lett., 18(3), 195–202, doi:10.1007/s003670050068, 1999.

Koç, N., Jansen, E. and Haflidason, H.: Paleoceanographic reconstructions of surface ocean conditions in the Greenland, Iceland and Norwegian seas through the last 14 ka based on diatoms, Quat. Sci. Rev., 12(2), 115–140, doi:10.1016/0277-3791(93)90012-B, 1993.

Koç, N., Klitgaard-Kristensen, D., Hasle, K., Forsberg, C. F. and Solheim, A.: Late glacial palaeoceanography of Hinlopen Strait, northern Svalbard, Polar Res., 21(2), 307–314, doi:10.1111/j.1751-8369.2002.tb00085.x, 2002.

Koenig, Z., Provost, C., Villacieros-Robineau, N., Sennéchael, N., Meyer, A., Lellouche, J.-M. and Garric, G.: Atlantic waters inflow north of Svalbard: Insights from IAOOS observations and Mercator

Ocean global operational system during N-ICE2015, J. Geophys. Res. Ocean., 122(2), 1254–1273, doi:10.1002/2016JC012424, 2017.

Kohler, J., James, T. D., Murray, T., Nuth, C., Brandt, O., Barrand, N. E., Aas, H. F. and Luckman, A.: Acceleration in thinning rate on western Svalbard glaciers, Geophys. Res. Lett., 34(18), L18502, doi:10.1029/2007GL030681, 2007.

Korsun, S. and Hald, M.: Modern Benthic Foraminifera off Novaya Zemlya Tidewater Glaciers, Russian Arctic, Arct. Alp. Res., 30(1), 61–77, doi:10.2307/1551746, 1998.

Korsun, S. and Hald, M.: Seasonal Dynamics of Benthic Foraminifera in a Glacially Fed Fjord of Svalbard, European Arctic, J. Foraminifer. Res., 30(4), 251–271, doi:10.2113/0300251, 2000.

Kremer, A., Stein, R., Fahl, K., Ji, Z., Yang, Z., Wiers, S., Matthiessen, J., Forwick, M., Löwemark, L., O'Regan, M., Chen, J. and Snowball, I.: Changes in sea ice cover and ice sheet extent at the Yermak Plateau during the last 160 ka – Reconstructions from biomarker records, Quat. Sci. Rev., 182, 93–108, doi:10.1016/j.quascirev.2017.12.016, 2018.

Kubischta, F., Knudsen, K. L., Kaakinen, A. and Salonen, V.-P.: Late Quaternary foraminiferal record in Murchisonfjorden, Nordaustlandet, Svalbard, Polar Res., 29(3), 283–297, doi:10.1111/j.1751-8369.2010.00173.x, 2010.

Kubischta, F., Knudsen, K. L., Ojala, A. E. K. and Salonen, V.-P.: Holocene benthic foraminiferal record from a high-Arctic fjord, Nordaustlandet, Svalbard, Geogr. Ann. Ser. A, Phys. Geogr., 93(4), 227–242, doi:10.1111/j.1468-0459.2011.00434.x, 2011.

Kug, J., Jeong, J., Jang, Y., Kim, B., Folland, C. K., Min, S. and Son, S.: Two distinct influences of Arctic warming on cold winters over North America and East Asia, Nat. Geosci., 8, 759–763, doi:10.1038/NGEO2517, 2015.

Łącka, M. and Zajączkowski, M.: Does the recent pool of benthic foraminiferal tests in fjordic surface sediments reflect interannual environmental changes? The resolution limit of the foraminiferal record, Ann. Soc. Geol. Pol., 86(1), 59–71, doi:10.14241/asgp.2015.019, 2016.

Łącka, M., Zajączkowski, M., Forwick, M. and Szczuciński, W.: Late Weichselian and Holocene palaeoceanography of Storfjordrenna, southern Svalbard, Clim. Past, 11(3), 587–603, doi:10.5194/cp-11-587-2015, 2015.

Landvik, J. Y., Bondevik, S., Elverhøi, A., Fjeldskaar, W., Mangerud, J., Salvigsen, O., Siegert, M. J., Svendsen, J. I. and Vorren, T. O.: The last glacial maximum of Svalbard and the Barents Sea area: Ice sheet extent and configuration, Quat. Sci. Rev., 17(1–3), 43–75, doi:10.1016/S0277-3791(97)00066-8, 1998.

Landvik, J. Y., Ingólfsson, Ó., Mienert, J., Lehman, S. J., Solheim, A., Elverhøi, A. and Ottesen, D.: Rethinking Late Weichselian ice-sheet dynamics in coastal NW Svalbard, Boreas, 34(1), 7–24, doi:10.1080/03009480510012809, 2005.

Lane, C. S., Brauer, A., Blockley, S. P. E. and Dulski, P.: Volcanic ash reveals time-transgressive abrupt climate change during the Younger Dryas, Geology, 41(12), 1251–1254, doi:10.1130/G34867.1, 2013.

Larsen, N. K., Funder, S., Linge, H., Möller, P., Schomacker, A., Fabel, D., Xu, S. and Kjær, K. H.: A Younger Dryas re-advance of local glaciers in north Greenland, Quat. Sci. Rev., 147, 47–58,

doi:10.1016/j.quascirev.2015.10.036, 2016.

Lauritzen, Ø.: Skrifter Nr. 176 - Investigations of Carboniferous and Permian sediments in Svalbard, Norsk Polarinstitutt, Oslo., 1981.

Lee, J. J.: Algal symbiosis in larger foraminifera, Symbiosis, 42, 63–75, 2006.

Lehman, S. J. and Forman, S. L.: Late Weichselian glacier retreat in Kongsfjorden, west Spitsbergen, Svalbard, Quat. Res., 37(2), 139–154, doi:10.1016/0033-5894(92)90078-W, 1992.

Levac, E., Lewis, M., Stretch, V., Duchesne, K. and Neulieb, T.: Evidence for meltwater drainage via the St. Lawrence River Valley in marine cores from the Laurentian Channel at the time of the Younger Dryas, Glob. Planet. Change, 130, 47–65, doi:10.1016/j.gloplacha.2015.04.002, 2015.

Lherminier, P., Meincke, J., Freiwald, A. and Schauer, U., Eds.: Circulation and Ecosystems in the Subpolar and Polar North Atlantic, Cruise No. 2, May 23 - September 16, 2006, Universität Hamburg. [online] Available from: https://www.tib.eu/de/suchen/id/awi%3Adoi~10.2312%252Fcr_msm02/, 2009.

Lind, S. and Ingvaldsen, R. B.: Variability and impacts of Atlantic Water entering the Barents Sea from the north, Deep. Res. Part I Oceanogr. Res. Pap., 62, 70–88, doi:10.1016/j.dsr.2011.12.007, 2012.

Linke, P. and Lutze, G. F.: Microhabitat preferences of benthic foraminifera—a static concept or a dynamic adaptation to optimize food acquisition?, Mar. Micropaleontol., 20(3–4), 215–234, doi:10.1016/0377-8398(93)90034-U, 1993.

Lisiecki, L. E. and Raymo, M. E.: A Pliocene-Pleistocene stack of 57 globally distributed benthic $\delta^{18}O$ records, Paleoceanography, 20(1), 1–17, doi:10.1029/2004PA001071, 2005.

Locarnini, R. A., Mishonov, A. V., Antonov, J. I., Boyer, T. P., Garcia, H. E., Baranova, O. K., Zweng, M. M., Paver, C. R., Reagan, J. R., Johnson, D. R., Hamilton, M. and Seidov, D.: World Ocean Atlas 2013 Volume 1: Temperature, edited by S. Levitus (Ed.) and A. Mishonov (technical Ed.), NOAA Atlas NESDIS 73., 2013.

Loeblich, A. R. and Tappan, H.: Foraminifera genera and their classification, Van Nostrand Reinhold, New York., 1988.

Loeng, H.: Features of the physical oceanographic conditions of the Barents Sea, Polar Res., 10(1), 5–18, 1991.

Lønne, I.: The influence of climate during and after a glacial surge - A comparison of the last two surges of Fridtjovbreen, Svalbard, Geomorphology, 207, 190–202, doi:10.1016/j.geomorph.2013.11.005, 2014.

Loubere, P. and Fariduddin, M.: Benthic Foraminifera and the flux of organic carbon to the seabed, in Modern Foraminifera, edited by B. K. Sen Gupta, pp. 181–199, Kluver Academic Publishers, New York., 2003.

Loubere, P. and Rayray, S.: Benthic foraminiferal assemblage formation: Theory and observation for the European Arctic margin, Deep Sea Res. Part I Oceanogr. Res. Pap., 115, 36–47, doi:10.1016/j.dsr.2016.05.004, 2016.

Lubinski, D. J., Polyak, L. and Forman, S. L.: Freshwater and Atlantic water inflows to the deep northern Barents and Kara seas since ca 13 ^{14}C ka: foraminifera and stable isotopes, Quat. Sci. Rev., 20, 1851–1879, doi:10.1016/S0277-3791(01)00016-6, 2001.

Luckman, A., Benn, D. I., Cottier, F., Bevan, S., Nilsen, F. and Inall, M.: Calving rates at tidewater glaciers

vary strongly with ocean temperature, Nat. Commun., 6(October), 8566, doi:10.1038/ncomms9566, 2015.

Mackensen, A.: On the use of benthic foraminiferal ^{13}C in palaeoceanography: constraints from primary proxy relationships, in Biogeochemical Controls on Palaeoceanographic Environmental Proxies, vol. 303, edited by W. E. N. Austin and R. H. James, pp. 121–133, Geological Society, London., 2008.

Mackensen, A. and Nam, S. Il: Taxon-specific epibenthic foraminiferal $\delta^{18}O$ in the Arctic Ocean: Relationship to water masses, deep circulation, and brine release, Mar. Micropaleontol., 113, 34–43, doi:10.1016/j.marmicro.2014.09.002, 2014.

Mackensen, A. and Schmiedl, G.: Brine formation recorded by stable isotopes of Recent benthic foraminifera in Storfjorden, Svalbard: palaeoceanographical implications, Boreas, 45(3), 552–566, doi:10.1111/bor.12174, 2016.

Mackensen, A., Sejrup, H.-P. P. and Jansen, E.: The distribution of living benthic foraminifera on the continental slope and rise off Southwest Norway, Mar. Micropaleontol., 9, 275–306, doi:10.1017/CBO9781107415324.004, 1985.

Mackensen, A., Schumacher, S., Radke, J. and Schmidt, D. N.: Microhabitat preferences and stable carbon isotopes of endobenthic foraminifera: Clue to quantitative reconstruction of oceanic new production?, Mar. Micropaleontol., 40(3), 233–258, doi:10.1016/S0377-8398(00)00040-2, 2000.

Mackensen, A., Schmiedl, G., Thiele, J. and Damm, E.: Microhabitat preferences of live benthic foraminifera and stable carbon isotopes off SW Svalbard in the presence of widespread methane seepage, Mar. Micropaleontol., 132(April), 1–17, doi:10.1016/j.marmicro.2017.04.004, 2017.

Mackiewicz, N. E., Powell, R. D., Carlson, P. R. and Molnia, B. F.: Interlaminated ice-proximal glacimarine sediments in Muir Inlet, Alaska, Mar. Geol., 57(1–4), 113–147, doi:10.1016/0025-3227(84)90197-X, 1984.

MacLachlan, S. E., Howe, J. A. and Vardy, M. E.: Morphodynamic evolution of Kongsfjorden-Krossfjorden, Svalbard, during the Late Weichselian and Holocene, in Fjord Systems and Archives, vol. 344, edited by J. A. Howe, W. E. N. Austin, M. Forwick, and M. Paetzel, pp. 195–205, Geological Society, London., 2010.

Majewski, W., Szczuciński, W. and Zajączkowski, M.: Interactions of Arctic and Atlantic water-masses and associated environmental changes during the last millennium, Hornsund (SW Svalbard), Boreas, 38(3), 529–544, doi:10.1111/j.1502-3885.2009.00091.x, 2009.

Mangerud, J.: Radiocarbon dating of marine shells including a discussion of the apparent age of recent shells from Norway., Boreas, 1, 143–172, doi:10.1111/j.1502-3885.1972.tb00147.x, 1972.

Mangerud, J. and Gulliksen, S.: Apparent radiocarbon ages of recent marine shells from Norway, Spitsbergen, and Arctic Canada, Quat. Res., 5(2), 263–273, doi:10.1016/0033-5894(75)90028-9, 1975.

Mangerud, J. and Landvik, J. Y.: Younger Dryas cirque glaciers in western Spitsbergen: smaller than during the Little Ice Age, Boreas, 36(3), 278–285, doi:10.1080/03009480601134827, 2007.

Mangerud, J., Lie, S. E., Furnes, H., Kristiansen, I. L. and Lømo, L.: A Younger Dryas Ash Bed in Western Norway, and Its Possible Correlations with Tephra in Cores from the Norwegian Sea and the North Atlantic, Quat. Res., 21, 85–104, 1984.

Manley, T. O.: Branching of Atlantic Water within the Greenland-Spitsbergen Passage: An estimate of recirculation, J. Geophys. Res., 100(C10), 20627, doi:10.1029/95JC01251, 1995.

Marchal, O., Cacho, I., Stocker, T. F., Grimalt, J. O., Calvo, E., Martrat, B., Shackleton, N., Vautravers, M., Cortijo, E., van Kreveld, S., Andersson, C., Koç, N., Chapman, M., Sbaffi, L., Duplessy, J., Sarnthein, M., Turon, J., Duprat, J. and Jansen, E.: Apparent long-term cooling of the sea surface in the northeast Atlantic and Mediterranean during the Holocene, Quat. Sci. Rev., 21(4–6), 455–483, doi:10.1016/S0277-3791(01)00105-6, 2002.

Masson-Delmotte, V., Schulz, M., Abe-Ouchi, A., Beer, J., Ganopolski, A., González Rouco, J. F., Jansen, E., Lambeck, K., Luterbacher, J., Naish, T., Osborn, T., Otto-Bliesner, B., Quinn, T., Ramesh, R., Rojas, M., Shao, X., Timmermann, A. and Rouco, J. F. G.: Climate Change 2013 - The Physical Science Basis, edited by Intergovernmental Panel on Climate Change, Cambridge University Press, Cambridge., 2014.

McCave, I. N. and Hall, I. R.: Size sorting in marine muds: Processes, pitfalls, and prospects for paleoflow-speed proxies, Geochemistry, Geophys. Geosystems, 7(10), doi:10.1029/2006GC001284, 2006.

McCave, I. N., Manighetti, B. and Beveridge, N. A. S.: Circulation in the glacial North Atlantic inferred from grain-size measurements, Nature, 374, 149–151, 1995a.

McCave, I. N., Manighetti, B. and Robinson, S. G.: Sortable silt and fine sediment size/composition slicing: parameters for palaeocurrent speed and palaeoceanography, Paleoceanography, 10(3), 593–610, doi:10.1029/94PA03039, 1995b.

McCusker, K. E., Fyfe, J. C. and Sigmond, M.: Twenty-five winters of unexpected Eurasian cooling unlikely due to Arctic sea-ice loss, Nat. Geosci., 9(October), 5–10, doi:10.1038/ngeo2820, 2016.

McGregor, H. V., Dupont, L., Stuut, J. B. W. and Kuhlmann, H.: Vegetation change, goats, and religion: a 2000-year history of land use in southern Morocco, Quat. Sci. Rev., 28(15–16), 1434–1448, doi:10.1016/j.quascirev.2009.02.012, 2009.

Meleshko, V. P., Johannessen, O. M., Baidin, A. V., Pavlova, T. V. and Govorkova, V. A.: Arctic amplification: does it impact the polar jet stream?, Tellus A, 68, 1–11, doi:10.3402/tellusa.v68.32330, 2016.

Meyers, P. A.: Organic geochemical proxies of paleoceanographic, paleolimnologic, paleoclimatic processes, Org. Geochem., 27(5/6), 213–250, 1997.

Milker, Y. and Schmiedl, G.: A taxonomic guide to modern benthic shelf foraminifera of the western Mediterranean Sea, Palaeontol. Electron., 15(2), 134, 2012.

Milker, Y., Schmiedl, G., Betzler, C., Andersen, N. and Theodor, M.: Response of Mallorca shelf ecosystems to an early Holocene humid phase, Mar. Micropaleontol., 90–91, 1–12, doi:10.1016/j.marmicro.2012.04.001, 2012.

Miller, G. H., Alley, R. B., Brigham-Grette, J., Fitzpatrick, J. J., Polyak, L., Serreze, M. C. and White, J. W. C.: Arctic amplification: Can the past constrain the future?, Quat. Sci. Rev., 29(15–16), 1779–1790, doi:10.1016/j.quascirev.2010.02.008, 2010a.

Miller, G. H., Brigham-Grette, J., Alley, R. B., Anderson, L., Bauch, H. A., Douglas, M. S. V., Edwards, M. E., Elias, S. a., Finney, B. P., Fitzpatrick, J. J., Funder, S. V., Herbert, T. D., Hinzman, L. D., Kaufman, D. S., MacDonald, G. M., Polyak, L., Robock, A., Serreze, M. C., Smol, J. P., Spielhagen,

R., White, J. W. C., Wolfe, A. P. and Wolff, E. W.: Temperature and precipitation history of the Arctic, Quat. Sci. Rev., 29(15–16), 1679–1715, doi:10.1016/j.quascirev.2010.03.001, 2010b.

Mori, M., Watanabe, M., Shiogama, H., Inoue, J. and Kimoto, M.: Robust Arctic sea-ice influence on the frequent Eurasian cold winters in past decades, Nat. Geosci., 7(October 2014), 869–874, doi:10.1038/ngeo2277, 2014.

Motyka, R. J., Hunter, L., Echelmeyer, K. A. and Connor, C.: Submarine melting at the terminus of a temperate tidewater glacier, LeConte Glacier, Alaska, U.S.A, Ann. Glaciol., 36, 57–65, doi:10.3189/172756403781816374, 2003.

Mulder, T. and Alexander, J.: The physical character of subaqueous sedimentary density flows and their deposits, Sedimentology, 48(2), 269–299, doi:10.1046/j.1365-3091.2001.00360.x, 2001.

Mulitza, S., Chiessi, C. M., Schefuß, E., Lippold, J., Wichmann, D., Antz, B., Mackensen, A., Paul, A., Prange, M., Rehfeld, K., Werner, M., Bickert, T., Frank, N., Kuhnert, H., Lynch-Stieglitz, J., Portilho-Ramos, R. C., Sawakuchi, A. O., Schulz, M., Schwenk, T., Tiedemann, R., Vahlenkamp, M. and Zhang, Y.: Synchronous and proportional deglacial changes in Atlantic Meridional Overturning and northeast Brazilian precipitation, Paleoceanography, doi:10.1002/2017PA003084, 2017.

Müller-Navarra, K., Milker, Y. and Schmiedl, G.: Natural and anthropogenic influence on the distribution of salt marsh foraminifera in the Bay of Tümlau, German North Sea, J. Foraminifer. Res., 46(1), 61–74, 2016.

Müller, J. and Stein, R.: High-resolution record of late glacial and deglacial sea ice changes in Fram Strait corroborates ice-ocean interactions during abrupt climate shifts, Earth Planet. Sci. Lett., 403, 446–455, doi:10.1016/j.epsl.2014.07.016, 2014.

Müller, J., Massé, G., Stein, R. and Belt, S. T.: Variability of sea-ice conditions in the Fram Strait over the past 30,000 years, Nat. Geosci., 2(11), 772–776, doi:10.1038/ngeo665, 2009.

Müller, J., Wagner, A., Fahl, K., Stein, R., Prange, M. and Lohmann, G.: Towards quantitative sea ice reconstructions in the northern North Atlantic: A combined biomarker and numerical modelling approach, Earth Planet. Sci. Lett., 306(3–4), 137–148, doi:10.1016/j.epsl.2011.04.011, 2011.

Müller, J., Werner, K., Stein, R., Fahl, K., Moros, M. and Jansen, E.: Holocene cooling culminates in sea ice oscillations in Fram Strait, Quat. Sci. Rev., 47, 1–14, doi:10.1016/j.quascirev.2012.04.024, 2012.

Müller, P. J., Kirst, G., Ruhland, G., von Storch, I. and Rosell-Melé, A.: Calibration of the alkenone paleotemperature index $U_{37}^{K'}$ based on core-tops from the eastern South Atlantic and the global ocean (60°N-60°S), Geochim. Cosmochim. Acta, 62(10), 1757–1772, doi:10.1016/S0016-7037(98)00097-0, 1998.

Murray, J. W.: Ecology and Applications of Benthic Foraminifera, Cambridge University Press, Cambridge. [online] Available from: http://www.cambridge.org/9780521828390, 2006.

Murton, J. B., Bateman, M. D., Dallimore, S. R., Teller, J. T. and Yang, Z.: Identification of Younger Dryas outburst flood path from Lake Agassiz to the Arctic Ocean., Nature, 464(7289), 740–743, doi:10.1038/nature08954, 2010.

Mysak, L. A.: Patterns of Arctic Circulation, Science, 293(1269), 1269–1270, doi:10.1126/science.1064217, 2001.

Newton, A. C. and Rowe, G. T.: The abundance of benthic calcareous Foraminifera and other meiofauna at a time series station in the Northeast Water Polynya, Greenland, J. Geophys. Res., 100(C3), 4423–4438, doi:10.1029/94JC02356, 1995.

Nilsen, F., Skogseth, R., Vaardal-Lunde, J. and Inall, M.: A Simple Shelf Circulation Model: Intrusion of Atlantic Water on the West Spitsbergen Shelf, J. Phys. Oceanogr., 46(4), 1209–1230, doi:10.1175/JPO-D-15-0058.1, 2016.

Norwegian Polar Institute: Kartdata Svalbard 1:100 000 (S100 Kartdata)/Map Data [Data set], [online] Available from: https://doi.org/10.21334/npolar.2014.645336c7, 2014.

Not, C. and Hillaire-Marcel, C.: Enhanced sea-ice export from the Arctic during the Younger Dryas, Nat. Commun., 3, 647, doi:10.1038/ncomms1658, 2012.

Notz, D. and Marotzke, J.: Observations reveal external driver for Arctic sea-ice retreat, Geophys. Res. Lett., 39(8), 1–6, doi:10.1029/2012GL051094, 2012.

Notz, D. and Stroeve, J.: Observed Arctic sea-ice loss directly follows anthropogenic CO2 emission, Science, 354(6313), 747–750, doi:10.1126/science.aag2345, 2016.

Ó Cofaigh, C. and Dowdeswell, J. A.: Laminated sediments in glacimarine environments: Diagnostic criteria for their interpretation, Quat. Sci. Rev., 20(13), 1411–1436, doi:10.1016/S0277-3791(00)00177-3, 2001.

Ó Cofaigh, C., Dowdeswell, J. A., Jennings, A. E., Hogan, K. A., Kilfeather, A., Hiemstra, J. F., Noormets, R., Evans, J., McCarthy, D. J., Andrews, J. T., Lloyd, J. M. and Moros, M.: An extensive and dynamic ice sheet on the west greenland shelf during the last glacial cycle, Geology, 41(2), 219–222, doi:10.1130/G33759.1, 2013.

Ohta, Y.: Hecla Hoek Rocks in Central and Western Nordaustlandet, Norsk Polarinstitutt, Oslo., 1982.

Olsen, J., Rasmussen, T. L. and Reimer, P. J.: North Atlantic marine radiocarbon reservoir ages through Heinrich event H4: a new method for marine age model construction, in Marine Tephrochronology, vol. 398, edited by W. E. N. Austin, P. M. Abbott, S. M. Davies, N. J. G. Pearce, and S. Wastegård, pp. 95–112, Geological Society, London., 2014.

Olsson, I. U.: Content of ^{14}C in marine mammals from Northern Europe, Radiocarbon, 22(3), 662–675, 1980.

Ottesen, D. and Dowdeswell, J. A.: Assemblages of submarine landforms produced by tidewater glaciers in Svalbard, J. Geophys. Res. Earth Surf., 111(1), F01016, doi:10.1029/2005JF000330, 2006.

Ottesen, D., Dowdeswell, J. A., Landvik, J. Y. and Mienert, J.: Dynamics of the Late Weichselian ice sheet on Svalbard inferred from high-resolution sea-floor morphology, Boreas, 36(3), 286–306, doi:10.1111/j.1502-3885.2007.tb01251.x, 2007.

Ottesen, D., Dowdeswell, J. A., Benn, D. I., Kristensen, L., Christiansen, H. H., Christensen, O., Hansen, L., Lebesbye, E., Forwick, M. and Vorren, T. O.: Submarine landforms characteristic of glacier surges in two Spitsbergen fjords, Quat. Sci. Rev., 27(15–16), 1583–1599, doi:10.1016/j.quascirev.2008.05.007, 2008.

Overland, J., Francis, J. A., Hall, R., Hanna, E., Kim, S.-J. and Vihma, T.: The Melting Arctic and Midlatitude Weather Patterns: Are They Connected?, J. Clim., 28(20), 7917–7932, doi:10.1175/JCLI-D-14-00822.1, 2015.

Overland, J. E.: A difficult Arctic science issue: Midlatitude weather linkages, Polar Sci., 10(3), 210–216,

doi:10.1016/j.polar.2016.04.011, 2015.

Overland, J. E., Dethloff, K., Francis, J. A., Hall, R. J., Hanna, E., Kim, S.-J., Screen, J. A., Shepherd, T. G. and Vihma, T.: Nonlinear response of mid-latitude weather to the changing Arctic, Nat. Clim. Chang., 6(11), 992–999, doi:10.1038/nclimate3121, 2016.

Overpeck, J. T., Otto-Bliesner, B. L., Miller, G. H., Muhs, D. R., Alley, R. B. and Kiehl, J. T.: Paleoclimatic Evidence for Future Ice-Sheet Instability and Rapid Sea-Level Rise, Science, 311(5768), 1747–1750, doi:10.1126/science.1115159, 2006.

Padman, L., Costa, D. P., Dinniman, M. S., Fricker, H. A., Goebel, M. E., Huckstadt, L. A., Humbert, A., Joughin, I., Lenaerts, J. T. M., Ligtenberg, S. R. M., Scambos, T. and Van Den Broeke, M. R.: Oceanic controls on the mass balance of Wilkins Ice Shelf, Antarctica, J. Geophys. Res. Ocean., 117(1), 1–17, doi:10.1029/2011JC007301, 2012.

Patterson, R. T. and Fishbein, E.: Re-examination of the statistical methods used to determine the number of point counts needed for micropaleontological quantitative research, J. Paleontol., 63(2), 245–248, doi:10.1017/S0022336000019272, 1989.

Pawłowska, J., Zajączkowski, M., Szczuciński, W., Zaborska, A., Kucharska, M., Jernas, P. E. and Forwick, M.: The influence of Coriolis force driven water circulation on the palaeoenvironment of Hornsund (S Spitsbergen) over the last century, Boreas, doi:10.1111/bor.12249, 2017.

Pearce, C., Seidenkrantz, M.-S., Kuijpers, A., Massé, G., Reynisson, N. F. and Kristiansen, S. M.: Ocean lead at the termination of the Younger Dryas cold spell., Nat. Commun., 4, 1664, doi:10.1038/ncomms2686, 2013.

Pearce, C., Seidenkrantz, M.-S., Kuijpers, A. and Reynisson, N. F.: A multi-proxy reconstruction of oceanographic conditions around the Younger Dryas–Holocene transition in Placentia Bay, Newfoundland, Mar. Micropaleontol., 112, 39–49, doi:10.1016/j.marmicro.2014.08.004, 2014.

Pearce, C., Varhelyi, A., Wastegård, S., Muschitiello, F., Barrientos, N., O´Regan, M., Cronin, T. M., Gemery, L., Semiletov, I., Backman, J. and Jakobsson, M.: The 3.6 ka Aniakchak tephra in the Arctic Ocean: a constraint on the Holocene radiocarbon reservoir age in the Chukchi Sea, Clim. Past, 13(4), 303–316, doi:10.5194/cp-13-303-2017, 2017.

Pérez-Hernández, M. D., Pickart, R. S., Pavlov, V., Våge, K., Ingvaldsen, R., Sundfjord, A., Renner, A. H. H., Torres, D. J. and Erofeeva, S. Y.: The Atlantic Water boundary current north of Svalbard in late summer, J. Geophys. Res. Ocean., 122(3), 2269–2290, doi:10.1002/2016JC012486, 2017.

Pfuhl, H. A. and Shackleton, N. J.: Two proximal, high-resolution records of foraminiferal fragmentation and their implications for changes in dissolution, Deep. Res. Part I Oceanogr. Res. Pap., 51(6), 809–832, doi:10.1016/j.dsr.2004.02.003, 2004.

Pinter, N., Scott, A. C., Daulton, T. L., Podoll, A., Koeberl, C., Anderson, R. S. and Ishman, S. E.: The Younger Dryas impact hypothesis: A requiem, Earth-Science Rev., 106(3–4), 247–264, doi:10.1016/j.earscirev.2011.02.005, 2011.

Polyak, L., Korsun, S., Febo, L. A., Stanovoy, V., Khusid, T., Hald, M., Paulsen, B. E. and Lubinski, D. J.: Benthic foraminiferal assemblages from the southern Kara Sea, a river-influenced Arctic marine environment, J. Foraminifer. Res., 32(3), 252–273, doi:10.2113/32.3.252, 2002.

Porter, S. C. and Denton, G. H.: Chronology of Neoglaciation in the North American Cordillera, Am. J. Sci.,

265(March), 177–210, doi:10.2475/ajs.265.3.177, 1967.

Prahl, F. G. and Wakeham, S. G.: Calibration of unsaturation patterns in long-chain ketone compositions for palaeotemperature assessment, Nature, 330(6146), 367–369, doi:10.1038/330367a0, 1987.

R Development Core Team: R: A Language and Environment for Statistical Computing, [online] Available from: http://www.r-project.org/, 2011.

Radić, V., Bliss, A., Beedlow, A. C., Hock, R., Miles, E. and Cogley, J. G.: Regional and global projections of twenty-first century glacier mass changes in response to climate scenarios from global climate models, Clim. Dyn., 42(1–2), 37–58, doi:10.1007/s00382-013-1719-7, 2014.

Rasmussen, S. O., Bigler, M., Blockley, S. P., Blunier, T., Buchardt, S. L., Clausen, H. B., Cvijanovic, I., Dahl-Jensen, D., Johnsen, S. J., Fischer, H., Gkinis, V., Guillevic, M., Hoek, W. Z., Lowe, J. J., Pedro, J. B., Popp, T., Seierstad, I. K., Steffensen, J. P., Svensson, A. M., Vallelonga, P., Vinther, B. M., Walker, M. J. C., Wheatley, J. J. and Winstrup, M.: A stratigraphic framework for abrupt climatic changes during the Last Glacial period based on three synchronized Greenland ice-core records: refining and extending the INTIMATE event stratigraphy, Quat. Sci. Rev., 106, 14–28, doi:10.1016/j.quascirev.2014.09.007, 2014a.

Rasmussen, T. L. and Thomsen, E.: The role of the North Atlantic Drift in the millennial timescale glacial climate fluctuations, Palaeogeogr. Palaeoclimatol. Palaeoecol., 210(1), 101–116, doi:10.1016/j.palaeo.2004.04.005, 2004.

Rasmussen, T. L. and Thomsen, E.: Pink marine sediments reveal rapid ice melt and Arctic meltwater discharge during Dansgaard-Oeschger warmings., Nat. Commun., 4(9037), 2849, doi:10.1038/ncomms3849, 2013.

Rasmussen, T. L. and Thomsen, E.: Brine formation in relation to climate changes and ice retreat during the last 15,000 years in Storfjorden, Svalbard, 76–78° N, Paleoceanography, 29, 911–929, doi:10.1002/2014PA002643, 2014.

Rasmussen, T. L., Thomsen, E., Ślubowska, M. A., Jessen, S., Solheim, A. and Koç, N.: Paleoceanographic evolution of the SW Svalbard margin (76° N) since 20,000 ^{14}C yr BP, Quat. Res., 67(1), 100–114, doi:10.1016/j.yqres.2006.07.002, 2007.

Rasmussen, T. L., Forwick, M. and Mackensen, A.: Reconstruction of inflow of Atlantic Water to Isfjorden, Svalbard during the Holocene: Correlation to climate and seasonality, Mar. Micropaleontol., 94–95, 80–90, doi:10.1016/j.marmicro.2012.06.008, 2012.

Rasmussen, T. L., Thomsen, E., Skirbekk, K., Ślubowska-Woldengen, M., Klitgaard Kristensen, D. and Koç, N.: Spatial and temporal distribution of Holocene temperature maxima in the northern Nordic seas: interplay of Atlantic-, Arctic- and polar water masses, Quat. Sci. Rev., 92, 280–291, doi:10.1016/j.quascirev.2013.10.034, 2014b.

Rasmussen, T. L., Thomsen, E. and Nielsen, T.: Water mass exchange between the Nordic seas and the Arctic Ocean on millennial timescale during MIS 4-MIS 2, Geochemistry, Geophys. Geosystems, 15(3), 530–544, doi:10.1002/2013GC005020, 2014c.

Ravelo, A. C. and Hillaire-Marcel, C.: The Use of Oxygen and Carbon Isotopes of Foraminifera in Paleoceanography, in Developments in Marine Geology - Proxis in Late Cenozoic Paleoceanography, edited by C. Hillaire-Marcel and A. de Vernal, pp. 735–764, Elsevier B.V., 2007.

Ray, G. C., McCormick-Ray, J., Berg, P. and Epstein, H. E.: Pacific walrus: Benthic bioturbator of Beringia, J. Exp. Mar. Bio. Ecol., 330(1), 403–419, doi:10.1016/j.jembe.2005.12.043, 2006.

Reimer, P. J., Bard, E., Bayliss, A., Beck, J. W., Blackwell, P. G., Ramsey, C. B., Buck, C. E., Cheng, H., Edwards, R. L., Friedrich, M., Grootes, P. M., Guilderson, T. P., Haflidason, H., Hajdas, I., Hatté, C., Heaton, T. J., Hoffmann, D. L., Hogg, A. G., Hughen, K. A., Kaiser, K. F., Kromer, B., Manning, S. W., Niu, M., Reimer, R. W., Richards, D. A., Scott, E. M., Southon, J. R., Staff, R. A., Turney, C. S. M. and van der Plicht, J.: IntCal13 and Marine13 Radiocarbon Age Calibration Curves 0–50,000 Years cal BP, Radiocarbon, 55(4), 1869–1887, doi:10.2458/azu_js_rc.55.16947, 2013.

Reusche, M., Winsor, K., Carlson, A. E., Marcott, S. A., Rood, D. H., Novak, A., Roof, S., Retelle, M., Werner, A., Caffee, M. and Clark, P. U.: ^{10}Be surface exposure ages on the late-Pleistocene and Holocene history of Linnébreen on Svalbard, Quat. Sci. Rev., 89, 5–12, doi:10.1016/j.quascirev.2014.01.017, 2014.

Rigual-Hernández, A. S., Colmenero-Hidalgo, E., Martrat, B., Bárcena, M. A., de Vernal, A., Sierro, F. J., Flores, J. A., Grimalt, J. O., Henry, M. and Lucchi, R. G.: Svalbard ice-sheet decay after the Last Glacial Maximum: New insights from micropalaeontological and organic biomarker paleoceanographical reconstructions, Palaeogeogr. Palaeoclimatol. Palaeoecol., 465, 225–236, doi:10.1016/j.palaeo.2016.10.034, 2017.

Rinterknecht, V., Jomelli, V., Brunstein, D., Favier, V., Masson-Delmotte, V., Bourlès, D., Leanni, L. and Schläppy, R.: Unstable ice stream in Greenland during the Younger Dryas cold event, Geology, 42(9), 759–762, doi:10.1130/G35929.1, 2014.

Risebrobakken, B., Dokken, T., Smedsrud, L. H., Andersson, C., Jansen, E., Moros, M. and Ivanova, E. V.: Early Holocene temperature variability in the Nordic Seas: The role of oceanic heat advection versus changes in orbital forcing, Paleoceanography, 26(4), doi:10.1029/2011PA002117, 2011.

Rohling, E. J. and Bigg, G. R.: Paleosalinity and δ^{18}O: A critical assessment, J. Geophys. Res., 103, 1307–1318, doi:10.1029/97jc01047, 1998.

Rohling, E. J. and Cooke, S.: Stable oxygen and carbon isotopes in foraminiferal carbonate shells, in Modern Foraminifera, edited by B. K. Sen Gupta, pp. 239–258, Kluver Academic Publishers, New York., 2003.

Røthe, T. O., Bakke, J., Vasskog, K., Gjerde, M., D'Andrea, W. J. and Bradley, R. S.: Arctic Holocene glacier fluctuations reconstructed from lake sediments at Mitrahalvøya, Spitsbergen, Quat. Sci. Rev., 109, 111–125, doi:10.1016/j.quascirev.2014.11.017, 2015.

Rudels, B.: Arctic ocean circulation, in Encyclopedia of Ocean Sciences, edited by J. H. Steele, K. K. Turekian, and S. A. Thorpe, pp. 211–225, Elsevier., 2009.

Rytter, F., Knudsen, K. L., Seidenkrantz, M.-S. and Eiriksson, J.: Modern Distribution of Benthic Foraminifera on the North Icelandinc Shelf and Slope, J. Foraminifer. Res., 32(3), 217–244, doi:10.2113/32.3.217, 2002.

Sakshaug, E.: Biomass and productivity distributions and their variability in the Barents Sea, ICES J. Mar. Sci., 54, 341–350, doi:10.1006/jmsc.1996.0170, 1997.

Saloranta, T. M. and Haugan, P. M.: Interannual variability in the hydrography of Atlantic water northwest of Svalbard, J. Geophys. Res., 106(C7), 13931–13943, doi:10.1029/2000JC000478, 2001.

Saloranta, T. M. and Svendsen, H.: Across the Arctic front west of Spitsbergen: High-resolution CTD sections from 1998-2000, Polar Res., 20(2), 177–184, doi:10.1111/j.1751-8369.2001.tb00054.x, 2001.

Salvigsen, O.: Radiocarbon-dated *Mytilus edulis* and *Modiolus modiolus* from northern Svalbard: Climatic implications, Nor. Geogr. Tidsskr. - Nor. J. Geogr., 56(2), 56–61, doi:10.1080/002919502760056350, 2002.

Salvigsen, O. and Høgvard, K.: Glacial history, Holocene shoreline displacement and palaeoclimate based on radiocarbon ages in the area of Bockfjorden, north-western Spitsbergen, Svalbard, Polar Res., 25(1), 15–24, doi:10.1111/j.1751-8369.2005.tb00021.x, 2006.

Salvigsen, O. and Österholm, H.: Radiocarbon dated raised beaches and glacial history of the northern coast of Spitsbergen, Svalbard, Polar Res., 1982(1), 97–115, doi:10.1111/j.1751-8369.1982.tb00473.x, 1982.

Sarnthein, M., van Kreveld, S., Erlenkeuser, H., Grootes, P. M., Kucera, M., Pflaumann, U. and Schulz, M.: Centennial-to-millennial-scale periodicities of Holocene climate and sediment injections off the western Barents shelf, 75° N, Boreas, 32(3), 447–461, doi:10.1080/03009480310003351, 2003.

Sarnthein, M., Grootes, P. M., Kennett, J. P. and Nadeau, M. J.: ^{14}C Reservoir Ages Show Deglacial Changes in Ocean Currents and Carbon Cycle, in Ocean Circulation: Mechanisms and Impacts - Past and Future Changes of Meridional Overturning, edited by A. Schmittner, J. C. H. Chiang, and S. R. Hemming, pp. 175–196, American Geophysical Union, Washington., 2007.

Schauer, U., Fahrbach, E., Osterhus, S. and Rohardt, G.: Arctic warming through the Fram Strait: Oceanic heat transport from 3 years of measurements, J. Geophys. Res. C Ocean., 109(6), 1–14, doi:10.1029/2003JC001823, 2004.

Schlitzer, R.: Ocean Data View, [online] Available from: http://odv.awi.de, 2015.

Schmidt, C., Morard, R., Almogi-Labin, A., Weinmann, A. E., Titelboim, D., Abramovich, S. and Kucera, M.: Recent invasion of the symbiont-bearing foraminifera pararotalia into the eastern mediterranean facilitated by the ongoing warming trend, PLoS One, 10(8), 1–25, doi:10.1371/journal.pone.0132917, 2015.

Schmiedl, G. and Mackensen, A.: Multispecies stable isotopes of benthic foraminifers reveal past changes of organic matter decomposition and deepwater oxygenation in the Arabian Sea, Paleoceanography, 21(4), 1–14, doi:10.1029/2006PA001284, 2006.

Schmiedl, G., Kuhnt, T., Ehrmann, W., Emeis, K.-C., Hamann, Y., Kotthoff, U., Dulski, P. and Pross, J.: Climatic forcing of eastern Mediterranean deep-water formation and benthic ecosystems during the past 22 000 years, Quat. Sci. Rev., 29(23–24), 3006–3020, doi:10.1016/j.quascirev.2010.07.002, 2010.

Schmittner, A., Bostock, H. C., Cartapanis, O., Curry, W. B., Filipsson, H. L., Galbraith, E. D., Gottschalk, J., Herguera, J. C., Hoogakker, B., Jaccard, S. L., Lisiecki, L. E., Lund, D. C., Martínez-Méndez, G., Lynch-Stieglitz, J., Mackensen, A., Michel, E., Mix, A. C., Oppo, D. W., Peterson, C. D., Repschläger, J., Sikes, E. L., Spero, H. J. and Waelbroeck, C.: Calibration of the carbon isotope composition ($\delta^{13}C$) of benthic foraminifera, Paleoceanography, 32, 1–19, doi:10.1002/2016PA003072, 2017.

Seidenkrantz, M.-S.: *Cassidulina teretis* Tappan and *Cassidulina neoteretis* new species (Foraminifera):

stratigraphic markers for deep sea and outer shelf areas, J. Micropalaeontology, 14(2), 145–157, doi:10.1144/jm.14.2.145, 1995.

Seidenkrantz, M.-S.: Benthic foraminifera as palaeo sea-ice indicators in the subarctic realm – examples from the Labrador Sea–Baffin Bay region, Quat. Sci. Rev., 79, 135–144, doi:10.1016/j.quascirev.2013.03.014, 2013.

Seidenkrantz, M.-S., Aagaard-Sorensen, S., Sulsbruck, H., Kuijpers, a., Jensen, K. G. and Kunzendorf, H.: Hydrography and climate of the last 4400 years in a SW Greenland fjord: implications for Labrador Sea palaeoceanography, The Holocene, 17(3), 387–401, doi:10.1177/0959683607075840, 2007.

Seidenkrantz, M.-S., Ebbesen, H., Aagaard-Sørensen, S., Moros, M., Lloyd, J. M., Olsen, J., Knudsen, M. F. and Kuijpers, A.: Early Holocene large-scale meltwater discharge from Greenland documented by foraminifera and sediment parameters, Palaeogeogr. Palaeoclimatol. Palaeoecol., 391, 71–81, doi:10.1016/j.palaeo.2012.04.006, 2013.

Sejrup, H.-P. and Guilbault, J.-P.: *Cassidulina reniforme* and *C. obtusa* (Foraminifera), taxonomy, distribution, and ecology, Sarsia, 65(2), 79–85, doi:10.1080/00364827.1980.10431476, 1980.

Sejrup, H. P., Haflidason, H. and Andrews, J. T.: A Holocene North Atlantic SST record and regional climate variability, Quat. Sci. Rev., 30(21–22), 3181–3195, doi:10.1016/j.quascirev.2011.07.025, 2011.

Serreze, M. C. and Barry, R. G.: Processes and impacts of Arctic amplification: A research synthesis, Glob. Planet. Change, 77(1–2), 85–96, doi:10.1016/j.gloplacha.2011.03.004, 2011.

Serreze, M. C., Barrett, A. P., Slater, A. G., Woodgate, R. A., Aagaard, K., Lammers, R. B., Steele, M., Moritz, R., Meredith, M. and Lee, C. M.: The large-scale freshwater cycle of the Arctic, J. Geophys. Res. Ocean., 111(11), 1–19, doi:10.1029/2005JC003424, 2006.

Sha, L., Jiang, H., Seidenkrantz, M. S., Knudsen, K. L., Olsen, J., Kuijpers, A. and Liu, Y.: A diatom-based sea-ice reconstruction for the Vaigat Strait (Disko Bugt, West Greenland) over the last 5000yr, Palaeogeogr. Palaeoclimatol. Palaeoecol., 403, 66–79, doi:10.1016/j.palaeo.2014.03.028, 2014.

Shackleton, N. J.: Attainment of isotopic equilibrium between ocean water and the benthonic foraminifera *Uvigerina*: isotopic changes in the ocean during the last glacial, Colloq. Int. du C.N.R.S, 219, 203–209 [online] Available from: https://epic.awi.de/32862/1/shackleton-1974.pdf, 1974.

Sheldon, C., Jennings, A., Andrews, J. T., Ó Cofaigh, C., Hogan, K., Dowdeswell, J. A. and Seidenkrantz, M. S.: Ice stream retreat following the LGM and onset of the west Greenland current in Uummannaq Trough, west Greenland, Quat. Sci. Rev., 147, 27–46, doi:10.1016/j.quascirev.2016.01.019, 2016a.

Sheldon, C. M., Seidenkrantz, M.-S., Pearce, C., Kuijpers, A., Hansen, M. J. and Christensen, E. Z.: Holocene oceanographic changes in SW Labrador Sea, off Newfoundland, The Holocene, 26(2), 274–289, doi:10.1177/0959683615608690, 2016b.

Skagseth, Ø.: Recirculation of Atlantic Water in the western Barents Sea, Geophys. Res. Lett., 35(11), 1–5, doi:10.1029/2008GL033785, 2008.

Skirbekk, K., Klitgaard Kristensen, D., Rasmussen, T. L., Koç, N. and Forwick, M.: Holocene climate variations at the entrance to a warm Arctic fjord: evidence from Kongsfjorden trough, Svalbard, in Fjord Systems and Archives, vol. 344, edited by J. A. Howe, W. E. N. Austin, M. Forwick, and M. Paetzel, pp. 289–304, Geological Society, London., 2010.

Skogseth, R., Haugan, P. M. and Jakobsson, M.: Watermass transformations in Storfjorden, Cont. Shelf Res.,

25, 667–695, doi:10.1016/j.csr.2004.10.005, 2005.

Slabon, P., Dorschel, B., Jokat, W., Myklebust, R., Hebbeln, D. and Gebhardt, C.: Greenland ice sheet retreat history in the northeast Baffin Bay based on high-resolution bathymetry, Quat. Sci. Rev., 154, 182–198, doi:10.1016/j.quascirev.2016.10.022, 2016.

Ślubowska-Woldengen, M., Rasmussen, T. L., Koç, N., Klitgaard-Kristensen, D., Nilsen, F. and Solheim, A.: Advection of Atlantic Water to the western and northern Svalbard shelf since 17,500 cal yr BP, Quat. Sci. Rev., 26(3–4), 463–478, doi:10.1016/j.quascirev.2006.09.009, 2007.

Ślubowska-Woldengen, M., Koç, N., Rasmussen, T. L., Klitgaard-Kristensen, D., Hald, M. and Jennings, A. E.: Time-slice reconstructions of ocean circulation changes on the continental shelf in the Nordic and Barents Seas during the last 16,000 cal yr B.P., Quat. Sci. Rev., 27(15–16), 1476–1492, doi:10.1016/j.quascirev.2008.04.015, 2008.

Ślubowska, M. A., Koç, N., Rasmussen, T. L. and Klitgaard-Kristensen, D.: Changes in the flow of Atlantic water into the Arctic Ocean since the last deglaciation: Evidence from the northern Svalbard continental margin, 80°N, Paleoceanography, 20(4), doi:10.1029/2005PA001141, 2005.

Small, D. and Fabel, D.: Was Scotland deglaciated during the Younger Dryas?, Quat. Sci. Rev., 145, 259–263, doi:10.1016/j.quascirev.2016.05.031, 2016.

Smik, L., Cabedo-Sanz, P. and Belt, S. T.: Semi-quantitative estimates of paleo Arctic sea ice concentration based on source-specific highly branched isoprenoid alkenes: A further development of the PIP_{25} index, Org. Geochem., 92, 63–69, doi:10.1016/j.orggeochem.2015.12.007, 2016.

Solignac, S., De Vernal, A. and Hillaire-Marcel, C.: Holocene sea-surface conditions in the North Atlantic - Contrasted trends and regimes in the western and eastern sectors (Labrador Sea vs. Iceland Basin), Quat. Sci. Rev., 23(3–4), 319–334, doi:10.1016/j.quascirev.2003.06.003, 2004.

Solomina, O. N., Bradley, R. S., Hodgson, D. A., Ivy-Ochs, S., Jomelli, V., Mackintosh, A. N., Nesje, A., Owen, L. A., Wanner, H., Wiles, G. C. and Young, N. E.: Holocene glacier fluctuations, Quat. Sci. Rev., 111, 9–34, doi:10.1016/j.quascirev.2014.11.018, 2015.

Solomina, O. N., Bradley, R. S., Jomelli, V., Geirsdottir, A., Kaufman, D. S., Koch, J., McKay, N. P., Masiokas, M., Miller, G., Nesje, A., Nicolussi, K., Owen, L. A., Putnam, A. E., Wanner, H., Wiles, G. and Yang, B.: Glacier fluctuations during the past 2000 years, Quat. Sci. Rev., 149, 61–90, doi:10.1016/j.quascirev.2016.04.008, 2016.

Spielhagen, R. F.: Hotspots in the Arctic: Natural archives as an early warning system for global warming, Geology, 40(11), 1055–1056, doi:10.1130/focus112012.1, 2012.

Spielhagen, R. F., Werner, K., Sørensen, S. A., Zamelczyk, K., Kandiano, E., Budeus, G., Husum, K., Marchitto, T. M. and Hald, M.: Enhanced modern heat transfer to the Arctic by warm Atlantic Water., Science, 331(6016), 450–453, doi:10.1126/science.1197397, 2011.

Stalling, D., Westerhof, M. and Hege, H.-C.: Amira: A Highly Interactive System for Visual Data Analysis, in The Visualization Handbook, edited by C. D. Hansen and C. R. Johnson, pp. 749–767, Elsevier. [online] Available from: https://amira.zib.de/, 2005.

Stein, R.: Arctic Ocean Sediments: Processes, proxies, and paleoenvironment, Elsevier B.V., Amsterdam., 2008.

Stein, R., Fahl, K. and Müller, J.: Proxy Reconstruction of Cenozoic Arctic Ocean Sea-Ice History – from

IRD to IP_{25}, Polarforschung, 82(1), 37–71, 2012.

Stein, R., Fahl, K., Schade, I., Manerung, A., Wassmuth, S., Niessen, F. and Nam, S. Il: Holocene variability in sea ice cover, primary production, and Pacific-Water inflow and climate change in the Chukchi and East Siberian Seas (Arctic Ocean), J. Quat. Sci., 32(3), 362–379, doi:10.1002/jqs.2929, 2017.

Steinsund, P. I.: Benthic foraminifera in surface sediments of the Barents and Kara Seas: modern and late Quaternary applications, University of Tromsø., 1994.

Stokes, C. R., Corner, G. D., Winsborrow, M. C. M., Husum, K. and Andreassen, K.: Asynchronous response of marine-terminating outlet glaciers during deglaciation of the Fennoscandian ice sheet, Geology, 42(5), 455–458, doi:10.1130/G35299.1, 2014.

Straneo, F., Hamilton, G. S., Sutherland, D. A., Stearns, L. A., Davidson, F., Hammill, M. O., Stenson, G. B. and Rosing-Asvid, A.: Rapid circulation of warm subtropical waters in a major glacial fjord in East Greenland, Nat. Geosci., 3(3), 182–186, doi:10.1038/ngeo764, 2010.

Streuff, K., Forwick, M., Szczuciński, W., Andreassen, K. and Ó Cofaigh, C.: Submarine landform assemblages and sedimentary processes related to glacier surging in Kongsfjorden, Svalbard, Arktos, 1(1), 14, doi:10.1007/s41063-015-0003-y, 2015.

Stroeve, J. C., Serreze, M. C., Holland, M. M., Kay, J. E., Malanik, J. and Barrett, A. P.: The Arctic's rapidly shrinking sea ice cover: A research synthesis, Clim. Change, 110(3–4), 1005–1027, doi:10.1007/s10584-011-0101-1, 2012.

Stuiver, M. and Braziunas, T. F.: Modeling atmospheric ^{14}C influences and ^{14}C ages of marine samples to 10,000 BC, Radiocarbon, 35(1), 137–189, 1993.

Svendsen, H., Beszczynska-Møller, A., Hagen, J. O., Lefauconnier, B., Tverberg, V., Gerland, S., Ørbæk, J. B., Bischof, K., Papucci, C., Zajączkowski, M., Azzolini, R., Bruland, O., Wiencke, C., Winther, J.-G. and Dallmann, W.: The physical environment of Kongsfjorden – Krossfjorden, an Arctic fjord system in Svalbard, Polar Res., 21(1), 133–166, 2002.

Svendsen, J. I. and Mangerud, J.: Holocene glacial and climatic variations on Spitsbergen, Svalbard, The Holocene, 7(1), 45–57, doi:10.1177/095968369700700105, 1997.

Svendsen, J. I., Elverhøi, A. and Mangerud, J.: The retreat of the Barents Sea Ice Sheet on the western Svalbard margin, Boreas, 25(4), 244–256, doi:10.1111/j.1502-3885.1996.tb00640.x, 1996.

Svendsen, J. I., Gataullin, V., Mangerud, J. and Polyak, L.: The glacial History of the Barents and Kara Sea Region, in Quaternary Glaciations-Extent and Chronology, edited by J. Ehlers and P. L. Gibbard, pp. 369–378, Elsevier, Amsterdam., 2004.

Svensson, A., Andersen, K. K., Bigler, M., Clausen, H. B., Dahl-Jensen, D., Davies, S. M., Johnsen, S. J., Muscheler, R., Parrenin, F., Rasmussen, S. O., Röthlisberger, R., Seierstad, I., Steffensen, J. P. and Vinther, B. M.: A 60 000 year Greenland stratigraphic ice core chronology, Clim. Past, 4(1), 47–57, doi:10.5194/cp-4-47-2008, 2008.

Syvitski, J. P. M., Burrell, D. C. and Skei, J. M.: Fjords: processes and products, Springer, New York., 1987.

Szczuciński, W. and Zajączkowski, M.: Factors Controlling Downward Fluxes of Particulate Matter in Glacier-Contact and Non-Glacier Contact Settings in a Subpolar Fjord (Billefjorden, Svalbard), in Sediments, Morphology and Sedimentary Processes on Continental Shelves, vol. 44, edited by M. Z. Li, C. R. Sherwood, and P. R. Hill, pp. 369–386, John Wiley & Sons, Ltd, Chichester, West

Sussex, UK., 2012.

Sztybor, K. and Rasmussen, T. L.: Diagenetic disturbances of marine sedimentary records from methane-influenced environments in the Fram Strait as indications of variation in seep intensity during the last 35 000 years, Boreas, 46(2), 212–228, doi:10.1111/bor.12202, 2017.

Taldenkova, E., Bauch, H. A., Gottschalk, J., Nikolaev, S., Rostovtseva, Y., Pogodina, I., Ovsepyan, Y. and Kandiano, E.: History of ice-rafting and water mass evolution at the northern Siberian continental margin (Laptev Sea) during Late Glacial and Holocene times, Quat. Sci. Rev., 29(27–28), 3919–3935, doi:10.1016/j.quascirev.2010.09.013, 2010.

Tarasov, L. and Peltier, W. R.: Arctic freshwater forcing of the Younger Dryas cold reversal., Nature, 435(7042), 662–665, doi:10.1038/nature03617, 2005.

Teichert, S., Woelkerling, W., Rüggeberg, A., Wisshak, M., Piepenburg, D., Meyerhöfer, M., Form, A. and Freiwald, A.: Arctic rhodolith beds and their environmental controls (Spitsbergen, Norway), Facies, 60(1), 15–37, doi:10.1007/s10347-013-0372-2, 2014.

Teigen, S. H., Nilsen, F., Skogseth, R., Gjevik, B. and Beszczynska-Möller, A.: Barotropic instability in the West Spitsbergen Current, J. Geophys. Res. Ocean., 116(7), 1–18, doi:10.1029/2011JC006974, 2010.

Telesiński, M. M., Spielhagen, R. F. and Lind, E. M.: A high-resolution Lateglacial and Holocene palaeoceanographic record from the Greenland Sea, Boreas, 43, 273–285, doi:10.1111/bor.12045, 2014.

Telesiński, M. M., Bauch, H. A., Spielhagen, R. F. and Kandiano, E. S.: Evolution of the central Nordic Seas over the last 20 thousand years, Quat. Sci. Rev., 121, 98–109, doi:10.1016/j.quascirev.2015.05.013, 2015.

Thompson, D. W. J. and Wallace, J. M.: The Arctic oscillation signature in the wintertime geopotential height and temperature fields, Geophys. Res. Lett., 25(9), 1297–1300, doi:10.1029/98GL00950, 1998.

Thornalley, D. J. R., McCave, I. N. and Elderfield, H.: Tephra in deglacial ocean sediments south of Iceland: Stratigraphy, geochemistry and oceanic reservoir ages, J. Quat. Sci., 26(2), 190–198, doi:10.1002/jqs.1442, 2011.

Trusel, L. D., Powell, R. D., Cumpston, R. M. and Brigham-Grette, J.: Modern glacimarine processes and potential future behaviour of Kronebreen and Kongsvegen polythermal tidewater glaciers, Kongsfjorden, Svalbard, in Fjord Systems and Archives, vol. 344, edited by J. A. Howe, W. E. N. Austin, M. Forwick, and M. Paetzel, pp. 89–102, Geological Society, London., 2010.

Untersteiner, N.: On the ice and heat balance in Fram Strait, J. Geophys. Res., 93(7), 527–531, 1988.

de Vernal, A., Bilodeau, G., Hillaire-Marcel, C. and Kassou, N.: Quantitative assessment of carbonate dissolution in marine sediments from foraminifer linings vs. shell ratios: Davis Strait, northwest North Atlantic, Geology, 20(6), 527–530, doi:10.1130/0091-7613(1992)020<0527:QAOCDI>2.3.CO;2, 1992.

de Vernal, A., Hillaire-Marcel, C. and Bilodeau, G.: Reduced meltwater outflow from the Laurentide ice margin during the Younger Dryas, Nature, 381, 774–777, 1996.

de Vernal, A., Hillaire-Marcel, C., Rochon, A., Fréchette, B., Henry, M., Solignac, S. and Bonnet, S.: Dinocyst-based reconstructions of sea ice cover concentration during the Holocene in the Arctic

Ocean, the northern North Atlantic Ocean and its adjacent seas, Quat. Sci. Rev., 79, 111–121, doi:10.1016/j.quascirev.2013.07.006, 2013.

Volkman, J. K.: A review of sterol markers for marine and terrigenous organic matter, Org. Geochem., 9(2), 83–99, doi:10.1016/0146-6380(86)90089-6, 1986.

Volkman, J. K., Barrett, S. M., Dunstan, G. A. and Jeffrey, S. W.: Geochemical significance of the occurrence of dinosterol and other 4-methyl sterols in a marine diatom, Org. Geochem., 20(1), 7–15, doi:10.1016/0146-6380(93)90076-N, 1993.

Waelbroeck, C., Duplessy, J. C., Michel, E., Labeyrie, L., Paillard, D. and Duprat, J.: The timing of the last deglaciation in North Atlantic climate records., Nature, 412(6848), 724–727, doi:10.1038/35106623, 2001.

Waelbroeck, C., Labeyrie, L., Michel, E., Duplessy, J. C., McManus, J. F., Lambeck, K., Balbon, E. and Labracherie, M.: Sea-level and deep water temperature changes derived from benthic foraminifera isotopic records, Quat. Sci. Rev., 21(1–3), 295–305, doi:10.1016/S0277-3791(01)00101-9, 2002.

Walczowski, W.: Frontal structures in the West Spitsbergen current margins, Ocean Sci., 9(6), 957–975, doi:10.5194/os-9-957-2013, 2013.

Walczowski, W. and Piechura, J.: Influence of the West Spitsbergen Current on the local climate, Int. J. Climatol., 31(7), 1088–1093, doi:10.1002/joc.2338, 2011.

Walker, M., Johnsen, S., Rasmussen, S. O., Popp, T., Steffensen, J.-P., Gibbard, P., Hoek, W., Lowe, J., Andrews, J., Björck, S., Cwynar, L. C., Hughen, K., Kershaw, P., Kromer, B., Litt, T., Lowe, D. J., Nakagawa, T., Newnham, R. and Schwander, J.: Formal definition and dating of the GSSP (Global Stratotype Section and Point) for the base of the Holocene using the Greenland NGRIP ice core, and selected auxiliary records, J. Quat. Sci., 24(1), 3–17, doi:10.1002/jqs.1227, 2009.

Wanner, H., Beer, J., Bütikofer, J., Crowley, T. J., Cubasch, U., Flückiger, J., Goosse, H., Grosjean, M., Joos, F., Kaplan, J. O., Küttel, M., Müller, S. a., Prentice, I. C., Solomina, O., Stocker, T. F., Tarasov, P., Wagner, M. and Widmann, M.: Mid- to Late Holocene climate change: an overview, Quat. Sci. Rev., 27(19–20), 1791–1828, doi:10.1016/j.quascirev.2008.06.013, 2008.

Wassmann, P.: Overarching perspectives of contemporary and future ecosystems in the Arctic Ocean, Prog. Oceanogr., 139, 1–12, doi:10.1016/j.pocean.2015.08.004, 2015.

Wefer, G. and Berger, W. H.: Isotope paleontology: growth and composition of extant calcareous species, Mar. Geol., 100, 207–248, doi:10.1016/0025-3227(91)90234-U, 1991.

Werner, K., Spielhagen, R. F., Bauch, D., Hass, H. C., Kandiano, E. and Zamelczyk, K.: Atlantic Water advection to the eastern Fram Strait — Multiproxy evidence for late Holocene variability, Palaeogeogr. Palaeoclimatol. Palaeoecol., 308(3–4), 264–276, doi:10.1016/j.palaeo.2011.05.030, 2011.

Werner, K., Spielhagen, R. F., Bauch, D., Hass, H. C. and Kandiano, E.: Atlantic Water advection versus sea-ice advances in the eastern Fram Strait during the last 9 ka: Multiproxy evidence for a two-phase Holocene, Paleoceanography, 28(2), 283–295, doi:10.1002/palo.20028, 2013.

Werner, K., Frank, M., Teschner, C., Müller, J. and Spielhagen, R. F.: Neoglacial change in deep water exchange and increase of sea-ice transport through eastern Fram Strait: Evidence from radiogenic isotopes, Quat. Sci. Rev., 92, 190–207, doi:10.1016/j.quascirev.2013.06.015, 2014.

Werner, K., Müller, J., Husum, K., Spielhagen, R. F., Kandiano, E. S. and Polyak, L.: Holocene sea subsurface and surface water masses in the Fram Strait - Comparisons of temperature and sea-ice reconstructions, Quat. Sci. Rev., 147, 194–209, doi:10.1016/j.quascirev.2015.09.007, 2016.

de Wet, G. A., Balascio, N. L., D'Andrea, W. J., Bakke, J., Bradley, R. S. and Perren, B.: Holocene glacier activity reconstructed from proglacial lake Gjøavatnet on Amsterdamøya, NW Svalbard, Quat. Sci. Rev., doi:10.1016/j.quascirev.2017.03.018, 2017.

Wilson, L. J., Hald, M. and Godtliebsen, F.: Foraminiferal faunal evidence of twentieth-century Barents Sea warming, The Holocene, 21(July), 527–537, doi:10.1177/0959683610385718, 2011.

Wollenburg, J.: Zur Taxonomie von rezenten benthischen Foraminiferen aus dem Nansen Becken, Arktischer Ozean, Bremerhaven., 1992.

Wollenburg, J.: Benthic foraminiferal assemblages in the Arctic Ocean : indicators for water mass distribution, productivity, and sea ice drift, University of Bremen., 1995.

Wollenburg, J. E. and Mackensen, A.: Living benthic foraminifers from the central Arctic Ocean: faunal composition, standing stock and diversity, Mar. Micropaleontol., 34, 153–185, 1998.

Wollenburg, J. E., Kuhnt, W. and Mackensen, A.: Changes in Arctic Ocean paleoproductivity and hydrography during the last 145 kyr: The benthic foraminiferal record, Paleoceanography, 16(1), 65–77, 2001.

Wollenburg, J. E., Knies, J. and Mackensen, A.: High-resolution paleoproductivity fluctuations during the past 24 kyr as indicated by benthic foraminifera in the marginal Arctic Ocean, Palaeogeogr. Palaeoclimatol. Palaeoecol., 204, 209–238, doi:10.1016/S0031-0182(03)00726-0, 2004.

Wouters, B., Martin-Espanol, A., Helm, V., Flament, T., van Wessem, J. M., Ligtenberg, S. R. M., van den Broeke, M. R. and Bamber, J. L.: Dynamic thinning of glaciers on the Southern Antarctic Peninsula, Science, 348(6237), 899–903, doi:10.1126/science.aaa5727, 2015.

Xiao, X., Fahl, K., Müller, J. and Stein, R.: Sea-ice distribution in the modern Arctic Ocean: Biomarker records from trans-Arctic Ocean surface sediments, Geochim. Cosmochim. Acta, 155, 16–29, doi:10.1016/j.gca.2015.01.029, 2015.

Yashayaev, I., Seidov, D. and Demirov, E.: A new collective view of oceanography of the Arctic and North Atlantic basins, Prog. Oceanogr., 132, 1–21, doi:10.1016/j.pocean.2014.12.012, 2015.

Young, N. E., Briner, J. P., Rood, D. H. and Finkel, R. C.: Glacier Extent During the Younger Dryas and 8.2-ka Event on Baffin Island, Arctic Canada, Science, 337(6100), 1330–1333, doi:10.1126/science.1222759, 2012.

Zajączkowski, M., Szczuciński, W., Plessen, B. and Jernas, P.: Benthic foraminifera in Hornsund, Svalbard: Implications for paleoenvironmental reconstructions, Polish Polar Res., 31(4), 349–375, doi:10.2478/v10183-010-0010-4, 2010a.

Zajączkowski, M., Szczuciński, W., Plessen, B. and Jernas, P.: Benthic foraminifera in Hornsund, Svalbard: Implications for paleoenvironmental reconstructions, Polish Polar Res., 31(4), 349–375, doi:10.2478/v10183-010-0010-4, 2010b.

Zamelczyk, K., Rasmussen, T. L., Husum, K., Haflidason, H., de Vernal, A., Ravna, E. K., Hald, M. and Hillaire-Marcel, C.: Paleoceanographic changes and calcium carbonate dissolution in the central Fram Strait during the last 20ka, Quat. Res., 78(3), 405–416, doi:10.1016/j.yqres.2012.07.006, 2012.

Zamelczyk, K., Rasmussen, T. L., Husum, K. and Hald, M.: Marine calcium carbonate preservation vs. climate change over the last two millennia in the Fram Strait: Implications for planktic foraminiferal paleostudies, Mar. Micropaleontol., 98, 14–27, doi:10.1016/j.marmicro.2012.10.001, 2013.

Versicherung an Eides Statt

gem. § 5 Abs. 5 der Promotionsordnung vom 15.07.2015

Ich, _____

(Vorname, Name, Anschrift, ggf. Matr.-Nr.)

versichere an Eides Statt durch meine Unterschrift, dass ich die vorstehende Arbeit selbständig und ohne fremde Hilfe angefertigt und alle Stellen, die ich wörtlich dem Sinne nach aus Veröffentlichungen entnommen habe, als solche kenntlich gemacht habe, mich auch keiner anderen als der angegebenen Literatur oder sonstiger Hilfsmittel bedient habe, und die zu Prüfungszwecken beigelegte elektronische Version der Dissertation mit der abgegebenen gedruckten Version identisch ist.

Ich versichere an Eides Statt, dass ich die vorgenannten Angaben nach bestem Wissen und Gewissen gemacht habe und dass die Angaben der Wahrheit entsprechen und ich nichts verschwiegen habe.

Die Strafbarkeit einer falschen eidesstattlichen Versicherung ist mir bekannt, namentlich die Strafandrohung gemäß § 156 StGB bis zu drei Jahren Freiheitsstrafe oder Geldstrafe bei vorsätzlicher Begehung der Tat bzw. gemäß § 161 Abs. 1 StGB bis zu einem Jahr Freiheitsstrafe oder Geldstrafe bei fahrlässiger Begehung.

_____ _____

Ort, Datum Unterschrift